2013

Fatigue Characterization Of Fire Resistant Syntactic Foam Core Material

Mohammad Mynul Hossain
North Carolina Agricultural and Technical State University

Fatigue Characterization of Fire Resistant Syntactic Foam Core Material

Mohammad Mynul Hossain

North Carolina A&T State University

A dissertation submitted to the graduate faculty

in partial fulfillment of the requirements for the degree of

DOCTOR OF PHILOSOPHY

Department: Mechanical Engineering

Major: Mechanical Engineering

Major Professor: Dr. Kunigal Shivakumar

Greensboro, North Carolina

2013

School of Graduate Studies
North Carolina Agricultural and Technical State University
This is to certify that the Doctoral Dissertation of

Mohammad Mynul Hossain

has met the dissertation requirements of
North Carolina Agricultural and Technical State University

Greensboro, North Carolina
2013

Approved by:

Dr. Kunigal Shivakumar Major Professor	Dr. Mannur Sundaresan Committee Member
Dr. Messiha Saad Committee Member	Dr. Shamsuddin Ilias Committee Member
Dr. Claude Lamb Committee Member	Dr. Ivatury Raju Committee Member
Dr. Samuel P. Owusu-Ofori Department Chair	Dr. Sanjiv Sarin Dean, The Graduate School

Biographical Sketch

Mohammad Mynul Hossain was born in Comilla, Bangladesh to Mr. Mohammad Abdul Mannan and Rezia Begum.He earned his B.Sc in Mechanical Engineering from Bangladesh University of Engineering & Technology, Dhaka, Bangladesh, in 2004. He received his M.Sc in Mechanical Engineering from Kongju National University, South Korea, in 2008. From 2004 to 2006, he was employed at Akij Cement Company Ltd, Bangladesh as a Mechanical Engineer (Shift Engineer) and later promoted to shift in-charge. At Akij Cement Company Ltd, His responsibility was to supervise engineer and technician involved in production and maintenance department.

He enrolled in the Department of mechanical Engineering Ph.D. program at the North Carolina Agriculture and Technical State University in 2008. His research is in the area of fatigue characterization of a fire resistant syntactic foam core for sandwich structure.

Dedication

I dedicate this success to my father, late Mr. Mohammad Abdul Mannan and my mother, Rezia Begum.

Acknowledgements

I wish to express my sincerest gratitude to the many individuals who supported and encouraged me both professionally and personally for the completion of this work. Foremost, I would like to thank my advisor Professor Dr. Kunigal Shivakumar. Admittedly, without his continued support, encouragement, patience and valuable advice, this work would not be possible. I greatly acknowledge to my committee members Dr. Mannur Sundaresan, Dr. Messiha Saad, Dr. Shamsuddin Illias and Dr. Ivatury Raju for reviewing my work and offering many useful recommendations.

I expressed my sincerest gratitude to the Center for Composite Materials Research (CCMR) at the North Carolina A&T State University and the Department of Mechanical Engineering for the opportunity to enroll me in this program. This research has been supported and funded by various organizations including Office of Naval Research (Dr. Yapa Rajapakse), U.S. Army Research Office (Dr. Larry Russell) and NASA university Research Center (URC)-Center for Aviation Safety (CAS). I greatly acknowledge these organizations and personnel for their financial and technical support to accomplish this research work. I would like to thank CCMR staff, especially, Mr. Matthew Sharpe and Mr. John Skujins, Dr. Shivalingappa Lingaiah for various assistance in completion of this work. It is my pleasure to acknowledge the contribution of my lab mates and, senior alumni specially Dr. Raghu Pandurangha, Dr. Jogi Gauwda, Dr. Paul Akangah, ABSM Rupan Talucdher, Anthony Cunningham, Hiba Ahmed, Rafid Kully and Kazi Al Imran for their support.

Finally, I would like to express my deepest appreciation to my parents, my wife Hoshna Ara Ovi and other family members for their lifelong sacrifices and belief in me. Their consistent mental support, love and affection always played a significant role in my journey in life.

Table of Contents

List of Figures……...…...x

List of Tables…….…...xiv

List of Symbols……..xv

Abstract 2

CHAPTER 1 Introduction..... 4

1.1 Background of Syntactic Foams and Eco-Core 4

1.2 Fatigue Test Parameters 8

1.2.1 Loading condition..... 8

1.2.2 Test control mode. 9

1.2.3 Stress ratio. 10

1.2.4 Loading frequency. 11

1.2.5 Test temperature. 11

1.2.6 Waveform. 11

1.3 Fatigue Life Models for Sandwich Structures 12

1.3.1 stress versus number of cycles (S-N) model. 12

1.3.2 Strength degradation model..... 15

1.3.3 Stiffness reduction model. 16

1.3.4 Cumulative damage model for variable amplitude loading. 20

1.4 Fatigue Test Methods for Foam Cores and Sandwich Beam 23

1.4.1 Compression-compression or tension-tension fatigue test methods. 23

1.4.2 Shear and flexural fatigue test methods. 24

1.5 Literature Review 24

1.5.1 Compression-compression fatigue. 24

1.5.2 Shear fatigue. 26

1.5.3 Flexural fatigue 27

1.6 Challenges and Gaps 29

1.7 Test Concept and Methodology 30

1.8 Objectives of the Research 31

1.9 Scope of the Dissertation 31

CHAPTER 2 Compression-Compression Fatigue Characterization 33

2.1 Introduction 33

2.2 Eco-Core Materials 33

2.3 Compression Static Test and Test Results 37

2.4 Fatigue Test 40

2.5 Fatigue Test Results and Discussion 43

2.5.1 Failure criteria and associated failure lives. 43

2.5.2 Stress-N diagram. 47

2.5.3 Stress ratio effect. 50

2.5.3.1 Stress versus N. 51

2.5.3.2 Stress range versus N. 52

2.5.3.3 Mean stress versus N. 52

2.6 Summary 53

CHAPTER 3 Shear Fatigue Characterization 55

3.1 Introduction 55

3.2 Material System 55

3.3 Design of Specimen 56

3.4 Fabrication of Sandwich Panel and Specimen 59

3.5 Static Shear Test, Results and Discussion 60

3.6 Shear Fatigue Test 63

3.7 Fatigue Test Results and Discussions 65

3.7.1 Failure modes and associated failure lives. 65

3.7.2 Stress analysis near face sheet-core interface region. 68

3.7.3 S-N Diagram. Normalized shear stress (τ_{max}/τ_c) versus number of load cycles (N) 71

3.8 Summary 74

CHAPTER 4 Flexural Fatigue Characterization 75

4.1 Introduction 75

4.2 Material System 76

4.3 Design of Specimen 76

4.4 Static Flexural Test and Results 78

4.5 Stress Analysis Near Face Sheet-Core Interface Region 82

4.6 Fatigue Test 83

4.7 Fatigue Test Results and Discussions 85

4.7.1 Failure definition and associated failure lives 85

4.7.2. S-N diagram. 89

4.8 Summary 92

CHAPTER 5 Concluding Remarks and Recommendation for Future Work 94

5.1 Conclusions 94

5.1.1 Compression-compression fatigue. 94

5.1.2 Shear fatigue. 95

5.1.3 Flexural fatigue 96

5.2 Recommendations for Future Works 97

5.2.1 Development of new test method for high cyclic frequency loading. 97

5.2.2 Development of fatigue life prediction model for variable amplitude loading. 97

5.2.3 Extend the study to tension-compression loading. 98

References 99

Appendix A 108

Appendix B 116

Appendix C 135

Appendix D 140

List of Figures

Figure 1.1. SEM image of conventional syntactic foam [9]. 6

Figure 1.2. Structural difference between Conventional syntactic foam and Eco-Core. 8

Figure 1.3. Three different fatigue loading conditions. 9

Figure 1.4. Nomenclature of different load ratio. 10

Figure 1.5. Nomenclature for constant stress amplitude loading. 13

Figure 1.6. Typical S-N diagram. 13

Figure 1.7. Normalized load Vs normalized number of cycles in sandwich composites under displacement control fatigue with logarithmic fit [59]. 19

Figure 1.8. Schematic illustration of determination of residual life: two-step loading [36]. 21

Figure 1.9. Eco-Core panel and test specimen configuration and loading. 30

Figure 2.1. Steps in fabricating Eco-Core panel 34

Figure 2.2. Compression test specimen. 34

Figure 2.3. Specimen layout. 35

Figure 2.4. Specimen selection process from panel 1: (a) Specimens numbered according to specimen number in specimen layout; (b) Specimen numbered according to ascending order of specimen density. 36

Figure 2.5. SEM image of Eco-Core. 37

Figure 2.6. Machine setup for compression static and fatigue test. 38

Figure 2.7. Static compression stress-strain responses of specimens (panel 1). 39

Figure 2.8. Onset, propagation and final failure images of static compression samples, panel 1. 40

Figure 2.9. Compression-compression fatigue loading. 42

Figure 2.10. Typical compliance versus cycles response of a C-C fatigue test with definition of three types of failure. 44

Figure 2.11. Compliance versus number of cycles (N) and the fatigue lives based on the three failure criteria. 46

Figure 2.12. Successive failure of the specimen (M-18) for σmin/σc =0.85 and R=10. 47

Figure 2.13. Normalized stress (σmin/σc) versus number of load cycles (N) for R=10 along with least square equation fit. Also shown is the equation with rounded off (solid line) constants. 48

Figure 2.14. Comparison of S-N equation with experimental data for R= 10, with constants rounded off. 49

Figure 2.15. Comparison of equation with experiment for R=5, with constants in equation are rounded off. 49

Figure 2.16. Normalized stress versus N for R= 10 and 5 for 2% compliance change. 51

Figure 2.17. Normalized stress range versus N for 2% compliance change for R= 10 and 5. 52

Figure 2.18. Normalized mean stress versus N for 2% compliance change for R= 10 and 5. 53

Figure 3.1. (a) Schematic of test specimen, loading and nomenclature (b) Shear force diagram (c) Bending moment diagram……..... 57

Figure 3.2. Failure load versus span/depth (S/d) ratio for Eco-Core sandwich beam based on two failure criteria. 58

Figure 3.3. Steps for fabricating face sheet. 59

Figure 3.4. Steps for fabricating Eco-Core sandwich panel. 60

Figure 3.5. Short beam shear test setup. 61

Figure 3.6. Load-deflection responses of short beam test specimens. 62

Figure 3.7. Typical static failure modes in Eco-Core sandwich beam (Crack is highlighted by white line). 63

Figure 3.8. Typical shear fatigue loading (R=0.1). 65

Figure 3.9. Compliance versus number of cycles (N) and the fatigue lives based on the three failure criteria. 66

Figure 3.10. Successive failure of the specimen (SSP-12) for τ_{max}/τ_c = 0.80 (crack is highlighted by white line). 67

Figure 3.11. Types of shear fatigue failure. 68

Figure 3.12. Stress state near the support and load points for delamination failure. 68

Figure 3.13. Shear stress distribution at section A, B, and C. 69

Figure 3.14. Normal stress distribution at section A, B, and C. 70

Figure 3.15. Through the thickness shear stress distribution for X= 0, $t_f/3$, $2t_f/3$, t_f, $2t_f$ and $4t_f$. .. 70

Figure 3.16. Maximum shear stress at the interface against X. 71

Figure 3.17. Normalized stress (τ_{max}/τ_c) versus number of load cycles test data and the power law equation for three failure criteria. 72

Figure 3.18. Comparison of S-N equation with the experimental data for 2%, 5% and 7% compliance failure criteria. 73

Figure 4.1. (a) Schematic of test specimen, loading and nomenclature (b) Shear force diagram (c) Bending moment diagram……..77

Figure 4.2. Failure load versus span/depth(S/d) ratio for Eco-Core sandwich beam based on shear and flexural failure criteria..... 78

Figure 4.3. Flexural test setup. 80

Figure 4.4. Stress versus deflection responses of flexural tests. 81

Figure 4.5. Typical static failure modes in Eco-Core sandwich beam specimen FSP-20 (Crack is highlighted by white line). 81

Figure 4.6. Shear stress distribution at section A, B, and C. 83

Figure 4.7. Normal stress distribution at section A, B, and C. 83

Figure 4.8. Typical flexural fatigue loading (R=0.1). 84

Figure 4.9. Compliance versus number of fatigue cycles (N) and the fatigue lives based on the three values (1%, 5% and 7%) of compliance change failure criteria. 88

Figure 4.10. Typical flexural fatigue failure sequence of a specimen (FSP-21) for σmax/σct = 0.80 (crack is highlighted by white line). 88

Figure 4.11. Comparison of normalized stress σmax/σct versus number of load cycles from experiment and equation for 1%, 5% and 7% change in compliance failure criteria. 91

Figure 4.12. Comparison of modified stress versus number of cycle equation with the experiment for the three failure criteria. 91

List of Tables

Table 2.1 Test Specimen and Properties 40

Table 2.2 Compression-Compression Fatigue Test Specimen and Loading for R=10, Panel 1(σ_c = -18.9 MPa) 42

Table 2.3 Compression-Compression Fatigue Test Specimen and Loading for R=5, Panel 2(σ_c = -20.3 MPa) 43

Table 2.4 Compression-Compression Fatigue Test Result for R= 10, panel 1 45

Table 2.5 Compression-Compression Fatigue Test Result for R= 5, panel 2 46

Table 2.6 Constants in the S-N Equation and Endurance Limit for R= 10 and 5 50

Table 3.1 Material Properties of Eco-Core and Face-sheet [12]…..……57

Table 3.2 Summary of Static Shear Strength Test 62

Table 3.3 Shear Fatigue Test Plan (R = 0.1, τ_c = 4.23 MPa) 64

Table 3.4 Shear Fatigue Equation Constants 67

Table 3.5 Flexural Static Test Results 73

Table 4.1 Flexural Static Test Results……...79

Table 4.2 Flexural Fatigue Test Plan for R=0.1(σ_{ct} = 9.97 MPa) 85

Table 4.3 Flexural Fatigue Test Results for R=0.1(σ_{ct} = 9.97 MPa) 87

Table 4.4 Flexural Fatigue Equation Constants 92

List of Symbols

σ_c = Core compression strength

$\Delta\sigma$ = Stress range

σ_{min} = Minimum applied stress

σ_{max} = Maximum applied stress

σ_{mean} = Mean applied stress

R = Load ratio or stress ratio

t_c = Core thickness.

t_f = Face sheet thickness.

d = Sandwich thickness.

S = Span of the beam.

b = Width of sandwich beam.

e = Edge distance from the support point.

P_f = Failure load.

D = Flexural rigidity of the sandwich beam.

E_c = Core elastic modulus (Tensile).

E_{ct} = Core tensile elastic modulus.

E_f = Face sheet elastic modulus.

σ_{ct} = Core tensile or flexural strength.

σ_{ult} = Core ultimate flexural strength.

τ_c = Core shear strength.

τ_{max} = Core maximum shear stress.

τ_{max} = Core minimum shear stress.

P_{max} = Maximum applied cyclic load in a single cycle.

P_{min} = Minimum applied cyclic load in a single cycle.

d_{max} = Displacement for the maximum applied cyclic load F_{max}.

d_{min} = Displacement for the minimum applied cyclic load F_{min}.

N = Number of cycles.

$N_{1\%}$ = Onset life based on 1% compliance change (for flexure load).

$N_{2\%}$ = Onset life based on 2% compliance change (for compression and shear load).

$N_{5\%}$ = Propagation life based on 5% compliance change.

$N_{7\%}$ = Total life based on 7% compliance change.

A_o = The material property constant.

α = Slope of the stress versus number of cycles curve.

*All the symbols listed here are from chapter 2 to chapter 4.

Abstract

Eco-Core is a fire resistant material for sandwich structural application; it was developed at NC A&T State University. The Eco-Core is made of very small volume of phenolic resin and large volume of flyash by a syntactic process. The process development, static mechanical and fracture, fire and toxicity safety and water absorption properties and the design of sandwich structural panels with Eco-Core was established and published in the literature. One of the important properties is needed for application in transportation vehicles is the fatigue performance under different stress states. Fatigue data are not available even for general syntactic foams. The objective of this research is to investigate the fatigue performance of Eco-Core under three types of stress states, namely, cyclic compression, shear and flexure, then document failure modes, and develop fatigue life equations for predicting life of Eco-Core sandwich panels. Compression-Compression fatigue was performed directly on Eco-Core cylindrical specimen, whereas shear and flexure fatigue tests were performed using sandwich beam made of E glass-Vinyl Ester face sheet and Eco-Core. Compression-compression fatigue test was conducted at two values of stress ratios (R=10 and 5) at the maximum compression stress (σ_{min}) range of 60% to 90% of compression strength (σ_c = 19.6 ± 0.25 MPa) for R=10 and 80% to 95% of compression strength for R=5. The failure modes were characterized by the material compliance change: On-set (2% compliance change), propagation (5%) and ultimate failure (7%). The number of load cycles correspond to each of these three damages were characterized as on-set, propagation and total lives. A similar approach was used in shear and flexure fatigue tests with stress ratio of R=0.1. The fatigue stress-number of load cycles data followed the standard power law equation for all three stress states. The constant of the equation were established for all three stress states and three failure modes. The fatigue life equation was

used to estimate endurance limit (10^6 cycles) of the material. Like metallic materials, the compression fatigue life of Eco-Core was found to be dependent on the stress range instead of maximum or mean cyclic stress. Furthermore shear and flexural ultimate failure of the core material was found to be due to a combination of shear and tensile stresses.

CHAPTER 1

Introduction

A background of foam core sandwich composites including syntactic foams and Eco-Core is presented. A review of fatigue test parameters, fatigue life models for characterization of foam core sandwich composites and general fatigue test methods are discussed. A literature survey on fatigue characterization of different metallic and polymeric foam core sandwich composite is also presented. Finally, challenges and technology gaps in the syntactic foam core sandwich beams, objective of the research, the scope of the dissertation are described.

1.1 Background of Syntactic Foams and Eco-Core

Sandwich structure core materials have received considerable amount of attention in recent years. This is because of their low density and unique functional properties such as impact energy absorption, sound absorption and high temperature tolerance. They are growing in use in sandwich structures, crash protection devices and the weight sensitive structural parts in transportation and aerospace applications. In sandwich structures, light weight core is covered on either side by two thin but stiff face sheets which are adhesively bonded or co-cured. The core is relatively thick, and carries the compression and shear loadings. The face sheet made of high strength and stiffness materials is relatively thin (1/10~1/20 of core thickness) and it carries the bending loads. The adhesive layer thickness is generally neglected as it is much smaller compared to face sheet or core thickness. The properties of sandwich composite mainly depend on the properties of the core and face sheets, their relative thicknesses and the integrity of bond between the two.

A variety of core materials are used in the composites industry. In aerospace applications honeycomb cores made from aluminum, phenolic-resin impregnated fiberglass, paper,

polypropylene and Aramid fiber are extensively utilized. Structures that are less weight critical and where cost is an important factor, core materials of end-grain balsa, closed-cell foams made from thermoplastics such as PVC or polyimide, carbon foams and syntactic foams are widely used. End-grain balsa wood is not suitable for complex shape construction. Besides, balsa wood suffers from non-uniform density, moisture swelling, rotting, and poor shear and transverse tension strengths. Plastic foams releases noxious gases when exposed to fire [1].

Syntactic foam is a special type of particulate composite where hollow spherical particles are bonded by matrix material. Here, matrix is considered to be the binder for the fillers. Matrix material can be made of metal, ceramic and polymers [2]; whereas filler particle can be made of hollow glass, carbon, steel, aluminum and polymer microbubbles of varying sizes (1 to 350 μm) [3, 4]. Polymeric matrices are of two types: thermoset and thermoplastic resin. Thermoset resins include epoxy resin, unsaturated polyesters, vinyl esters, phenolics, polyurethanes, and silicones. Thermoplastic resins are polyethylene, polystyrene, polyvinyl chloride, etc. Syntactic foams possess lower density compared to solid particulate or the matrix material, generally lower than 1 g/cc, which make the material to be buoyanent applications.

Syntactic foams are usually a two phase material, matrix and microballoons. However, during fabrication some air or gases can be entrapped within the matrix. The micro structure of syntactic foams under Scanning Electron Microscope (SEM) is shown in Figure 1.1. The syntactic foams are macroscopically isotropic [5] and its properties can be tailored by varying its density. This density variation is achieved in two different ways. One is by varying the radius ratio of different microballoons [6] and other is by changing the volume fraction [7] of microballoons in the structure. Processing and mechanical properties of syntactic foam have been investigated by a number of researchers for example [6, 8-12]. Effect of fiber reinforcement

on mechanical properties of syntactic foam has also been studied in [13-16] and found that a small amount of fibers reinforcement is required to increase fracture toughness. Nanoclay reinforcement was investigated in [18].

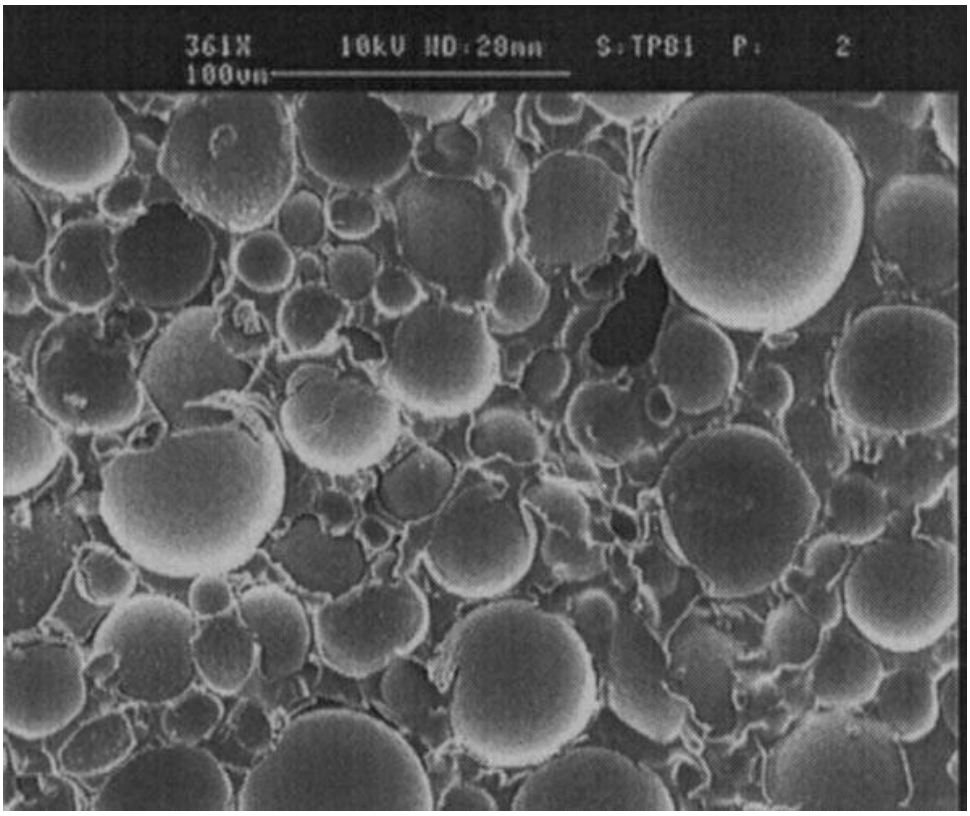

Figure 1.1. SEM image of conventional syntactic foam [9].

A number of properties such as high specific compressive strength [18], low moisture absorption and excellent damping properties [19, 20], higher thermal [21] and electrical insulation [22] properties, self-healing [23] and radar transparent [24] properties make syntactic foams suitable for many structural applications compared to open cell structural foams or balsa [2]. Syntactic foams were initially developed as buoyancy aid materials for deep sea applications [25]. They are now found to be useful in marine, aerospace, petroleum and mass transport industries [26, 27]. Although Syntactic foams are multi-functional composites and can be fabricated in a functionally graded configuration, but there are many limitations such as

brittleness, joining, repair, higher density and susceptibility to fire.

Although the general polymeric syntactic foams have found to have wide application in marine, aerospace and other transportation industries, the main problems is its susceptibility to fire. These foams contain about 50% weight of resin or 43 to 50% of gross weight of volatiles (depending on the char yield of resin), which fuels the fire once a fire is started. As a solution to this fire problem, Shivakumar et al. [11] developed a special class of syntactic foam called "Eco-Core". Eco-Core contains very low percent of volatiles (3-6% by weight) and the matrix material is dispersed in a large volume of inert material that makes the material to be fire tolerant. Another difference between Eco-Core and conventional syntactic foam is that the microbubbles are coated with a thin layer of high char resin to make sphere to sphere contact while the general syntactic foam is mixed and casted. Microbubbles used in Eco-Core are Cenospheres that it is extracted from fly ash produced by coal burn electric thermal power plants. The Figure 1.2 shows the structural difference between conventional syntactic foam and Eco-Core. Major highlights of Eco-Core are:

- Inexpensive and manufactured from a waste product
- Excellent fire resistant
- Nontoxic in fire
- Superior mechanical properties
- Good thermal and sound insulator
- Adaptable to existing manufacturing facility.
- Moldable and shapeable.

Potential field of application for Eco-Core material is in sandwich structures as a fire containment structures in marine ships, mass transportation structures (subway train), fire walls

in buildings, automobiles, and anywhere where fire is a major concern.

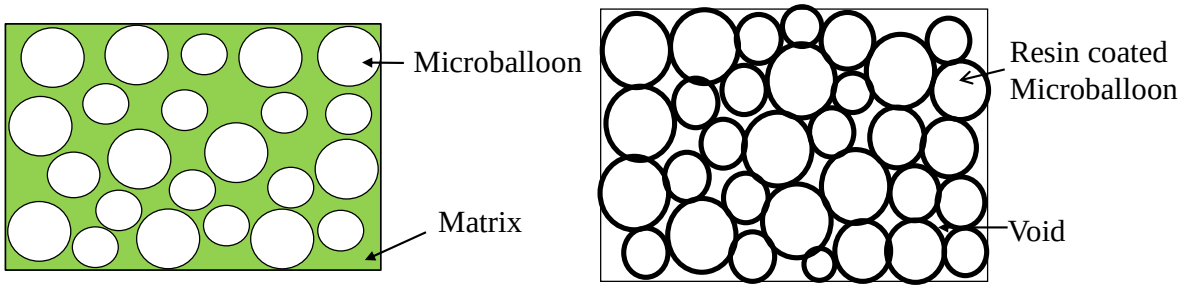

(a) Conventional syntactic foam (b) Eco-Core

Figure 1.2. Structural difference between Conventional syntactic foam and Eco-Core.

The processing, static mechanical, fire and toxicity properties of Eco-Core material as well as energy absorption and sea water resistance are presented in [1, 11, 15, 28]. Design of sandwich panels with Eco-Core is presented in [12]. All transportation structures are subjected to vibration or cyclic loads and fatigue performance of Eco-Core under various stress states needs to be established before it can be used in structural applications.

1.2 Fatigue Test Parameters

There are several parameters that have greater or less influence on fatigue life and failure modes of materials. These parameters include loading condition, test control mode, stress ratio, loading frequency, waveform, test temperature, etc. In designing the fatigue test program, decision should be made taking into account the influence of these parameters. Influences of above parameters are discussed below.

1.2.1 Loading condition. Composite structures are rarely subjected to uniform constant amplitude loading in service. The load could fluctuate randomly according to a vehicle operation and environmental condition thus creating a load spectrum. This type of loading could be presented as a series of block loading. Different fatigue loading conditions are schematically shown in Figure 1.3.

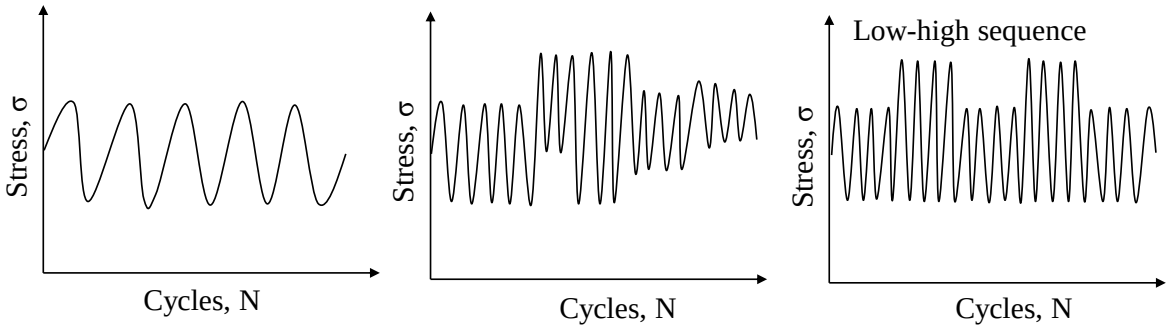

(a) Constant amplitude loading (b) Variable amplitude loading (c) Block loading

Figure 1.3. Three different fatigue loading conditions.

In literature, several articles are available on fatigue behavior of laminate composites under block loading [29-31], variable amplitude loading [32] and multi-axial loading conditions [33-35]. However, limited results are available on fatigue behavior of foam core and foam core sandwich composite [36] and none on variable amplitude loading and multi-axial fatigue loading. Clark et al. [36] investigated the fatigue behavior of Airex C70.130 foam core sandwich beams under two-step and block loading conditions using four-point bending. They used a combination of low-high and high-low loads to investigate the influence of load sequence on fatigue life. Clark et al. concluded that load sequence affects the fatigue life and a high/low load combination is more damaging than a low/high load combination. So, loading pattern plays a significant role in fatigue failure behavior and life prediction of composite materials.

1.2.2 Test control mode. Fatigue test can be performed under load or displacement (or strain) control. In load control mode, load is kept constant, deformation of the material increased with increasing number of load cycles as damage accumulated in the material and finally material fails. The load control mode is preferred for establishing S-N equation, to examine the load sequence effect on fatigue life [29-31] and also for applying a spectrum loading on a specimen or structural component [32]. On the other hand, displacement control is used in case of smooth damage development. In this case the specimen cyclic displacement is kept constant

and the load decreases continuously with number of cycles. Therefore the examined material does not fail suddenly. Displacement control mode is preferred in testing fatigue crack propagation studies [37].

1.2.3 Stress ratio. ($R= \sigma_{min}/\sigma_{max}$) is defined as the ratio of minimum cyclic stress to maximum cyclic stress. It helps to determine whether the applied load is tensile or compressive or a combination of both which are schematically shown in Figure 1.4.

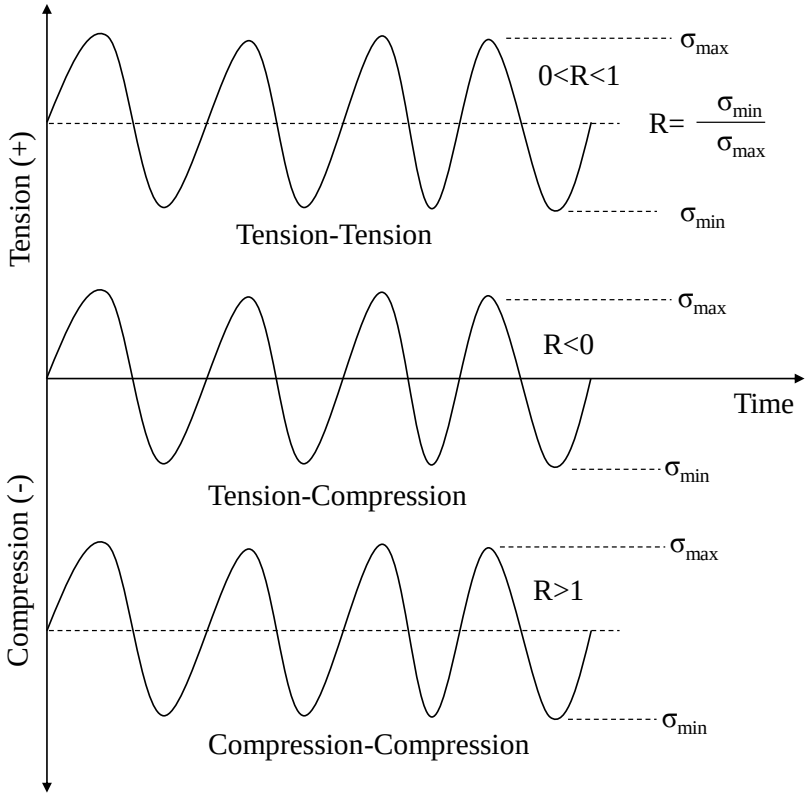

Figure 1.4. Nomenclature of different load ratio.

R<0 corresponds to a fatigue test with either compression-tension or tension-compression loading. 0<R<1 represent the fatigue test under tension-tension loading and R>1 corresponds to a fatigue test under compression-compression loading. Composite materials behave differently under tension fatigue and under compression fatigue because their mechanisms are different under these loading conditions, which in turn reflect the stress ratio effect [38]. Therefore, the

successful design of a testing program requires correct selection of loading cases, in keeping with the application for which the material is intended.

1.2.4 Loading frequency. In contrast to metallic materials, fatigue life of composite materials is considerably affected by the loading frequency. Several researchers concluded that the dependence of fatigue life on loading frequency is due to the heating of the material at higher frequencies, or creep fatigue at lower frequencies, or the interaction of both [39-44]. Mechanical energy dissipated during each stress-strain hysteresis loop is transformed into heat causing greater rise of localized temperature in the material. When this energy cannot be dissipated into the environment, it rises the temperatures of the specimen close to or even higher than the glass transition temperature of the matrix that in turn reduces the fatigue life of the specimen. This is a common phenomenon that researchers have observed at high loading frequency tests. Standards concerning the development of S-N curves for laminate and sandwich composite materials [45], provides no specific direction about loading frequency concern. The only prerequisite is that no significant changes in temperature must be observed.

1.2.5 Test temperature. For most of the testing programs in the literature, experimental results were obtained under ambient temperature conditions. This is because this type of test is simpler, less expensive, and provides basic information about material fatigue behavior. However, in practice, structures are subjected to combined thermo-mechanical loading [47] and therefore information about fatigue behavior of the structures under similar conditions is important to meet the design requirement. In general, fatigue strength of composite materials decreases with increased temperature of the composite materials.

1.2.6 Waveform. The shape of the applied waveform can affect the fatigue results. The sinusoidal waveform is the most commonly used since it can be easily generated and can be

assumed to be more realistic one compared to other types of loading that represent sudden changes, like the triangular, step (square) and saw-tooth waveforms.

In the present basic fatigue characterization, constant amplitude, load control test at room (ambient) temperature under three types of loading are conducted. The loadings are: compression-compression, shear, and flexure with R ratio of 10, 5, 0.1 and 0.1, respectively.

1.3 Fatigue Life Models for Sandwich Structures

In literature, there are several fatigue life models for sandwich structures were reported. These models are typically based on Stress versus number of cycles (S-N) diagram, strength degradation, stiffness reduction, cumulative damage model, or combination of these approaches. A brief description of these approaches is discussed:

1.3.1 stress versus number of cycles (S-N) model. The S-N approach is based on a simple curve fit to the experimental data of stress to number of cycles to cause failure. This is a commonly used approach to establish the endurance limit. In S-N approach, the test specimens are loaded in constant amplitude i.e. load between maximum (σ_{max}) or minimum stress (σ_{min}) until the specimen fails by a defined failure. The mean stress (σ_{mean}), and stress amplitude (σ_{amp}) are calculated by the equations (1.1) and (1.2), respectively. All this terms are illustrated in Figure 1.5.

$$\sigma_{mean} = \frac{\sigma_{max}+\sigma_{min}}{2} \tag{1.1}$$

$$\sigma_{amp} = \frac{\sigma_{max}-\sigma_{min}}{2} \tag{1.2}$$

The typical S-N plot (linear scale) is shown in Figure 1.6. In S-N diagram, the total life of the specimen is plotted, where total life defines the number of cycles required to fatigue crack initiation plus the number of cycles required to propagate the fatigue crack up to final failure. The stress, σ in equations (1.1) and (1.2) can be replaced by strain or even stress intensity factor

depending on type of the model needed.

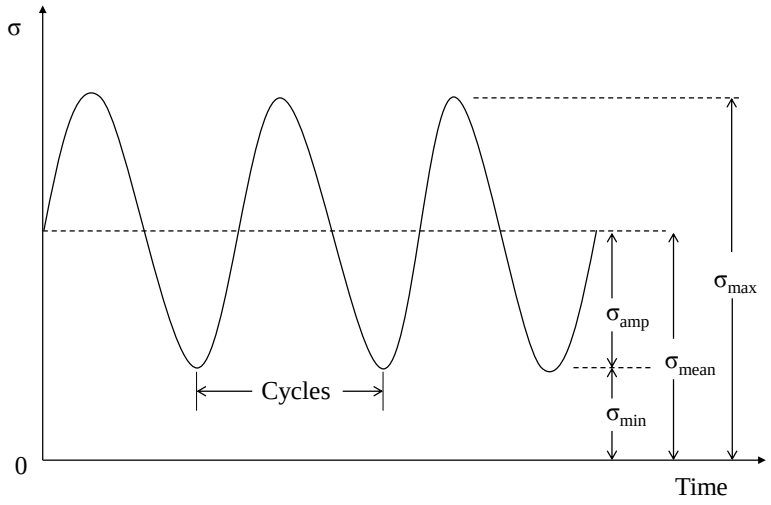

Figure 1.5. Nomenclature for constant stress amplitude loading.

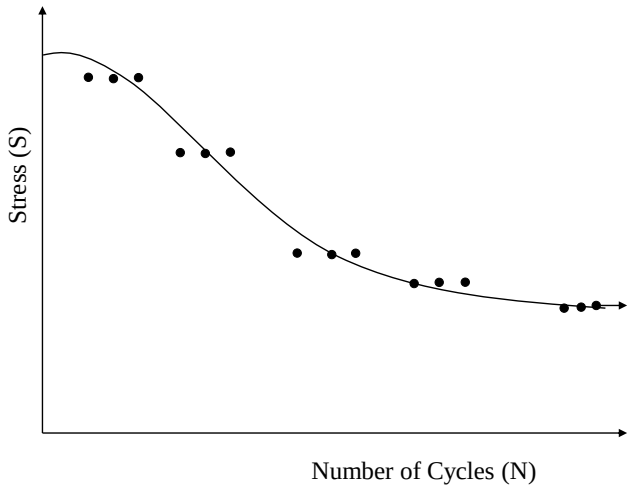

Figure 1.6. Typical S-N diagram.

In constant amplitude loading, many engineering materials show a plateau in S-N curve after 10^6 or 10^7 cycles. At this load (stress) level, the specimen is assumed to take infinite number of load cycles before failure. This load/stress is called threshold level or endurance limit (10^6 or 10^7 cycles). After this threshold level, the test is generally stopped and the corresponding results are represented by an arrow in S-N plot (Figure 1.6) indicating that material is not failed.

Under constant amplitude loading, the fatigue life of a material may change radically

when the applied minimum load or load amplitude is changed while maintaining the same maximum applied load. To overcome this problem, the load ratio, *R* is introduced which is defined by equation (1.3). The fatigue characterization of a new material is generally involved fatigue testing at different load ratios.

$$R = \frac{\sigma_{min}}{\sigma_{max}} \tag{1.3}$$

Kanny and Mahfuz [48] studied the flexural fatigue performance of PVC foam core sandwich composite for different foam core densities and developed a simple fatigue life expression for PVC foam core sandwich beam which is given by

$$N = C\Delta\sigma^{-m} \tag{1.4}$$

here, *N* is the number of cycles to failure, *C* is a material constant, $\Delta\sigma$ is the stress range (σ_{max} - σ_{min}), and m is the slope. By taking logarithms on both sides of equation (1.4) and rearranging, the final equation for straight line on the S-N curve was defined as

$$log\Delta\sigma = -\frac{1}{m} logN + C^{*} \tag{1.5}$$

where, *1/m* is the slope of the straight line S-N curve in a log-log plot and C^{*}= *(logC)/m* is the material constant.

Burman and Zenkert [49, 50] studied the shear fatigue performance of Divinycell H100 and Rohacell WF51 foam core sandwich beam for transverse loading condition using damaged and undamaged specimens. They proposed a simple fatigue life expression based on weibull function of S-N data. The expression is based on two fitting parameter weibull function as

$$\tau(N) = \tau_{th} + (\hat{\tau} - \tau_{th}) e^{-\log\left(\frac{N}{a}\right)^{b}} \tag{1.6}$$

here, τ is the shear stress in the beam for given number of load cycles to failure, τ_{th} is the fatigue threshold (or endurance limit),$\hat{\tau}$ is the static ultimate shear stress, N is the number of cycles to failure, and *a* and *b* are the curve fitting parameters. In the experimental studies of fatigue, τ_{th} can

be determined by setting a limit on the number of load cycles and monitoring the damage. Their study showed a reasonable agreement between experimental and analytical results.

Later, Burman and Zenkert [51, 52] studied the fatigue performance of Divinycell and Rohacell foam of different densities under tension, compression and shear loadings. They showed that fatigue stress-life data can be represented by Basquin's law type relation which was defined as

$$\Delta\sigma = B(N)^{-1/\beta} \tag{1.7}$$

where $\Delta\sigma$ is the stress range, N is the number of cycles to failure, B is the fitting constant and $-1/\beta$ is the slope of the relation.

1.3.2 Strength degradation model. The life prediction model based on strength degradation approach describes the degradation of initial strength during fatigue life. This method is also called as wear-out model. Sendeckyz [53] used this approach to predict the fatigue life of fiber reinforced polymer matrix composite. This model requires only two parameters to describe the strength degradation in fatigue loading. One parameter represents the strength degradation and the other a relative fatigue life. Sendeckyz's life prediction model is summarized by the equations (1.8) to (1.13), respectively.

In this model, the probability distribution of static strength σ_s is described by a two-parameter weibull distribution:

$$P(\sigma_s) = exp\left[-\left(\frac{\sigma_s}{\beta}\right)\right]^{\alpha} \tag{1.8}$$

where β is a scale parameter and α is a shape parameter.

In constant amplitude fatigue at a maximum fatigue stress σ_a, the residual strength σ_r after n cycles is related to the initial static strength σ_s, by a deterministic equation, a wear-out model:

$$\sigma_s = \sigma_a\left[\left(\frac{\sigma_r}{\sigma_a}\right)^{1/s} + (n-1)f\right]^{s} \tag{1.9}$$

where, *s* and *f* are experimental parameters. The parameter *s* is the absolute value of the asymptotic slope at long life on a log-log plot of S-N curve [53]. Therefore, *s* can describe the strength degradation rate. Fatigue failure occurs when the residual strength decreases to the maximum fatigue stress i.e. when $\sigma_a = \sigma_r$. Thus the relationship between the static strength (σ_s) and fatigue stress (σ_a) is given by

$$\sigma_s = \sigma_a[1 + (n-1)f]^s \tag{1.10}$$

The resulting fatigue life distribution is then

$$P(n) = exp\left\{-\left\{\frac{\sigma_a[1+(n-1)f]^s}{\beta}\right\}^{\alpha}\right\} \tag{1.11}$$

The residual strength distribution after *n* cycles also follows from equation (1.9) and (1.10) as

$$P\left(\frac{\sigma_r}{n}\right) = exp\left\{-\left[\left(\frac{\sigma_r}{\beta}\right)^{\frac{1}{s}} + \left(\frac{\sigma_a}{\beta}\right)^{\frac{1}{s}} f(n-1)\right]^{\alpha s} + \left(\frac{\sigma_s}{\beta}\right)^{\alpha}\right\} \tag{1.12}$$

Experimentally, the static strength distribution is determined from the ranked static strength data using the median rank as

$$p(\sigma_{si}) = 1 - \frac{i-0.3}{M+0.4} \tag{1.13}$$

where σ_{si} is the *i*th strength and *M* is the total number of data.

Later, Dai and Hahn [54] extended Sendeckyz's [53] wear-out model to develop model for fatigue life and core fatigue failure of sandwich beams. They developed for PVC core material and applied to Balsa core.

1.3.3 Stiffness reduction model. Many researchers investigated the robustness of stiffness reduction approach in predicting the fatigue life for both laminate and sandwich composites. This is because residual stiffness can be monitored nondestructively and can be related to residual strength and fatigue life of the specimen. Wu et al. [55], Philippidis and Vassilopoulos [56] and Whitworth [57] used the stiffness reduction approach to predict the

fatigue life of laminate composite and suggested that stiffness reduction approach is an accurate way to predict the fatigue life of laminate composite. Judawisastra et al. [58] used the stiffness reduction approach in predicting the fatigue life of polyurethane (PUR) foam core sandwich composite. Clark et al. [36] proposed a model based on stiffness reduction approach for life prediction of foam core sandwich composite made of Airex C70.130 foam core and hybrid glass/kevlar/epoxy face sheet for both single step and multi-step fatigue loading conditions.

The term fatigue modulus or stiffness is defined as the ratio between the applied stress and the resulting strain at a given number of cycles. This modulus is a function of loading cycles *n* and applied stress level $r = \tau_a/\tau_u$ where τ_a is the applied fatigue stress and τ_u is the ultimate static stress. According to the model of Clark et al., the rate of decrease of fatigue modulus from an initial static value can be expressed as:

$$G_f(n) = G_o \quad \text{for } n \ll n_{if}$$

$$G_f(n) = G_o - Ae^{(n-n_{if})c} \text{ for } n \geq n_{if} \tag{1.14}$$

where, $G_f(n)$ is the transient fatigue modulus, G_o is the instantaneous static modulus, A and C are the material constants, n is the number of fatigue cycles imposed and n_{if} is the number of cycles to initial damage. $G_f(n)$ is the ratio of applied fatigue shear stress to the fatigue component of the resultant shear strain ($G_f(n) = \frac{\tau_a}{\gamma_f(n)}$). They derived a non-linear S-N equation by rearranging the equation (1.14) and the non-linear S-N equation becomes

$$N_f = n_{if} + \frac{ln[B(1-r)]}{C} \tag{1.15}$$

where $B = G_o/A$ can be used to predict the number of cycles at failure for different applied stress levels.

El Mahi et al. [59] studied the flexural fatigue behavior of PVC foam core and E-

glass/epoxy face sheet sandwich composite. In this study, they used the life prediction model of Clark et al. [36] and compared the results with the experimental data. Fatigue tests were conducted both in displacement control and load control and two different equations were developed for load and displacement control modes. In the displacement control, d_{mean} is the static mean displacement (midspan deflection in the three-point bend test) and d_{am} is the amplitude of the applied sinusoidal waveform. During the tests the decrease in load (stiffness) according to the number of cycles is recorded. Figure 1.8 represents the typical load reduction (F_{max}/F_{omax}) as function of number of cycles for a mean displacement $d_{\mathrm{mean}} = 0.5d_{\mathrm{u}}$, where d_{u} is the value of the failure displacement in the static tests for an amplitude $d_{\mathrm{am}} = 1.75$mm. Here, F_{max} is the maximum applied load and F_{omax} is the maximum load at the first cycle. The result shows that the failure of the specimen proceeds in three stages: (i) an initial stage characterized by rapid load reduction; (ii) an intermediate stage in which an additional load reduction occurred at a much slower rate; and (iii) a final stage, in which rapid load reduction is observed as specimen failure is approached. Load reduction is related to the decrease of the flexural fatigue modulus. The load reduction can be expressed as a logarithmic function as

$$\frac{F_{max}}{F_{omax}} = 1 - A_d ln(n) \tag{1.16}$$

where F_{omax} is the maximum applied load in the first cycle and A_d depends on the applied displacement levels and the material properties. A_d can be described according to different load levels r by a power function as

$$A_d = a_{od} \times r^{a_d} \tag{1.17}$$

where a_{od} and a_d are the parameters that depends on the material properties and the loading conditions. The load expression according to the number of cycles and the applied displacement level thus becomes:

$$\frac{F_{max}}{F_{omax}} = 1 - a_{od} r^{a_d} ln(n) \tag{1.18}$$

The parameters a_{od} and a_d can be determined experimentally.

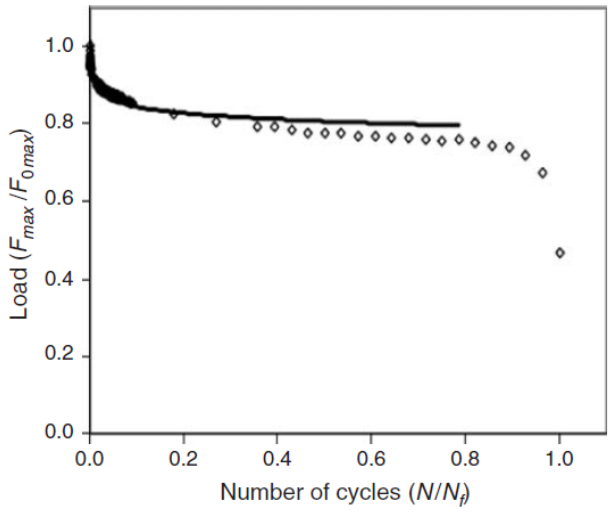

Figure 1.7. Normalized load Vs normalized number of cycles in sandwich composites under displacement control fatigue with logarithmic fit [59].

This load or stiffness reduction approach was found to be valid for only the first two stages of failures namely, initial damage and intermediate stages. Similarly Degrieck and van Paepegem [60] also used stiffness reduction approach and found that the method is not always valid third stage of failure (final failure). Thus the stiffness reduction model is not valid up to complete failure. The failure condition for predicting the fatigue life can be predefined by a certain percentage of stiffness reduction generally referred to as $N\alpha$ where α is the percentage of load reduction. According to the study of El Mahi et al., the expression for predicting the fatigue life in displacement control corresponding to a load reduction of $\alpha\%$ can be derived from the equation (1.18) as

$$N_{d\alpha} = exp\left(\frac{1-\beta}{a_{od} \times r^{a_d}}\right) \tag{1.19}$$

where $\beta = 1 - \frac{\alpha}{100}$

Similarly, in the case of fatigue test with load control, the critical number of cycles $N_{F\alpha}$ corresponding to a displacement increase of $\alpha\%$ is derived as

$$N_{F\alpha} = -\frac{1}{C_{oF} r^{c_F}} ln(\beta) \tag{1.20}$$

A limitation of this concept is that it cannot be used for displacement level r_d and load level r_F near the unity, where the failure occurs very rapidly and specimen fracture before significant reduction in load or increase in displacement.

1.3.4 Cumulative damage model for variable amplitude loading. Several researchers attempted to study the fatigue behavior of laminated composite based on cumulative damage model for example [53, 61]. However, limited work was published in the literature on the use of cumulative damage model for studying the fatigue behavior of sandwich composites. Clark et al. [36] studied the use of cumulative damage model for sandwich composite based on stiffness reduction approach for two-step loading. In this experimental investigation, the core material used was Airex C70.130 and the face sheet was made of hybrid glass/Kevlar/epoxy. A general damage model defining the fatigue damage parameter, *D* was defined assuming constant frequency and environmental conditions. Fatigue damage, *D* accumulates from an initial damage state zero at zero cycles to unity at final failure.

For constant amplitude loading

$$D = 0 \ @ \ n = 0,$$
$$D = 1 \ @ \ n = N_f, \tag{1.21}$$

For a sequence of 'm' loadings:

$$D = 0 \ @ \ n = 0,$$
$$D = \sum_{i=1}^{m} \Delta D_i = 1 \ @ \ n = N_f, \tag{1.22}$$

where D_i is the damage experienced at load level i, n is the number of cycles, N_f is the number of

cycles to failure. The total damage is the summation of all the damage components at each load Level. Thus for two-step loading, the residual life of a beam can be determined from the residual damage, *Dr* which is schematically presented in Figure 1.9.If N_1 and N_2 are the expected lives under the first and second loads, respectively, then the remaining damage can be expressed as

$$D_r = 1 - D_{12} \tag{1.23}$$

where D_{12} is the level of damage experienced under the first stress level and equated to an amount of damage at the start of loading at the second stress level. The remaining life is therefore the number of cycles to failure under second stress level N_2, minus the number of cycles under the second load that equates to the already damage level D_{12} under the first load.

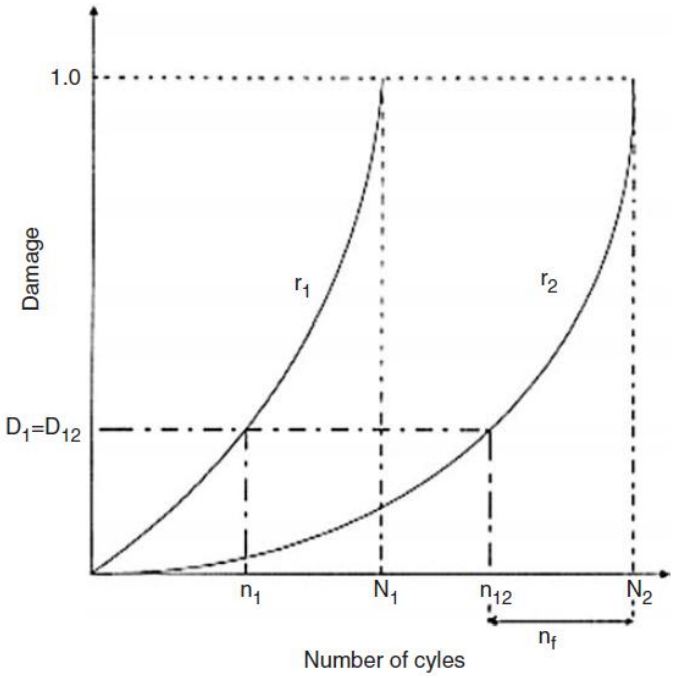

Figure 1.8. Schematic illustration of determination of residual life: two-step loading [36].

Different forms of the cumulative damage parameter, *D*, can be chosen depending on the degree of linearity of the degradation response. Three different models were proposed. The first model is linear, based on 'number of cycles', the second model is based on changes of 'modulus' and the third model is based on changes of 'strain'. Damage is assumed to initiate when fatigue

damage is first observed, i.e., at $n=n_{if}$. At $n=N_f$, the damage is equal to unity. For the purpose of all cumulative damage models investigated, it was assumed that:

$$D(n) = 0, \text{ where } n \leq n_{if}$$

$$0 \leq D(n) \leq 1, \text{ where } n_{if} \leq n \leq N_f \quad (1.24)$$

Model 1: According to this model, the amount of damage at a given cyclic stress level is equal to the ratio of the number of cycles at a given stress level to the number of cycles required to cause fatigue failure at that stress level. In this case, the damage model occurs after the initiation of damage and can be expressed as:

$$D(n) = \frac{(n-n_{if})}{(N_f-n_{if})}, \text{ where } n \geq n_{if} \quad (1.25)$$

Model 2: The damage function was defined in terms of the fatigue modulus as:

$$D(n) = \frac{G_o-G_f(n)}{G_o-G_f(N_f)} \quad (1.26)$$

where $G_f(n)$ and G_o are defined as the transient fatigue modulus and instantaneous static modulus, respectively, and $G_f(N_f)$ is the fatigue modulus at failure. The relation between $G_f(n)$ and G_o is:

$$G_f(n) = G_o, \text{ where } n \leq n_{if},$$

$$G_f(n) = G_o - Ae^{(-n_{if})C}, \text{ where } n \leq n_{if}, \quad (1.27)$$

where A and C are material constants to be determined from experimental data. Using equation (1.27), equation (1.26) was modified as:

$$D(n) = \frac{e^{(n-n_{if})C}}{e^{(N_f-n_{if})C}} \text{ where } n \geq n_{if} \quad (1.28)$$

Model 3: In this case the damage function was defined in terms of shear strain as:

$$D(n) = \frac{\gamma(n)-\gamma(0)}{\gamma(N_f)-\gamma(0)} \quad (1.29)$$

Again following the equation (1.27) and stress-strain relationships, the damage function can be modified as:

$$D(n) = \left[\frac{r}{1-r}\right]\left[\frac{e^{(n-n_{if})c}}{B-e^{(n-n_{if})}}\right] \text{ where } n \geq n_{if} \quad (1.30)$$

where $B=G_o/A$.

In summary most of the core materials studied were polymeric foams (PVC, Airex, Divinycell, Rohacell) and Balsa and their properties are different from syntactic foams. Syntactic foams are brittle compare to the above cores. No failure model was reported for syntactic foam sandwich panels.

1.4 Fatigue Test Methods for Foam Cores and Sandwich Beam

Fatigue tests are divided into three different types: smooth specimen tests to obtain total fatigue life, pre-cracked specimen tests to obtain crack propagation data, and structural testing where the fatigue life of a specific application is verified. In determining the fatigue life of foam core materials in tension, compression, shear and flexural stress states using smooth specimens, either solid foam core or foam core sandwich beam specimens is used, and corresponding test methods are discussed below.

1.4.1 Compression-compression or tension-tension fatigue test methods. There are no well-defined test standards for compression-compression or tension-tension fatigue testing of foam core materials. The test standards used for the static properties may also be used for fatigue testing. The standard test method for static compressive properties of rigid cellular plastics is ASTM D621-10 [45] which is equivalent to ISO 844 [46], standard test method for flatwise static compressive properties of sandwich cores is ASTM C365-05 [45] and standard test method for static tensile and tensile adhesion properties of rigid cellular plastics is ASTM D1623-10 [46] which is also similar to test standard ASTM D638-10 (Standard test method for tensile properties

of plastics) [45]. All these tests standards mentioned above may be used only for compression-compression or tension-tension fatigue testing of foam core with some modification. None of them can be used for compression-tension or tension-compression fatigue testing i.e. for $R<0$.

1.4.2 Shear and flexural fatigue test methods. Block shear test method ASTM C273-07a [45] or four-point bending test method ASTM C393-06 [45] are the two methods commonly used to determine the static shear properties of foam core materials in sandwich constructions. The block shear test procedure may also be used for fatigue tests following ASTM C394-00 [45]. However, the major drawback of block shear test method is that the specimen geometry creates stress concentrations at the corners of the core material which cause premature crack initiation and failure in both static and fatigue loading conditions. The four-point bend test method, ASTM C393-06 is an alternative effective test method in investigating the shear strength and failure modes of sandwich beams. This test method is also successfully used to investigate the shear fatigue life and fatigue failure modes of foam core sandwich beams **[**48-51, 74, 75]. Three-point bending test following ASTM C393-06 is also used to investigate the flexural fatigue performance of foam core sandwich beam [48, 71-73].

1.5 Literature Review

A literature on fatigue characterization of of polymeric and aluminum (Al) alloy foams and foam core sandwich composite specimen is presented here. The type of loading included compression-compression, shear and bending. Types of foams are PVC foams, open cell Duocel and closed cell Alporas Al foams, and balsa. Very little fatigue study on syntactic foam has been reported in open literature and is present last.

1.5.1 Compression-compression fatigue. Zenkert and Burman [51, 62] studied the compression-compression fatigue of closed cell Divinycell H-grade (H60, H100 and H200) and

Rohacell F-grade (WF51, WF110 and WF200) foams. In their study, they reported that compression fatigue failure was by crush band formation and propagation in the thickness direction resulting in cell wall compaction. This crush band formation was reflected by a sudden drop in displacement in load control fatigue test. The stress-life data can be represented by a Basquin's law and the slopes of the equation depends on the density of the material. Harte et al. [63] studied the compression-compression fatigue performance of an open cell Duocel and closed cell Alporas Al foam. Their study concluded that the typical failure mode is by progressive shortening of the specimen by crush band formation. Zhou and Soboyejo [64] studied the macro/micro scale fatigue mechanisms and the effect of heat treatment on Duocel open cell Al foams. The foams were tested as fabricated (F), annealed (O) and T6-strengthened conditions. From their study, it can be concluded that fatigue damage is associated with the nucleation of surface crack and growth within the individual struts followed by formation of macroscopic deformation bands which causes abrupt strain jumps. Heat treatment affected the macro-scale fatigue behavior. The abrupt strain jump leads to the formation of heterogeneous deformation band in the as-fabricated and T6-strengthened foams whereas for annealed foam, the deformation band was relatively homogeneous. Besides, annealed foams exhibited better fatigue strength compared to the T6-strengthened and the as-fabricated foams. Sugimura et al. [65] studied the compression fatigue behavior of closed cell Alporas aluminum foam. In their study, they reported that typical failure mode of the foam is by the formation of deformation bands. Each band densifies with a thickness equal to cell the size. The bands originate from plastically buckled membranes preferentially at the largest cells in the medium. This deformation band is governed by an abrupt increase in strain. Hakamada et al. [66] studied the cyclic compression fatigue behavior of porous Al fabricated by spacer method and compared them with those of

conventionally fabricated porous Al (Alporas). In this study, they didn't observe any distinct strain jump for porous Al produced by the spacer method. The strain jump, which was due to localization deformation, was observed in Alporas Al. They suggested that the absence of the distinct strain jump under cyclic compression for the porous Al produced by the spacer method is due to the uniform cell structure. Kolluri et al. [67] studied the cyclic compression fatigue behavior of closed-cell Al foam both with and without lateral constraint. Their study showed that while the early stages of strain accumulation due to fatigue loading are independent of constraint, the rapid strain accumulation stage behaviors are sensitive to the constraint. In both cases, no fatigue effects (strain accumulation) were observed when the maximum stress of the fatigue cycle was 60% of the quasi-static plastic strength of the foam. Stress-life diagrams, constructed with two different critical strain accumulation failure criteria (4 and 10%), show a marginal improvement of fatigue life under constraint when failure life is defined as 10%. All the compression fatigue studies discussed above are related to polymer and metallic foams and no compression fatigue studies were found in open literature for syntactic foams.

1.5.2 Shear fatigue. Zenkert and Burman [51, 52] studied the shear fatigue of Divinycell H100 and Rohacell (WF51, WF110 and WF200) polymer foams of different densities using composite face sheet sandwich beam specimens using four-point bending. Their study showed that cores fail by shear by a formation of crack at angle ranging between 45^{o} and 70^{o} with the face sheet [51]. They also observed that the face sheet tensile failure at low stress levels [52]. Thomson et al. [69] studied the effect of core and face sheet debond on shear fatigue life of PVC sandwich beams. They established a critical crack size below which the crack has no effect on the fatigue life of the beam. Harte et al. [70] studied fatigue strength of a closed cell aluminum alloy foam core sandwich beams of different span to depth ratios and established a design map to

display fatigue strength and failure modes as a function of specimen geometry. All the shear fatigue studies discussed above are related to polymer and metallic foams and no shear fatigue studies were found in open literature for syntactic foams.

1.5.3 Flexural fatigue. Dai and Hahn [71] studied the flexural fatigue properties of balsa wood for short and long beam specimens. Their study concluded that short beam failed by core shear as expected, forming large crack started at the center of the core and propagated into the compression and tension side. For a long beam, the first damage initiated in the face sheet tension laminate by ply cracking, fiber breaks, and debonding followed by crushing of the core on the compression side of the beam. Kanny and Mahfuz [48] studied the influence of loading frequency on flexural fatigue behavior of PVC foam core sandwich composite. Fatigue test was performed on PVC foam core sandwich beams at frequencies of 3 and 15 Hz. They found that fatigue life increased with increase in frequency. In both cases, fatigue failure was dominated by 45^{o} core shear crack. The crack path and crack propagation rates varied with loading frequency. Kulkarni et al. [72] studied the flexural fatigue characteristics of sandwich structures with polymer (PVC) foam core using sandwich beam. Their study concluded that sandwich specimen first failed by debonding between skin and core and finally core shear failure by forming a 45^{o} crack with the neutal axis. They developed a fatigue model based on fatigue damage of core material and correlated it with the experimental data. Kanny et al. [73] studied the flexural fatigue behavior of cross-linked PVC foam cores of three different densities (H130, R260 and R300). Their study concluded that foam core failed by first forming an 80-85^{o} angle of crack on tension side of the beam and this crack quickly propagated towards the compression side of the beam causing total collapse of the specimen. Kanny et al. [74] also studied the effect of elevated temperature on fatigue behavior of PVC foam core sandwich composite. In this study, they

conducted test at three different temperatures (room temperature, 40^{o}C and 80^{o}C) and found that, fatigue life decreased with increased temperature and there was a slight change in mechanism of core failure. Shenoi et al. [75] studied the flexural fatigue behavior of polymer composite sandwich beams using ten-point loading configuration for three different polymer foams (AIREX R63.80, AIREX R90.200 and AIREX C70.130) using frequency of 0.33, 0.50 and 0.91 Hz and load ratio of R=0. Their study concluded that AIREX R63.80 sandwich composite failed by core shear near the supports whereas AIREX R90.200 and AIREX C70.130 sandwich composite first failed by face-sheet tension failure on tension side of the specimen, followed by catastrophic failure of the core. Based on literature review and their experimental results, they reported that the effects of frequency do not have much significance in the range of 0-1.0 Hz but may have some effect at about 5 Hz frequency, which may cause decrease in fatigue properties. Based on available data in literature they also reported that stress ratio R has a great influence on fatigue life of sandwich beams. The loading configuration (three-point bending or four-point bending) and waveform shape (sinusoidal, slamming and square wave) type does not seem to greatly influence the form of the S-N curve. Freeman et al. [76] studied the fatigue behavior of polyurethane foam core sandwich composite with two different densities (0.164 g/cc and 0.106 g/cc) of core material using four-point bend specimen that was already impact tested. Their study showed that fatigue failure mode depends on face sheet thickness. For low density foam with thick (four layers) and thin (two layers) face sheets, failure mode was by core shear initiated between core and face sheet interface under one of load points, followed by propagation of shear cracks to the top and bottom face sheets and finally leading to specimen failure. Impact damage had no influence on fatigue failure mode. However, for higher density foam with thin face sheet, fatigue failure mode was changed from core shear to core bending failure. Bending failure

initiated at the damage created in the core by the impact and slowly propagated from the center until it reached both ends of the sample. Zenkert and Burman [49, 50] studied fatigue properties of Divinycell H100 and Rohacell WF51 using four-point bending. In their study, they used both undamaged and damaged specimen and concluded that both undamaged and damaged specimen failed by core shear forming a 45^{o} crack with the neutral axis. In case of undamaged specimens, failure initiation was from neutral axis. On the other hand for the damaged specimen, the damage was initiated from corner of the butt joints and tip of the interfacial Teflon insert. The only paper that is related to syntactic foam was by Ferreira et al. [77]. They studied the effect of volume percent of microbubbles and reinforcing fibers (glass or carbon) on flexural fatigue behavior of syntactic foams. They found that fatigue strength increased by 30% by the addition of a small (<1%) percentage of fibers (glass or carbon) as a reinforcing material. However at higher filler content, the fatigue strength decreased and fatigue degradation rate increased.

1.6 Challenges and Gaps

As explained in previous sections most of the fatigue characterization in literature was on PVC, aluminum foam and balsa core sandwich panels subjected to bending loads. Only one reference [77] related to syntactic foam was found in the literature that too was for bending load. No results are reported for compression and shear fatigue loading. In addition, Eco-Core is a low binder content with sphere to sphere contact foam and no data was found for such material in the literature. Therefore, a comprehensive fatigue characterization of Eco-Core under three primary types of fatigue loading: compression, shear and flexural are under taken. These stress states are experienced by Eco-Core when used alone or as a core material in sandwich panels or structures. Types of failures and associated lives are measured and documented. Based on the fatigue data, simple stress-life equations are developed.

1.7 Test Concept and Methodology

Eco-Core material is envisioned to be used in compression, shear, and bending bearing members. Although one can think of direct tension fatigue testing, because of its brittleness the material is not suitable for such applications. Therefore, only compression, shear, and flexure fatigue testing are considered. The compression fatigue was performed directly on the Eco-Core material whereas the shear and flexure tests were performed on sandwich specimen to avoid premature failure under load points by indentation and rubbing of loading rollers on the material. The Eco-Core is fabricated as a rectangular panel of size 355.6x355.6 mm by 25.4 mm thick. The cylindrical compression specimen was extracted by 27.9 mm diameter core cutter (See Figure 1.9b). A separate sandwich panel (Figure 1.9a) with FGI 1854 glass fiber/vinyl ester composite laminate face sheet (thickness of 1/18 of core thickness) was fabricated by adhesively bonding composite face sheets to top and bottom surface of Eco-Core panel. A sketch of the sandwich panel is shown in Figure 1.9a.

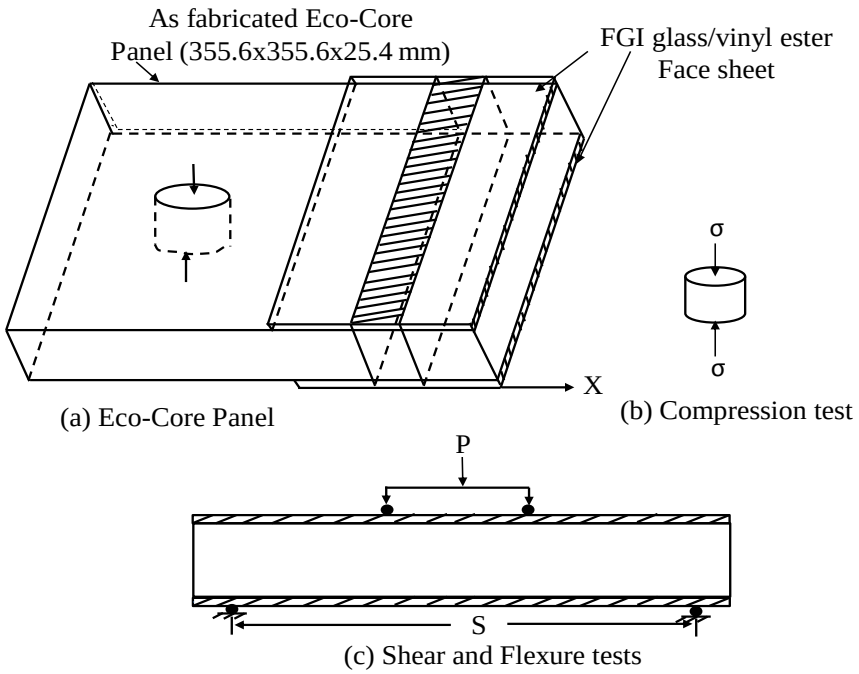

Figure 1.9. Eco-Core panel and test specimen configuration and loading.

Four point loading (Figure 1.9c) was used for shear and flexure testing with different span-thickness ratios. Quarter-point loading was used for shear and one-third load points was used for flexure testing. Chapter 3 and 4 describe more details of the study.

1.8 Objectives of the Research

The overall objective of this research is to establish fatigue performance of "Eco-Core" material under three different fatigue stress states, namely compression, shear and flexure. Then identify failure modes for onset, propagation, and final failure and then the associated lives. Finally, establish stress-life equation for the three stress states and associated failure modes. Cylindrical Eco-Core samples are used for compression-compression fatigue and Eco-Core sandwich beam is used for shear and flexure test. The sandwich face sheet is made of FGI glass/vinyl ester composite laminate. Each of the three load conditions is presented in a separate chapter.

1.9 Scope of the Dissertation

The dissertation consists of five chapters. In Chapter 1, an overview of syntactic foam, Eco-Core, fatigue test parameters, fatigue life models for sandwich structures and a literature review on fatigue characterization of foam core sandwich composites are presented. Chapter 2 presents the Eco-Core processing and its compression static and fatigue characterization. Compression static characterization includes validating compressive strength, its failure modes and failure mechanisms. Compression fatigue characterization includes two values of R, endurance limit and identification of failure modes and mechanisms. Chapter 3 presents the design of Eco-Core sandwich specimen for shear loading, fabrication of Eco-Core sandwich panel and specimen, and static shear and fatigue shear tests. Characterization includes verifying shear strength, establishing endurance strength and studying shear failure modes and

mechanisms for both static and cyclic loadings. Then an explanation of failure modes from the stress states in sandwich core and face sheet interface is under taken. Chapter 4 presents the design of Eco-Core sandwich specimen for flexure, fabrication of Eco-Core sandwich panel and specimen, and static flexure and fatigue flexure tests. Characterization includes verifying flexural strength, establishing endurance strength and studying flexural failure modes and mechanisms for both static and cyclic loading. Then the explanation of failure modes from the stress states in sandwich core and face sheet interface is under taken. Finally, the concluding remarks and recommendations for future work are presented in chapter 5.

CHAPTER 2

Compression-Compression Fatigue Characterization

2.1 Introduction

In this chapter, Compression-Compression fatigue performance of Eco-Core is described. The static test was conducted following ASTM C365 with some modification and the same test setup was used for fatigue test. For both static and fatigue tests, cylindrical specimens was used. The specimen diameter was 28 mm (1.1 in) and height was 25 mm (1 in). The specimen densities were within the range of 0.53 g/cc to 0.54 g/cc, a less than 2% variation. Compression fatigue test was conducted using sinusoidal loading frequency of 2 Hz and stress ratio R of 10 and 5. Tests were conducted at different stress levels (σ_{min}/σ_c) and a PC based data acquisition system stored fatigue load, stroke displacement and time. This data was converted to compliance and number of cycles and created compliance versus number of cycles curves. Fatigue life was determined for 2%, 5% and 7% compliance change failure criteria. This data was used to establish stress-number of cycles (S-N) relation. The macro-scale fatigue failure and associated mechanism was investigated by analyzing the failure images taken from beginning to end of the test. These images were taken by a digital camera. This work was published in open literature [79].

2.2 Eco-Core Materials

A class of fly ash known as Cenosphere grade XL 150 supplied by Sphere Services Inc. and phenol-formaldehyde resole binder resin, Durite SC 1008 supplied by Mektech Composities Inc. were used to formulate Eco-Core [11]. The resin was diluted with alcohol at a weight ratio of 10:1. Then fly ash was mixed with resin solution at a weight ratio of 5:1, where 5 and 1 represent the weight ratio of fly ash and solid resin, respectively. The mixture was mixed in a

low-shear planetary motion mixer so that fly ash was uniformly coated with resin. The fly ash mixture was then charged into a compression mold of dimensions 356 x 356 x 25 mm in a steel frame, compressed by a laboratory hot press that was preheated to a temperature of 82^{o}C. The preheated panel was then cured at 163^{o}C for 30 minutes at 1.55 MPa (224 psi) pressure. The panel was finally post cured in a convection oven at 163^{o}C for 4-1/2 hours and all the steps in fabricating Eco-Core panel are shown in Figure 2.1.

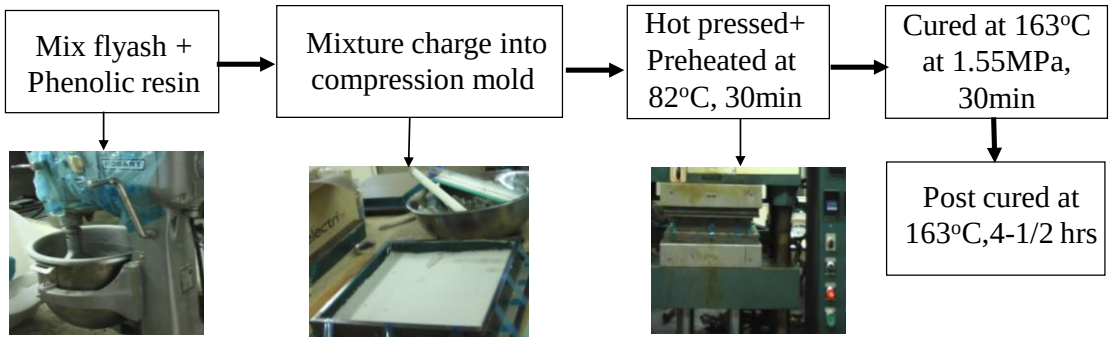

Figure 2.1. Steps in fabricating Eco-Core panel.

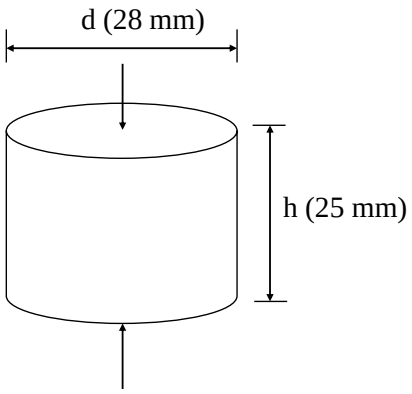

Figure 2.2. Compression test specimen.

Two panels (panel 1 and 2) were fabricated following the steps stated in the previous section. These panels were used to extract cylindrical specimens 28 mm (1.1 in) diameter and 25 mm (1 in) height (Figure 2.2) using a core cutter of internal diameter 28.6 mm (1-1/8 in). The specimen dimensions and bulk density were measured and recorded. Specimens from the panels

1 and 2 were fatigue tested at two values of stress ratio R=10 and 5. Note that stress ratio values are not conventional to what is commonly used, because of the negative sign was used for compression stress. R= $\sigma_{min}/\sigma_{max}$ is 10 and 5 in case of compression fatigue while it is 0.1 and 0.2 on an absolute value basis. The average bulk densities of the specimens for the panels 1 and 2 were 0.536 g/cc and 0.532 g/cc, respectively. Specimens within ± 0.5% of the average value of the density were selected for testing. The specimen layout for panel 1 is shown in Figure 2.3. The way of selecting specimens from panel-1 for static and fatigue test are shown and Figure 2.4 and similar procedure was applied in case of selecting specimen from panel-2, which are attached in Appendix B.1. In figure 2.4a, specimens are numbered according to specimen number in specimen layout (Figure 2.3) whereas in figure 2.4b, specimens are numbered according to ascending order of specimen density. More clearly, specimen number was 1 for the specimen of lowest density and specimen number was 64 for the specimen of highest density. Between these two ranges, specimen number was selected based on the position of the specimen density. Selected specimens for static and fatigue test are listed in Tables 2.1, 2.2 and 2.3 for R=10 and 5, respectively.

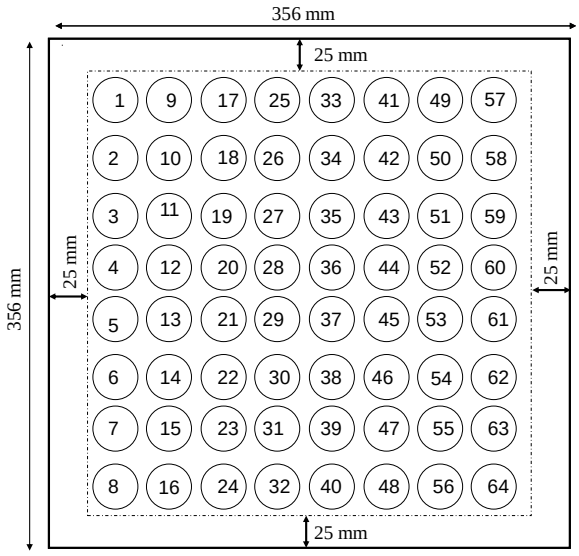

Figure 2.3. Specimen layout.

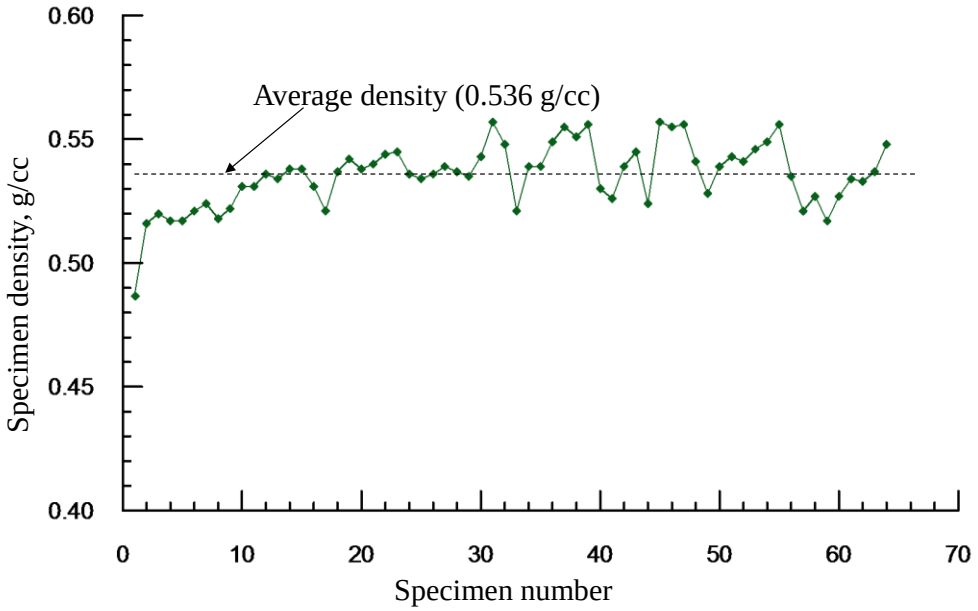

(a)

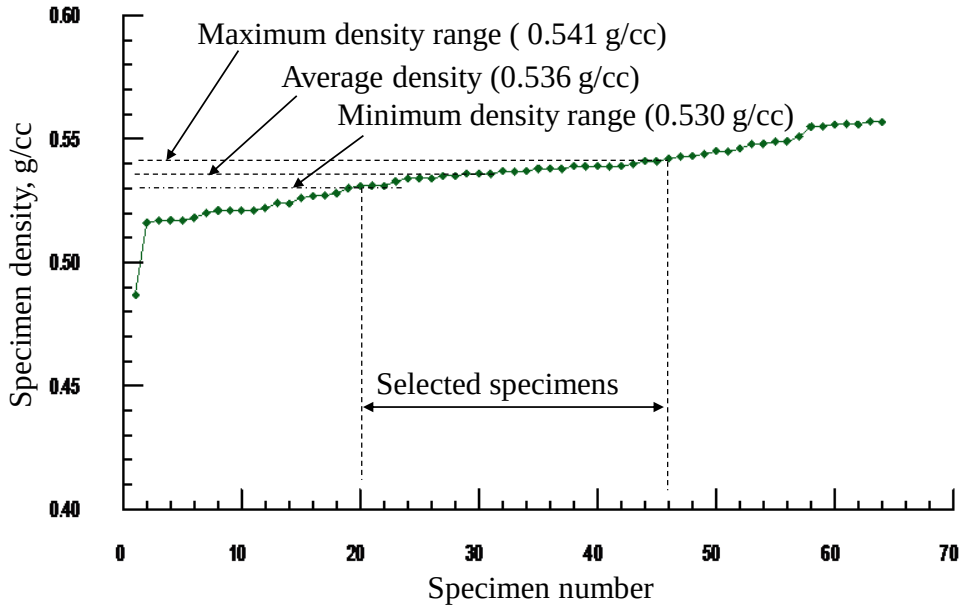

(b)

Figure 2.4. Specimen selection process from panel 1: (a) Specimens numbered according to specimen number in specimen layout; (b) Specimen numbered according to ascending order of specimen density.

Scanning electron microscope (SEM) image of Eco-Core specimen is shown in Figure

2.5. Notice several features: size of microspheres about 20-75µm; a thin layer of resin coating on microbubbles; sphere to sphere contact with open interstitial region. The broken microbubbles are due to machining. The features represent the very low binder content of the material. Before performing the test, the top and bottom surface of each specimen was coated with graphite fine powder to reduce the friction between specimen and platen contact area.

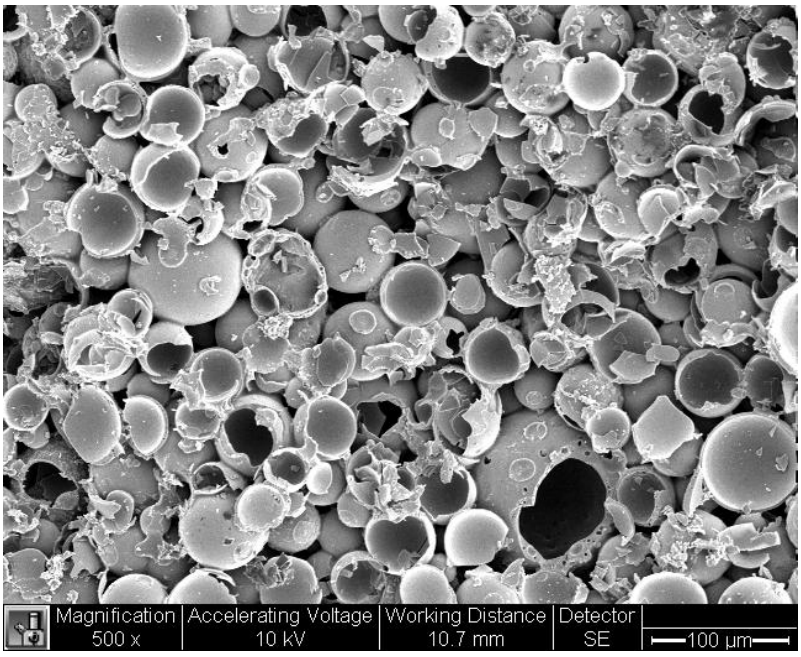

Figure 2.5. SEM image of Eco-Core.

2.3 Compression Static Test and Test Results

Compression static test was performed to measure compression strength and modulus, their variability and failure modes of Eco-Core. The static compression test was performed using an MTS servo-hydraulic test machine and the machine setup is shown in Figure 2.6. The specimen was compressed between two platens at a constant displacement rate of 1.27mm/min (0.05in/min) while load and displacement were recorded at every one-half second. The specimen deformation was continuously monitored by a high speed camera for post processing later. The load deformation was recorded until the specimen is completely compressed. Compression stress

and strain were calculated from load/cross sectional area and displacement/initial height, respectively.

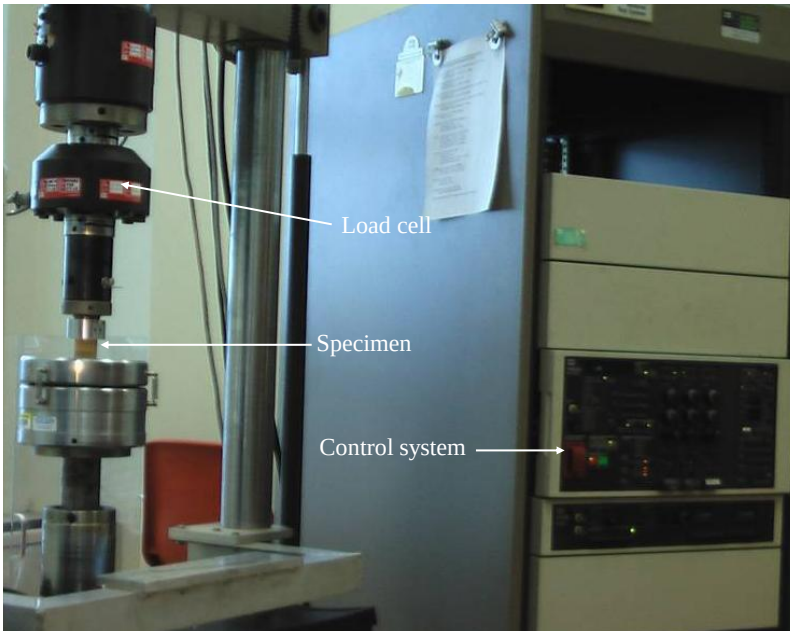

Figure 2.6. Machine setup for compression static and fatigue test.

Figure 2.7 shows compression stress-strain response for five Eco-Core samples for panel 1 and compression stress-strain response of the five Eco-Core samples is attached in Appendix B.2. The stress-strain response is almost linear till the maximum stress is reached. After that, stress suddenly drops, remains constant or both with increase in strain. Then stress gradually decreases with increase in strain and finally material crushes. The crushing strain in this type of unconfined compression could be as high as 30%, but only results upto about 10% strain is shown in Figure 2.7. Each of failure steps, respectively, represent the failure initiation by breakage of binder around the microbubble, which generally starts at the mid height or edge (top or bottom) of the specimen as a crush band, followed by failure progression in thickness direction and finally leading to ultimate failure. All these features were imaged by a high speed camera; only selected pictures are shown in Figure 2.8. Failure in the material first initiated at the

middle of the specimen due to bond breakage between the microbubbles causing a crush band, the crush band propagated in thickness direction, finally leading to axial (longitudinal) cracking of the specimen. A similar failure mode was also observed by Panduranga et al. [14, 78]. Maximum stress before failure onset was considered to be strength of the material. The average compressive strength (σ_c) was -18.9MPa (-2,743psi) with a standard deviation (STD) of 0.28MPa (41psi). Compression elastic modulus was calculated from the linear slope of stress-strain curve (Figure 2.7). The average modulus was 1.74GPa (253ksi) with a STD of 0.11 GPa (16ksi) for panel 1. Whereas for panel 2, σ_c was -20.3MPa (-2,945 psi) with a STD of 0.45 MPa (65psi) and average modulus of 1.55GPa (225ksi) with a STD of 0.01GPa (1.45ksi). The results for the two panels are consistent. Compressive strengths and moduli of tested specimen from panel 1 and 2 are listed in Table 2.1. By applying the statistical error mean, the average compression strength and modulus of Eco-Core is 19.6 ± 0.25 MPa and 1.65 ± 0.05 MPa, respectively.

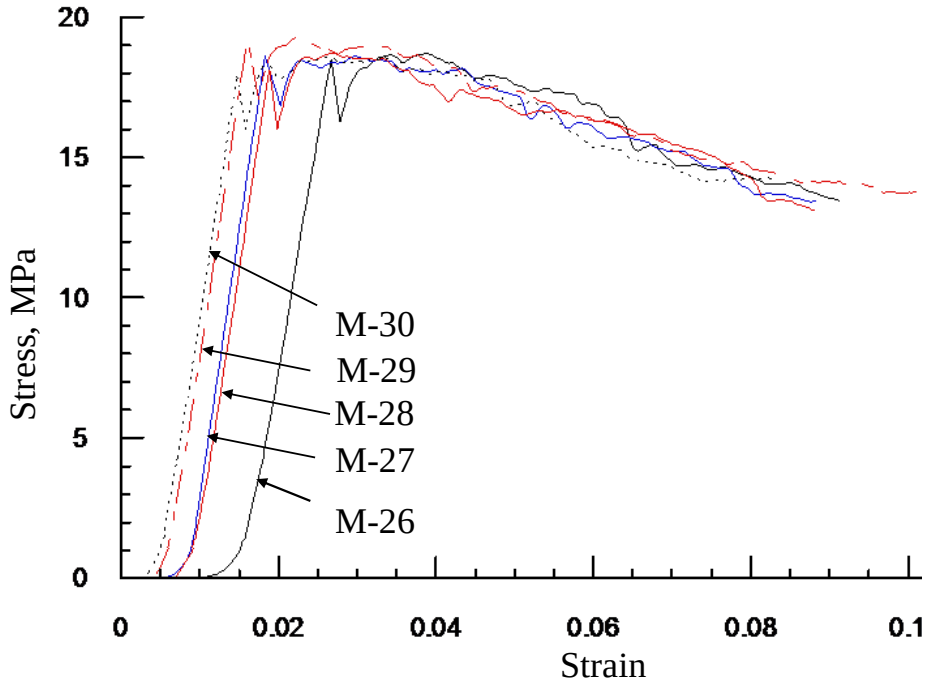

Figure 2.7. Static compression stress-strain responses of specimens (panel 1).

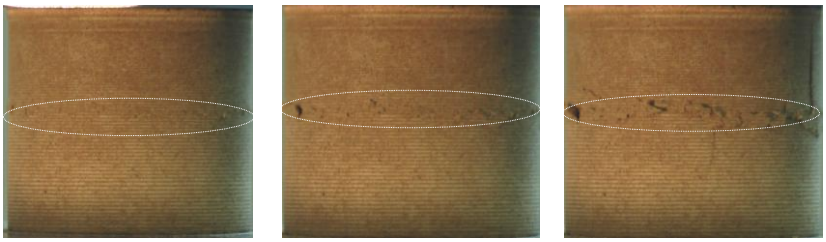

(a) Onset (b) Progression (c) Final failure

Figure 2.8. Onset, propagation and final failure images of static compression samples, panel 1.

Table 2.1

Test Specimen and Properties

Panel no	Specimen ID	Specimen Geometry		Specimen Density, g/cc	Compression		
		Diameter, mm	height, mm		Failure Load, N	Strength, MPa	Modulus, GPa
1	M-26	29.770	25.630	0.536	13,050	18.76	1.44
	M-27	29.850	25.630	0.539	13,295	19.02	1.87
	M-28	29.740	25.640	0.537	13,033	18.75	1.79
	M-29	29.810	25.620	0.535	12,993	18.62	1.76
	M-30	29.770	25.630	0.540	13,513	19.42	1.84
	Average					18.91	1.74
	STD					0.28	0.11
	SEM					0.13	0.05
2	M-13	29.172	26.416	0.529	13,135	19.65	1.55
	M-26	29.228	26.213	0.532	13,317	19.92	1.54
	M-38	29.158	26.060	0.537	13,936	20.87	1.55
	M-43	29.158	26.162	0.531	13,397	20.06	1.54
	M-47	29.102	26.060	0.533	13,664	20.54	1.56
	Average					20.30	1.55
	STD					0.45	0.11
	SEM					0.20	0.00

2.4 Fatigue Test

Compression-compression fatigue tests were conducted under a sinusoidal cyclic load of frequency 2Hz and two stress ratios of R = 10 and 5, respectively. Fatigue testing for R=10, used specimens from panel 1 and corresponding average strength (σ_c) used was -18.9MPa (-2,743psi).

For R=5, specimens from panel 2 were used with a corresponding average strength of 20.3MPa (2,945 psi). Typical compression cyclic load is shown in Figure 2.9. σ_{min} is the maximum compression or algebraically minimum stress. Similarly, σ_{max} is algebraically maximum stress or the minimum compression stress. Preliminary tests showed that for R=10, all the tested specimens for σ_{min}/σ_c= 0.6 exceeded 10^6 cycles and for R= 5, at σ_{min}/σ_c= 0.8 all tested specimen exceeded 10^6 cycles without failure. Therefore, the stress levels selected were above the limiting stress. The endurance limit for this class of materials needs to be 10^7-10^9 cycles depending on the application. However because of limitations of test time and equipment, the testing was limited to 10^6 cycles and this is used as the endurance limit. Six different stress levels (σ_{min}/σ_c) in the range of 0.6 to 0.9 for R = 10 and four different stress levels in the range of 0.8 to 0.95 for R = 5 were chosen. Tables 2.2 and 2.3 lists stress levels and number of replication of tests. The same static test setup was used for fatigue test (Figure 2.6). Three to four specimens were tested for each stress ratio. All the cyclic compression tests on specimens were performed in the thickness direction of the panel. Both load (P) and displacement (d) and numbers of load cycles (N) were collected using a PC based acquisition system. The load-displacements recorded were used to calculate compliance which is the ratio of change in displacements between the consecutive maximum and minimum loads and the loads difference. The fatigue life is defined as the number of cycles to failure. The failure is defined by the compliance change criteria, which is defined later. To investigate the macro-scale fatigue failure mechanisms, a digital camera was set up to record the deformation sequence. Since each fatigue test lasted for hours to days, images were taken only for selective intervals between the beginning and end of the test (unstable failure). The image sequences were then analyzed to understand the fatigue failure mechanism at the macro-scale.

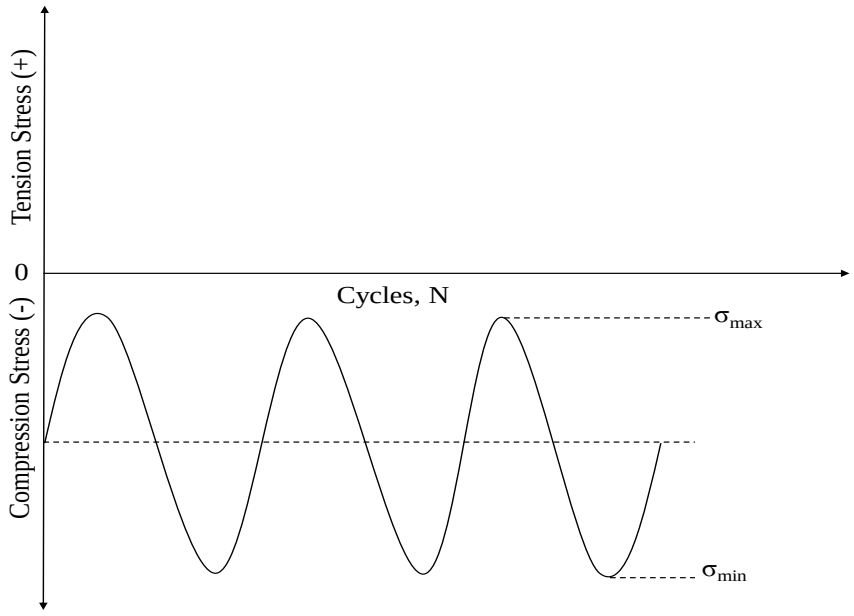

Figure 2.9. Compression-compression fatigue loading.

Table 2.2

Compression-Compression Fatigue Test Specimen and Loading for R=10, Panel 1(σ_c = -18.9 MPa)

Specimen ID	Density, g/cc	σ_{min}/σ_c	σ_{min}, MPa	Diameter,mm	P_{min}, N
M-14	0.538	0.90	-17.02	29.799	11,872
M-24	0.536			29.827	11,890
M-61	0.534			29.716	11,805
M-56	0.535			29.785	11,858
M-10	0.531	0.85	-16.08	29.785	11,205
M-15	0.538			29.799	11,213
M-18	0.537			29.840	11,245
M-52	0.541	0.80	-15.13	29.592	10,404
M-13	0.534			29.854	10,586
M-12	0.536			29.827	10,568
M-62	0.533	0.75	-14.18	29.716	9,835
M-16	0.531			29.785	9,883
M-48	0.540			29.564	9,719
M-50	0.539	0.70	-13.24	29.785	9,225
M-20	0.538			29.868	9,274
M-34	0.539			29.689	9,163
M-21	0.540	0.60	-11.35	29.840	7,935
M-25	0.534			29.564	7,788

Table 2.3

Compression-Compression Fatigue Test Specimen and Loading for R=5, Panel 2(σ_c = -20.3 MPa)

Specimen ID	Density, g/cc	σ_{min}/σ_c	σ_{min}, MPa	Diameter, mm	$P_{min,}$ N
M-46	0.533	0.95	-19.292	29.130	12,857
M-30	0.535			29.158	12,882
M-55	0.536			29.102	12,832
M-39	0.527	0.90	-18.279	29.116	12,170
M-31	0.528			29.172	12,217
M-19	0.539			29.102	12,158
M-52	0.531	0.85	-17.258	29.158	11,524
M-44	0.534			29.158	11,524
M-51	0.527			29.130	11,502
M-27	0.535	0.80	-16.245	29.172	10,858
M-45	0.533			29.144	10,837
M-11	0.526			29.172	10,858

2.5 Fatigue Test Results and Discussion

2.5.1 Failure criteria and associated failure lives. Failure is a subjective term; to define failure specimen compliance is used. Typical compliance versus number of cycles of a fatigue test is shown in Figure 2.10. The response can be divided into three zones: Initial or onset where the specimen shows onset of damage; slow propagation of damage where the material densifies in thickness direction yet specimen has not lost its strength and fast damage progression or ultimate failure (material crushed) that is leading to solidification of the sample. The onset can also be treated as first breakage of bond between the microbubbles. The three different failures are defined as onset, propagation and final failure. They are categorized as 2%, 5%, and 7% respectively. The number of load cycles required for 2% compliance change is defined as onset life, required for 5% compliance change is defined as propagation life and required for 7% compliance change is defined as the total life. Selection of these compliance limits was based on the profile of the compliance versus number of load cycles.

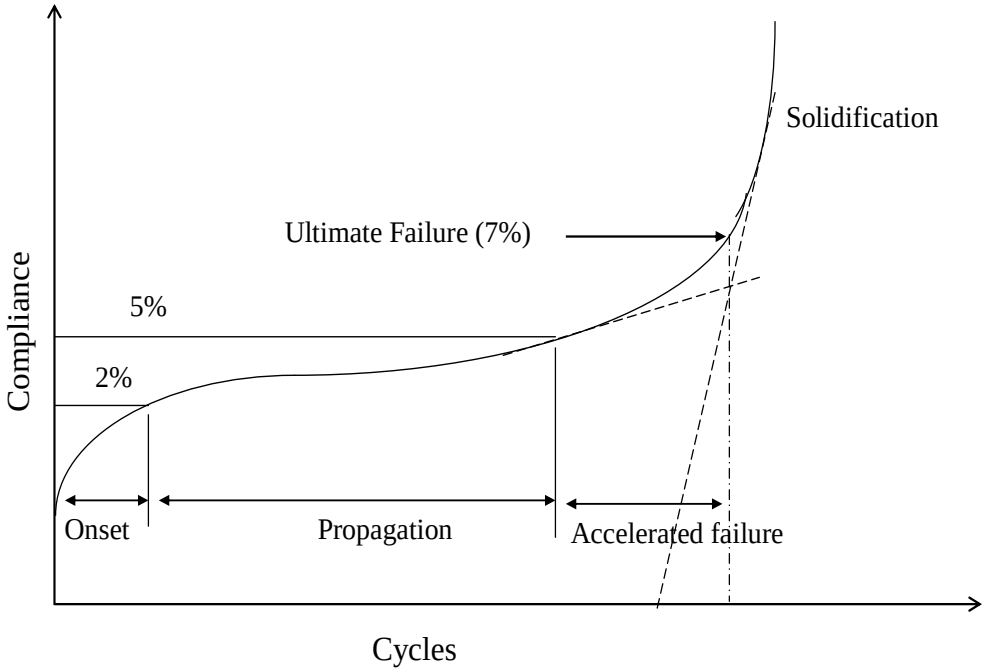

Figure 2.10. Typical compliance versus cycles response of a C-C fatigue test with definition of three types of failure.

Compliance appears to be arbitrary but can be related to damage onset, and accumulation [36] as in the stiffness reduction models [59]. Furthermore, a small variation of the compliance values has minimal impact on the fatigue lives. The compliance change criteria were used in estimating fatigue lives. The Figure 2.11 shows compliance versus number of cycles response for Eco-Core sample M-18 for σ_{min}/σ_c= 0.85 and response for all other samples are included in Appendix B.3 through B.12 for R=10 and 5, respectively. The three failure zones and their lives are clearly identifiable; the associated damage images are shown in Figure 2.12. The first image (a) was taken before loading the specimen; image (b) was taken after the onset of damage (2% compliance), notice the crush band; and images (c), (d), (e) were taken for successive propagation of crush band indicating the damage propagation in Eco-Core. Image (f) was taken around 7% compliance change. After 7% compliance change, the specimen failed within few load cycles. The damage sequences were similar for all the tests for R= 10 and 5. Therefore, the

formation of crush band, progression and final collapse of crush bands is the compression fatigue failure mechanism of Eco-Core. The collapse of the material was not apparent in the region outside of the crush band which happens mostly in the middle or edge (top or bottom) of the specimens based on the weak region in the specimen. This behavior is similar to that of static failure of Eco-Core. The fatigue lives for each of the three failure criteria for all tests are listed in Tables 2.4 and 2.5 for R= 10 and 5, respectively. Those specimens that did not fail in 10^6 cycles were static tested to measure the residual strength. Residual strengths are tabulated in Tables 2.4 and 2.5. To determine and understand the endurance limit of the material and the fatigue degradation rate, the data is presented by normalized maximum compression stress (σ_{min}/σ_c) versus the number of load cycles (N) through S-N diagram in Figures 2.13 through Figure 2.15.

Table 2.4

Compression-Compression Fatigue Test Result for R= 10, panel 1

Specimen ID	Cycles to failure	Residual Strength, MPa	Cycles for Compliance Change		
			$N_{2\%}$	$N_{5\%}$	$N_{7\%}$
M-14	914	-	295	740	820
M-24	1615	-	325	920	1480
M-61	602	-	65	390	520
M-56	4290	-	2,070	3820	4150
M-10	16,013	-	1,400	11650	13800
M-15	20,139	-	3,700	8,900	17,020
M-18	24,843	-	2,800	21,300	23,300
M-52	71,212	-	7,000	43,900	60,400
M-13	118,008	-	53,000	112,200	116,600
M-12	282,261	-	116,000	264,000	273,000
M-62	543,712	-	334,000	520,000	538,500
M-16	906,328	-	832,000	882,000	895,000
M-48	No*	18.155	725,000	-	-
M-50	No*	18.727	-	-	-
M-20	No*	17.796	650,000	-	-
M-34	No*	19.692	-	-	-
M-21	No*	18.541	-	-	-
M-25	No*	16.155	-	-	-

* indicates no failure

Table 2.5

Compression-Compression Fatigue Test Result for R= 5, panel 2

Specimen ID	Cycles to Failure	Residual Strength, MPa	Cycles for Compliance Change		
			$N_{2\%}$	$N_{5\%}$	$N_{7\%}$
M-46	2,318	-	570	1,920	2,140
M-30	2,497	-	1,850	2,240	2,410
M-55	10,057	-	5,800	8,800	9,500
M-39	9,053	-	4,300	7,350	8,500
M-31	2,973	-	780	2,600	2,860
M-19	4,366	-	1,500	4,090	4,250
M-52	119,663	-	67,000	113,500	117,550
M-44	No*	21.464	-	-	-
M-51	33,587	-	21,300	31,350	32,400
M-27	No*	20.565	250,000	-	-
M-45	No*	20.995	-	-	-
M-11	986,982	-	835,000	955,000	963,600

*No indicating no failure

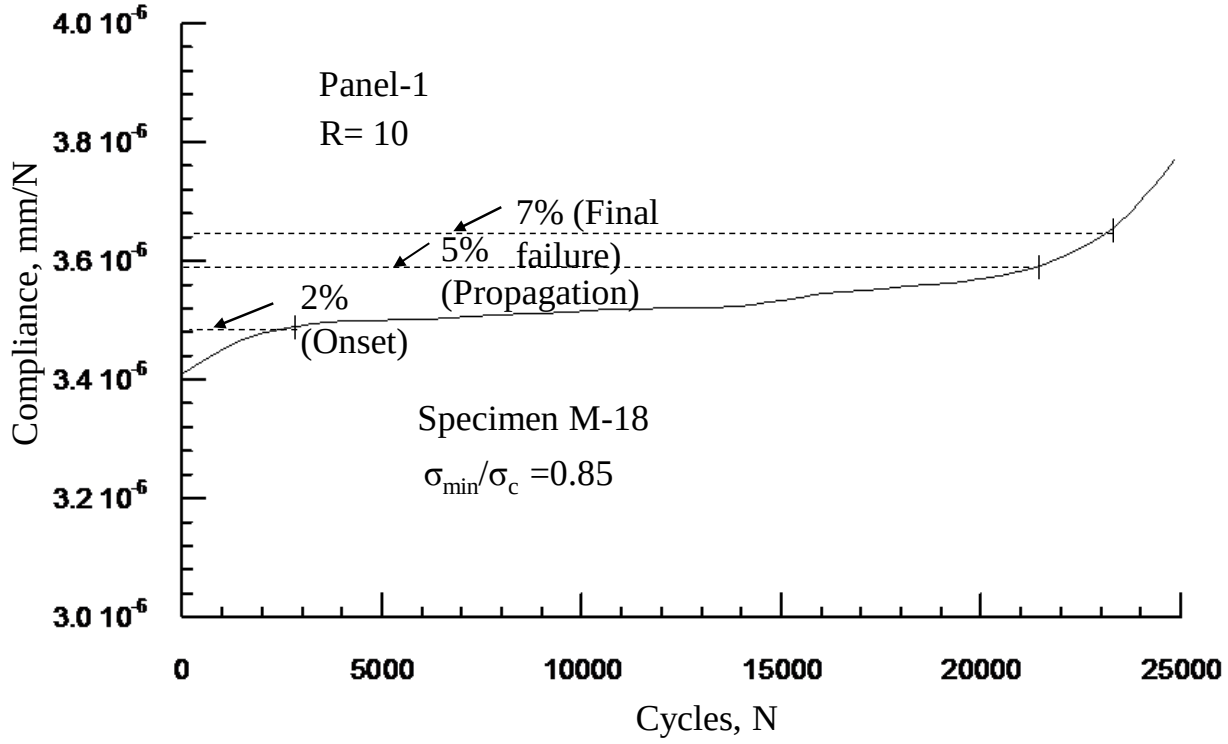

Figure 2.11. Compliance versus number of cycles (N) and the fatigue lives based on the three failure criteria.

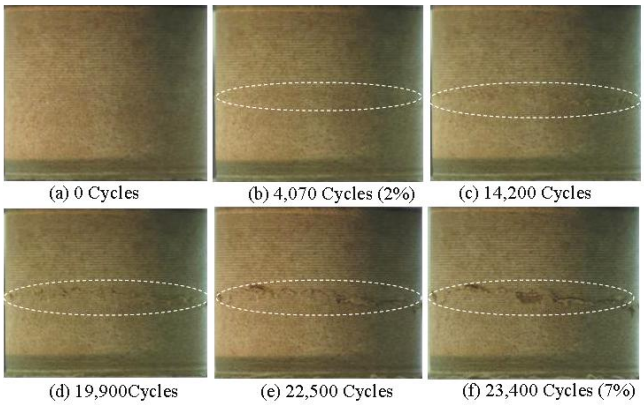

Figure 2.12. Successive failure of the specimen (M-18) for σmin/σc =0.85 and R=10.

2.5.2 Stress-N diagram. Plot of σ_{min}/σ_c versus load cycle (N) data of Eco-Core in Table 2.4 for R=10 are shown in Figure 2.13. The failure onset (2% compliance change), propagation (5%) and final failure (7%) are shown separately in Figures 2.13 a, b and c, respectively. Both the normalized maximum stress (σ_{min}/σ_c) and number of load cycles (N) are in log-log scale, a typical of fatigue data representation. In all three figures, the data (symbols) follows a straight line path. A least squared fit of data was performed and are represented by broken lines. The form of equation follows a power law of the form equation (2.1).

$$\left(\frac{\sigma_{min}}{\sigma_c}\right) = A_o N^{\alpha} \tag{2.1}$$

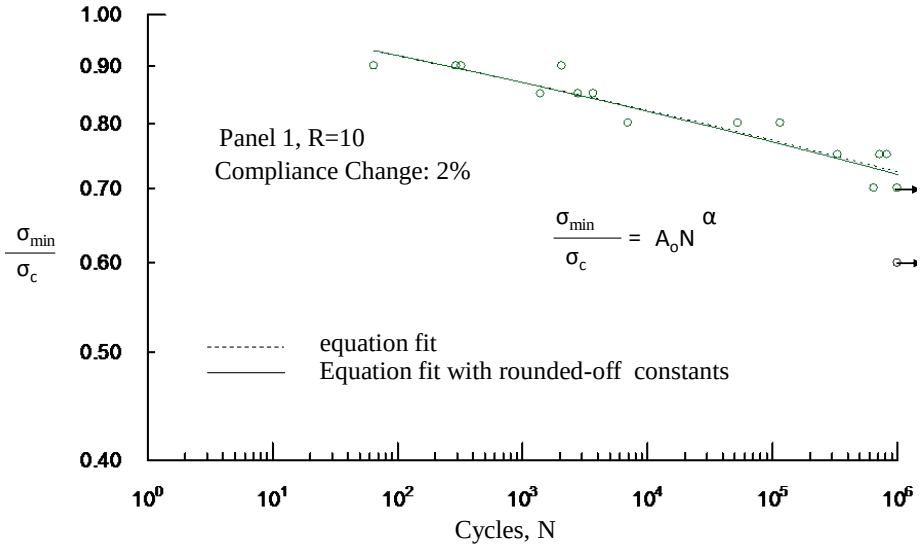

(a) Based on 2% compliance change failure

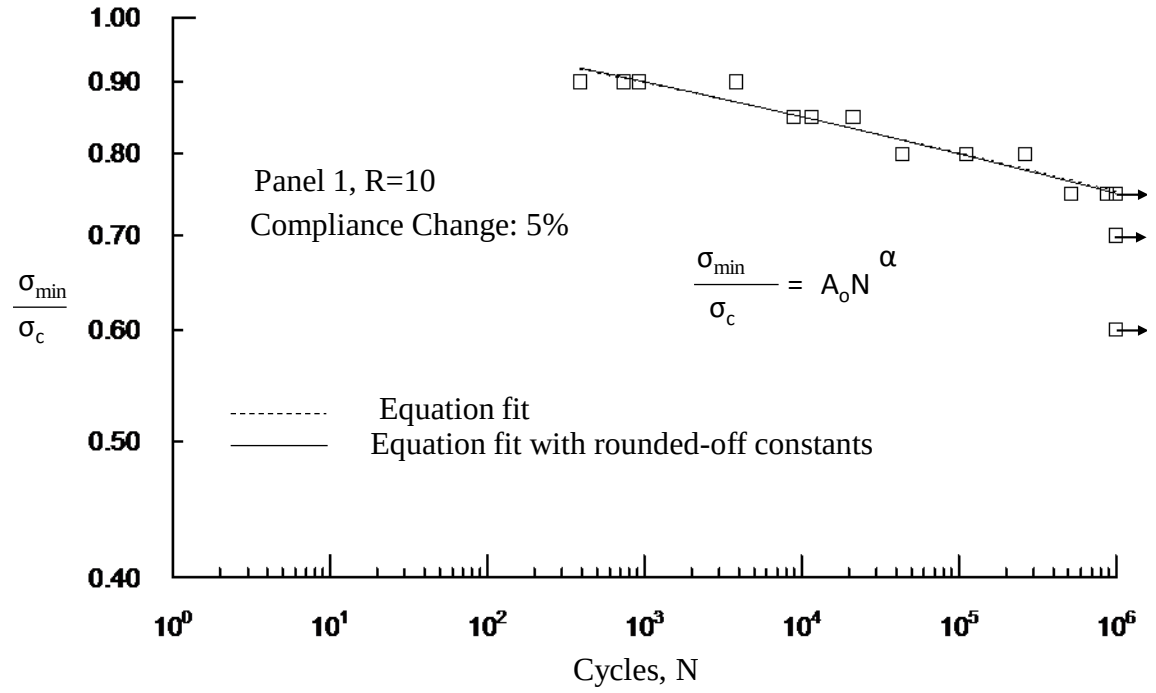

(b) Based on 5% compliance change failure

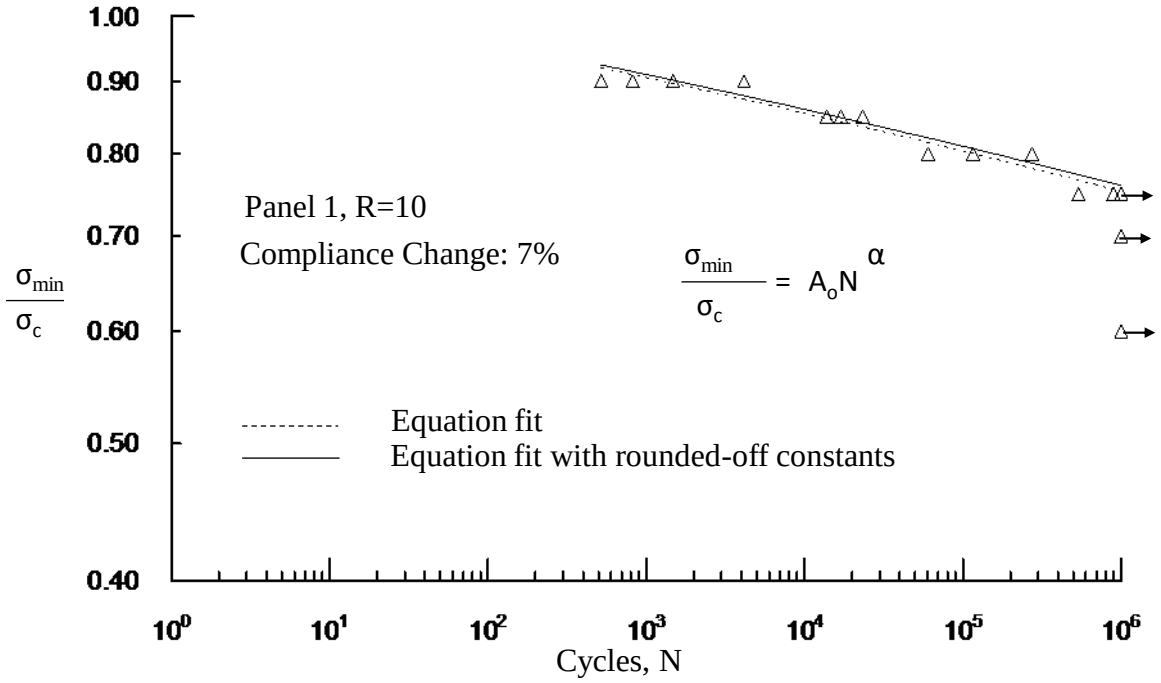

(c) Based on 7% compliance change failure

Figure 2.13. Normalized stress (σmin/σc) versus number of load cycles (N) for R=10 along with least square equation fit. Also shown is the equation with rounded off (solid line) constants.

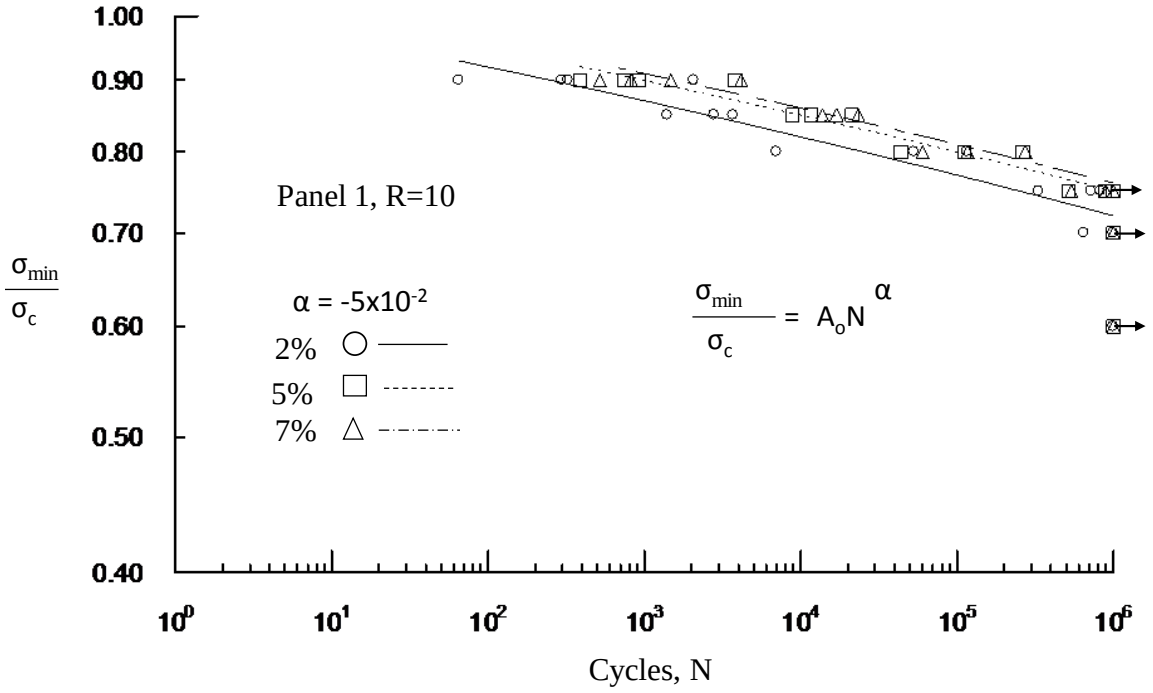

Figure 2.14. Comparison of S-N equation with experimental data for R= 10, with constants rounded off.

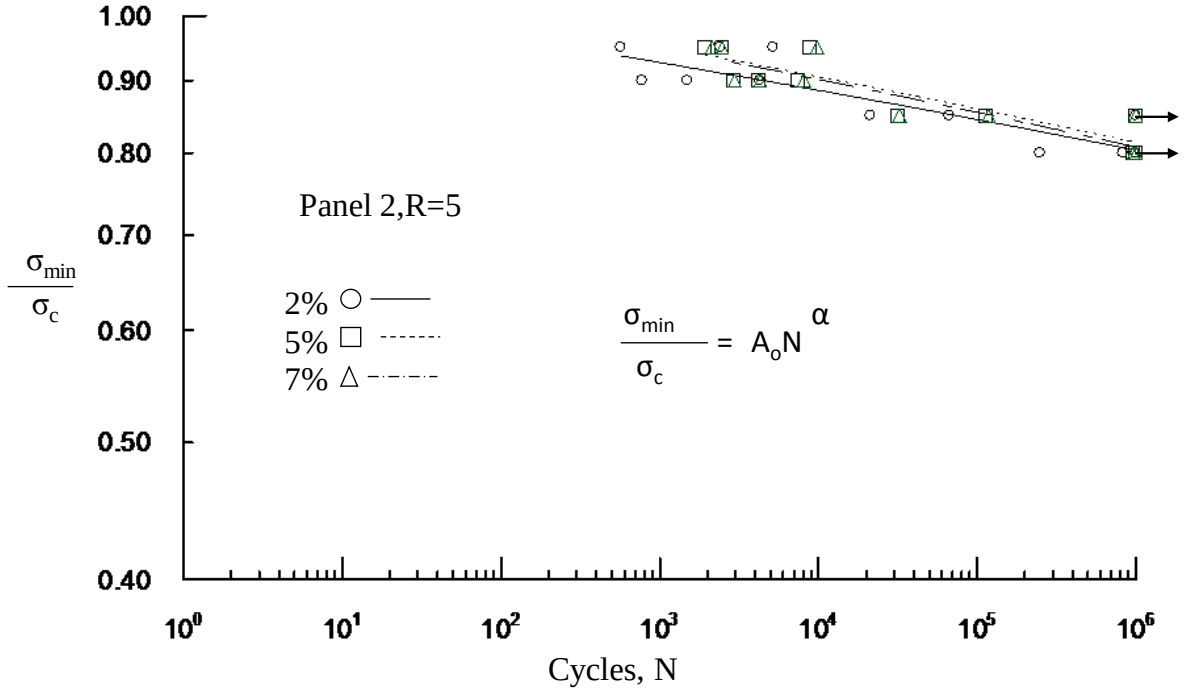

Figure 2.15. Comparison of equation with experiment for R=5, with constants in equation are rounded off.

The constant A_o is the material constant and α represents the degradation rate of the material. The raw values of constant A_o and the exponent α for all three cases of failure are listed in Table 2.6 for both R=10 and 5. For R=10, the values of α are nearly same whereas the constant A_o varied for each of the failure criteria and shows an ascending trend from onset to final failure. The broken lines in the Figure 2.13 represent the equation (2.1) using raw values of A_o and α and are found to represent the data very well. The constants A_o and α were rounded-off to two decimal places, these rounded values are listed also in Table 2.6. The solid lines in Figure 2.13 represent the equation 1 with rounded values of A_o and α. Results of rounded-off constants in equation (2.1) are compared with the test data for R=10 and 5 in Figure 2.14 and 2.15, respectively. The rounded values of A_o and α fit with the test data very well. Results in Figures 2.14 and 2.15 are used to estimate endurance limit ($N \geq 10^6$). Estimated endurance limit for R=10 and 5 are listed in Table 2.6.

Table 2.6

Constants in the S-N Equation and Endurance Limit for R= 10 and 5

Load ratio, R	Failure criteria	Constants				Endurance limit
	Compliance Change	Fitted		Rounded		
		A_o	α	A_o	α	
10	2%	1.0171	-0.04888	1.02	-0.05	$0.72\sigma_c$
	5%	1.0451	-0.04878	1.05		$0.75\sigma_c$
	7%	1.0582	-0.05088	1.06		$0.76\sigma_c$
5	2%	1.0504	-0.04051	1.05	-0.041	$0.80\sigma_c$
	5%	1.0852	-0.04586	1.09	-0.046	$0.82\sigma_c$
	7%	1.0893	-0.04654	1.09	-0.047	$0.82\sigma_c$

2.5.3 Stress ratio effect. The effect of R ratio on fatigue life is examined from the point of view of cyclic stress range and mean stress. Most metallic material's responses are dependent on stress range. As Eco-Core also behaves like an isotropic material, the stress range effect is investigated. Here both test data and equation are examined in three different ways: normalized

cyclic stress versus N; stress range versus N; and mean stress versus N. Here only the onset (2% compliance change) results are shown, however same trend was found for other two failure modes. Results for damage progression (5% compliance change) ultimate failure (7% compliance change) are attached in Appendix B.

2.5.3.1 Stress versus N. Normalized stress (σ_{min}/σ_c) versus N data in Tables 2.4 and 2.5 for R=10 and 5 for damage onset (2% compliance change) failure are shown in Figure 2.16. σ_{min}/σ_c versus N for damage progression (5% compliance change) and ultimate failure (7% compliance change) are attached in Appendix B.13. From figure 2.16, it can be seen that for a given stress (σ_{min}/σ_c), the fatigue life of a specimen for R=5 is larger than for R=10. The slope for R=10 is greater than for R=5. Alternately, strength degradation rate is larger for R=10 than for R=5. Consequently, the estimated endurance limit (N= 10^6 cycles) for R=5 is larger than R=10 by about 7%.

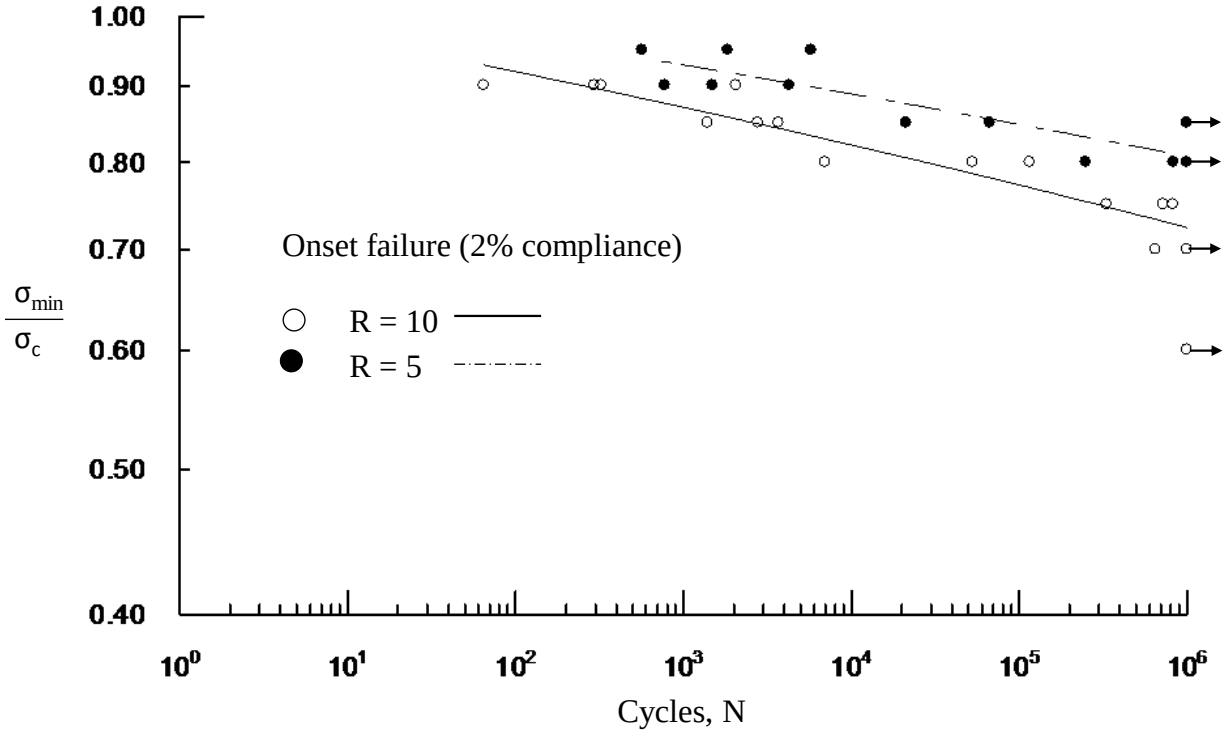

Figure 2.16. Normalized stress versus N for R= 10 and 5 for 2% compliance change.

2.5.3.2 Stress range versus N. The σ_{min}/σ_c versus N data in Figure 2.16 is transferred to normalized stress range ($\Delta\sigma/\sigma_c$) versus N using the equation 2.2 and are presented in Figure 2.17 for damage onset (2% compliance change) for both R=10 and 5. $\Delta\sigma/\sigma_c$ versus N for damage progression (5% compliance change) and ultimate failure (7% compliance change) are attached in Appendix B.14.

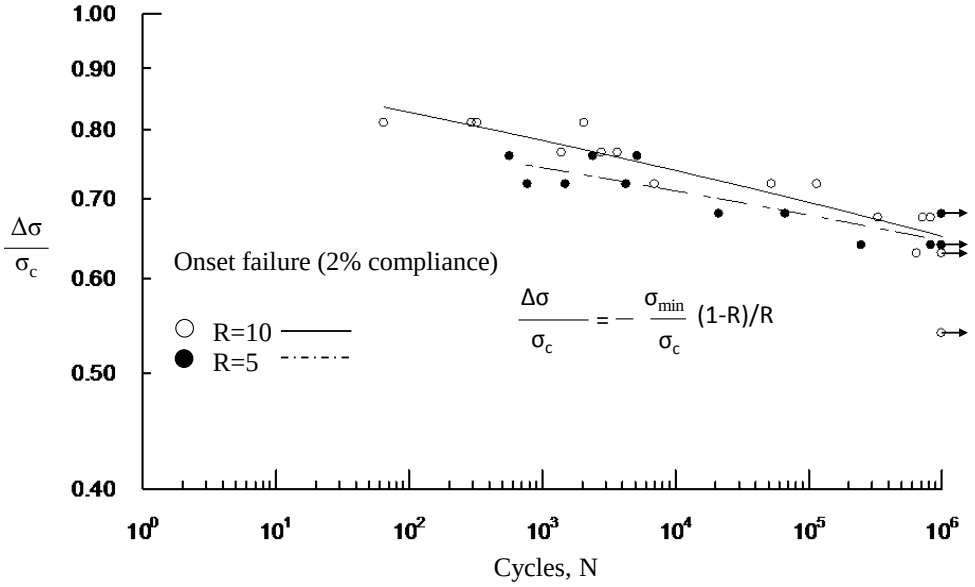

Figure 2.17. Normalized stress range versus N for 2% compliance change for R= 10 and 5.

From Figure 2.17, it can be seen that the two data are closer and almost interspersed with each other. This shows that that the fatigue life of Eco-Core depends on stress range and the R ratio effect could be included when the loading is expressed as

$$\frac{\Delta\sigma}{\sigma_c} = -\frac{\sigma_{min}}{\sigma_c} * \frac{(1-R)}{R} \tag{2.2}$$

As expected and can be seen in Figure 2.17 that R= 10 has higher stress range than R=5. Because of this reason, the degradation rate for R=10 is slightly higher than for R=5. These results are in agreement with what is observed for metals.

2.5.3.3 Mean stress versus N. The σ_{min}/σ_c versus N data in Figure 2.16 is transferred to normalized mean stress (σ_{mean}/σ_c) versus N through the equation 2.3 and the results are plotted in

Figure 2.18 for damage onset (2% compliance change) for both R=10 and 5. σ_{mean}/σ_c versus N for damage progression (5% compliance change) and ultimate failure (7% compliance change) are attached in Appendix B.15.

In Figure 2.18, symbols represent the test data and lines represent the equation. The data for R=10 and 5 are shifted apart as in Figure 2.16 for σ_{min}/σ_c. Thus the mean stress versus N representation of fatigue data does show dependency of R value.

$$\frac{\sigma_{mean}}{\sigma_c} = \frac{\sigma_{min}}{2\sigma_c}\left(1 + \frac{1}{R}\right) \tag{2.3}$$

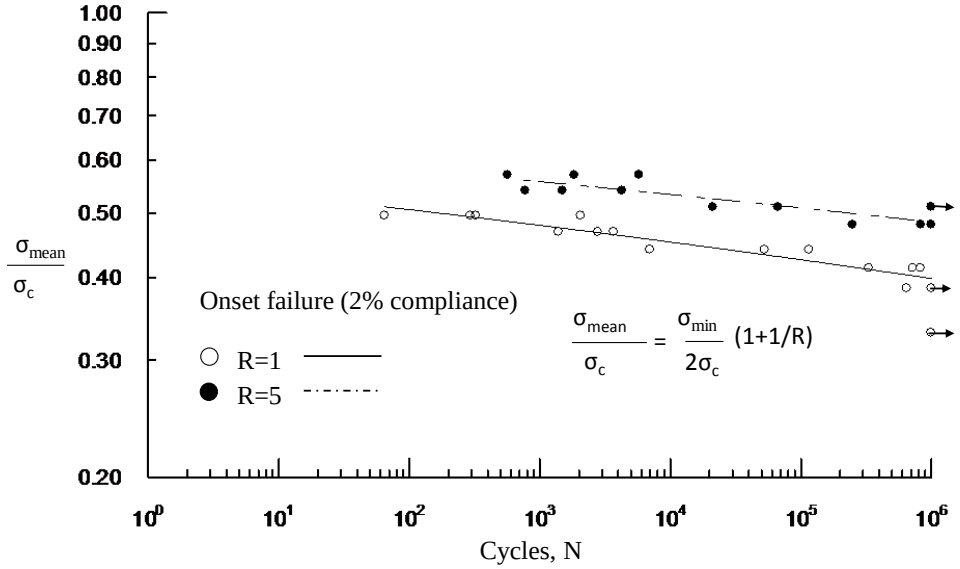

Figure 2.18. Normalized mean stress versus N for 2% compliance change for R= 10 and 5.

2.6 Summary

Static compression and compression-compression fatigue tests were conducted on a fire resistant Eco-Core material for two values of stress ratios (R= 10 and 5). Fatigue stress (σ_{min}/σ_c) ranged 0.9 to 0.6 for R=10 and 0.95 to 0.8 for R=5. Here σ_{min} is the maximum compression stress (algebraically minimum) and σ_c is the compression strength of Eco-Core. The compression strength of Eco-Core is 19.6± 0.25 MPa. The study showed that Eco-core has well defined failure modes and associated fatigue lives.

Eco-Core's failure can be classified as three types: damage on-set, progression and final failure. Damage on-set is characterized by formation of a single crush band at the middle or edge of the specimen, which corresponds to 2% change in compliance; damage progression is characterized by crush band propagation, which corresponds to 5% change in compliance; and final failure characterized by 7% compliance change. The three failure modes were found to be same for both static and fatigue loadings.

Based on 1 million cycles endurance limit was found to be $0.72\sigma_c$, $0.75\sigma_c$ and $0.76\sigma_c$, respectively for on-set, propagation and final failure for R=10 while it is $0.81\sigma_c$, $0.82\sigma_c$ and $0.82\sigma_c$, respectively for R=5. The S-N (number of load cycles) data follows a well-defined power law equation, $\sigma_{min}/\sigma_c = A_o N^{\alpha}$. Constants of the equation were established for all three modes of failures and the two stress ratios. The Eco-Core fatigue life was found to be less sensitive to R ratio when expressed in terms of stress range versus number of load cycles that is similar to what was observed in most metallic materials.

CHAPTER 3

Shear Fatigue Characterization

3.1 Introduction

In this chapter, shear fatigue performance of Eco-Core sandwich beam is presented. The static test was conducted following ASTM C393 and the same test setup was used for fatigue test. For both static and fatigue tests, Eco-Core sandwich beams made of three ply (0/90/0) woven roving FGI 1854 glass fiber/Vinyl ester face sheet were used. The thicknesses of fabricated core (t_c) and face sheet (t_f) were 25.4 mm and 1.50 mm, respectively. The average density of the Eco-Core panel was 0.50 g/cc. The length and width of the Short beam sandwich specimens were 130 mm and 51 mm, respectively. The specimen span (S) was set to 80 mm with an average sandwich thickness (d) of 26.9 mm that results in S/d of 3 and t_f/d of 1/18. Shear fatigue test was conducted using sinusoidal loading with a frequency of 2 Hz and stress ratio R of 0.1. Tests were conducted at different stress levels (τ_{max}/τ_c) and a PC based data acquisition system was used to store fatigue load, stroke displacement and time. This data was converted to compliance and number of cycles and created compliance-number of cycles curves. Fatigue life was determined based on 2%, 5% and 7% compliance change failure criteria and corresponding stress-number of cycles (S-N) diagram were established. The macro-scale fatigue failure mechanism was investigated by analyzing the selective images of the specimen taken from beginning to end of the test by a digital camera. This work is published in open literature [82].

3.2 Material System

A class of fly ash known as Cenosphere grade XL 150 supplied by Sphere Services Inc. and phenol-formaldehyde resole binder resin, Durite SC 1008 supplied by Mektech Composities Inc. were used to formulate Eco-Core [11]. Eco-Core panel fabrication process was already

discussed in chapter 2. Four core panels were fabricated with an average bulk density of 0.5 g/cc. These panels were used as a core to fabricate sandwich panels.

Face sheets were fabricated by using woven roving three layers (0/90/0) of FGI-1854 glass fabric and vinyl ester composite laminate by a vacuum assisted resin transfer molding process [80, 83]. FGI 1854 glass fabric was supplied by Fiber Glass Inc and vinyl ester was supplied by Dow Chemicals. Sandwich panels were fabricated by bonding the face sheets to Eco-Core on top and bottom surfaces using Loctite Hysol E-90FL adhesive as explained in [12].

3.3 Design of Specimen

Short beam shear test specimen was designed as per the guidelines and the material properties are given in the reference [12], which are also listed in Table 3.1. Four point loaded sandwich beam was selected to avoid direct contact of the load on the core material and reduce the stress concentration and wear damage caused in fatigue test. Although the lap shear test (ASTM C394) specimen was also be used in honey comb sandwich beams, here a four-point bend loaded specimen used because of ease of loading. The specimen nomenclature is shown in Figure 3.1. Here t_c is the core thickness, t_f is the face sheet thickness, d is the design depth of sandwich beam $(d = t_c + t_f)$, S is the span of the beam and e is the edge distance from the support point. The symbols σ_c, τ_c, E_c, and G_c define core compression strength, shear strength, compression modulus and shear modulus, respectively. Similarly, the core tensile modulus and strength are defined by E_{ct} and σ_{ct}, respectively. Properties of Eco-Core given in Table 3.1 [12] are for core material that was determined from direct tension, compression and shear tests. The nominal thicknesses of the core and face sheet are 25.4 mm and 1.40 mm, respectively and the width of the specimen is 51 mm. The test specimen was designed using the core shear and core tension (flexure) failure criteria. The failure load (P_f) for core shear and core tension are derived

from beam theory from maximum shear and bending moment (see Figure 3.1b and 3.1c) and are given by Equations (3.1) and (3.2), respectively.

Table 3.1

Material Properties of Eco-Core and Face-sheet [12]

Material	Tensile		Compressive		Transverse Shear	
	Modulus,	Strength,	Modulus,	Strength,	Modulus,	Strenght,
Face sheet[83]	29.20	512.50	31.90	363.40	4.00	77.10
Eco-Core[11]	2.54	6.46	1.14	21.85	0.97	4.61

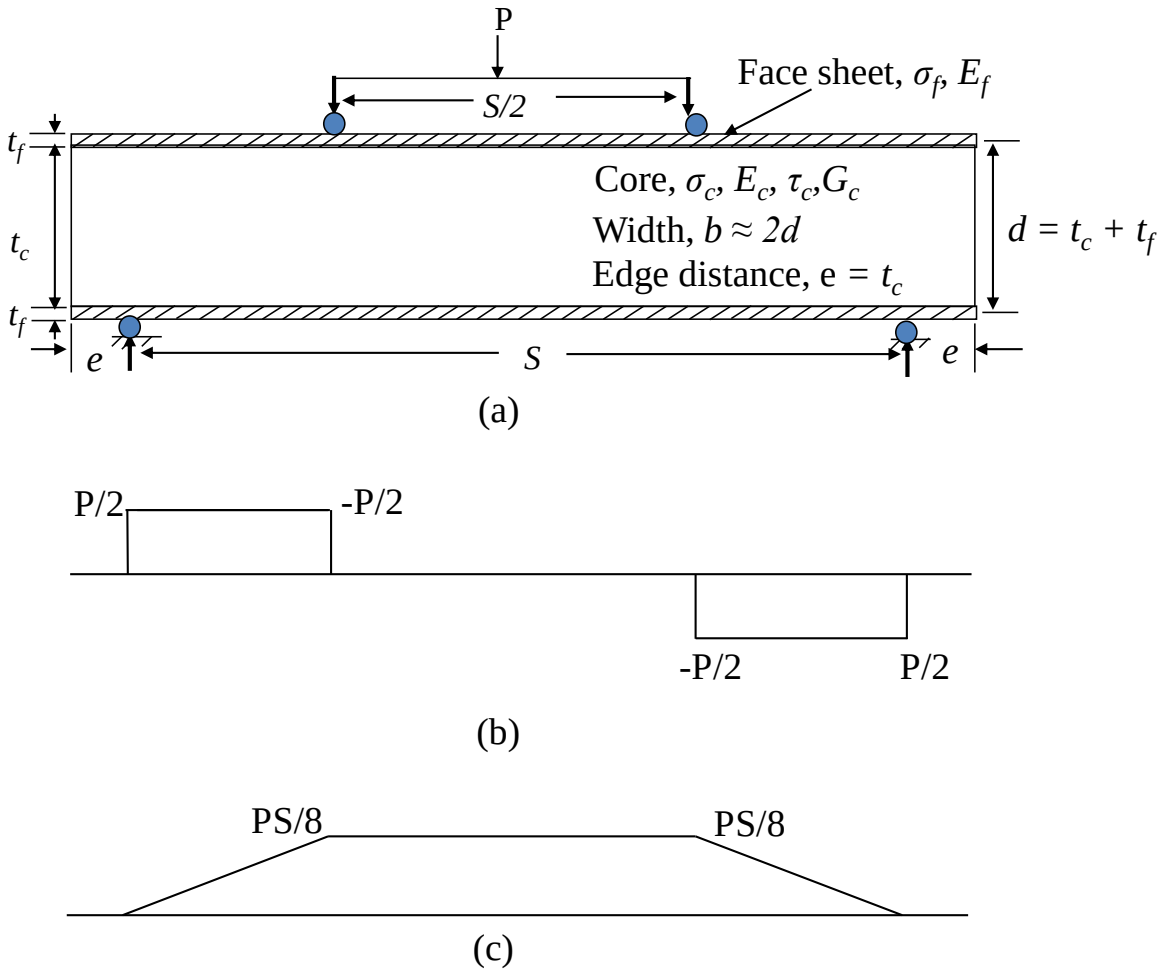

Figure 3.1. (a) Schematic of test specimen, loading and nomenclature (b) Shear force diagram (c) Bending moment diagram.

$$\frac{P_f}{b} = 2\tau_c d \tag{3.1}$$

$$\frac{P_f}{b} = \frac{16D\sigma_{ct}}{St_cE_{ct}} \tag{3.2}$$

where, σ_{ct} and E_{ct} are the core tensile strength and modulus, respectively. The D is flexural rigidity of the sandwich beam and is given by Equation (3.3).

$$D = \frac{E_f t_f^3}{6} + \frac{E_f t_f d^2}{2} + \frac{E_c t_c^3}{12} \tag{3.3}$$

Normalized failure loads of these two failure criteria are shown in Figure 3.2 as a function of span to depth (S/d) ratio. The core shear failure is represented by a horizontal broken line and core tension failure by a solid line. Intersection of the two lines represents the potential for both failures. The two curves intersect at S/d = 4. Therefore, S/d of 3.0 was selected so that core shear failure is the dominant failure mode. The failure load per unit width (P_f/b) of the beam is 247 N/mm.

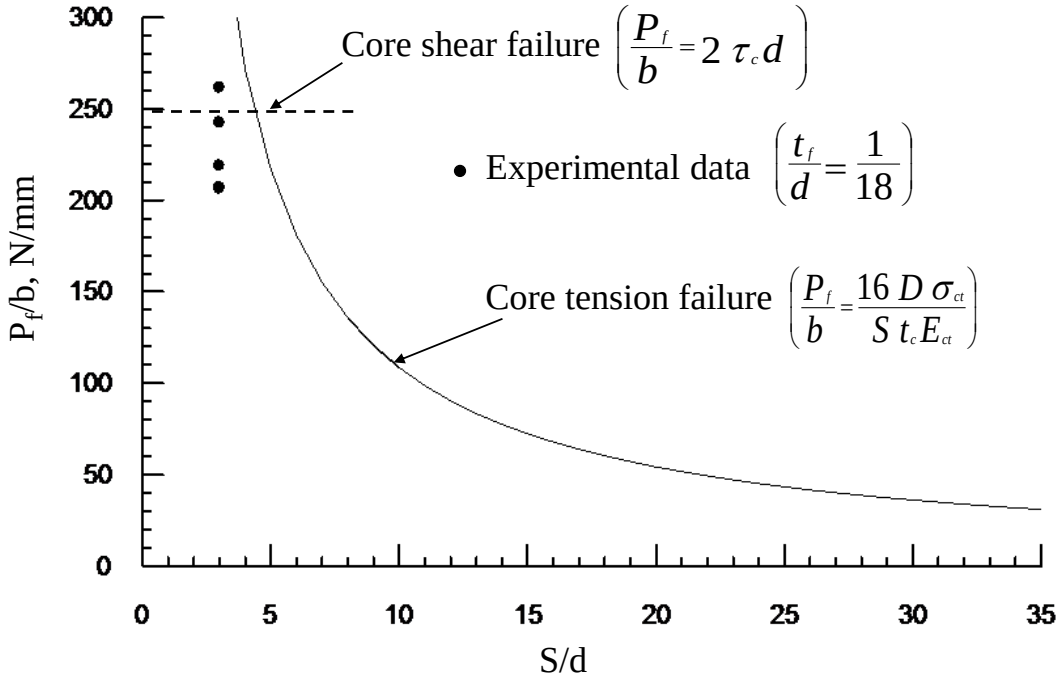

Figure 3.2. Failure load versus span/depth (S/d) ratio for Eco-Core sandwich beam based on two failure criteria.

3.4 Fabrication of Sandwich Panel and Specimen

Three-ply symmetric (0/90/0) woven roving FGI 1854 glass fabric/vinyl ester composite face sheets of 1,270 mm X 810 mm in size were fabricated by Vacuum Assisted Resin Transfer Molding (VARTM) as explained in references [80, 81]. Steps in fabricating glass/vinyl ester face sheet are shown in Figure 3.3. The average thickness of the fabricated face sheet was 1.50 mm. The large face sheet was cut into 356 mm X 356 mm pieces which is consistent with the core panel size. The face sheets were bonded to core panel using Loctite Hysol E-90FL toughened and medium viscosity epoxy adhesive. This adhesive has tensile strength of 13 MPa, lap shear strength of 5.9 MPa and elongation of 64%. Adhesive bonded sandwich panels were cured in a vacuum bag at a pressure of 0.051 MPa (15 in of Hg) at room temperature for 12 hours. The adhesive layer thickness was about 250 µm (0.01 in) after cure. Steps in fabricating Eco-Core sandwich panel is shown in Figure 3.4.

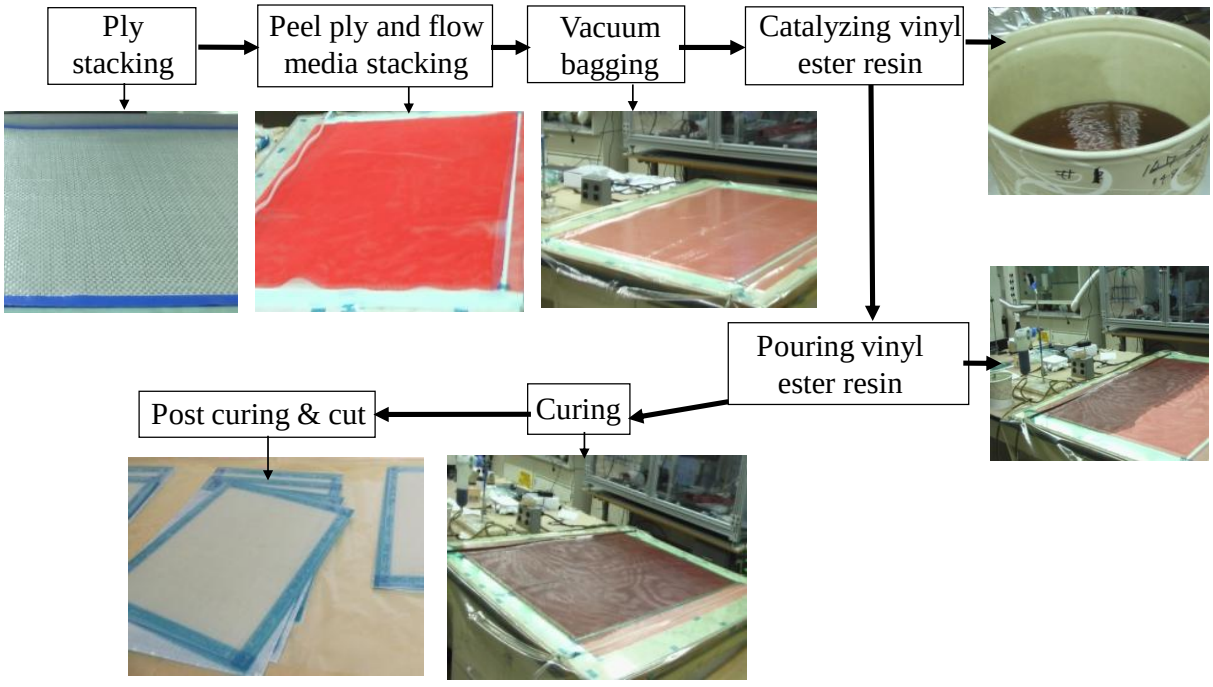

Figure 3.3. Steps for fabricating face sheet.

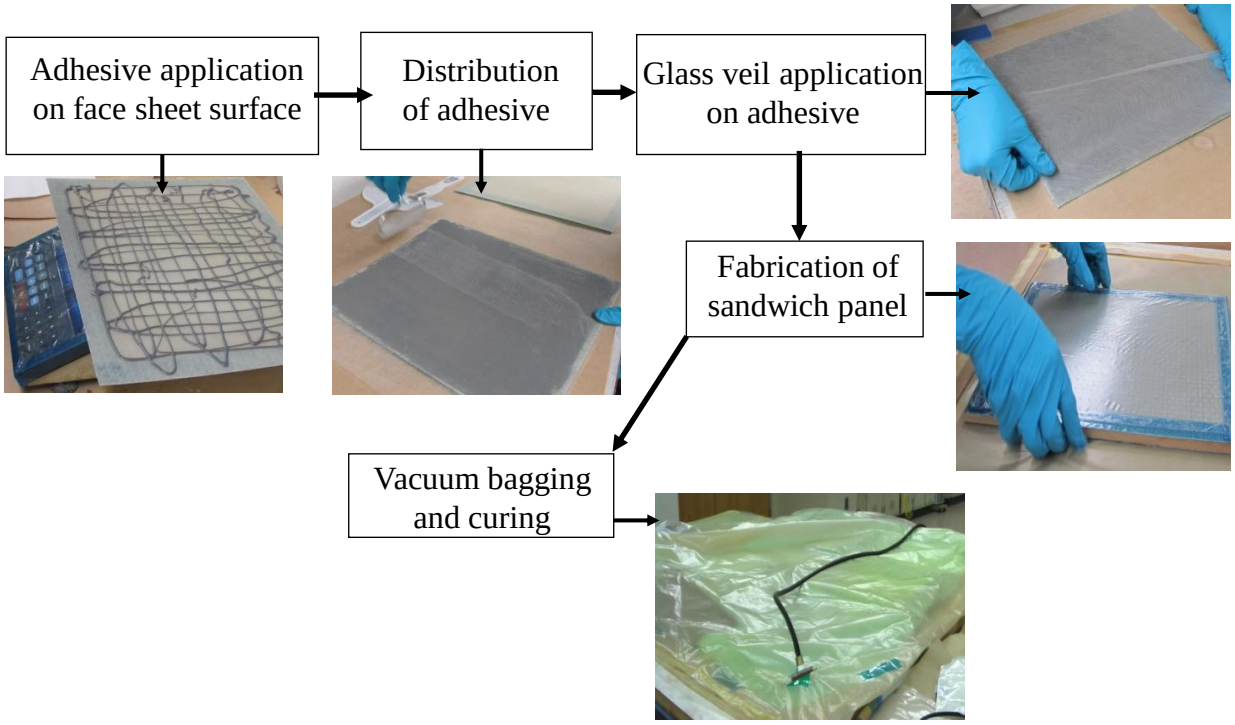

Figure 3.4. Steps for fabricating Eco-Core sandwich panel.

Short beam sandwich specimens of 130 mm long and 51 mm wide were machined. Specimen dimensions were precisely measured and are listed in Table 3.2 and 3.3. The specimen span (*S*) was set to 80 mm with an average *d* of 26.9 mm that results in *S/d* of 3 and t_f/d of 1/18.

3.5 Static Shear Test, Results and Discussion

Static shear tests were performed to validate the shear strength used in design of test specimen, record core failure modes, and to precisely measure the shear strength of the core material. The test was conducted using a MTS servo-hydraulic test machine following ASTM C393 by applying quarter point loading (Figures 3.1). A deflection transducer (LVDT) was placed under the specimen at the mid span for direct measurement of deflection (Figure 3.5). The specimen was loaded at a constant cross-head speed of 0.5 mm/min (0.02in/min). Load and deflection were recorded at every one-half second and the associated failure modes were monitored by a high speed camera.

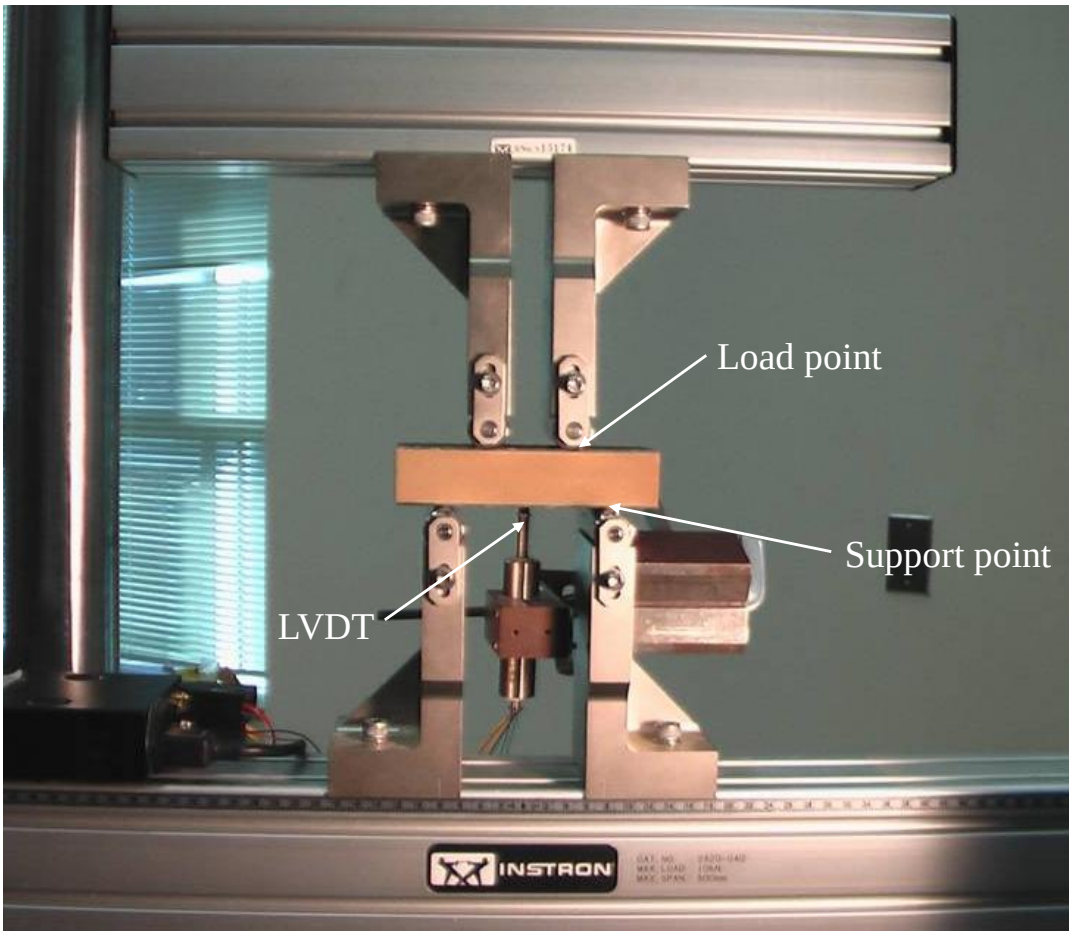

Figure 3.5. Short beam shear test setup.

Figure 3.6 shows the load-deflection responses of five test specimens. The load-deflection response was almost linear until the first failure load was reached. After that, a sudden load drop was observed that is similar to brittle fracture. The load at the first load drop was considered as the failure load of the specimen. The three specimens (SSP-03, SSP-07 and SSP-22) failed at nearly the same load where as two specimens (SSP-14 and SSP-18) failed at slightly lower loads.

Shear strengths for first three specimens ranged from 4.08 to 4.87 MPa, whereas the specimens SSP-14 and SSP-18 ranged from 3.84 to 3.85 MPa. The average shear strength (τ_c) was 4.23MPa (0.61ksi) with a standard deviation (STD) of 0.45MPa (0.07ksi) and standard error

mean (SEM) of 0.20MPa (0.03ksi). This average strength is about 8% lower than that of reference [12], which is reasonable when comparing the direct strength and sandwich panel strength. The test results are listed in Table 3.2. The normalized failure loads (P_f/b) of the test are shown by solid circles in Figure 3.2.

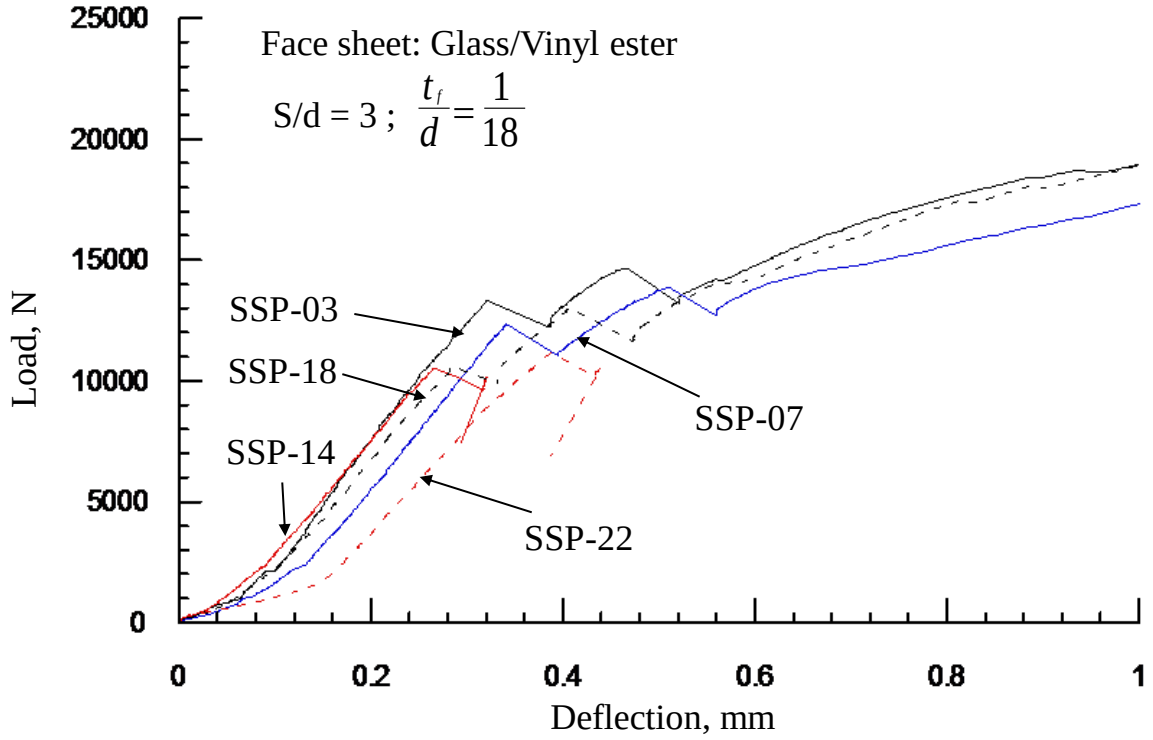

Figure 3.6. Load-deflection responses of short beam test specimens.

Table 3.2

Summary of Static Shear Strength Test

specimen ID	Specimen Parameters				Shear	
	S, mm	b, mm	t_c, mm	t_f, mm	P_f, N	τ_c, MPa
SSP-03	80	50.9	25.4	1.5	13,326	4.87
SSP-07	80	50.9	25.4	1.5	12,352	4.51
SSP-14	80	51.1	25.4	1.5	10,533	3.84
SSP-18	80	51.1	25.4	1.5	10,577	3.85
SSP-22	80	51.1	25.4	1.5	11,187	4.08
Average					11,595	4.23
STD					1,215	0.45
SEM					543	0.20

Figure 3.7 illustrates the typical shear failure of the Eco-Core material. The typical shear cracks occurred at an angle of 45^{o} in the core near the mid thickness of the specimen and between the bottom support and top load point. The load drops as soon as the crack forms. Two types of crack formation were observed from the high speed images. One is a single crack (see Figure 3.7a) and other one is the two symmetric cracks (Figure 3.7b) both possibilities are expected. Both types of cracks extended up to the face sheets and stops. With continued loading, the cracks turns into an interfacial delamination, which results in a final failure.

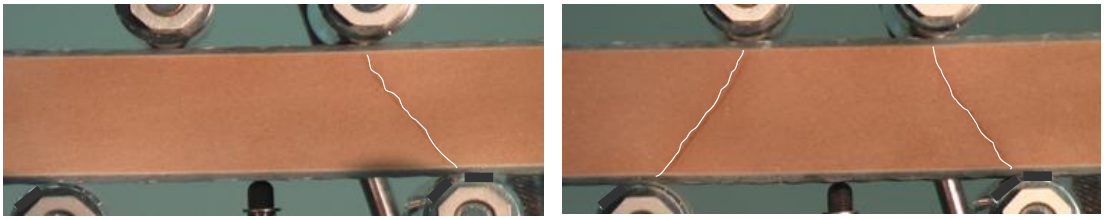

(a) Single shear crack (b) Symmetrically double shear crack

Figure 3.7. Typical static failure modes in Eco-Core sandwich beam (Crack is highlighted by white line).

3.6 Shear Fatigue Test

Shear fatigue tests were conducted under a sinusoidal cyclic load of frequency 2Hz and stress ratio of R = 0.1. Typical shear cyclic loading is shown in Figure 3.8. The endurance limit requirement depends on the applications, which vary from 10^{7}-10^{9} cycles. Because of limitations of equipment and test time, the testing was limited to 10^{6} cycles and the 10^{6} cycles was used as the endurance limit. Four different stress levels (τ_{max}/τ_{c}) in the range of 0.9 to 0.7 were chosen and are listed in Table 3.3. The shear fatigue test plan such as stress ratio, maximum shear stress, and the associated load are shown in Table 3.3. Four specimens were tested for each stress ratio. Load, stroke displacement and time were collected using a PC based data acquisition system. Data acquisition procedure was different for each stress level (τ_{max}/τ_{c}). For $\tau_{max}/\tau_{c} = 0.9$, data was collected for 5 seconds at every one minute interval, for $\tau_{max}/\tau_{c} = 0.8$, the data was collected for 5

second at every 2 minute interval. For τ_{max}/τ_c = 0.75 and 0.70, data was collected for 5 seconds at every five minute interval. Times recorded during cyclic loading were converted to cycles by multiplying time with the number two. The displacements recorded were converted into the compliance, which is the ratio of change in displacements and the change in loads between the consecutive maximum and minimum loads. The fatigue life was defined as the number of cycles to failure. To investigate the macro-scale fatigue failure, a digital camera was set up close to the specimen to record any failure. Since each fatigue test lasted for hours to days, images were taken only for selective intervals between the beginning and end of the test (unstable failure). The image sequences were then analyzed to understand the fatigue failure and its mechanisms.

Table 3.3

Shear Fatigue Test Plan (R = 0.1, τ_c = 4.23 MPa)

Specimen ID	τ_{max}/τ_c	Specimen geometry				τ_{max}, MPa	P_{max}, N
		S, mm	b, mm	t_c, mm	t_f, mm		
SSP-02	0.90	80	51.0	25.4	1.5	3.81	10,444
SSP-11		80	50.9	25.4	1.5		10,433
SSP-16		80	51.1	25.4	1.5		10,474
SSP-21		80	51.2	25.4	1.5		10,485
SSP-12	0.80	80	51.1	25.4	1.5	3.38	9,292
SSP-25		80	51.2	25.4	1.5		9,310
SSP-10		80	50.8	25.4	1.5		9,238
SSP-09		80	51.2	25.4	1.5		9,301
SSP-31	0.75	80	51.1	25.4	1.5	3.17	8,706
SSP-05		80	50.9	25.4	1.5		8,672
SSP-26		80	50.9	25.4	1.5		8,681
SSP-15		80	51.2	25.4	1.5		8,723
SSP-04	0.70	80	50.9	25.4	1.5	2.96	8,098
SSP-19		80	50.9	25.4	1.5		8,106
SSP-24		80	51.2	25.4	1.5		8,146
SSP-29		80	51.1	25.4	1.5		8,138

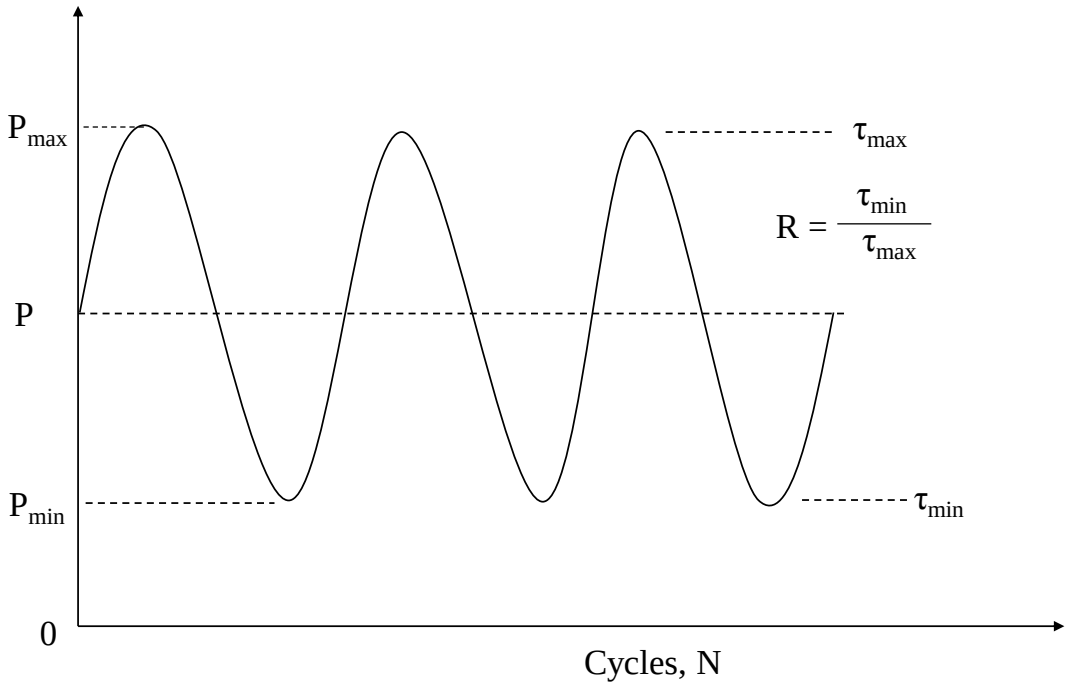

Figure 3.8. Typical shear fatigue loading (R=0.1).

3.7 Fatigue Test Results and Discussions

3.7.1 Failure modes and associated failure lives. The fatigue failure was characterized by change in compliance. Figure 3.9 shows compliance versus number of fatigue load cycles of the test specimen SSP-12 for a shear loading of τ_{max}/τ_c= 0.80. The compliance plots for other samples were similar and are presented in Appendix C.1 through C.3. The compliance response was found to be divided into three types: failure onset, progression and ultimate failure. The associate three failures were characterized by three different values of compliance change, namely, 2%, 5% and 7%. This classification is same as that was used for compression fatigue failure in chapter 2 [79]. Each of these compliance changes was represented by different stages of shear cracks. The 2% compliance change was usually associated with formation of shear crack near the mid thickness of the specimen. The 5% compliance change was represented by crack propagation to the face sheets. Finally, the 7% compliance change was represented by the crack arrest after meeting the face sheets or the interfacial delamination between face sheet and core.

The number of cracks associated with these failure stages could be a single crack, symmetrically located two cracks or a multiple cracks as shown in Figure 3.11 which is similar to static shear tests. All failure resulted from shear cracks at about 45^o to beam axis. Fatigue lives of the specimen for the three failure criteria are listed in Table 3.4 for different τ_{max}/τ_c. Those specimens that did not completely fail in 10^6 cycles were static tested to measure the residual strength. Residual strengths are also tabulated in Tables 3.4.

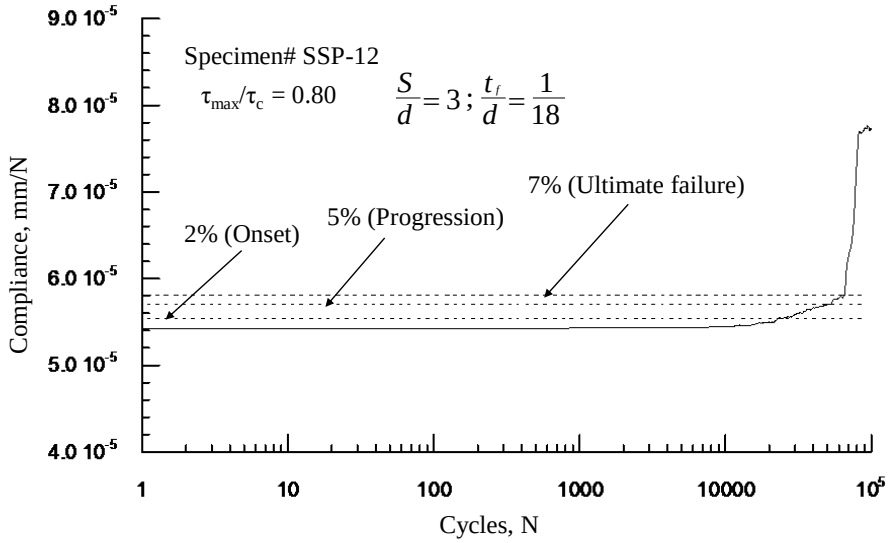

Figure 3.9. Compliance versus number of cycles (N) and the fatigue lives based on the three failure criteria.

The Figure 3.10 shows edge view of the specimen SSP-12 before starting test, 66,950, 72,600, and 82,300 cycles representing the different levels of failure. Based on edge view analysis of specimens at different stress levels, three types of failure modes corresponding to three values of compliance change were observed which are schematically shown in Figure 3.11. At ultimate failure (Figure 3.10c), sometimes multiple shear cracks with interfacial delamination near load/support points were observed. This type of crack occurred mostly when the number of load cycles to failure was large. Delamination near the concentrated cyclic loads was considered to be due to multi axial stress state, a combination of interfacial shear and tensile bending stress.

Figure 3.12 shows the possible stress states at load and support locations. A detailed finite element analysis was performed on the test specimen and a summary of the results is presented below.

Table 3.4

Shear Fatigue Test Results (R= 0.1)

Specimen ID	τ_{max}/τ_c	Cycles when test stopped	Residual strength, MPa	Cycles for compliance change		
				$N_{2\%}$	$N_{5\%}$	$N_{7\%}$
SSP-02	0.90	133,950		3,250	6,160	8,500
SSP-11		346,509		2,975	7,145	7,300
SSP-16		10,128		1,190	3,280	3,460
SSP-21		124,827		360	915	980
SSP-12	0.80	166,926		22,800	52,600	67,500
SSP-25		339,689		3,500	10,200	15,600
SSP-10		1,000,000		140,300	220,090	250,400
SSP-09		698,719		110,600	264,200	325,500
SSP-31	0.75	504,861		148,500	235,200	274,500
SSP-05		903,899		180,300	350,500	470,500
SSP-26		123,104		4,360	11,540	17,820
SSP-15		208,300		41,570	80,150	85,013
SSP-04	0.70	1,000,000	5.78	570,500	1,000,000	1,000,000
SSP-19		1,000,000	4.68	330,500	430,800	515,500
SSP-24		1,000,000		171,500	460,200	554,200
SSP-29		1,000,000		284,600	390,600	590,300

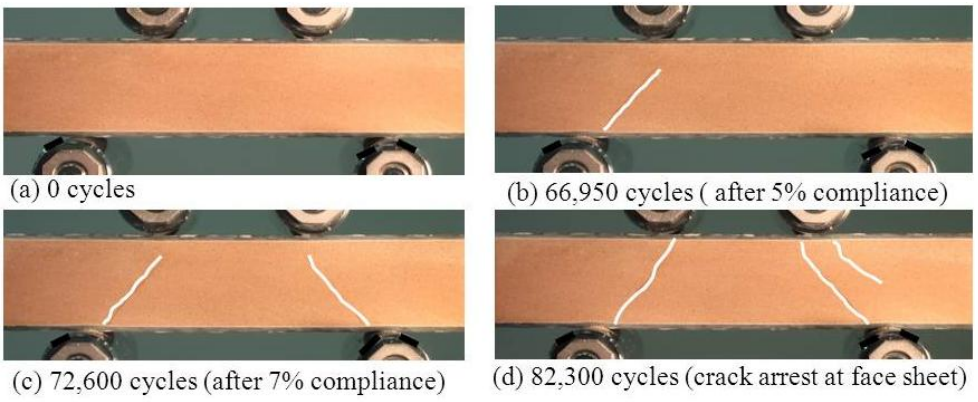

Figure 3.10. Successive failure of the specimen (SSP-12) for τ_{max}/τ_c = 0.80 (crack is highlighted by white line).

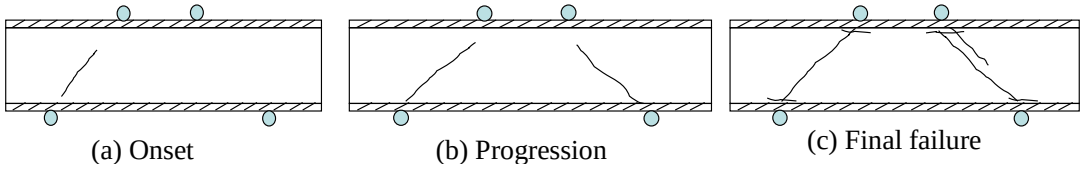

Figure 3.11. Types of shear fatigue failure.

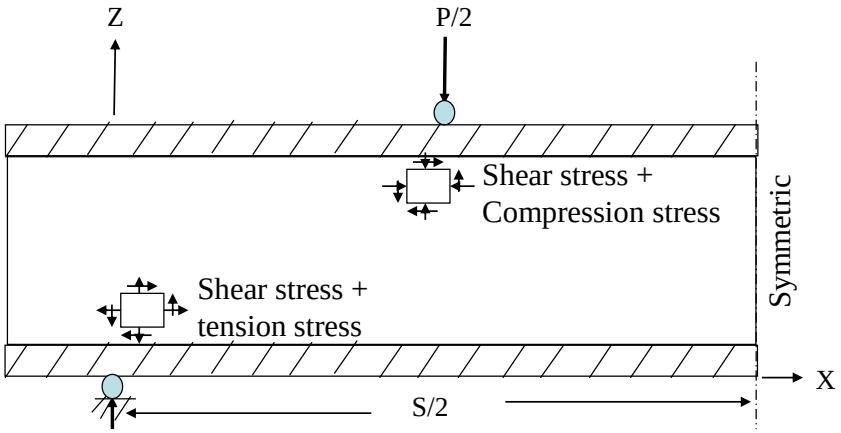

Figure 3.12. Stress state near the support and load points for delamination failure.

3.7.2 Stress analysis near face sheet-core interface region. A 2-D finite element analysis (FEA) of the test sandwich beam was conducted to understand the stress field near the support location. Details of the FEA are given in the Appendix A. Here only required figures are shown to explain the possibility of core-face sheet interfacial debond in fatigue testing.

Figure 3.13 shows the shear stress distribution through the thickness of the core material (no face sheet) at three locations between the support and load point (see in sketched picture). The location B and C are about t_f distance from the support and load points, respectively. As expected, the shear stress distribution at B and C are reflection of each other about the mid-plane. The maximum shear stress is about $2.6\tau_{av}$ at the core-face sheet interface. The shear stress at A at half-way between support and load points is symmetric about the mid-plane and nearly flat curve as expected in sandwich beams (depending on the relative modulus of face sheet and core). The maximum shear stress is about $1.1\tau_{av}$. These results conclude that if the shear failure occurs at

mid-way between the support and load points, it is due to maximum shear at the mid-plane of the beam. If the failure occurs near the support or load point, it may be because of shear concentration at the interface. Because the interface is resin densified and the interfacial strength could be much higher than the core shear strength.

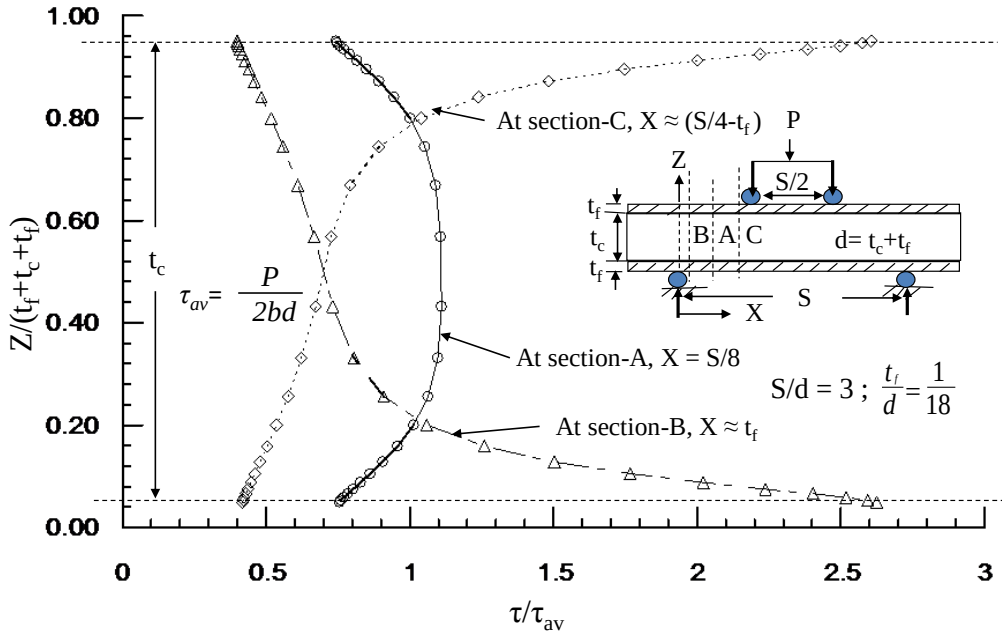

Figure 3.13. Shear stress distribution at section A, B, and C.

To examine the state of normal stress near the interface, the bending stresses plotted through the thickness at the same three sections (A, B and C) in Figure 3.14. As clearly shown that the bending stress near the interface of the section B is tensile (before it becomes compressive at the interface) while the bending stress at C near the support is compressive. Therefore high interfacial shear stress and tensile stress near the support at section B may the reason for initiation of delamination in fatigue loading. To establish the location of maximum interfacial shear stress from the support, the through the thickness shear distribution are plotted for X= 0, $t_f/3$, $2t_f/3$, t_f, $2t_f$ and $4t_f$ (see Figure 3.15). Maximum shear stress at the interface is plotted against X in Figure 3.16. This plot clearly shows that the shear stress is maximum at

about one mm or about $2t_f/3$ distance from the support. Hence the hypothesis is that the maximum interfacial shear stress and tension bending stress together may be causing interfacial debond between the Eco-Core and the composite face sheet.

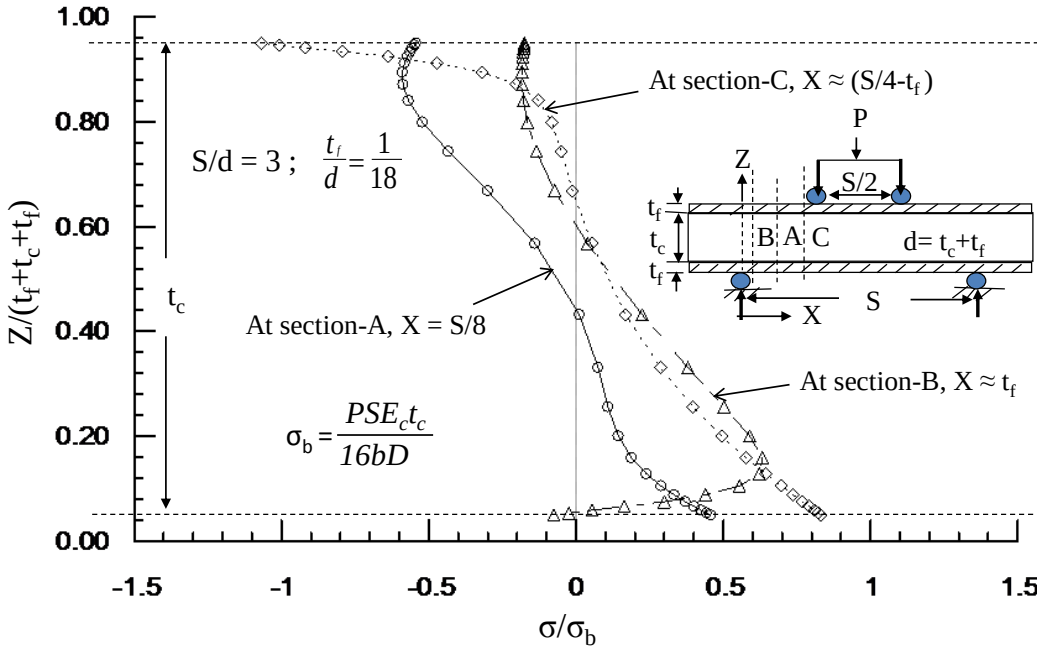

Figure 3.14. Normal stress distribution at section A, B, and C.

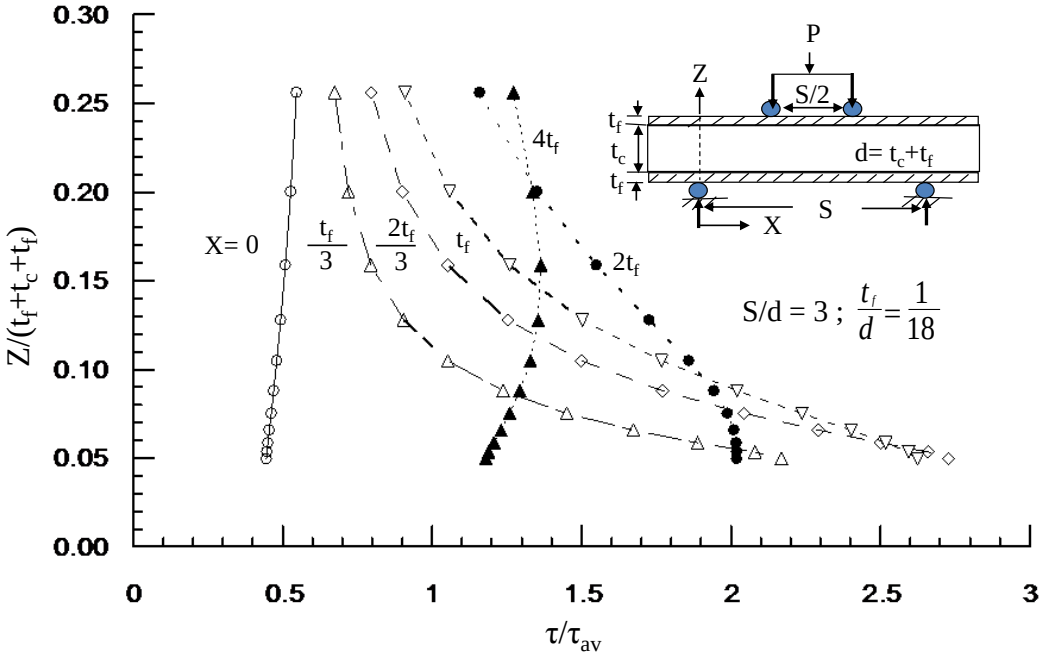

Figure 3.15. Through the thickness shear stress distribution for X= 0, $t_f/3$, $2t_f/3$, t_f, $2t_f$ and $4t_f$.

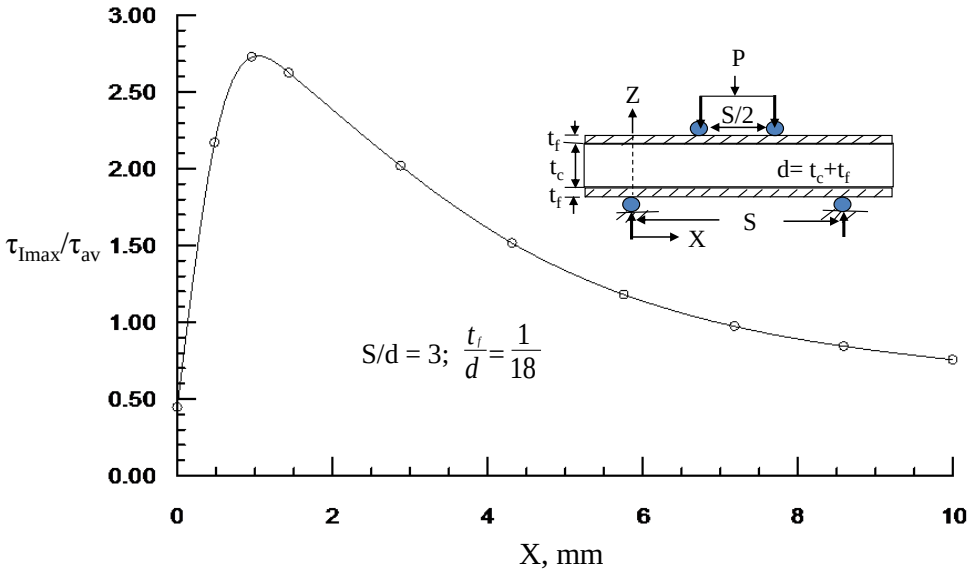

Figure 3.16. Maximum shear stress at the interface against X.

3.7.3 S-N Diagram. Normalized shear stress (τ_{max}/τ_c) versus number of load cycles (N) for 2%, 5%, and 7% compliance change criteria are shown in Figures 3.17a through 3.17c, respectively. Both abscissa and the ordinates are in log-log scale. The log-log fatigue data fits a power law Equation (3.4).

$$\frac{\tau_{max}}{\tau_c} = A_o N^{\alpha} \tag{3.4}$$

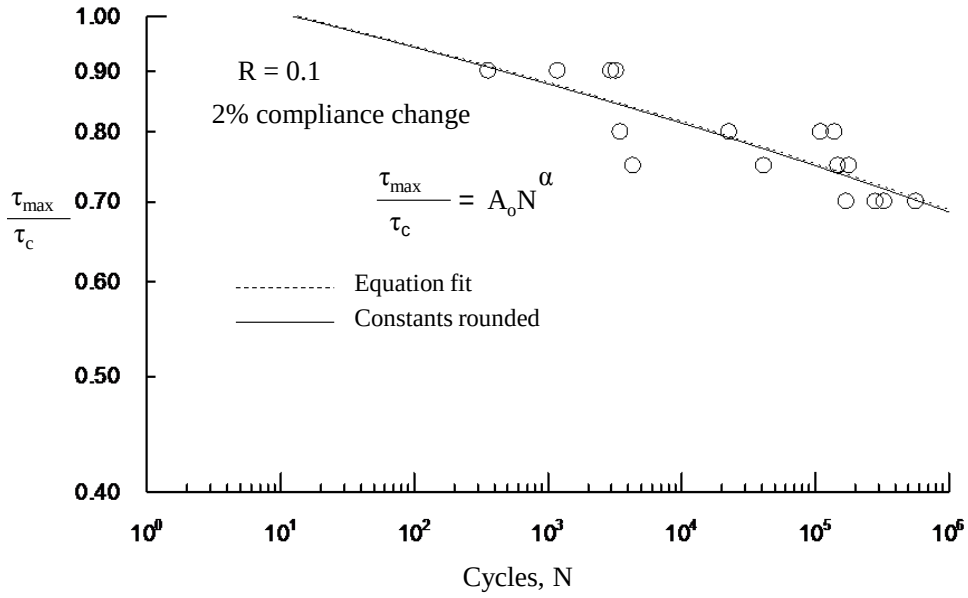

(a) Based on 2% compliance change failure

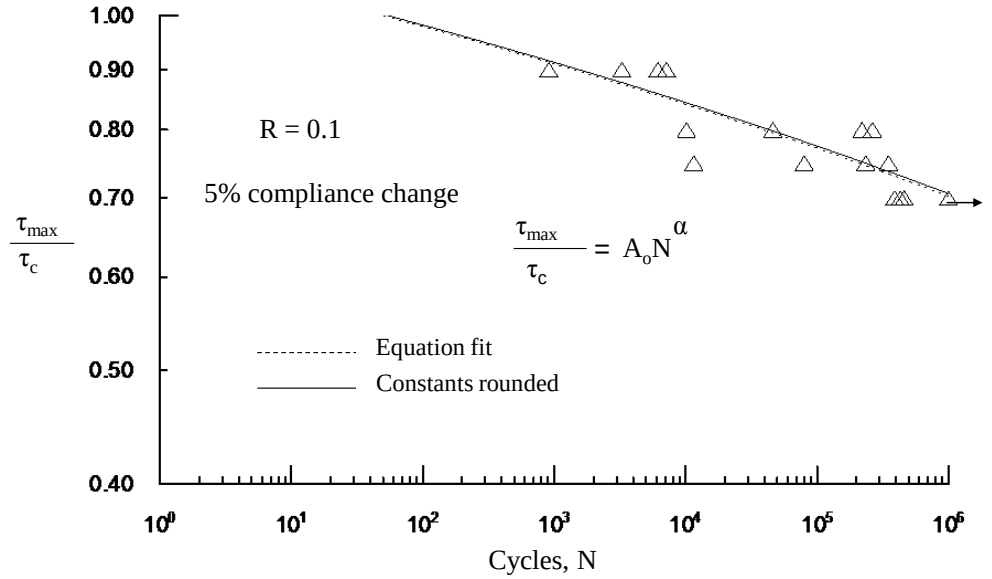

(b) Based on 5% compliance change failure

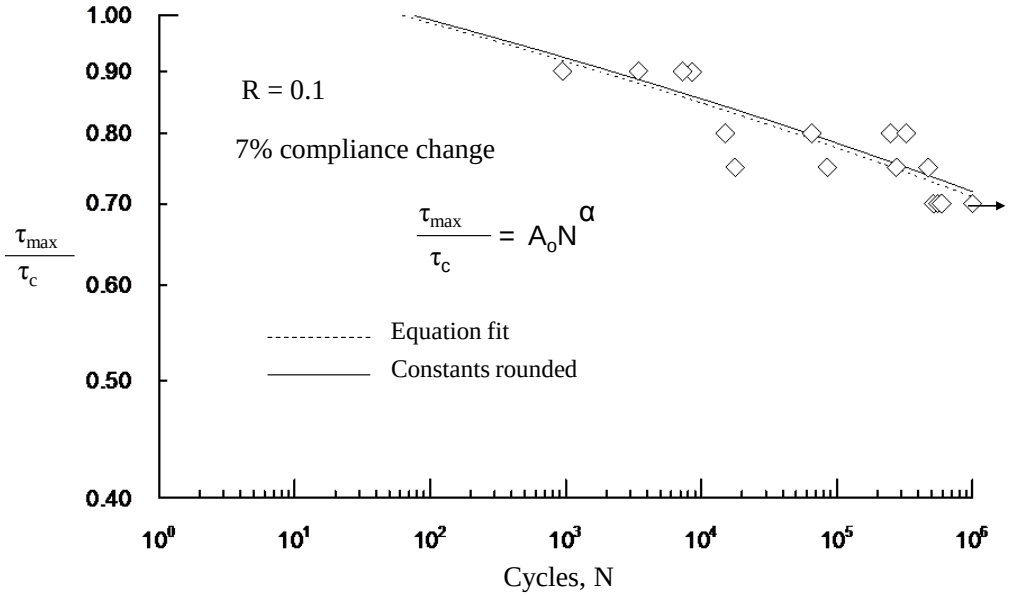

(c) Based on 7% compliance change failure

Figure 3.17. Normalized stress (τ_{max}/τ_c) versus number of load cycles test data and the power law equation for three failure criteria.

A least square equation fit was performed to determine the constants (A_o and α) of the power law for the three types of failure and the values of the constant are listed in Table 3.5. The equation, as fitted, is represented by broken lines. The constants when rounded to two

significants are shown by solid lines. The rounded values of A_o and α fits the original regression equation and the experimental data very well.

Table 3.5

Shear Fatigue Equation Constants

Failure criteria	Constants fitted		Constants rounded	
Compliance change	A_o	α	A_o	α
2%	1.072	-0.0638	1.07	-0.064
5%	1.118	-0.0692	1.12	-0.069
7%	1.125	-0.0693	1.13	-0.069

The constant of A_o is the material property and α is the fatigue degradation rate. Theoretically, when N=1, A_o should be equal to unity and that scenarios is not feasible. A summary of results with the final fatigue equation for the three types of failure is shown in Figure 3.18. The fatigue equation was extrapolated to 10^6 load cycle to determine the endurance limit ($N \geq 10^6$), which is defined as the stress at 10^6 load cycles. This was found to be about $0.68\tau_c$ for onset (2% compliance change), about $0.70\tau_c$ for propagation (5%) and about $0.71\tau_c$ for final failure (7%).

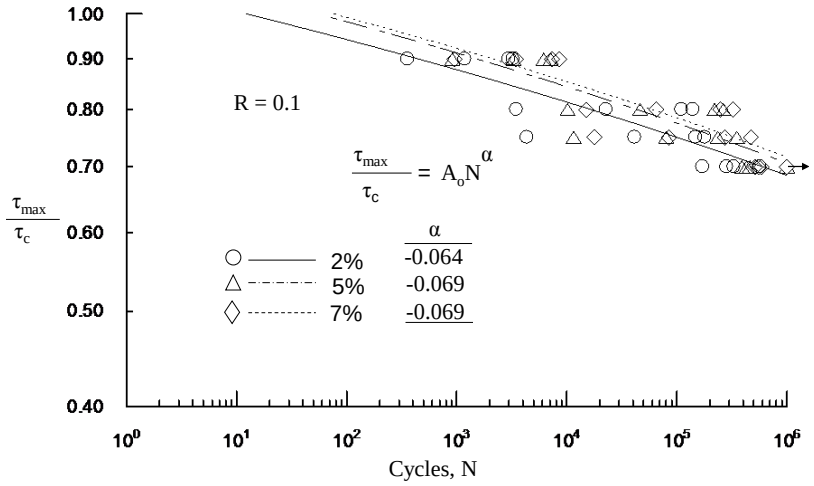

Figure 3.18. Comparison of S-N equation with the experimental data for 2%, 5% and 7% compliance failure criteria.

3.8 Summary

Eco-Core sandwich beams made of woven roving FGI 1854 glass/Vinyl ester face sheet were used to study core shear fatigue performance. The loading frequency was 2Hz with a load ratio R= 0.1. The core density was 0.5 g/cc. Specimen configuration was designed to produce shear failure. Fatigue tests were conducted at τ_{max}/τ_c values of 0.9 to 0.7, where τ_{max} is the maximum cyclic shear stress and τ_c is the shear strength of the Eco-Core, which is 4.23 ± 0.20 MPa.

Shear fatigue failure of Eco-Core sandwich specimen were classified into three types: damage onset, damage progression and ultimate shear failure. These failures were characterized by 2%, 5% and 7% changes in compliance and corresponding life represented the failure lives. The 7% compliance change life is also classified as the total fatigue life of the core material. These three failure are classified a onset of 45^o single shear crack, multiple shear cracks, and multiple shear cracks with an interfacial delamination. The Interfacial delamination is attributed to combination of high interfacial shear stress and tensile bending stress.

The fatigue stress-load cycle (S-N) data followed a well-known power law equation, $\tau_{max}/\tau_c = A_o N^{\alpha}$. The constants A_o and α were established for all three types of failure. Based on 1 million cycles, the endurance limit was found to be $0.68\tau_c$, $0.70\tau_c$ and $0.71\tau_c$, respectively for onset, propagation and ultimate failures.

CHAPTER 4

Flexural Fatigue Characterization

4.1 Introduction

In this chapter, flexural fatigue performance of Eco-Core sandwich beam is described. The static test was conducted following ASTM C393 standard, the same test setup was used for flexural fatigue test. For both static and fatigue flexure tests, Eco-Core sandwich beams made of woven roving FGI 1854 glass/Vinyl ester face sheet were used. The thicknesses of fabricated core (t_c) and face sheet (t_f) were 25.4 mm and 1.50 mm, respectively. The average density of the Eco-Core panel was about 0.52 g/cc. The length and width of the long beam sandwich specimens were 320 mm and 51 mm, respectively. The specimen span (S) was set to 269 mm with an average sandwich thickness (d) of 26.9 mm that results in S/d of 10 and t_f/d of 1/18. Flexural fatigue test was conducted using sinusoidal loading with a frequency of 2 Hz and stress ratio R of 0.1. Tests were conducted at different stress levels (σ_{max}/σ_{ct}), where σ_{max} is the maximum cyclic bending stress in the core and σ_{ct} is the bending tensile strength of the core. A PC based data acquisition system was used to store fatigue load, stroke displacement and time. This data were converted to compliance and number of cycles, which was then used to create compliance-number of cycles curves. As previously explained, the fatigue failure was characterized by damage onset, progression and final failures. These failures were found to be equivalent to compliance change of 1%, 5% and 7%, respectively and corresponding number of cycles reflected the fatigue lives for damage onset, progression and final failure. This number of cycles data was used to determine S-N relationship. The macro-scale fatigue failure mechanism was investigated by analyzing the damage images of the test samples taken from beginning to end of the test.

4.2 Material System

Eco-Core sandwich panels were fabricated first preparing Eco-Core panels from fly ash and phenol-formaldehyde resole binder resin. Then fabricating FGI 1854 glass fiber/vinyl ester composite laminate and bonding the face sheets on top and bottom face sheets of the Eco-Core using a room temperature cure. Details of the fabrication of sandwich panels are given in chapter 3, section 4.

4.3 Design of Specimen

Flexural test specimen was designed as per the guidelines given in the reference [12] and using the material properties given in Table 3.1 in chapter 3. The Eco-Core properties were taken from reference [11] and the composite face sheet properties were taken from reference [83]. Transverse shear modulus of face sheet listed in Table 3.1 in chapter 3 and in reference [12] was assumed. It should be noted that compressive strength and modulus of Eco-Core listed in Table 3.1 is slightly different from that is listed in [79]. In that study, the average value of compressive strength and modulus was 19.61 MPa and 1.65 GPa, respectively. In designing the specimen, Eco-Core was treated as isotropic and the face sheet as orthotropic. Four point loaded sandwich beam was selected to avoid direct contact of the load on the core material and reduce the stress concentration under the load point. The direct load contact with solid core may lead to premature failure under load points by cyclic loading due to indentation and rubbing of loading rollers on the material. The specimen geometric parameters are defined in Figure 4.1 and the parameters are defined in chapter 3, section 3.

The nominal thicknesses of the core and face sheet are 25.4 mm and 1.40 mm, respectively and the width of the specimen is 51 mm. The design equation for core shear and core tension failure is similar to those derived in chapter 3 by equations 3.1 and 3.2, respectively.

Because the loading is one-third point loading, expression for the maximum bending moment is PS/6 (Figure 4.1 c) instead of PS/8, which leads an expression for maximum bending stress in the core is given by

$$\sigma_{max} = \frac{P_f S t_c E_{ct}}{12 D b} \tag{4.1}$$

Or the normalized failure load, P_f is given by

$$\frac{P_f}{b} = \frac{12 D \sigma_{ct}}{S t_c E_{ct}} \tag{4.2}$$

where, t_c, σ_{ct} and E_{ct} are the core thickness, core tensile strength and modulus, respectively. D and b are the flexural rigidity and width of the sandwich beam, respectively.

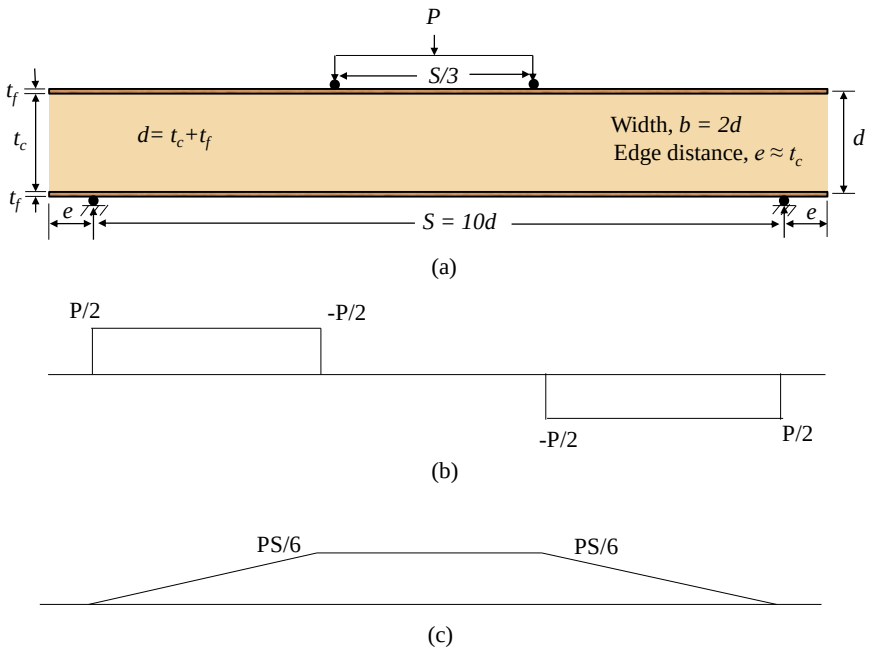

Figure 4.1. (a) Schematic of test specimen, loading and nomenclature (b) Shear force diagram (c) Bending moment diagram.

Normalized failure loads for core shear and core tension failure criteria are shown in Figure 4.2 as a function of span to depth (*S/d*) ratio. The core shear failure is represented by a horizontal broken line and core tension failure (σ_{ct} = 6.46 MPa based on tension test value) by a solid line. Intersection of the two lines represents the potential for both failures. The two curves

intersect at S/d = 3.5. Therefore, S/d of 10 was selected so that core tension failure is the dominant failure mode and also the specimen length is short enough to conduct fatigue test using the existing test fixtures.

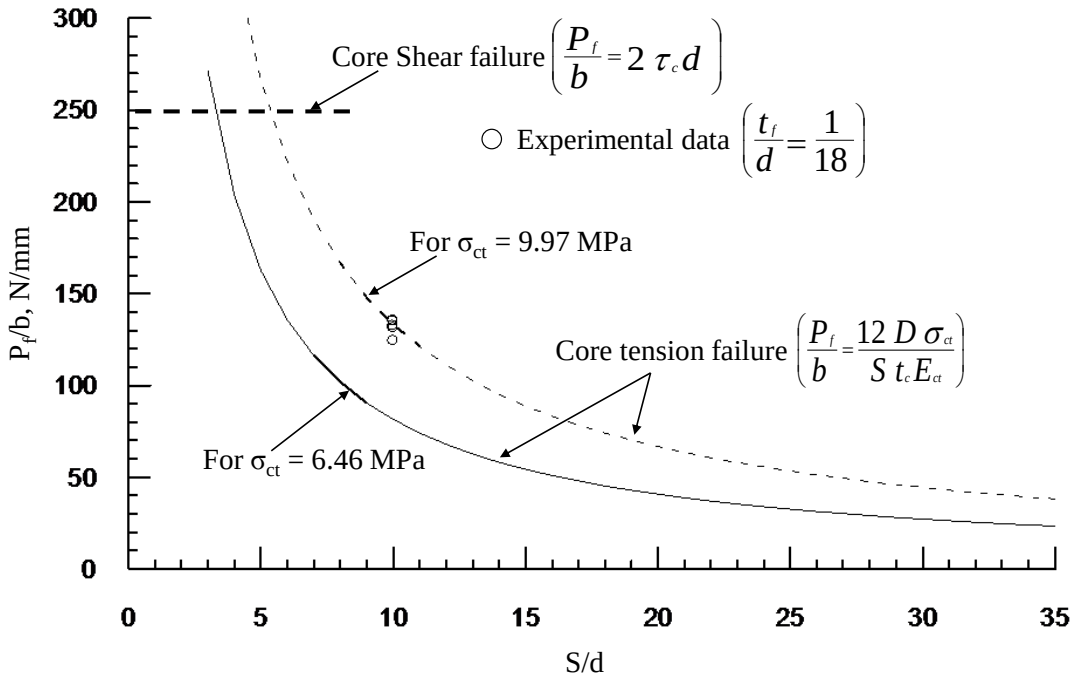

Figure 4.2. Failure load versus span/depth(S/d) ratio for Eco-Core sandwich beam based on shear and flexural failure criteria.

4.4 Static Flexural Test and Results

Static flexural tests were performed to validate the core tension strength used in design of test specimen and identify the core failure modes. The test was conducted using an MTS servo-hydraulic test machine following ASTM C393 by applying four-point loading (Figures 4.1). A deflection transducer (LVDT) was placed under the specimen at the mid span for direct measurement of deflection (Figure 4.3). The specimen was loaded at a constant cross-head speed of 1.27 mm/min (0.05in/min). Load and deflection were recorded at every one-half second and the associated failure modes were monitored by a high speed camera. Five specimens were tested. The specimen number, geometric parameters, and failure loads of all tested specimens

were recorded and listed in Table 4.2. Figure 4.4 shows the load-deflection response of the tested specimens. Figure 4.4a shows the response for all five tested specimens and Figure 4.4b shows the detailed response for the specimen FSP-20. Each load drop in Figure 4.4b indicates a formation of crack. The maximum load before the first load drop (#1) represent the first vertical flexural crack appeared in the tension side of the core (between the load points) was considered as the flexural failure load of the core. As load increased additional cracks formed between the load-span, their sequence is represented by white lines in Figure 4.5 and also mapped in Figure 4.4b. All these cracks started at the bottom interface between the core and face sheet, and propagated up to about mid-thickness of the core and stopped. The final failure was started by forming a tension crack under one of the load points followed by a 45^o shear crack near that load point and then ultimate failure by interfacial delamination, see Figure 4.5d and also in Figure 4.4b. Similar failure modes were observed by Shivakumar and Chen [12].

Table 4.1

Flexural Static Test Results

Specimen ID	Specimen geometry				$d= t_c+t_f$, mm	Failure Load, N	Strength,MPa
	S, mm	b, mm	t_c,mm	t_f, mm			
FSP-20	269	51.0	25.4	1.5	26.9	6761	10.03
FSP-11	269	51.2	25.4	1.5	26.9	6939	10.26
FSP-16	269	50.9	25.4	1.5	26.9	6872	10.22
FSP-28	269	51.1	25.4	1.5	26.9	6352	9.41
FSP-04	269	51.2	25.4	1.5	26.9	6716	9.94
Average						6728	9.97
STD						228	0.34
SEM						102	0.15

The specimens FSP-20, FSP-11, FSP-16 and FSP-04 failed at nearly the same load whereas specimens FSP-28 had slightly lower failure load. The flexural core strength (σ_{cl}) of all tested specimens was calculated using the Equation (4.3) and is listed in Table 4.1. In measuring

the flexural strength, the core tensile modulus (E_c) of 2.54 GPa and flexural rigidity (D) of 19.01 MN.mm were used.

$$\sigma_{ct} = \frac{P_f S t_c E_c}{12 D b} \tag{4.3}$$

The average flexural strength (σ_{ct}) was 9.97MPa (1.446ksi) with a standard error mean (SEM) of 0.15MPa (0.02ksi). This strength value is 54% larger than that of Shivakumar et al. [12] data, where core tensile strength measured by uniaxial tension test of Eco-Core sample of core density 0.47 g/cc. The present result was from flexural test and the average core density was 0.52 g/cc. The density and the test method difference may be the reason for difference in strengths. The flexural design curve P_f/b versus span for the new value of flexural strength (9.97 MPa) is shown by the broken line in the Figure 4.2. Symbols represent the test data. This experimental data is used for designing specimen for fatigue test.

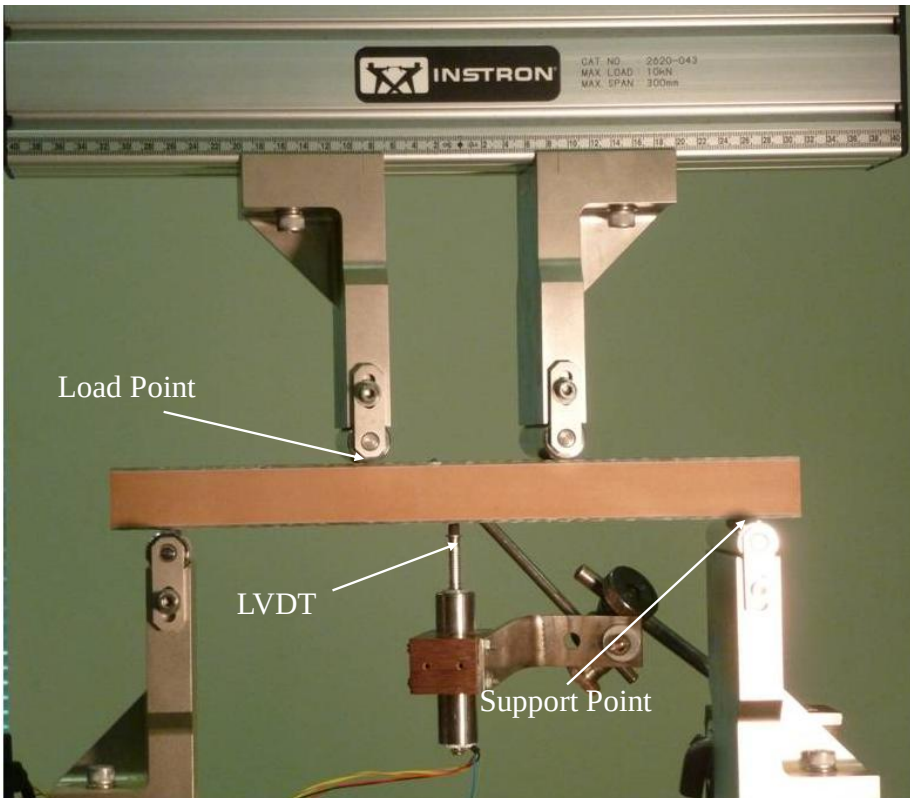

Figure 4.3. Flexural test setup.

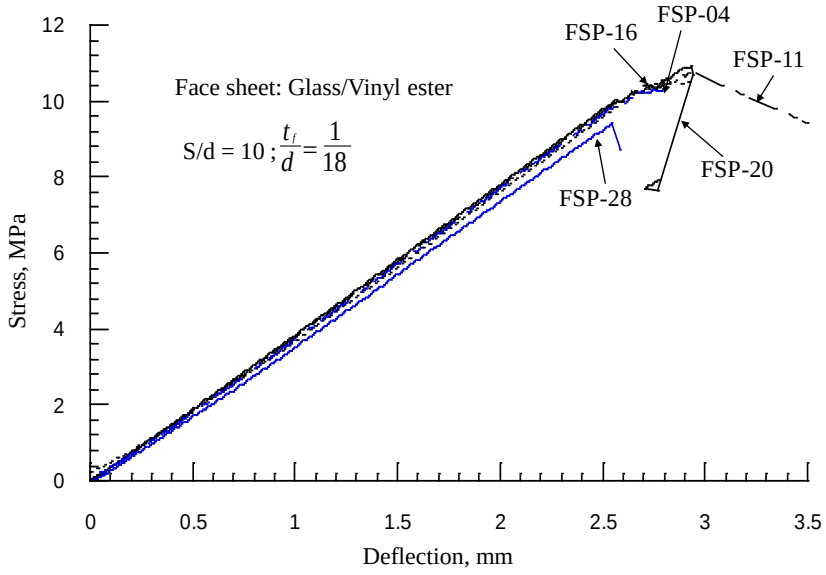

(a) For all tested specimens

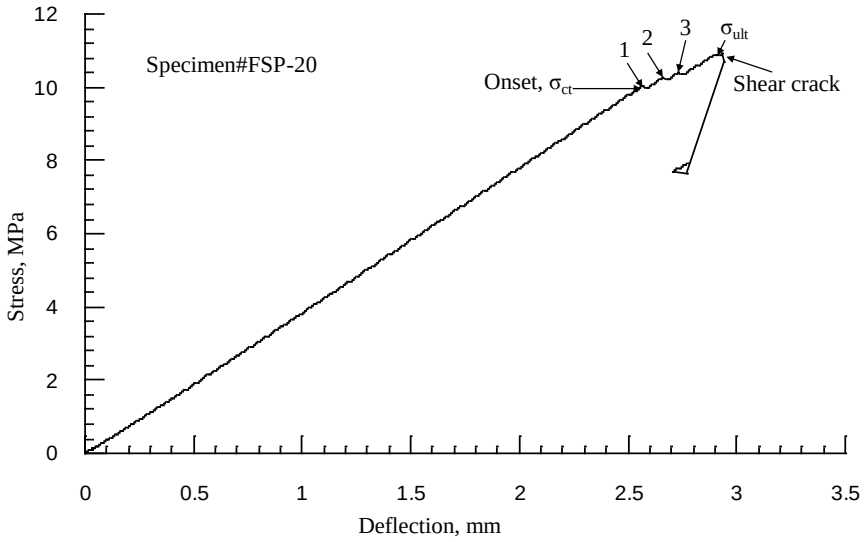

(b) Details for the specimen # FSP-20

Figure 4.4. Stress versus deflection responses of flexural tests.

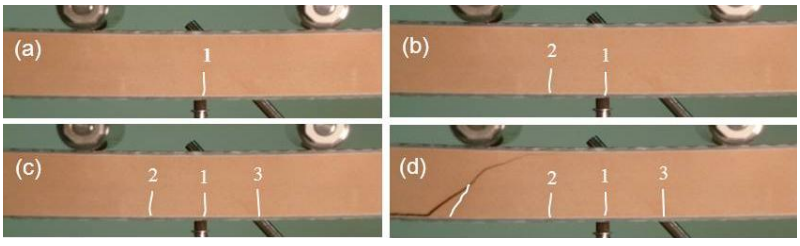

Figure 4.5. Typical static failure modes in Eco-Core sandwich beam specimen FSP-20 (Crack is highlighted by white line).

4.5 Stress Analysis Near Face Sheet-Core Interface Region

A 2-D finite element analysis (FEA) of the test sandwich beam was conducted to understand the stress field near the critical location. Details of the FEA are given in the Appendix A. Here only required figures are shown to explain the possibility of final core shear failure followed by core-face sheet interfacial debond in fatigue testing.

Figure 4.6 shows the shear stress distribution through the thickness of the core material (no face sheet) at three locations between the support and load point and in the symmetric region (see in insert picture). The location B and C are about t_f distance from the support and load points, respectively. As expected, the shear stress distribution at B and C are reflection of each other about the mid-plane. The maximum shear stress is about $2.6\tau_{av}$ at the core-face sheet interface. The shear stress at A at half-way between support and load points is symmetric about the mid-plane and nearly flat curve as expected in sandwich beams (depending on the relative modulus of face sheet and core). The maximum shear stress is about $1.1\tau_{av}$. These results conclude that if the shear failure occurs at mid-way between the support and load points, the failure is due to maximum shear at the mid-plane of the beam. If the failure occurs near the support or load point, the failure may be because of shear concentration at the interface. Because the interface is resin densified, the interfacial strength could be much higher than the core shear strength. Because of symmetry, the shear stresses at section D are zero. So, if there is any failure between two loading points, it will be due to bending stresses.

To examine the state of normal stress near the interface, the bending stresses plotted through the thickness at the same three sections (A, B, C and D) in Figure 4.7. As clearly shown that the bending stress near the interface of the section B is tensile (before it becomes compressive at the interface) while the bending stress at C is tensile at tension side and it is

nearly same as that at section D. Hence the hypothesis is that combination of shear stress and high tensile stress near the load point at section C may the reason for initiation of tension crack followed by shear crack under one of the load points in fatigue loading.

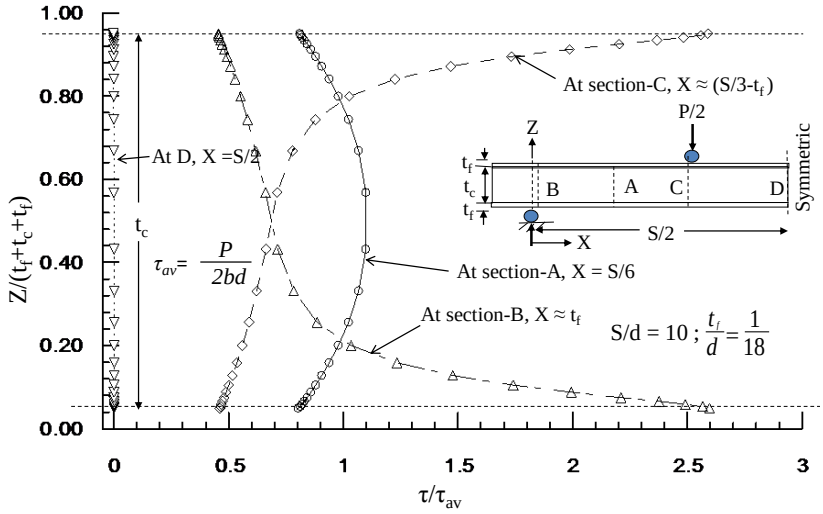

Figure 4.6. Shear stress distribution at section A, B, and C.

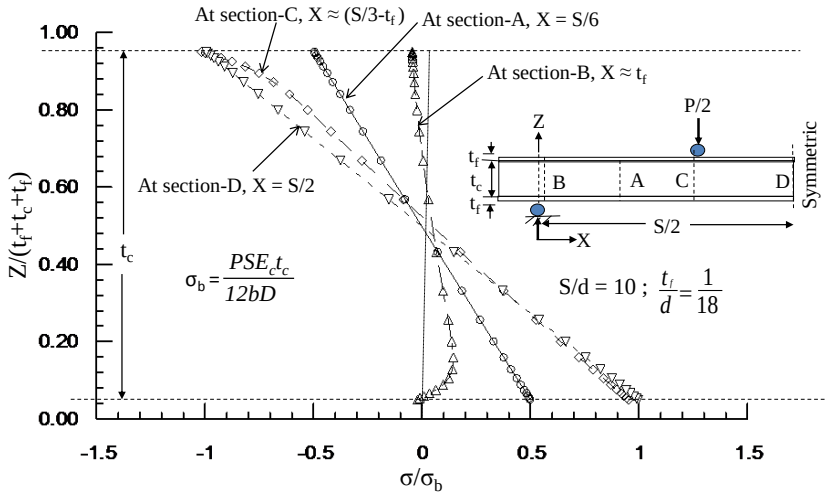

Figure 4.7. Normal stress distribution at section A, B, and C.

4.6 Fatigue Test

Flexural fatigue tests were conducted under a sinusoidal cyclic load of frequency 2Hz and stress ratio R = 0.1. The test setup was similar as used for static test. Typical flexural cyclic loading is shown in Figure 4.8.

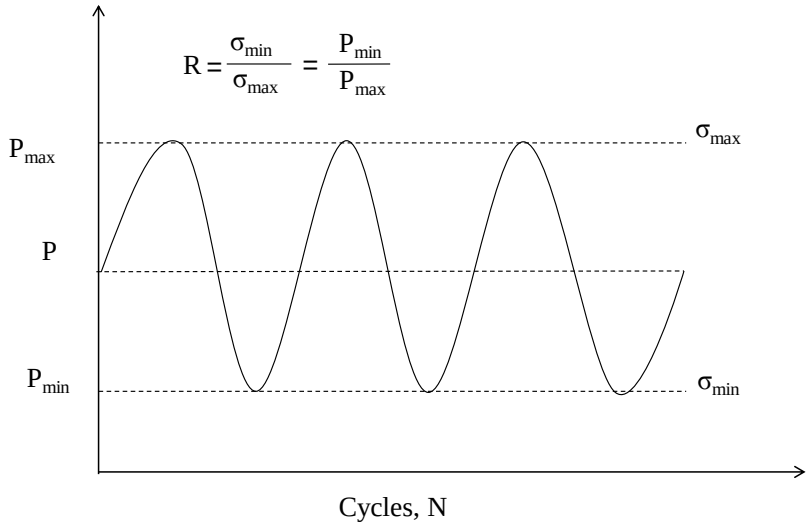

Figure 4.8. Typical flexural fatigue loading (R=0.1).

The endurance limit requirement depends on the application, which generally range 10^7-10^9 cycles for marine applications. Because of limitations of equipment and test time, the testing was limited to 10^6 cycles and the 10^6 cycles was used as the endurance limit for analysis of the results. Four different stress levels (σ_{max}/σ_{ct}) in the range of 0.9 to 0.7 were chosen, where σ_{max} is the maximum cyclic flexural stress in the core material. For each stress level, four specimens were tested. The specimen number and loading are listed in Table 4.2. Load, stroke displacement and time were recorded using a PC based data acquisition system. Data acquisition procedure was different for each stress level (σ_{max}/σ_{ct}). For σ_{max}/σ_{ct} = 0.9, data were collected for 5 seconds at every one minute intervals, for σ_{max}/σ_{ct} = 0.8, the data were collected for 5 seconds at every 2 minute intervals. For σ_{max}/σ_{ct} = 0.75 and 0.70, data were collected for 5 seconds at every five minute intervals. Times recorded in seconds during cyclic loading were converted to cycles by multiplying time by two (2Hz loading frequency) to obtain number of cycles. The load and displacements recorded were converted into the compliance, which is the ratio of change in displacements and the change in loads between the consecutive maximum and minimum loads for a single load cycle and is defined by

$$\text{Compliance} = \frac{d_{max} - d_{min}}{P_{max} - P_{min}} \quad (4.4)$$

where, d_{max} is the displacement for the maximum applied load P_{max} and d_{min} is the displacement for minimum applied load P_{min} for a single cycle.

To investigate the macro-scale fatigue failure, a digital camera was set up close to the specimen to record the failure mode. Since each fatigue test lasted for hours to days, images were taken only for selective intervals between the beginning and end of the test (unstable failure). The image sequences were then analyzed to understand the fatigue failure and its mechanisms.

Table 4.2

Flexural Fatigue Test Plan for R=0.1(σ_{ct} = 9.97 MPa)

Specimen ID	σ_{max}/σ_{ct}	σ_{max}, MPa	Thickness t_c, mm	Width b, mm	Span S, mm	P_{max}, N
FSP-02	0.90	8.97	25.4	51.2	269	6062
FSP12			25.4	51.4	269	6093
FSP-24			25.4	51.2	269	6069
FSP-17			25.4	51.2	269	6062
FSP-03	0.80	7.98	25.4	51.1	269	5380
FSP-06			25.4	51.4	269	5420
FSP-10			25.4	51.3	269	5407
FSP-21			25.4	51.5	269	5423
FSP-09	0.75	7.48	25.4	51.3	269	5065
FSP-29			25.4	51.3	269	5065
FSP-23			25.4	51.2	269	5055
FSP-22			25.4	51.2	269	5060
FSP-05	0.70	6.98	25.4	51.4	269	4739
FSP-08			25.4	51.3	269	4725
FSP-18			25.4	51.1	269	4713
FSP-14			25.4	51.4	269	4739

4.7 Fatigue Test Results and Discussions

4.7.1 Failure definition and associated failure lives. The fatigue failure was characterized by change in compliance which is similar to strength or stiffness reduction models. Figure 4.9 shows compliance versus number of fatigue load cycles of the test specimen FSP-21

for a flexural loading of $\sigma_{max}/\sigma_{ct} = 0.80$. The compliance plots for other samples were similar and are presented in appendix D.1 through D.3. The compliance response was found to be divided into three types: failure onset, progression and ultimate failure. The three failures were characterized by three different values of compliance change, namely, 1%, 5% and 7%, similar the values were used in compression [79] and shear [82] fatigue tests. Except, here 1% compliance change criteria was used for failure onset, because this failure was clear with a formation of vertical flexural cracks. Each of these compliance changes was represented by different stages of damage formation. The 1% compliance change can be usually associated with the formation of a vertical crack in the core on tension region of the specimen, specifically between the two load points. The 5% compliance change can be represented the accumulation of damage by formation of multiple vertical cracks between two load points of four-point test. Finally, the 7% compliance change can be represented by a formation of 45^o shear crack in the core under one of the load points in the beam. Selection of these compliance limits was based on the profile of the compliance versus number of load cycles (See Figure 4.9). The number of load cycles required to cause each of the compliance change is called fatigue life. According to the three compliance changes (1%, 5% and 7%), there are three fatigue lives which are represented by $N_{1\%}$, $N_{5\%}$ and $N_{7\%}$, respectively (See Figure 4.9). A small variation of these values has minimal impact on the fatigue lives.

The Figure 4.10 shows the fatigue failure mode of Eco-Core sandwich specimen FSP-21. The white lines represent the crack pattern. The first image (a) was taken before loading the specimen; image (b) was taken just after the formation of first vertical crack (about 1% compliance change); images (c) and (d) were taken for successive formation of multiple vertical cracks (within 5% compliance change). Each vertical crack matches with the compliance jump in

Figure 4.9. Image (e) was taken after the formation of 45^o shear crack under one of the loading points in tension side. Image (f) was taken after the shear crack linked between top and bottom face sheets. The linking of shear crack with top and bottom face sheet is happened mostly around 7% compliance change in the specimen. The damage sequences were similar for all the tested specimens. Therefore, typical flexural fatigue failure of Eco-Core sandwich beam is by formation of single vertical crack, multiple vertical cracks in the core in tension side between two load points and followed by a 45^o shear crack in the core under one of the load points, which finally reach the two ends of the core. This behavior is similar to that of static flexural failure of Eco-Core sandwich beams.

Table 4.3

Flexural Fatigue Test Results for R=0.1(σ_{ct} = 9.97 MPa)

Specimen ID	σ_{max}/σ_{ct}	Cycles when test stopped	Cycles for compliance change			No of Cycles at1st crack
			$N_{1\%}$	$N_{5\%}$	$N_{7\%}$	
FSP-02	0.90	16,846	1,208	5,998	16,074	1,225
FSP12		5,708	1,519	2,429	4,735	458
FSP-24		6,625	2,410	4,754	6,257	2,400
FSP-17		3,048	420	2,677	2,979	486
FSP-03	0.80	37,158	7,288	21,324	32,114	7,315
FSP-06		467,469	12,186	64,845	273,429	1,096
FSP-10		122,285	9,162	24,227	101,742	8,953
FSP-21		101,146	1,425	28,025	97,940	1,288
FSP-09	0.75	1,000,000	78,986	689,900	1,000,000	23,000
FSP-29		502,418	71,834	297,576	458,139	67,213
FSP-23		630,323	64,047	299,991	598,766	59,823
FSP-22		1,000,000	79,117	690,566	1,000,000	41,720
FSP-05	0.70	1,000,000	235,280	1,000,000	1,000,000	164,900
FSP-08		1,000,000	327,223	1,000,000	1,000,000	518,000
FSP-18		1,000,000	192,747	793,615	1,000,000	313,200
FSP-14		607,595	73,250	444,130	575,328	130,000

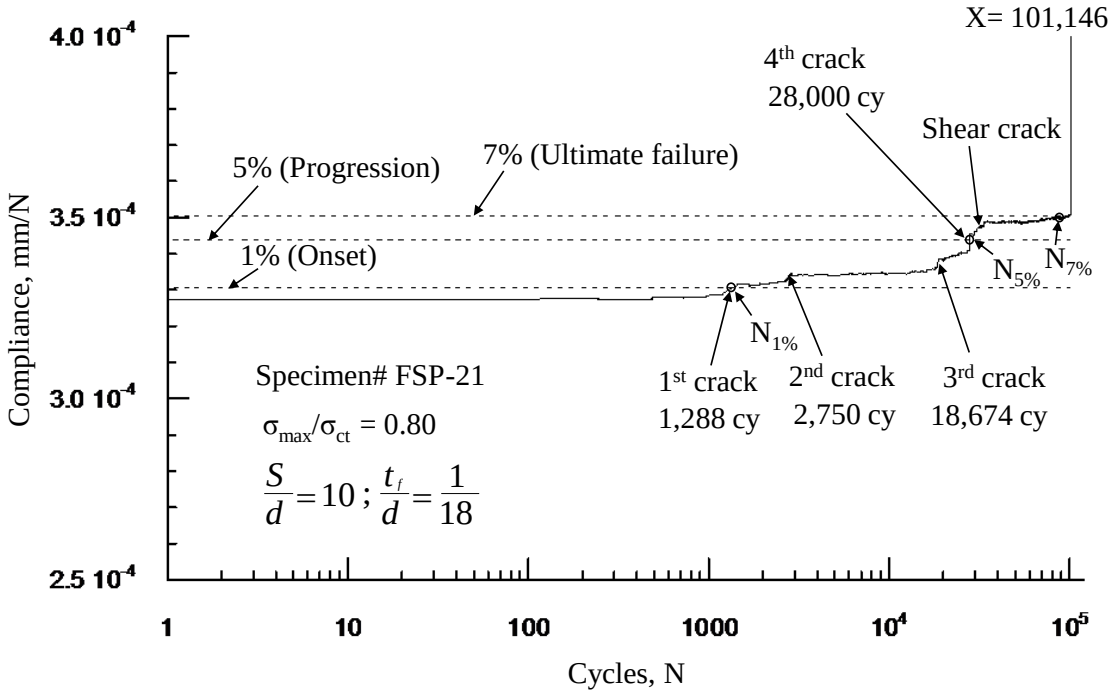

Figure 4.9. Compliance versus number of fatigue cycles (N) and the fatigue lives based on the three values (1%, 5% and 7%) of compliance change failure criteria.

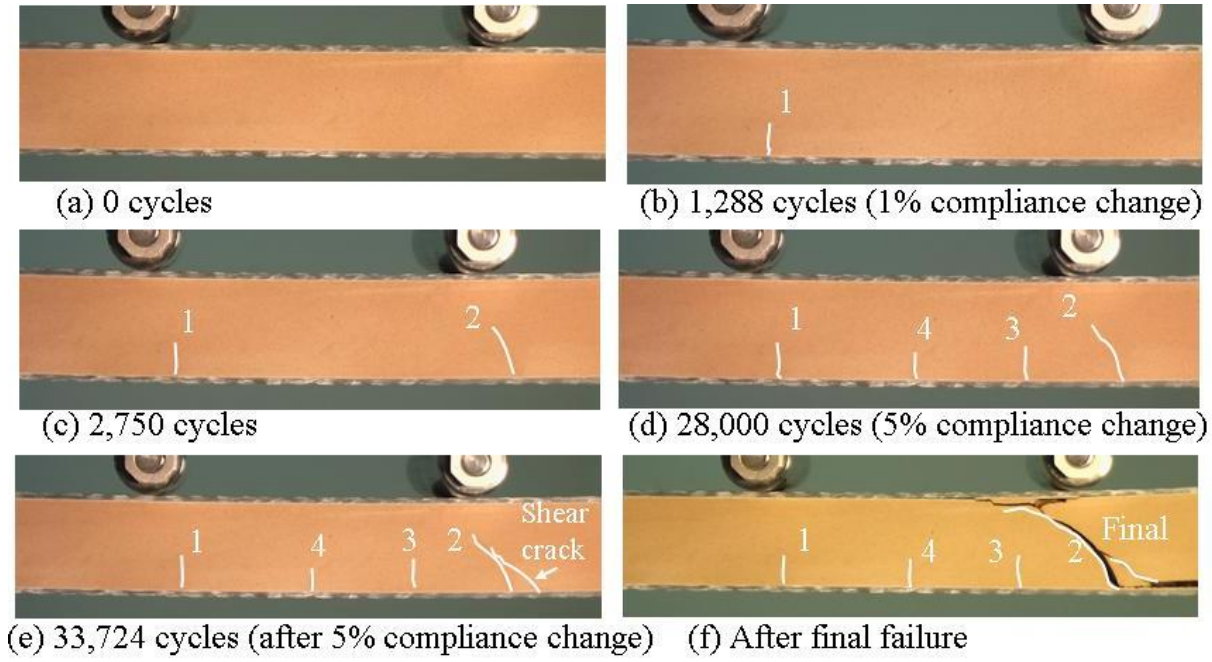

Figure 4.10. Typical flexural fatigue failure sequence of a specimen (FSP-21) for σmax/σct = 0.80 (crack is highlighted by white line).

4.7.2. S-N diagram. The fatigue load cycles (N) for 1%, 5%, and 7% change in compliance for different stress values of tested specimens are listed in Table 4.3. The same data are plotted in Figure 4.11a through 4.11c for onset (1% compliance change), propagation (5%) and ultimate failure (7%), respectively. The normalized maximum tensile stress (σ_{max}/σ_{ct}) and number of load cycles (N) were plotted in log-log scale, a typical of fatigue data representation. The test data was fit a power law equation (4.5) using a least square regression.

$$\frac{\sigma_{max}}{\sigma_{ct}} = A_o N^{\alpha} \tag{4.5}$$

Here A_o is the material property constant and the exponent, α is the slope of the log-log curve represents the fatigue degradation rate. Theoretically, when N=1, A_o should be equal to unity and this scenario is not feasible. The computed values of A_o and the exponent α for all three cases of failure are listed in Table 4.4. The values of α were nearly the same for damage onset and progression but for final failure it is slightly higher. The constant A_o shows an ascending trend from onset to final failure. The Table 4.4 also lists the final rounded values of A_o and α. The rounded α values are -0.071, -0.074 and -0.079 for damage onset, progression and ultimate failure, respectively. This indicates that flexural strength degradation rate of the core increases with increasing damage. The broken and solid lines in Figure 4.11 represent the equation (4.5) using raw values and rounded values of A_o and α, respectively. Both fits agree with the experimental data. The final fatigue equation for the three types of failure along with experimental data is shown in Figure 4.12. The fatigue equation was extrapolated to 10^6 load cycle to calculate the endurance limit ($N \geq 10^6$). The endurance value was found to be about $0.65\sigma_{ct}$ for onset (1% compliance change), about $0.70\sigma_{ct}$ for propagation (5%) and about $0.71\sigma_{ct}$ for final failure (7%). The equation could be extrapolated to 10^7 and 10^8 cycles but there is no data is available to validate the equation.

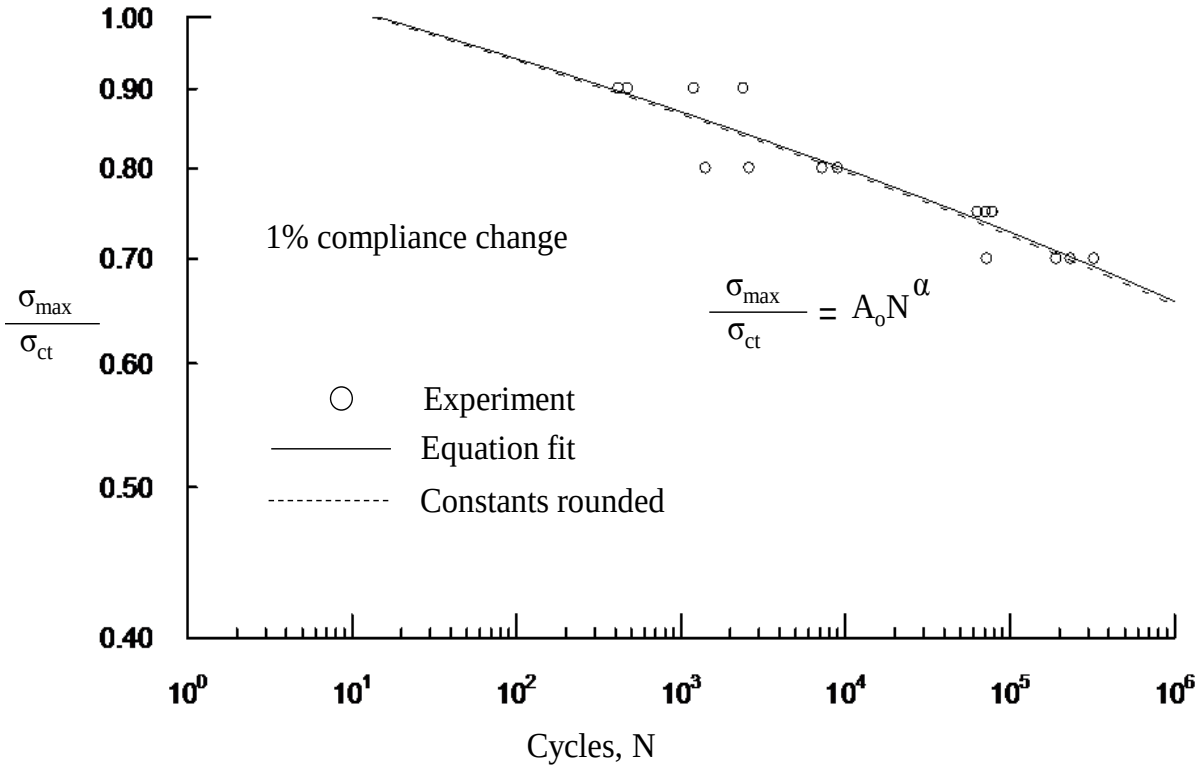

(a) Based on 1% compliance change failure criteria

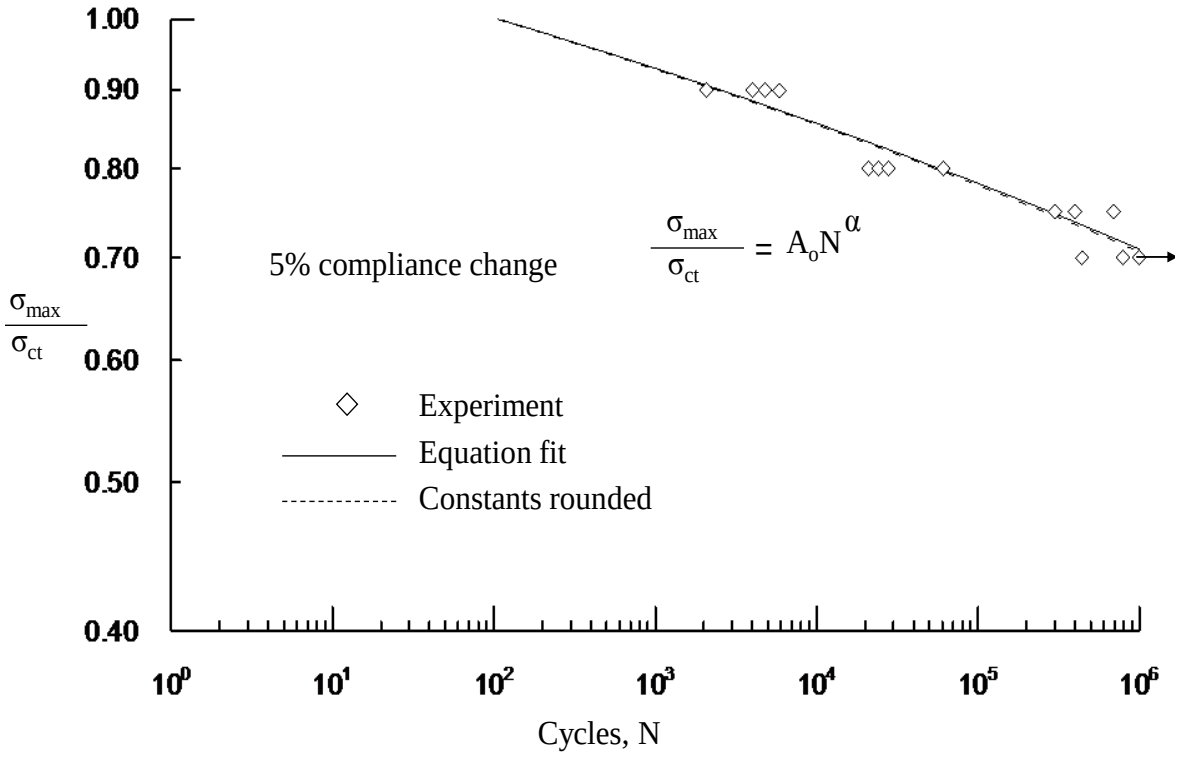

(b) Based on 5% compliance change failure

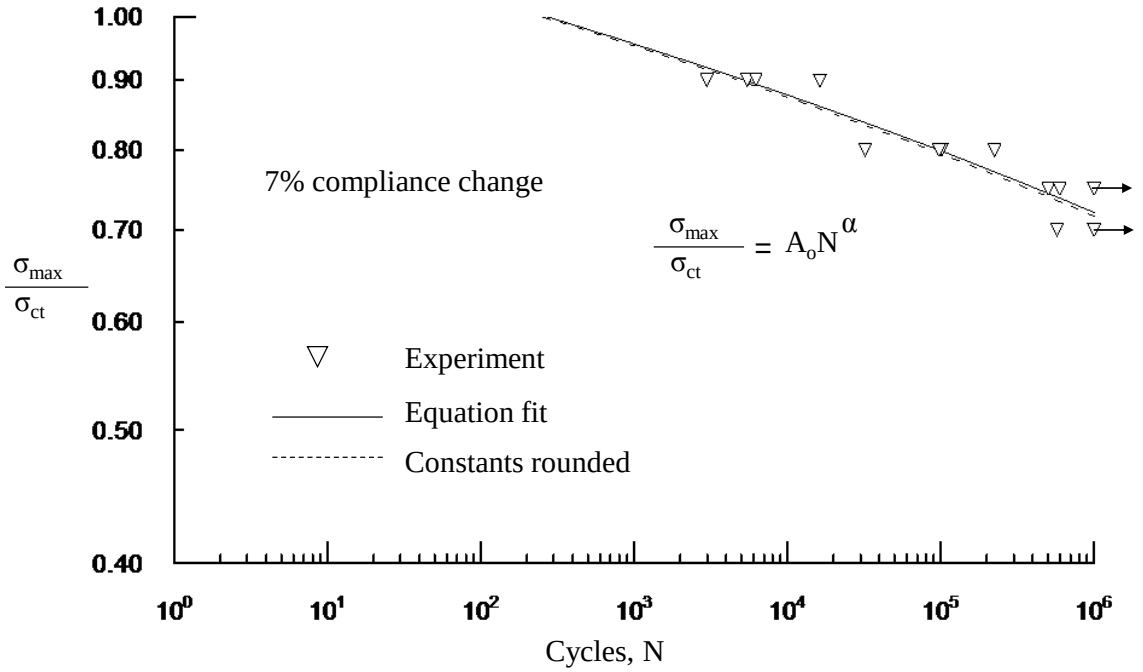

(c) Based on 7% compliance change failure

Figure 4.11. Comparison of normalized stress σmax/σct versus number of load cycles from experiment and equation for 1%, 5% and 7% change in compliance failure criteria.

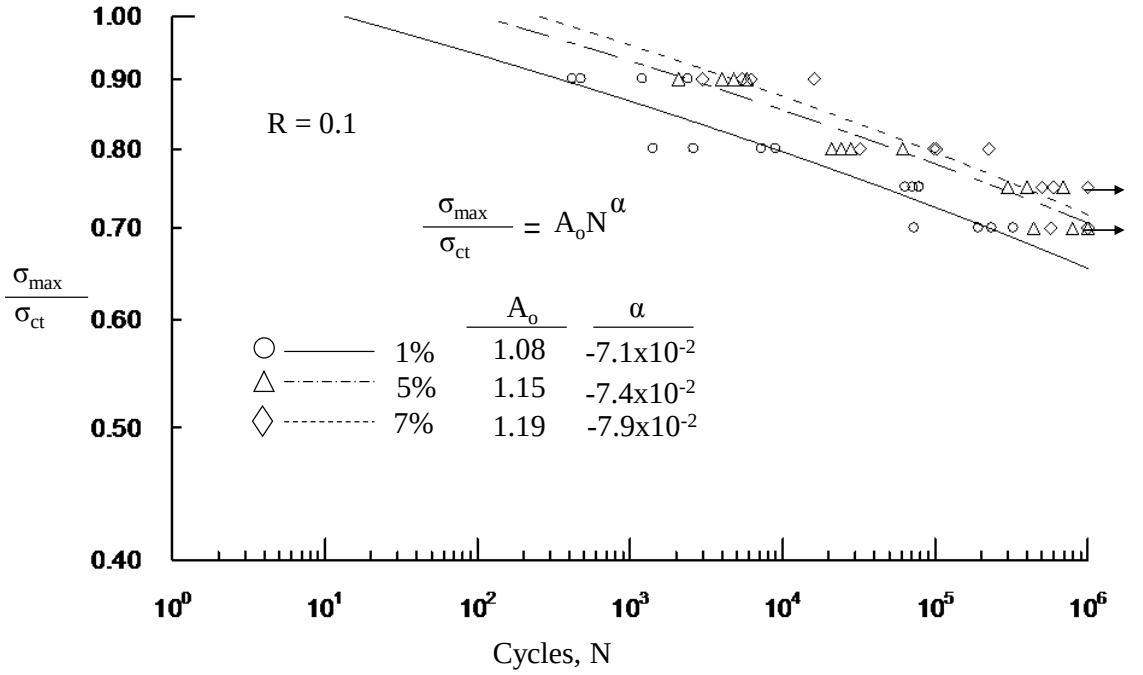

Figure 4.12. Comparison of modified stress versus number of cycle equation with the experiment for the three failure criteria.

Table 4.4

Flexural Fatigue Equation Constants

Failure criteria	Constants fitted		Constants rounded	
Compliance change	A_o	α	A_o	α
1%	1.0825	-0.0708	1.08	-0.071
5%	1.1498	-0.0735	1.15	-0.074
7%	1.1914	-0.0785	1.19	-0.079

4.8 Summary

Eco-Core sandwich beams made of woven roving FGI 1854 glass/Vinyl ester face sheet and a fire resistant Eco-Core were used to study core flexural fatigue performance. The loading frequency was 2Hz with the load ratio R= 0.1.The Eco-Core density was ranging from 0.515 g/cc to 0.522 g/cc with an average bulk density of 0.518 g/cc. Specimen configuration was designed to produce core tension failure. Static flexural tests were conducted using ASTM C393 to verify the core tension strength (σ_{ct}) that was found to be 9.97 ± 0.15 MPa for the specimen produced in this study. This is about 54% higher than the uniaxial tensile strength of the material that was reported previously. The failure modes were tension cracks in the core followed by shear failure.

Fatigue tests were conducted at σ_{max}/σ_{ct} values of 0.9 to 0.7, where σ_{max} is the maximum cyclic flexural stress. The fatigue test setup was same as used for static test. The study showed that flexural fatigue failure mode of Eco-Core material was by first formation of vertical cracks in the core in tension side followed by a formation of 45^o shear crack in the core under one of the load points. These failure modes are similar to that of static flexural failures. Flexural fatigue failure of Eco-Core sandwich beam occurred in three stages: damage onset, damage progression and ultimate failure. These failures were characterized by 1%, 5% and 7% changes in compliance and associated number of cycles as their failure lives. The 7% compliance change was considered to be total fatigue life of the core.

The fatigue stress-load cycle (S-N) data followed the well-known power law equation, $\sigma_{max}/\sigma_{ct} = A_o N^{\alpha}$. The constants A_o and α were established for all three types of failures. The damage degradation rate increased with damage state of the core material. Based on 1 million cycles, the endurance limit was found to be $0.65\sigma_{ct}$, $0.70\sigma_{ct}$ and $0.71\sigma_{ct,}$ respectively for damage onset, propagation and ultimate failure.

CHAPTER 5

Concluding Remarks and Recommendation for Future Work

5.1 Conclusions

Eco-Core is a special class of syntactic foam made by high volume of flyash and a small volume of phenolic resin, where flyash is collected from coal burn thermal power plants. Because of very low volatile content in the mixture, it has demonstrated to be a fire resistant material for composite sandwich structures applications. Except for one flexure fatigue article on general class of syntactic foam, there is no other article on fatigue characterization of syntactic foams. Therefore, a comprehensive fatigue characterization of fire resistant Eco-Core materials was undertaken. Three stress states were considered, namely, compression-compression, shear and flexural stress states. Compression fatigue was performed directly on Eco-Core cylindrical specimen, whereas the shear and flexure fatigue were performed using E glass-Vinyl ester face sheet sandwich beam specimen to avoid direct load contact and avoid wear damage between the support rollers. The Eco-Core specifics of the study and the conclusions are summarized in the following sections. The endurance limit was determined based on one million load cycles because of limitation of test equipment and duration of test that required more than 1 million cycles. All tests were conducted in a load control mode with loading frequency of 2 Hz and core specimen density of about 0.5 g/cc. The load, displacement and time were recorded continuously using a PC based data acquisition system. From this data, compliance versus number of load cycles was generated. Edge of the specimen was imaged in regular interval to document the damage modes of onset, progression and final failure for both static and fatigue tests.

5.1.1 Compression-compression fatigue. Compression-Compression fatigue study on Eco-Core was conducted for two values of stress ratios (R= 10 and 5). Tests were conducted at

maximum compression stress (σ_{min}) varied from 60% to 90% of compression strength (σ_c) for R=10 and 80% to 95% of compression strength for R=5. The compression strength of Eco-Core depends on the material density and its value for panels 1 and 2 were 18.9 ± 0.13 MPa and 20.3 ± 0.00 MPa, respectively with the average values of two panels was 19.6 ± 0.25 MPa. The study showed that Eco-core has well defined failure modes and associated fatigue lives. The failure modes were classified into: damage on-set; damage progression, and final failure.

- Damage on-set was characterized by formation of a single crush band at the middle or at top or bottom edge of the specimen; damage progression was characterized by crush band propagation, and final failure was characterized by 7% increase in compliance. Damage onset and progression were characterized by 2% and 7% increase in compliance. The number of load cycles required for these three compliance changes are defined as onset life, progression life and total life, respectively. The three failure modes were found to be same for both static and fatigue loadings.
- The stress versus number of load cycles (S-N) data followed a well-defined power law equation, $\sigma_{min}/\sigma_c = A_o N^{\alpha}$. Constants of the equation were established for all three modes of failures.
- Based on 1 million cycles, the endurance limit was found to be $0.72\sigma_c$, $0.75\sigma_c$ and $0.76\sigma_c$, respectively, for on-set, propagation and final failure for R=10 while it is $0.81\sigma_c$, $0.82\sigma_c$ and $0.82\sigma_c$, respectively, for R=5.
- Finally, compression-compression fatigue life was found to be dependent on cyclic stress range similar to a behavior that of metallic materials.

5.1.2 Shear fatigue. Shear fatigue performance of Eco-Core sandwich beam was studied using a specimen of span to depth ratio of three and load ratio of R= 0.1. Normalized maximum

shear stress (τ_{max}/τ_c) was ranging from 0.7 to 0.9. Shear fatigue failure of Eco-Core sandwich specimen were also classified into three types: damage onset, damage progression and ultimate shear failure. Each of these failures corresponds to 2%, 5% and 7% changes in compliance. Shear failure initiated as a 45^o angle of single shear crack and progressed to multiple shear cracks that spanned between top and bottom face sheets. At low fatigue shear stress a core-face sheet interfacial delamination were also found.

- The fatigue stress-load cycle (S-N) data found to follow the well known power law equation, $\tau_{max}/\tau_c = A_o N^{\alpha}$. The constants A_o and α were established for all three types of failure.
- Based on 1 million cycles, the endurance shear strength was found to be $0.68\tau_c$, $0.70\tau_c$ and $0.71\tau_c$, respectively for onset, propagation and ultimate failure.

5.1.3 Flexural fatigue. Flexural fatigue performance of Eco-Core sandwich beam was studied using a specimen with a span-depth ratio of 10 and load ratio of 0.1. This specimen configuration was found to produce core tension failure The Eco-Core bulk density was slightly higher and it was about 0.52 g/cc. Fatigue tests were conducted at normalized maximum stress σ_{max}/σ_{ct} ranged from 0.7 to 0.9, where σ_{ct} is the flexural strength of Eco-Core and it was found to be 9.97 ± 0.15 MPa.

The study showed that flexural fatigue failure mode was by first formation of vertical tension cracks in the core between the load points of the four-point bend specimen, and then followed by a formation of 45^o shear crack in the core under one of the load points. Fatigue failure modes were found to be similar to that of static flexural failure of the beam. Flexure failure modes were classified into three types: damage onset, damage progression and ultimate failure. These failures were found to be associated with 1%, 5% and 7% increase in compliance. Note that the on-set compliance change reduced to 1% in contrast to 2% in compression and shear failure because the

flexure failure was clear.

- The fatigue stress-load cycle (S-N) data followed the well-known power law equation, $\sigma_{max}/\sigma_{ct} = A_o N^{\alpha}$. The constants A_o and α were established for all three types of failures.
- Based on 1 million cycles, the endurance limit was found to be $0.65\sigma_{ct}$, $0.70\sigma_{ct}$ and $0.71\sigma_{ct,}$ respectively, for onset, propagation and ultimate failures.
- A detailed finite element stress analysis of shear and flexure specimens was conducted to understand the stress states at failure. Final failure of the shear specimen could also be associated with both high interfacial shear stress and bending stress at the interface between the core and face sheet. For flexure specimen, it was due to combination of high bending stress and interfacial shear stress.

5.2 Recommendations for Future Works

5.2.1 Development of new test method for high cyclic frequency loading. Eco-Core material is developed to use sandwich structural applications. This core has a potential to be used in marine, aerospace and transport industries as a fire and toxicity safe structural core. Generally, life of these structures range from 30-50 years yielding on 10^7-10^9 load cycles. Determining the endurance limit of these numbers of cycles will take months to years for each specimen. Conventional hydraulic system may not be suitable for such tests. Therefore, a suitable test method apparatus needs to be developed so that an experiment is completed in a reasonable time period.

5.2.2 Development of fatigue life prediction model for variable amplitude loading. The constant amplitude fatigue life model was developed for Eco-Core in compression, shear and flexure stress states was based on constant amplitude loading. But for practical applications, these models have to be extended and validated for variable amplitude loading.

5.2.3 Extend the study to tension-compression loading. Most structures also experience tension-compression stress during their life cycles. Unfortunately, the test fixture to apply tension-compression loading is difficult to design, fabricate and operate. Such a test fixture needs to be developed and validated. Then it can be extended to tension-compression fatigue loading.

References

1. Argade, S., Shivakumar, K., Sadler, R., Sharpe, M., Swaminathan, G., and Sorathia, U. (2004). Mechanical fire resistance properties of a core Material. SAMPE 2004, May 16-20, Long Beach, CA.
2. Landrock, A. (1995). Handbook of plastic foams: types, properties, manufacture, and applications: William Andrew Publishing.
3. Lee, S. (1993). Handbook of composite reinforcements: VCH Publishers, Inc
4. d'Almeida, J. (1999). An analysis of the effect of the diameters of glass microspheres on the mechanical behavior of glass-microsphere/epoxy-matrix composites. Composites science and technology, Vol.59, pp. 2087-2091.
5. Gupta, N., Priya, S., Islam, R., Ricci, W. (2006). Characterization of mechanical and electrical properties of epoxy-glass microballoon syntactic composites. Ferroelectrics, Vol.345,pp. 1-12.
6. Gupta, N., Woldesenbet, E. and Mensah, P. (2004). Compression properties of syntactic foams: effect of cenosphere radius ratio and specimen aspect ratio. Composites Part A: Applied Science and Manufacturing, Vol. 35(1), pp. 103-111.
7. Gupta, N. and Woldesenbet, E. (2004). Microballoon wall thickness effects on properties of syntactic foams. Journal of cellular plastics, Vol. 40,pp. 461-480.
8. Devi, K., John, B., Nair, C.P., Ninan, K.N. (2007). Syntactic foam composites of epoxy-allyl phenol-bismaleimide ternary blend—Processing and properties. Journal of applied polymer science, Vol.105, pp. 3715-3722.
9. Rizzi, E., Papa, E., and Corigliano, A. (2000). Mechanical behavior of a syntactic foam:experiments and modeling. International Journal of Solids and Structures, Vol.37,

pp. 5773-5794.

10. Kim, H.S. and Oh, H.H (2000). Manufacturing and impact behavior of syntactic foam. Journal of applied polymer science, Vol.76, pp. 1324-1328.
11. Shivakumar, K., Argade, S.D, Sadler R.L., Sharpe. M.M., Dunn, L, Swaminathan, G,, Sorathia, U. (2006). Processing and Properties of a lightweight Fire Resistant Core Material for Sandwich Structures. Journal of Advanced Materials, Vol. 38, pp. 32-38.
12. Shivakumar, K. and Chen, H. (2010). Structural Performance of Eco-Core Sandwich Panels. Major Accomplishments in Composite Materials and Sandwich Structures, pp. 381-406.
13. Gupta, N., Karthikeyan, C. and Sankaran, S. (1999). Correlation of processing methodology to the physical and mechanical properties of syntactic foams with and without fibers. Materials characterization, Vol.43,pp. 271-277.
14. Karthikeyan, C., Sankaran, S. and Kumar, J. (2001). Processing and compressive strengths of syntactic foams with and without fibrous reinforcements. Journal of applied polymer science, Vol.81,pp. 405-411.
15. Panduranga, R., Shivakumar, K. and Russell, Jr L. (2007). Energy Absorption Performance of Eco-Core–A Syntactic Foam, *48th AIAA/ASME/ASCE/AHS/ASC Structures, Structural Dynamics, and Materials Conference,* April 23-26, Honolulu, HI.
16. Panduranga, R., Russell, Jr L., and Shivakumar, K. (2007). Fracture toughness enhancement of flyash based Eco-Core by glass fiber reinforcement, 22nd annual technical conference of the American Society for Composites, September 17-19, Seattle, WA.
17. John, B., Nair, C. and Ninan, K. (2010). Effect of nanoclay on the mechanical, dynamic mechanical and thermal properties of cyanate ester syntactic foams. Materials Science and Engineering: A, Vol.527,pp. 5435-5443.

18. Nji, J. and Li, G. (2008). A CaO enhanced rubberized syntactic foam. Composites Part A: Applied Science and Manufacturing, Vol.39,pp. 1404-1411.
19. Kireitseu, M., Hui, D. and Tomlinson, G. (2008). Advanced shock-resistant and vibration damping of nanoparticle-reinforced composite material. Composites Part B: Engineering, Vol.39, pp. 128-138.
20. Gui, M.C., Wang, D.B., Wu, J.J., Yuan, G.J. and Li, C.G. (2000). Deformation and damping behaviors of foamed Al–Si–SiC composite. Materials Science and Engineering: A, Vol.286,pp. 282-288.
21. Sauvant-Moynot, V., Gimenez, N. and Sautereau, H. (2006). Hydrolytic ageing of syntactic foams for thermal insulation in deep water: degradation mechanisms and water uptake model. Journal of materials science, Vol.41,pp. 4047-4054.
22. Shutov, F. (1983). Foamed polymers. Cellular structure and properties. Industrial Developments, pp. 155-218.
23. Li, G. and John, M. (2008). A self-healing smart syntactic foam under multiple impacts. Composites science and technology, Vol.68, pp. 3337-3343.
24. Boyd, J., Sitt, H., Ryang, H. and Blermann, T. (1990). Structures exhibiting improved transmission of ultrahigh frequency electromagnetic radiation and structural materials which allow their construction, Google Patents.
25. Shutov, F., Klempner, D. and Frisch, K. (1991). Handbook of Polymeric Foams and Foam Technology. New York: Hanser Publishers, 1991. 381.
26. Sorathia, U. and Perez, I. (2004). Improving the fire safety of composite materials for naval applications. SAMPE 2004, May 16-20, Long Beach, CA.
27. Shutov, F. (1986). Syntactic polymer foams.Chromatography/Foams/Copolymers, pp.

63-123.

28. Sadler, R.L., Sharpe, M., Panduranga, R., and Shivakumar, K. (2009). Water immersion effect on swelling and compression properties of Eco-Core, PVC foam and balsa wood. Composite Structures, Vol. 90, pp. 330-336.
29. Paepegem, W., Degrieck, J.(2002). Effects of load sequence and block loading on the fatigue response of fiber-reinforced composites. Mechanics of Advanced material Structure, Vol.9, pp.19-35.
30. Harris, B., Gathercole, N., Reiter, H. and Adam, T. (1997). Fatigue of Carbon-fibre-reinforced plastics under block-loading conditions. Composite Part A, Vol.28, pp. 327-337.
31. Gamstedt, E.K. and Sjogren, B.A. (2002). An experimental Investigation of the Sequence Effect in Block Amplitude Loading of Cross-ply Composite Laminates, Int Journal of Fatigue, Vol. 24, pp. 437-446.
32. Philippidis, T., Vassilopoulos, A. (2004). Life prediction methodology for GFRP laminates under spectrum loading. Composite Part A- Applied Science, Vol. 35, pp. 657-666.
33. Philippidis, T., Vassilopoulos, A. (1999). Fatigue strength prediction under multiaxial stress, Journal of Composite material, Vol. 33, pp. 1578-1599.
34. Philippidis, T., Vassilopoulos, A. (2002). Complex stress state effect on fatigue life of GRP laminates. Part 11: Theoretical formulation, International Journal of Fatigue, Vol. 24, pp. 825-830.
35. Philippidis, T., Vassilopoulos, A. (2004). Fatigue of glass fibre reinforced plastics under complex stress states, In the Handbook of Advanced Materials: Enabling New Designs, J Wessel, ed., Wiley- Inter science.
36. Clark, S.D., Shenoi, R.A. and Allen, H.G. (1999). Modeling the fatigue behavior of

sandwich beams under monotonic, 2-step and block loading regimes, Composite Science and Technology, Vol. 59, pp. 471-486.

37. Brunner, A.J., Murphy, N., Pinter, G. (2009). Development of a standardized procedure for the characterization of interlaminar delamination propagation in advanced composites under fatigue mode 1 loading conditions. Engineering Fracture Mechanics, Vol. 76, pp. 2678-2689.
38. Kadi, H., Ellyin, F. (1994). Effect of stress ratio on the fatigue failure of fiberglass reinforced epoxy laminae. Composites, Vol. 25, pp. 917-924.
39. Saff, C. (1983). Effect of load frequency and lay-up on fatigue life of composites, in Long-Term Behavior of Composites, ASTM STP 813, TK O'Brien, ed., pp.78-91.
40. Sun, C.T., Chan, W.S. (1979). Frequency effect on the fatigue life of laminated composite, in Composite Materials: Testing and Design (fifth conference), ASTM STP 674, SW Tsai, ed., pp. 418-430.
41. Rotem, A.(1993). Load frequency effect on the fatigue strength of isotropic laminates. Composite Science Technology, Vol. 46, pp. 129-138.
42. Burman, M. and Zenkert, D. (1997). Fatigue of Foam Core Sandwich Beams-1: Undamaged Specimens, International Journal of Fatigue, Vol. 19(7), pp. 551-561.
43. Shenoi, R.A., Clark, S.D. and Allen, H.G. (1995). Fatigue behavior of polymer composite sandwich beams, Journal of Composite Materials, Vol. 29, pp. 2423-2446.
44. Sharma, S.C., Murthy, H.N.N. and Krishna, M. (2004). Interfacial studies in fatigue behavior of polyurethane sandwich structures, Journal of reinforced plastics and composites, Vol. 23, pp. 893-903.
45. Annual Book of the ASTM Standards, American Society for Testing and Materials, ASTM Intenational, West Conshohocken, PA.

46. ISO 844 (2004). Rigid cellular plastics-Determination of Compression Properties.

47. Sims G.D. Fatigue test methods, problems, and standards, In Fatigue in Composites, B Harris , ed., Woodhead Publishing, pp. 36-62.

48. Kanny, K. and Mahfuz, H. (2005). Flexural fatigue characteristics of sandwich structures at different loading frequencies. Composite Structures, Vol.67, pp. 403-410.

49. Burman, M. and Zenkert, D. (1997). Fatigue of foam core sandwich beams-1: Undamaged specimens. International Journal of Fatigue, Vol.19, pp.551-561.

50. Burman, M. and Zenkert, D. (1997). Fatigue of foam core sandwich beams-2: Effect of initial damage. International Journal of Fatigue, Vol. 19(7), pp. 563-578.

51. Zenkert, D. and Murman, M. (2009). Tension, compression and shear fatigue of a closed cell polymer foam. Composite Science and Technology, Vol. 69, pp. 785-792.

52. Zenkert, D. and Burman, M. (2011). Failure mode shifts during constant amplitude fatigue loading of GFRP/foam core sandwich beams. International Journal of Fatigue, Vol.33, pp. 217-222.

53. Sendeckyj, G. P. (19991). Life prediction for resin-matrix composite materials. Composite Materials Series, Vol. 4, pp. 431-483.

54. Dai, J. and Hahn, H.T. (2004). Fatigue analysis of sandwich beams using a wear-out model. Journal of Composite Materials, Vol.38, pp. 581-589.

55. Wu, W.F., Lee, L.J. and Choy, S.T. (1996). A study of fatigue damage and fatigue life of composite laminates, Journal of Composite Materials, Vol. 30, pp. 123-137.

56. Philippidis, T. and Vassilopoulos, A. (1999). Fatigue of composite laminates under off-axis loading, International Journal of Fatigue, Vol. 21, pp. 253-262.

57. Whitworth, H.A. (1998). A stiffness degradation for composite laminates under fatigue

loading, Composite Structures, Vol. 40, pp. 95-101.

58. Judawisastra, H., Ivens, J. Verpoest, I. Fatigue of 3D sandwich fabric composites under core shear loading, ICCM 12.
59. Mahi, A., Farook, K., Sahraoui, S. and Bezazi, A. (1992). Modeling the flexural behavior of sandwich composite materials under cyclic fatigue, Materials & design, Vol. 25, pp. 199-208.
60. Degrieck, J. and Paepegem, W. (2001). Fatigue damage modeling of fiber-reinforced composite Material: review, Applied Mechanics Review, Vol. 54, pp. 279-299.
61. Epaarachchi, J. and Clausen, P. (2005). A new cumulative fatigue damage model for fiber reinforced plastic composites under step/discrete loading, Composites: Part A, Vol. 36, pp. 1236-1245.
62. Zenkert, D. and Burman, M. (2010). Fatigue of a closed-cell foams in compression, Journal of Sandwich Structures and Materials, Vol. 13, pp. 467-478.
63. Harte, A.M., Fleck, N.A. and Ashby, M.F. (1999). Fatigue Failure of An Open Cell and A Closed Cell Aluminium alloy Foam. Acta mater Vol. 47, pp. 2511-2524.
64. Zhou, J., Soboyejo, W.O. (2004). Compression-Compression fatigue of open cell aluminum foams: macro-/micro-mechanisms and the effects of heat treatment. Mater Sci and Eng A Vol. 369, pp. 23-35.
65. Sugimura, Y., Rabiei, A., Evans, A.G., Harte, A.M. and Fleck, N.A. (1999). Compression Fatigue of a Cellular Al Alloy. Mater Sci and Eng Vol. 269, pp.38-48.
66. Hakamada, M., Kuromura, T., Chino, Y., Yamada, Y.,Chen, Y., Kusuda, H., Mabuchi, M. (2007). Monotonic and cyclic compressive properties of porous aluminum fabricated by spacer method. Materials Science and Engineering A Vol. 459, pp. 286-293.
67. Kolluri, M., Mukherjee, M., Garcia-Moreno, F., Banhart, J., Ramamurty, U. (2008).

Fatigue of laterally constrained closed cell aluminum foam. Acta Materialia. Vol. 56, pp. 1114-1125.

68. Amsterdam, E., Hosson, J.T.M.D., Onck, P.R. (2006). Failure Mechanisms of closed-cell aluminum foam under monotonic and cyclic loading. Acta Materialia. Vol. 54, pp. 4465-4472.
69. Thomson, R., Khan, M., Mouritz, A. (1998). Shear properties of sandwich composite containing defects, Composite Structures, Vol. 42, pp. 107-118.
70. Harte, A., Fleck, N., Ashby, M. (2001). The fatigue strength of sandwich beams with an aluminum alloy foam core, International Journal of Fatigue, Vol. 23, pp. 499-507.
71. Dai, J., Hahn, H. (2003). Flexural behavior of sandwich beams fabricated by vacuum-assisted resin transfer molding, Composite Structures Vol. 61, pp.247-253.
72. Kulkarni, N., Mahfuz, H., Jeelani, S., Carlsson, LA. (2003). Fatigue crack growth and life prediction of foam core sandwich composites under flexural loading. Comp Struct Vol. 59, pp. 499-505.
73. Kanny, K., Mahfuz, H.,Carlsson, L., Thomas, T. and Jeelani, S. (2002). Dynamic mechanical analysis and flexural fatigue of PVC foams. Composite Structures Vol. 58, pp. 175-183.
74. Kanny, K., Mahfuz, H., Thomas, T. and Jeelani, S. (2004). Temperature effects on the fatigue behavior of foam core sandwich structures, Polymers and Polymer Composites, Vol.12, pp. 551-559.
75. Shenoi, R. A., Clark, S.D. and Allen, H.G. (1995). Fatigue behavior of polymer composite sandwich beams, Journal of Composite Materials Vol. 29, pp. 2423-2445.
76. Freeman, B., Schwingler, E., Mahinfalah, M., Kellogg, K. (2005). The effect of low-velocity impact on the fatigue life of sandwich composite, Composite Structures Vol.70, pp. 374-381.

77. Ferreira J.A.M., Salviano K., Costa J.D. and Capela, C. (2010). Fatigue behavior in hybrid hollow microspheres/fibre reinforced composites. J Mater Sci Vol. 45, pp. 3547-3553.

78. Panduranga, R. (2010). High strain response of Eco-Core and its modification, PH.D. Dissertation, Mechanical Engineering Department, North Carolina A&T State University, Greensboro, NC.

79. Hossain, M.M., and Shivakumar, K. (2011). Compression Fatigue Performance of a Fire Resistant Syntactic Foam, Comp. Struct. Vol. 94, pp. 290-298.

80. Smith, S., Shivakumar, K. (2000). Evaluation of Interfacial Fracture Toughness of VARTM Sandwich Panels using the Mode-1 cracked Beam Specimen, AIAA-2000-1493.

81. Sadler, R., Shivakumar, K., Sharpe, M. (2002). Interlaminar fracture properties of split angle-ply composites, Proceedings of the SAMPE Technical Conference and Exhibition, Long-Beach, CA.

82. Hossain, M.M., and Shivakumar, K. (2012). Shear fatigue characterization of fire resistant syntactic foam core composite sandwich panel, Proceeding of SAMPE TECH 2012, October 22-25, Charleston, SC.

83. Shivakumar, k.,Swaminathan, G. and Sharpe, M. (2006). Carbon/Vinyl Ester composites for enhanced performance in marine applications, J Reinforced Plastics and Composites Vol.25, pp.1101-1116.

Appendix A

Finite Element Analysis of Four-point Bend Shear and Flexure Test Specimen

During shear fatigue test, sometimes multiple shear cracks with interfacial delamination near load/support points were observed as shown in Figure A.1. In flexural fatigue test, near the final failure stage, a shear crack followed by delamination was observed under one of the load points as shown in Figure A.2. To understand the stress states in the core and face sheet interface regions of the sandwich beams, a detailed nonlinear 2-D finite element analysis (FEM) was conducted. A summary of the results is presented below.

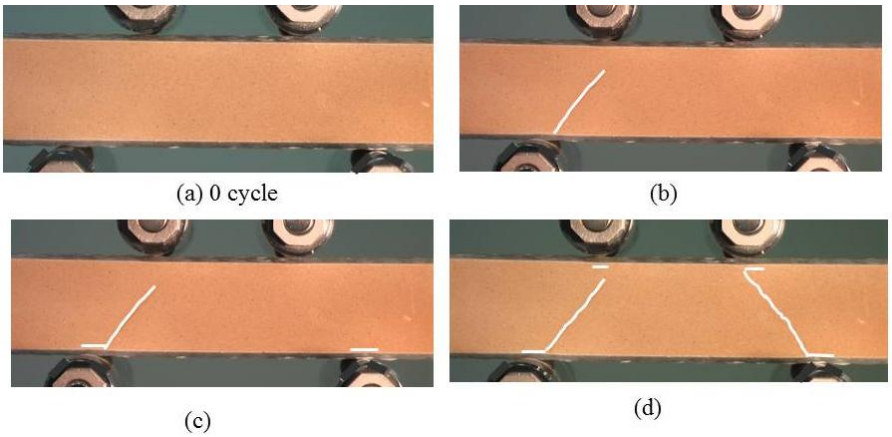

Figure A.1. Successive failure of the specimen (SSP-10) for $\tau_{max}/\tau_c = 0.80$ at shear fatigue test.

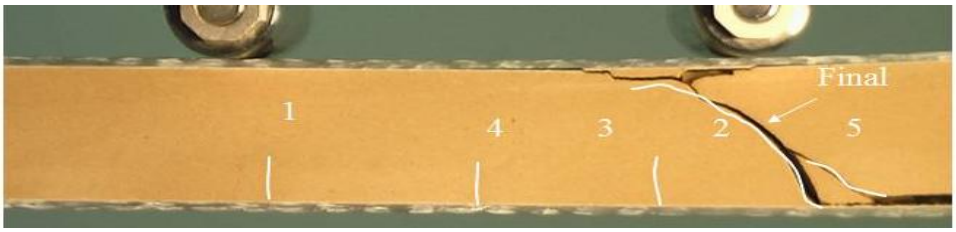

Figure A.2. Final failure of the specimen (SSP-10) for $\sigma_{max}/\sigma_{ct} = 0.80$ at flexure fatigue test.

A.1 Finite Element Model

The shear and flexural test specimen shown in Figure A.3 was analyzed by ANSYS finite element code. Figure A.4 shows the symmetric one-half of the FEA model for both shear (Figure A.4a) and flexure (Figure 4.b) sandwich specimens with the origin at the left support. The figure

also shows the boundary condition and the loading applied at S/4 point on the face sheet for shear test specimen and at S/3 for flexure test specimen. The loading and support were modeled by steel elements to simulate realistic load transfer mechanism. Both specimens were idealized by 4-noded Plane-42 elements. Line contact elements were used between the support cylindrical roads and the specimen. The shear model had 6,636 elements and flexure model had 12,622 elements. Material properties of Eco-Core and face sheet were taken from the literature [11, 12, 83] and listed in Table A.1.

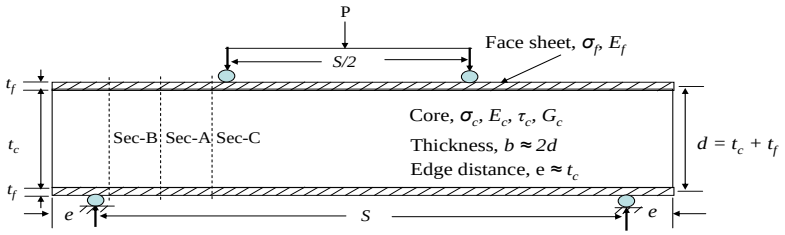

(a) Shear test specimen.

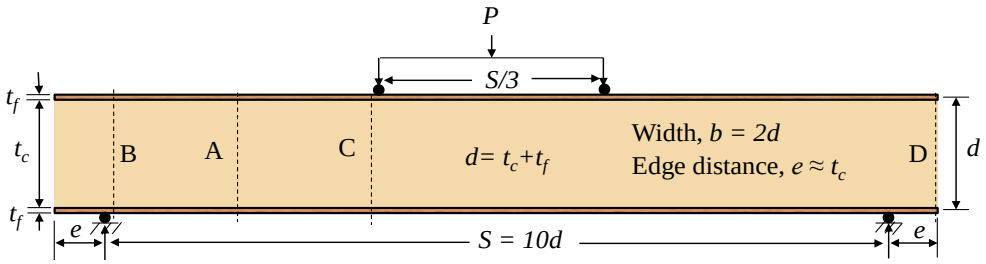

(b) Flexure test specmen.

Figure A.3. Schematic of test specimen, loading and nomenclature.

A.2 Finite Element Analysis

A Geometric nonlinear contact analysis was conducted using ANSYS finite element code for an applied load P = failure on-set load in the static test. Although the contact region varied with load, the deformation and stress distribution in the region of interest remained linear with load. Transverse shear and bending stresses were examined at Section A, B and C for shear test specimen (Figure A.3a) and at section A, B, C and D for flexure test (Figure A.3b). The section

B and C are about t_f distance from the support and load points, section A at half-way between support and load points and section D is in symmetric region. All stresses were normalized by beam theory solutions for comparison.

Table A.1

Material Properties of Eco-Core and Face sheet [12].

Materials	Density, g/cc	Material properties										
		Strength, MPa		Young modulous, GPa						Poisson's ratio		
		Tensile	Shear	E_x	E_y	E_z	G_{xy}	G_{yz}	G_{zx}	ν_{xy}	ν_{yz}	ν_{zx}
Eco-Core	0.50	6.46	4.61	2.54	-	-	77.10	-	-	0.17	-	-
face sheet	-	512.50	77.10	29.20	23.90	23*	4.50	4.30	4.0*	0.16	0.14	0.15*

* Assumed

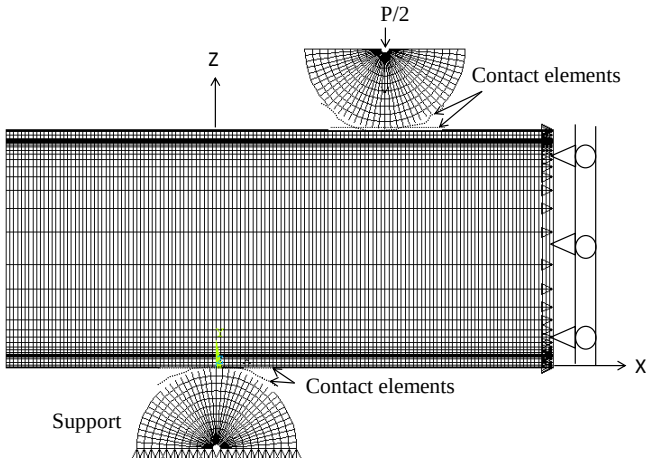

(a) Eco-Core sandwich beam for shear test.

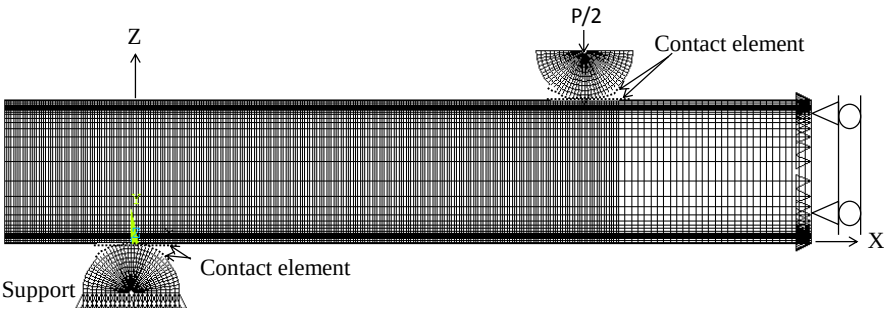

(b) Eco-Core sandwich beam for flexure test.

Figure A.4. Finite element models Eco-Core sandwich beam.

A.3 Results

A.3.1. Shear test specimen. Figure A.5 shows the shear stress distribution through the thickness of the core material (no face sheet) at three locations between the support and load point (see in sketched picture). The location B and C are about t_f distance from the support and load points, respectively. The shear stress distribution at B and C are reflection of each other about the mid-plane. The maximum shear stress is about $2.6\tau_{av}$ at the core-face sheet interface. The shear stress at A at half-way between support and load points is symmetric about the mid-plane and nearly flat curve as expected in sandwich beams (depending on the relative modulus of face sheet and core). The maximum shear stress is about $1.1\tau_{av}$. These results conclude that if the shear failure occurs at mid-way between the support and load points, it is due to maximum shear at the mid-plane of the beam. If the failure occurs near the support or load point, it may be because of shear concentration at the interface. Because the interface is resin densified and the interfacial strength could be much higher than the core shear strength.

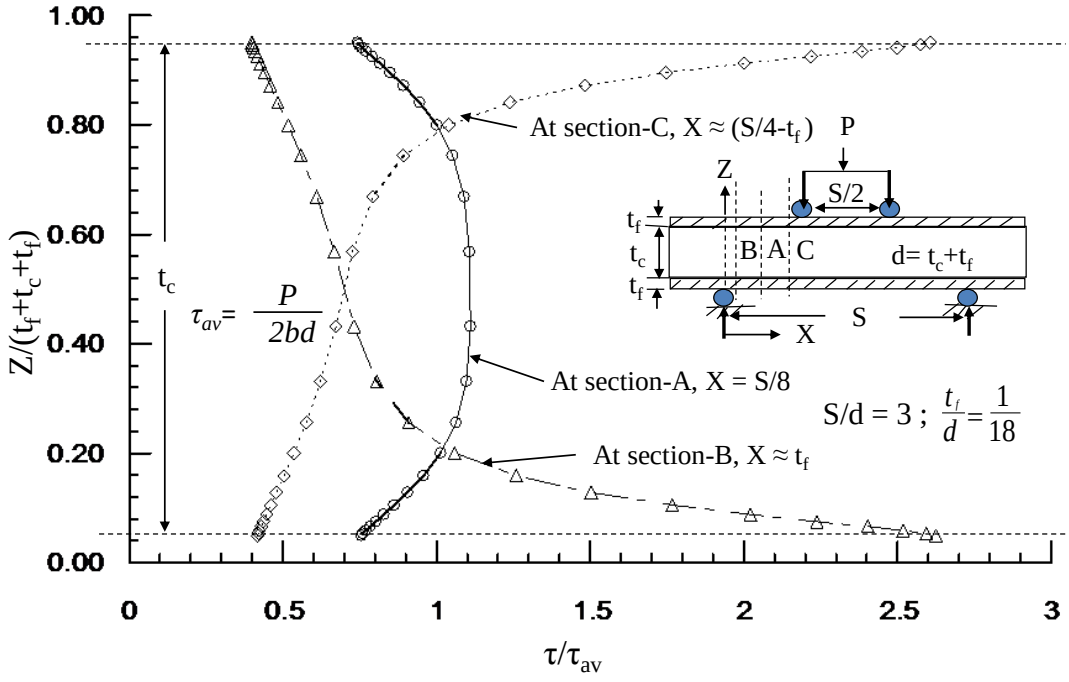

Figure A.5. Shear stress distribution at section A, B, and C.

To examine the state of normal stress near the interface, the bending stresses plotted through the thickness at the same three sections (A, B and C) in Figure A.6. As clearly shown that the bending stress near the interface of the section B is tensile (before it becomes compressive at the interface) while the bending stress at C near the support is compressive. Therefore high interfacial shear stress and tensile stress near the support at section B may the reason for initiation of delamination in fatigue loading. To establish the location of maximum interfacial shear stress from the support, the through the thickness shear distribution are plotted for X= 0, $t_f/3$, $2t_f/3$, t_f, $2t_f$ and $4t_f$ (see Figure A.7). Maximum shear stress at the interface is plotted against X in Figure A.8. This plot clearly shows that the shear stress is maximum at about one mm or about $2t_f/3$ distance from the support. Hence the hypothesis is that the maximum interfacial shear stress and tension bending stress together may be causing interfacial debond between the Eco-Core and the composite face sheet in shear fatigue test.

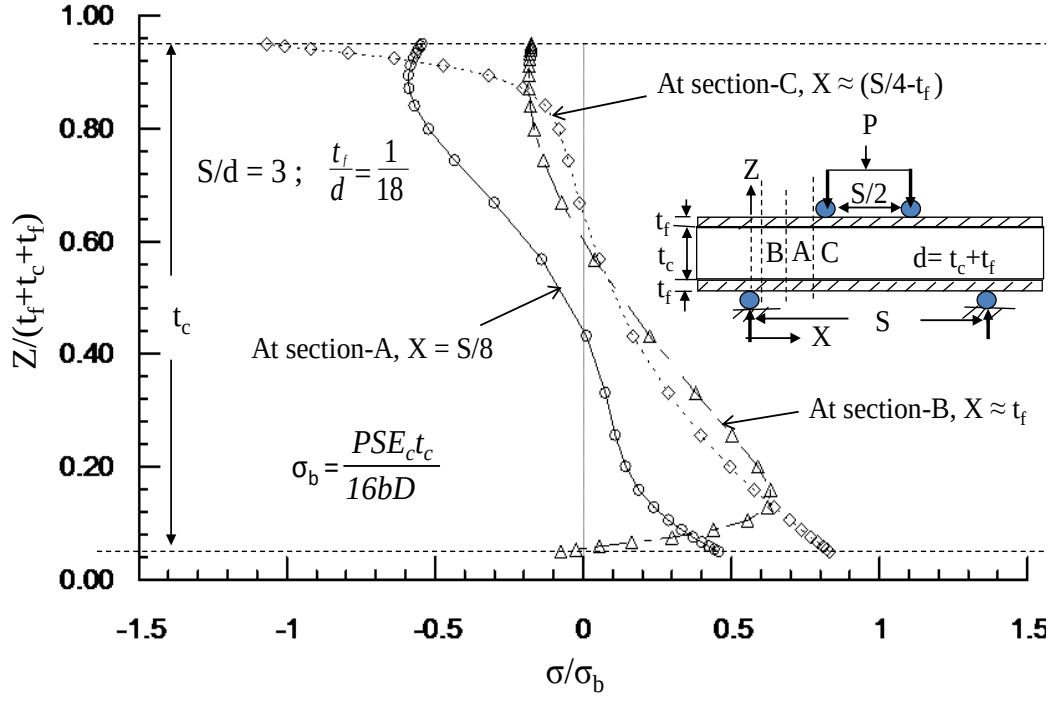

Figure A.6. Normal stress distribution at section A, B, and C.

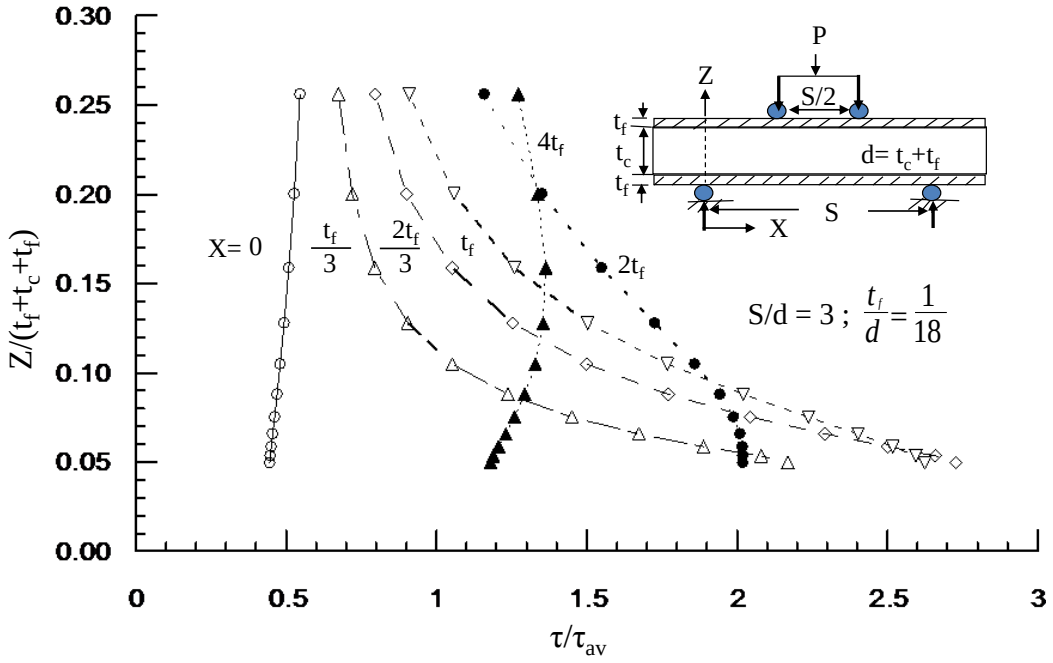

Figure A.7. Through the thickness shear stress distribution for X= 0, $t_f/3$, $2t_f/3$, t_f, $2t_f$ and $4t_f$.

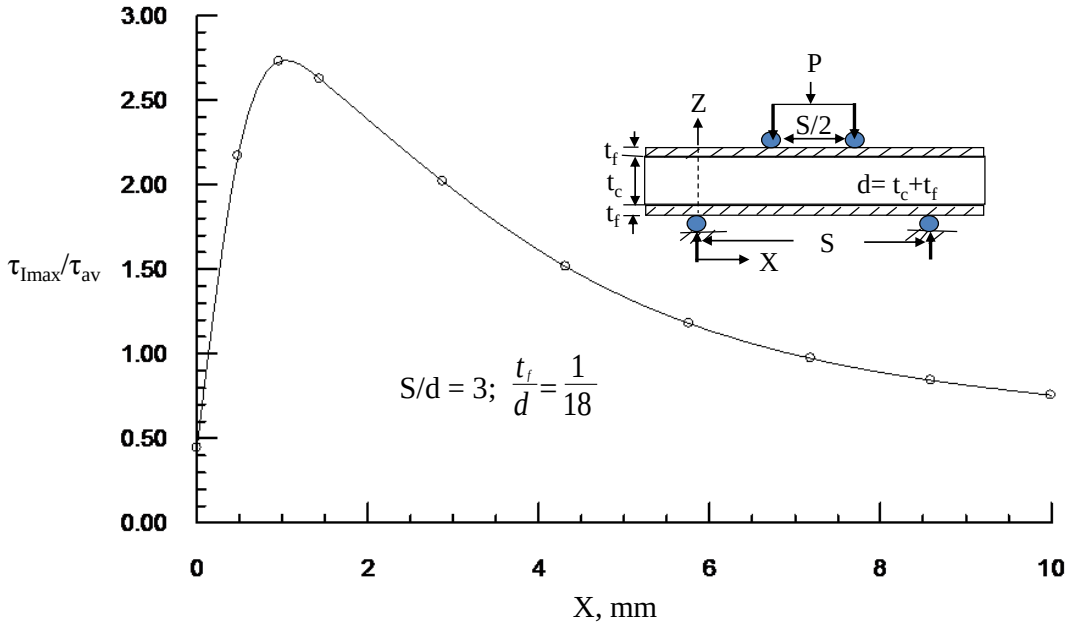

Figure A.8. Maximum shear stress at the interface against X.

A.3.2. Flexural test specimen. Figure A.9 shows the shear stress distribution through the thickness of the core material (no face sheet) at three locations between the support and load point and in the symmetric region (see in insert picture). The behavior of shear stress distribution

at three locations between support and load points is similar to that for shear test specimen. Here, the maximum shear stress is also about $2.6\tau_{av}$ at the core-face sheet interface. If the failure occurs near the support or load point, it may be because of shear concentration at the interface. Because the interface is resin densified, the interfacial strength could be much higher than the core shear strength. The shear stress at D, because symmetric region, is zero. So, if there is any failure between two loading points, it will because of bending stress.

To examine the state of normal stress near the interface, the bending stresses plotted through the thickness at the same four sections (A, B, C and D) in Figure A.10. As clearly shown that the bending stress near the interface of the section B is tensile (before it becomes compressive at the interface) while the bending stress at C is tensile at tension side and it is almost same as at section D. Hence the hypothesis is that combination of shear stress and high tensile stress near the load point at section c may the reason for initiation of tension crack followed by shear crack under one of the load points in fatigue loading.

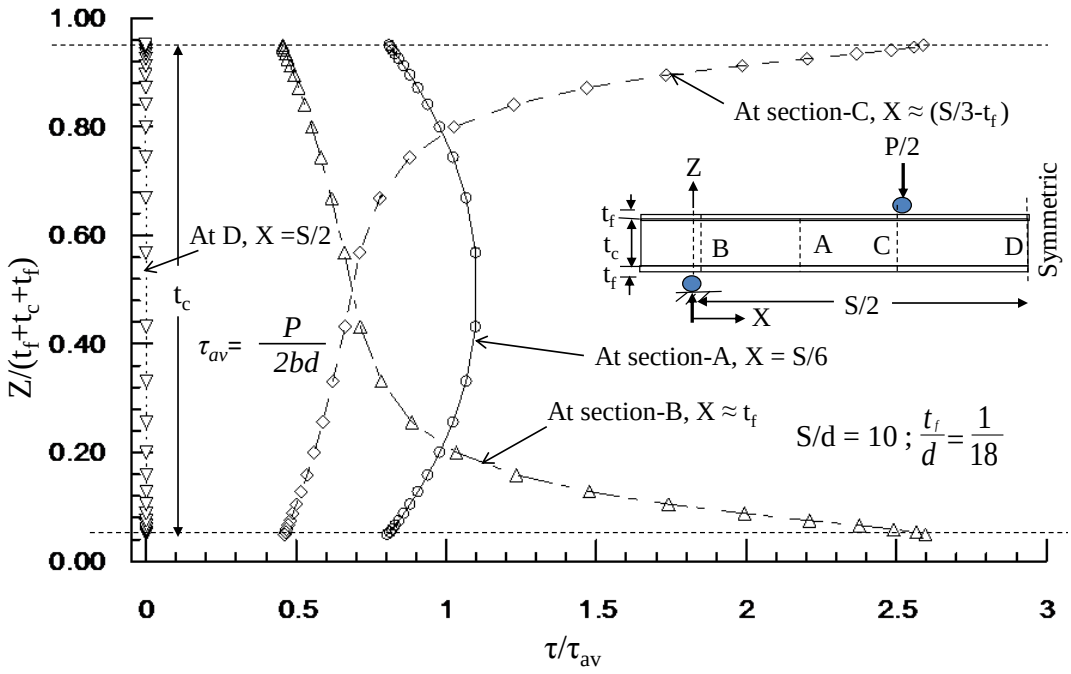

*Figure A. 9.*Shear stress distribution at section A, B, and C.

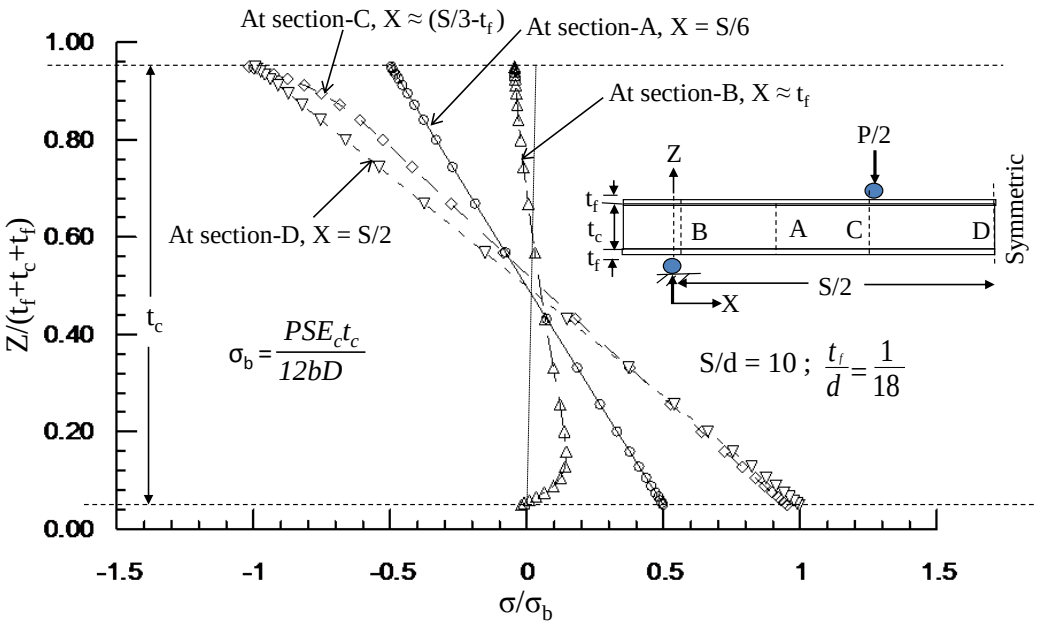

Figure A 10. Normal stress distribution at section A, B, and C.

Appendix B

Additional Figures of Chapter 2

Selection process of specimens for static and fatigue test from panel 2, static compression stress-strain response of the specimen (panel 2), compliance versus number of cycles(N) curves of the fatigue tested specimens for σ_{max}/σ_c = 0.90, 0.80, 0.75, 0.70 and 0.60 for R=10, and σ_{max}/σ_c = 0.95, 0.90, 0.85 and 0.80 for R=5 are given below.

B.1 Specimen Selection Process from Panel 2

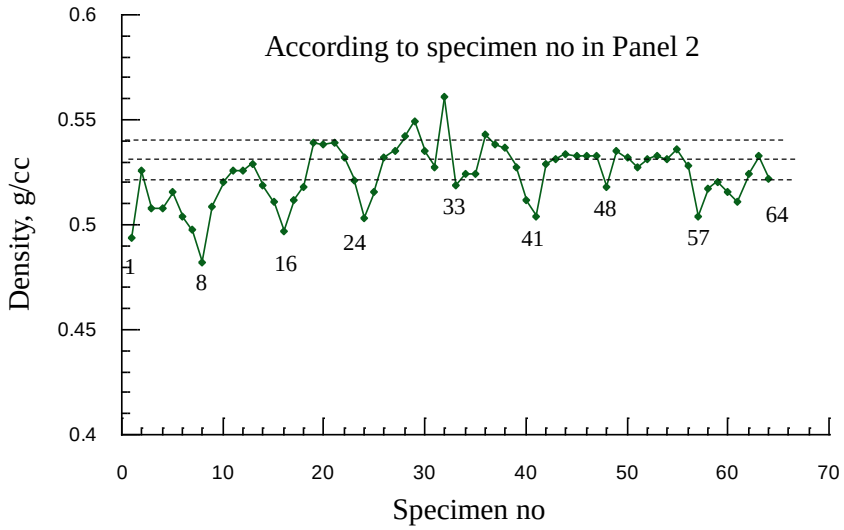

(a) Specimens numbered according to specimen number in specimen layout

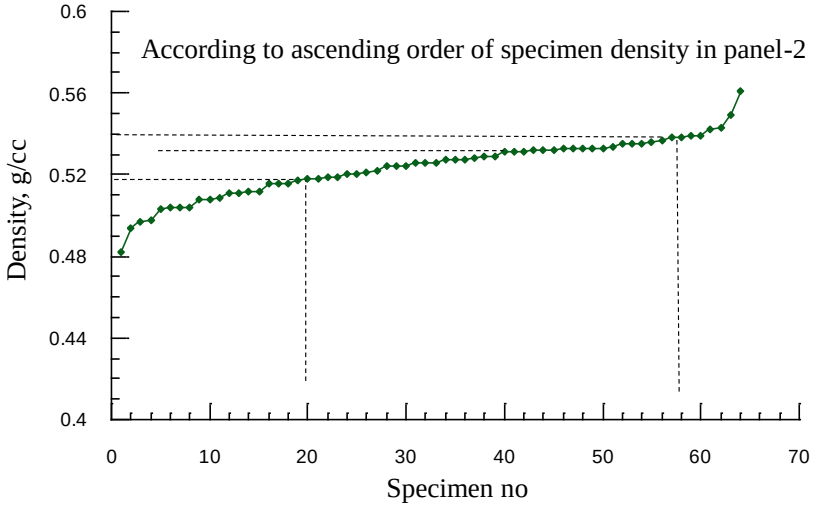

(b) Specimen numbered according to ascending order of specimen density.

Figure B 1. Specimen selection process from panel 2.

B.2 Static Compression Stress-Strain Response of the Specimen (Panel 2)

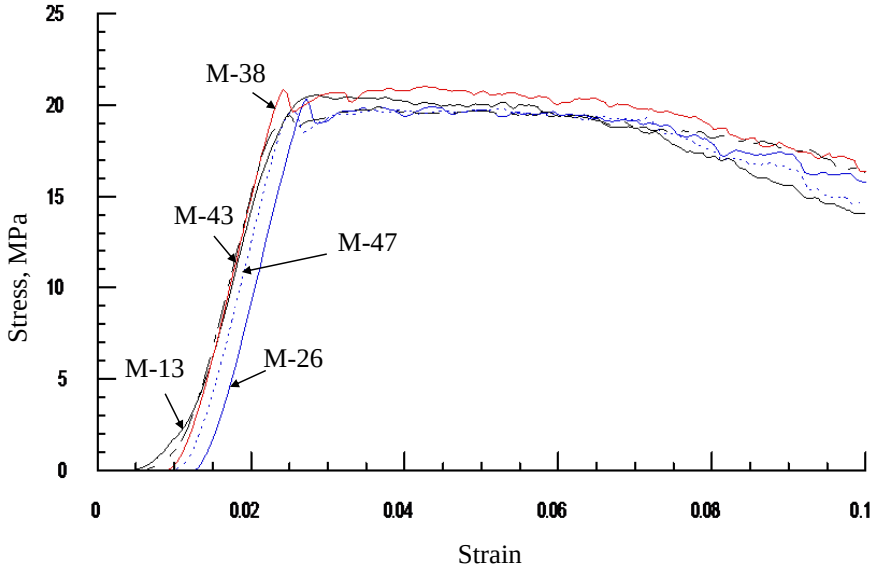

Figure B 2. Static Compression stress-strain response of the specimen (Panel 2).

B.3 Compliance Versus Number of Cycles Curves of the Specimens for σ_{max}/σ_c = 0.90, R=10.

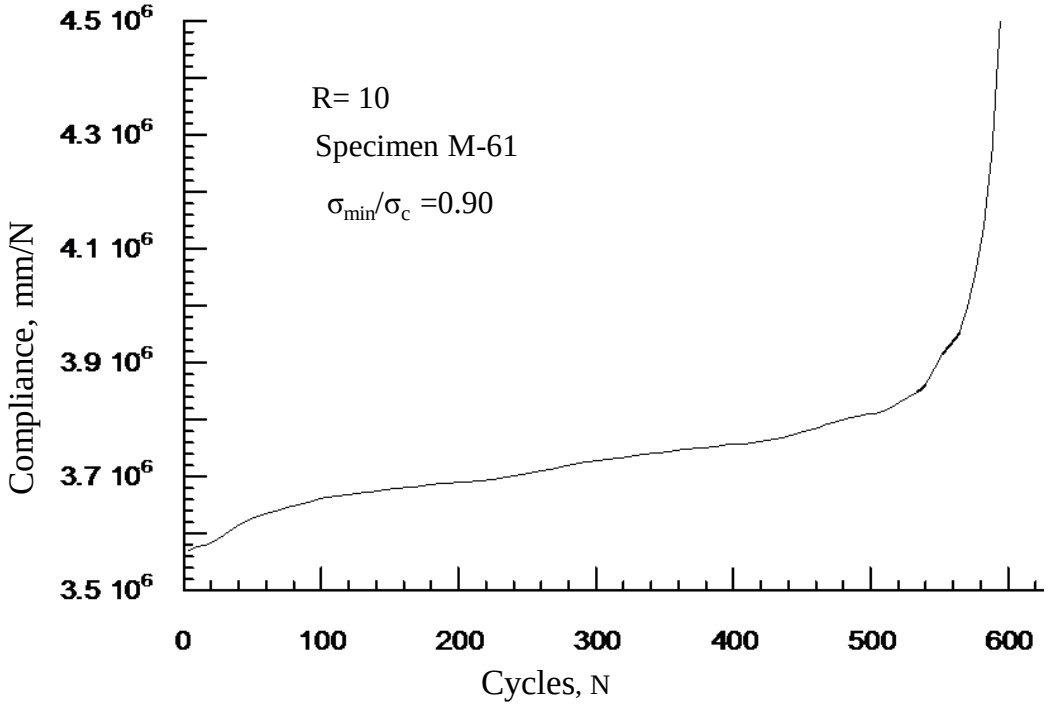

(a) Compliance Versus number of cycles curve for specimen M-61

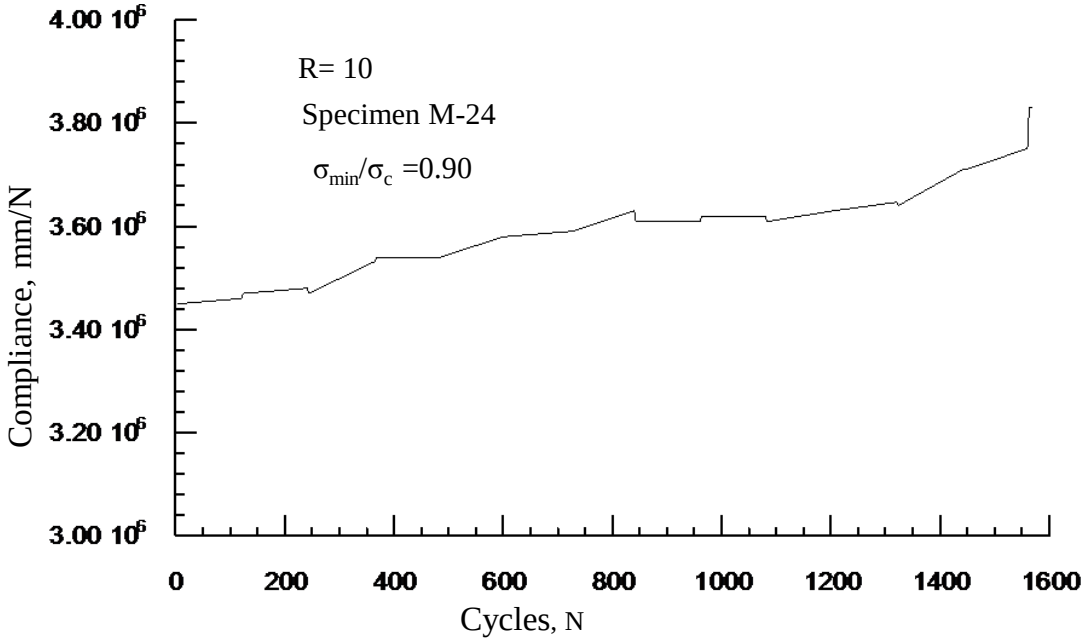

(b) Compliance Versus number of cycles curve for specimen M-24

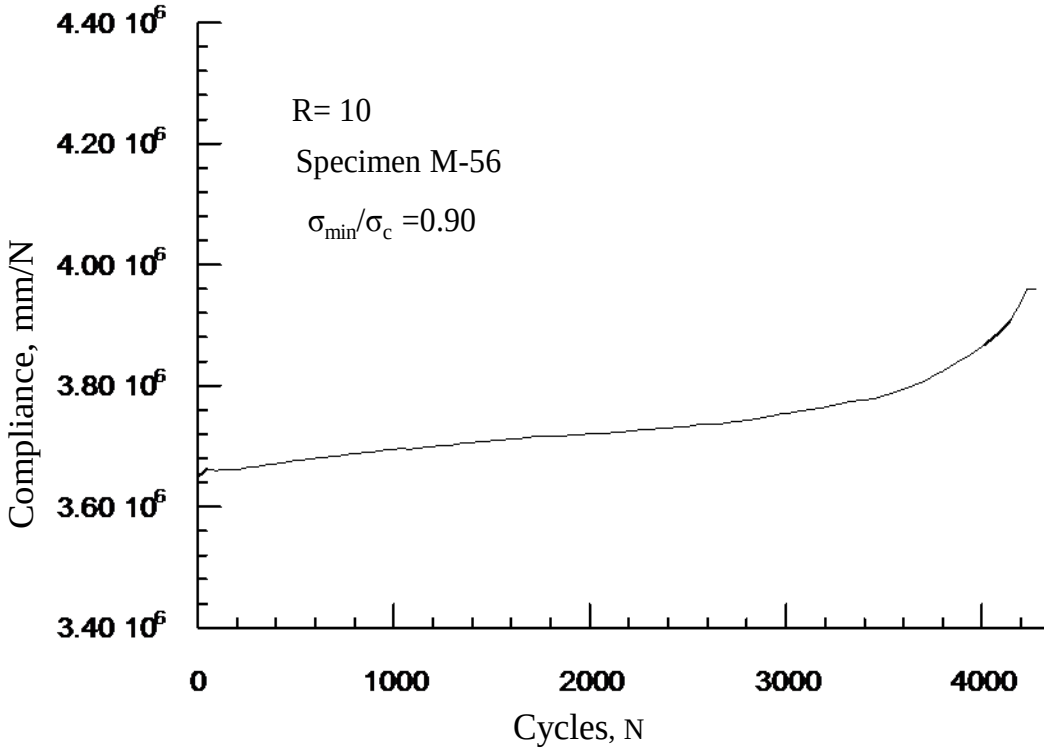

(c) Compliance Versus number of cycles curve for specimen M-61

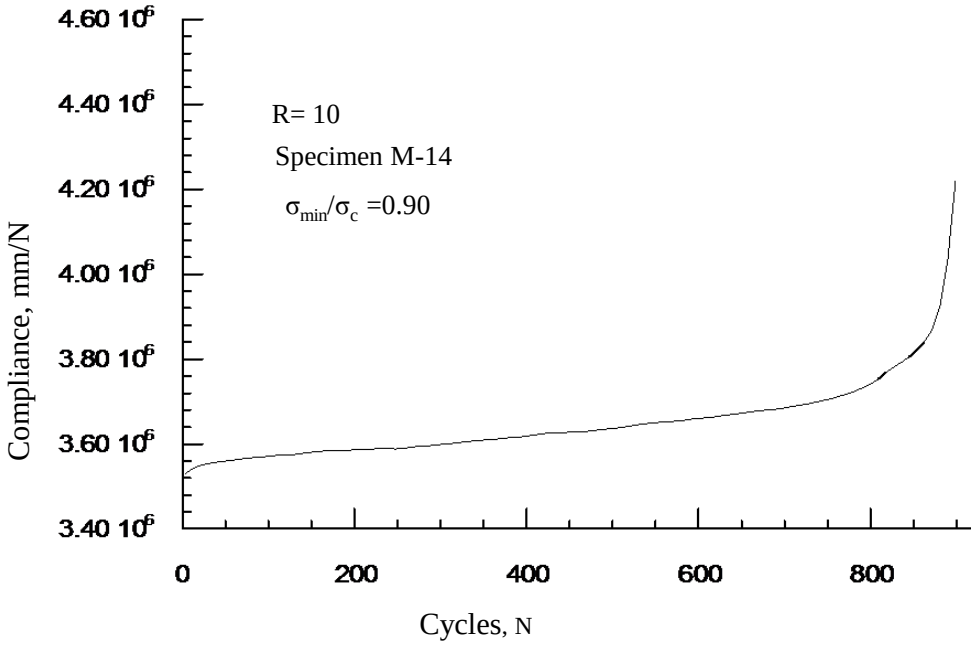

(d) Compliance Versus number of cycles curve for specimen M-14

Figure B 3. Compliance versus number of cycles (M-61, M-24, M-56 and M-14) for σ_{min}/σ_c = 0.90, R=10.

B.4 Compliance Versus Number of Cycles Curves of the Specimens for σ_{max}/σ_c = 0.85, R=10.

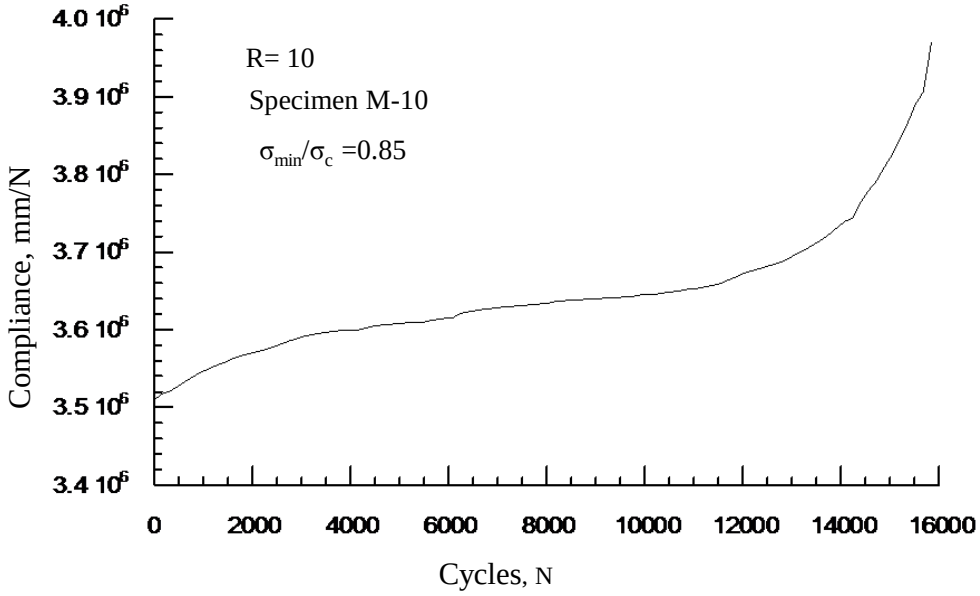

(a) Compliance Versus number of cycles curve for specimen M-10

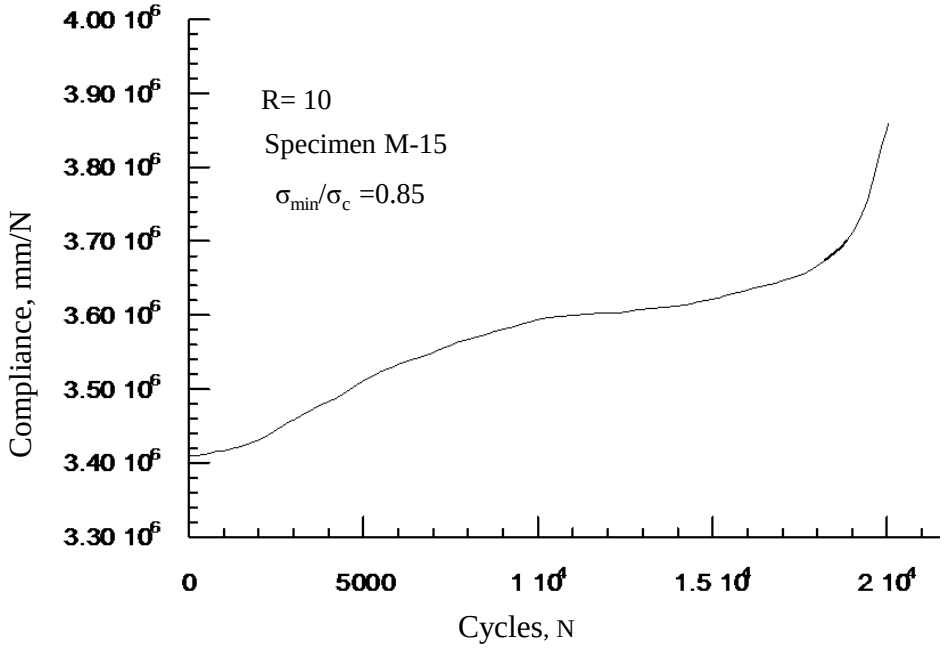

(b) Compliance Versus number of cycles curve for specimen M-15

Figure B 4. Compliance versus number of cycles (M-10, M-15) for $\sigma_{min}/\sigma_c = 0.85$, R=10.

B.5 Compliance Versus Number of Cycles Curves of the Specimens for $\sigma_{max}/\sigma_c = 0.80$, R=10.

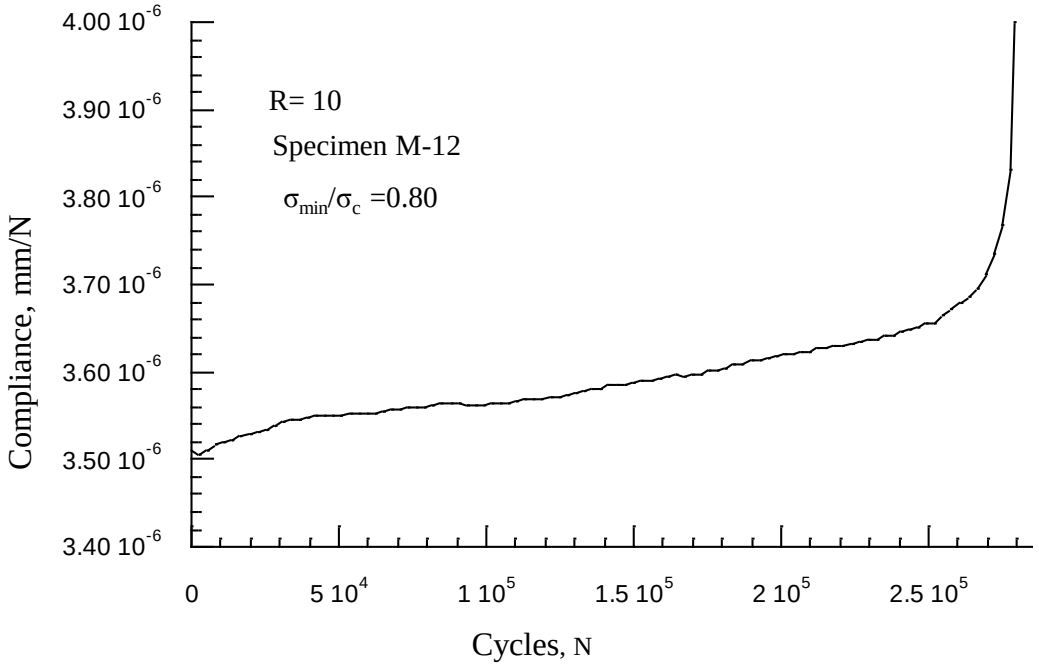

(a) Compliance Versus number of cycles curve for specimen M-12

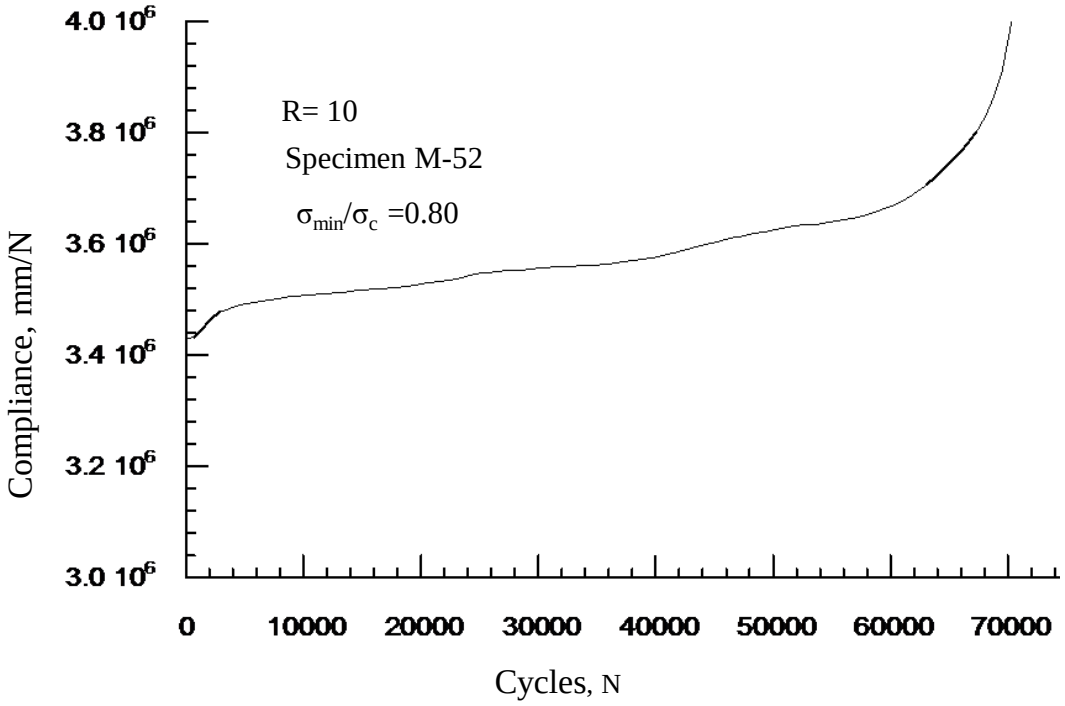

(b) Compliance Versus number of cycles curve for specimen M-52

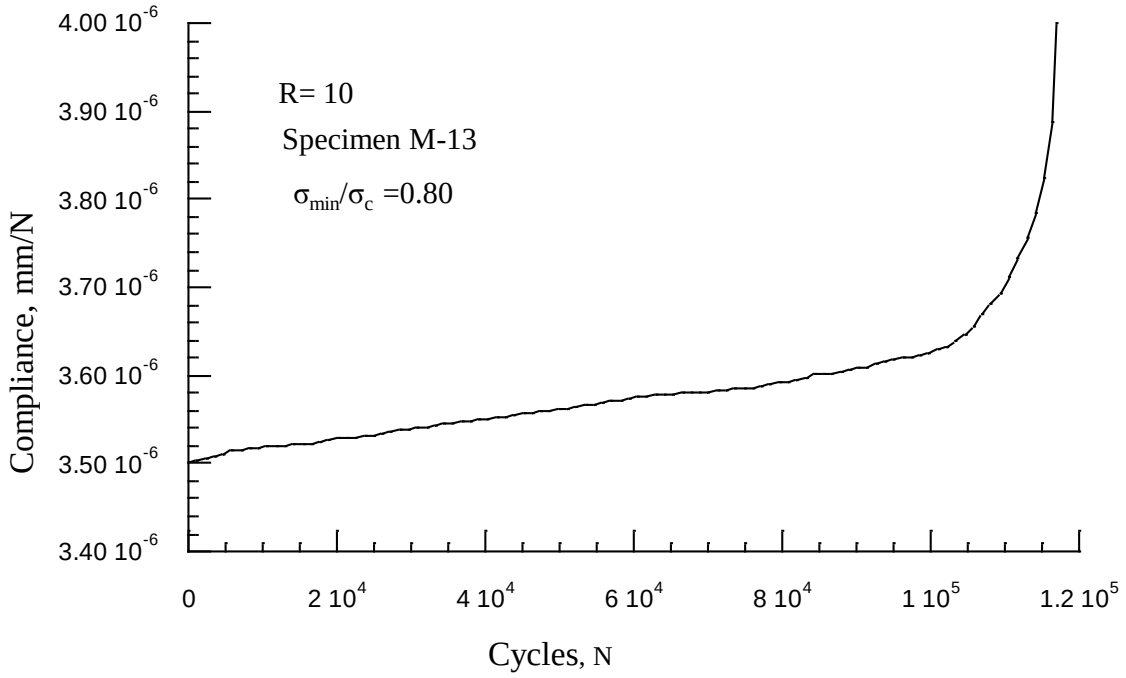

(c) Compliance Versus number of cycles curve for specimen M-13

Figure B 5. Compliance versus number of cycles (M-12, M-52, M-13) for $\sigma_{min}/\sigma_c = 0.80$, R=10.

B.6 Compliance Versus Number of Cycles Curves of the Specimens for σ_{max}/σ_c = 0.75, R=10.

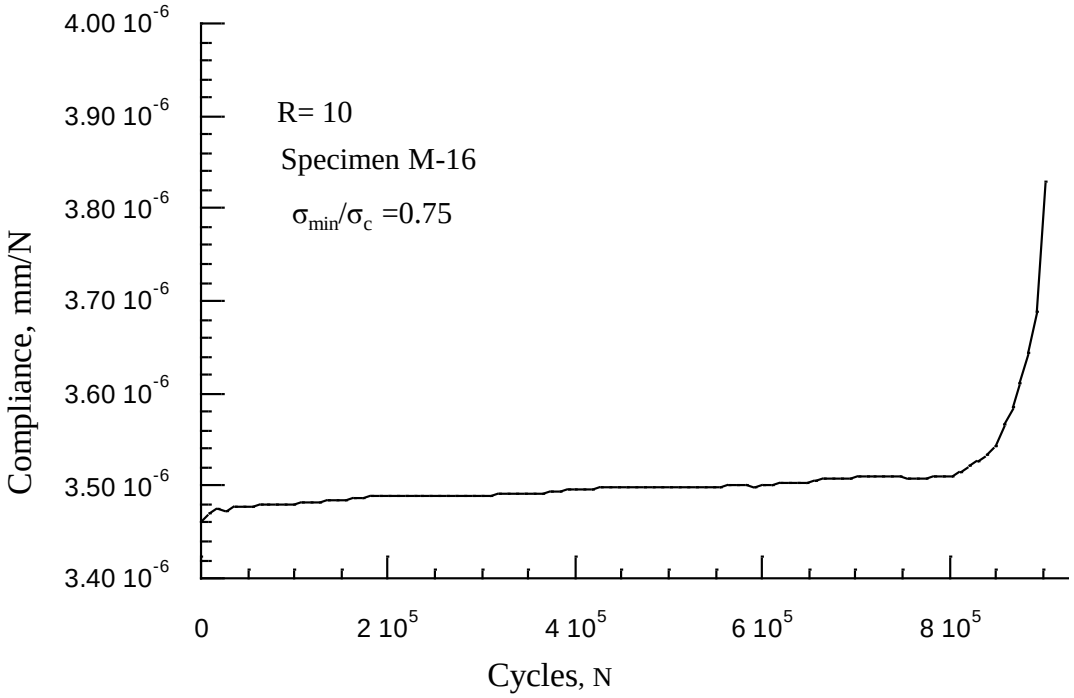

(a) Compliance Versus number of cycles curve for specimen M-16

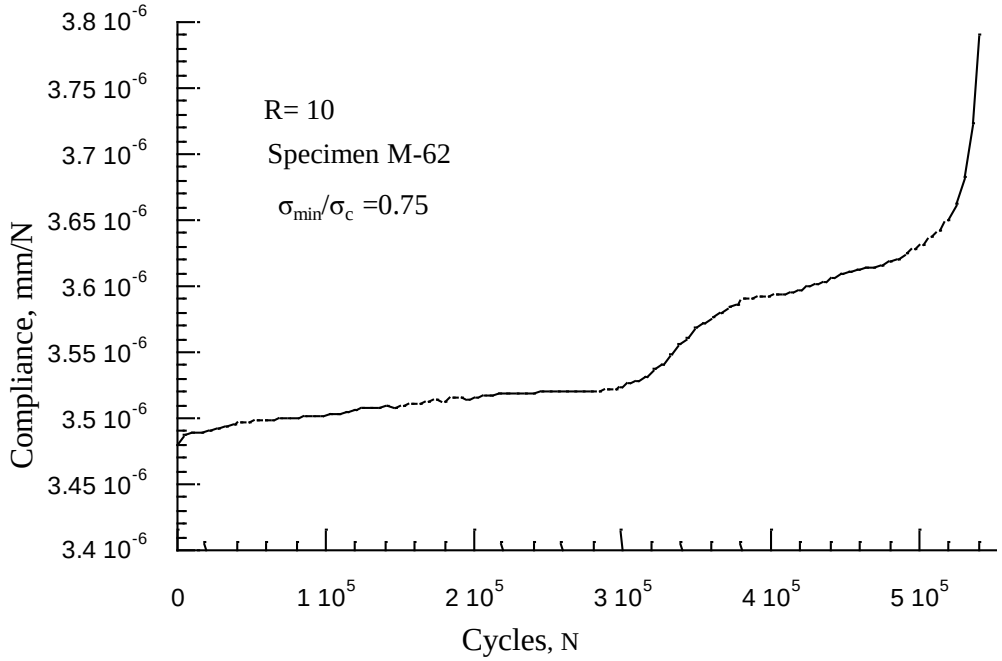

(b) Compliance Versus number of cycles curve for specimen M-62

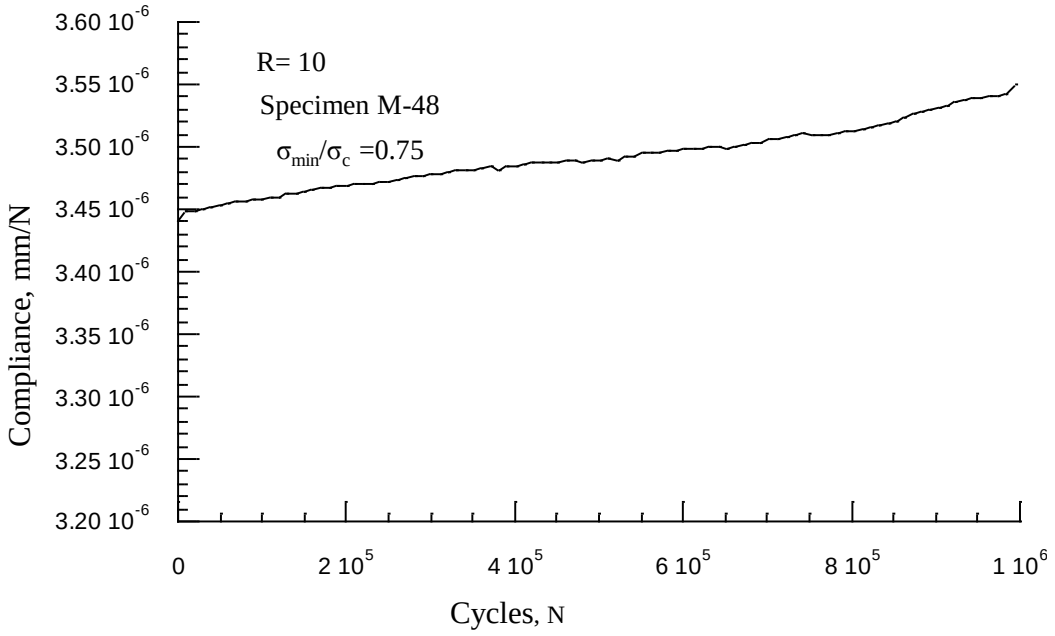

(c) Compliance Versus number of cycles curve for specimen M-48

Figure B 6. Compliance versus number of cycles M-16, M-62, M-48) for $\sigma_{min}/\sigma_c = 0.75$, R=10.

B.7 Compliance Versus Number of Cycles Curves of the Specimens for $\sigma_{max}/\sigma_c = 0.70$, R=10.

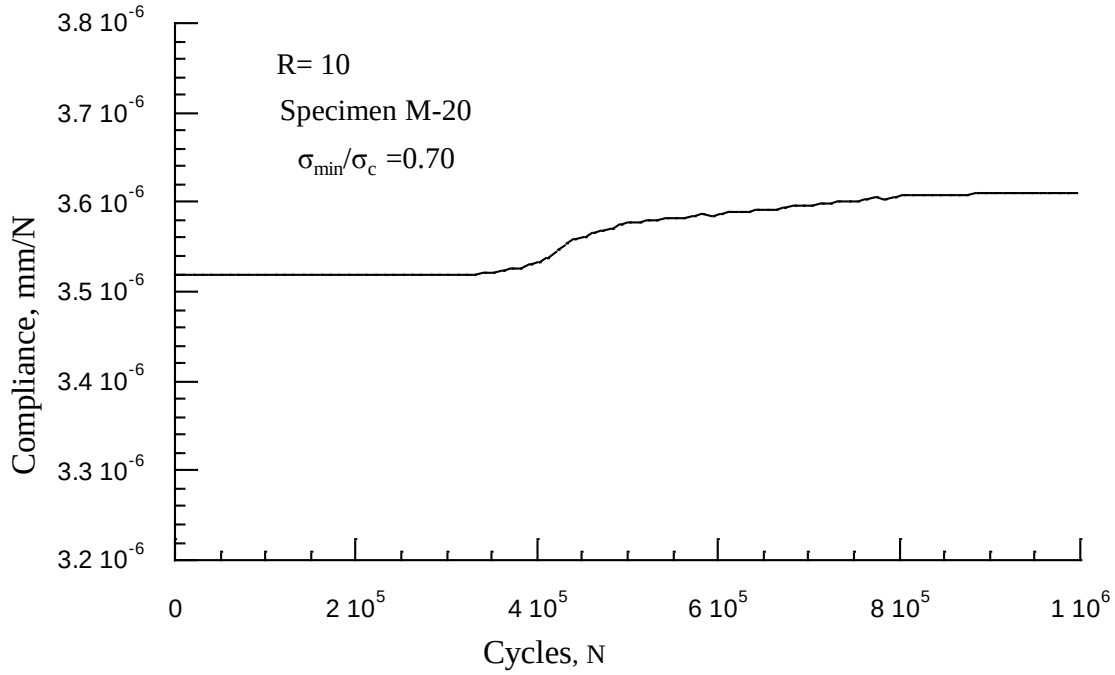

(a) Compliance Versus number of cycles curve for specimen M-20

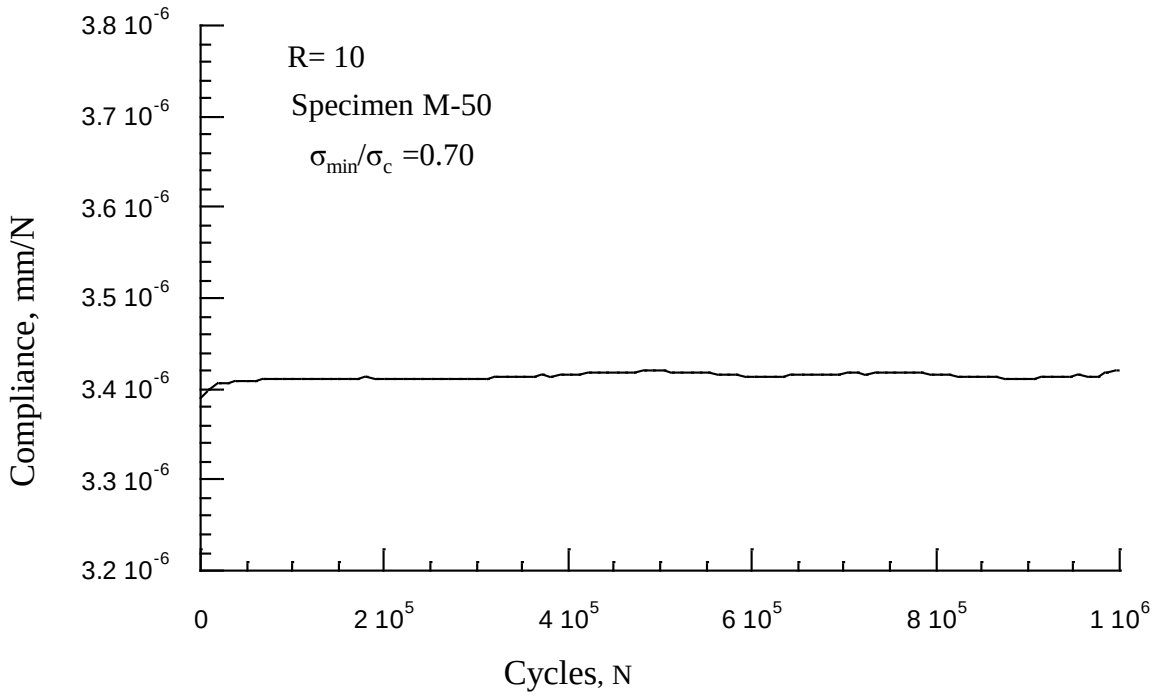

(b) Compliance Versus number of cycles curve for specimen M-50

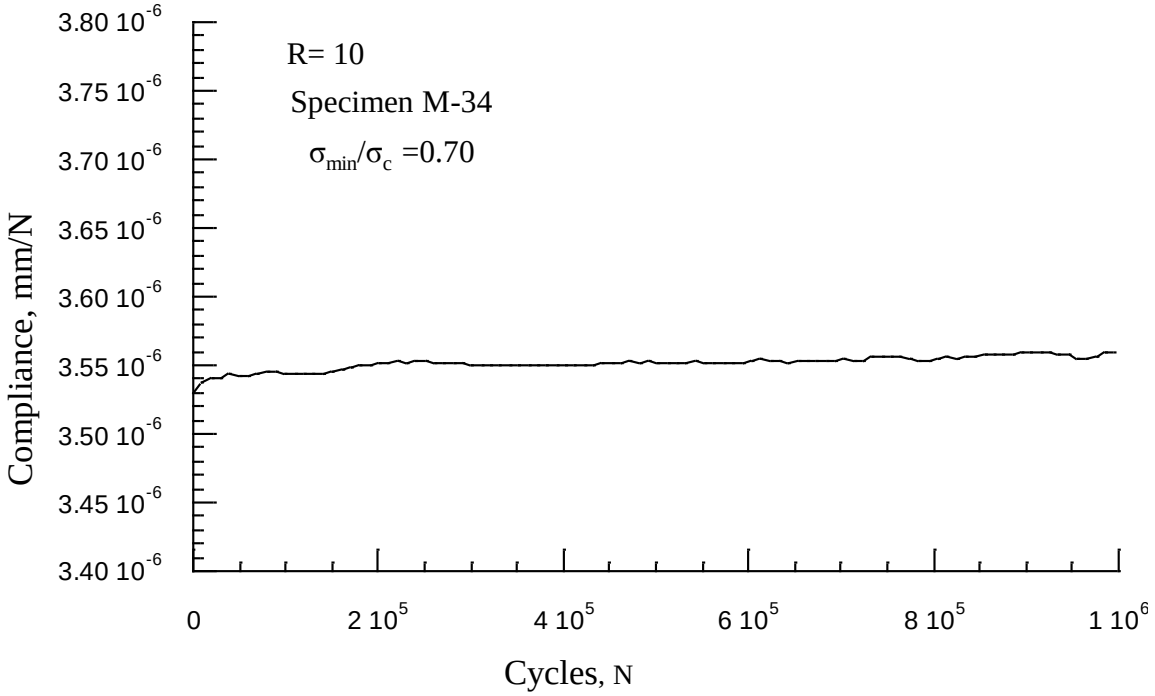

(c) Compliance Versus number of cycles curve for specimen M-34

Figure B 7. Compliance versus number of cycles (M-20, M-50, M-34) for $\sigma_{min}/\sigma_c = 0.70$, R=10.

B.8 Compliance Versus Number of Cycles Curves of the Specimens for σ_{max}/σ_c = 0.60, R=10.

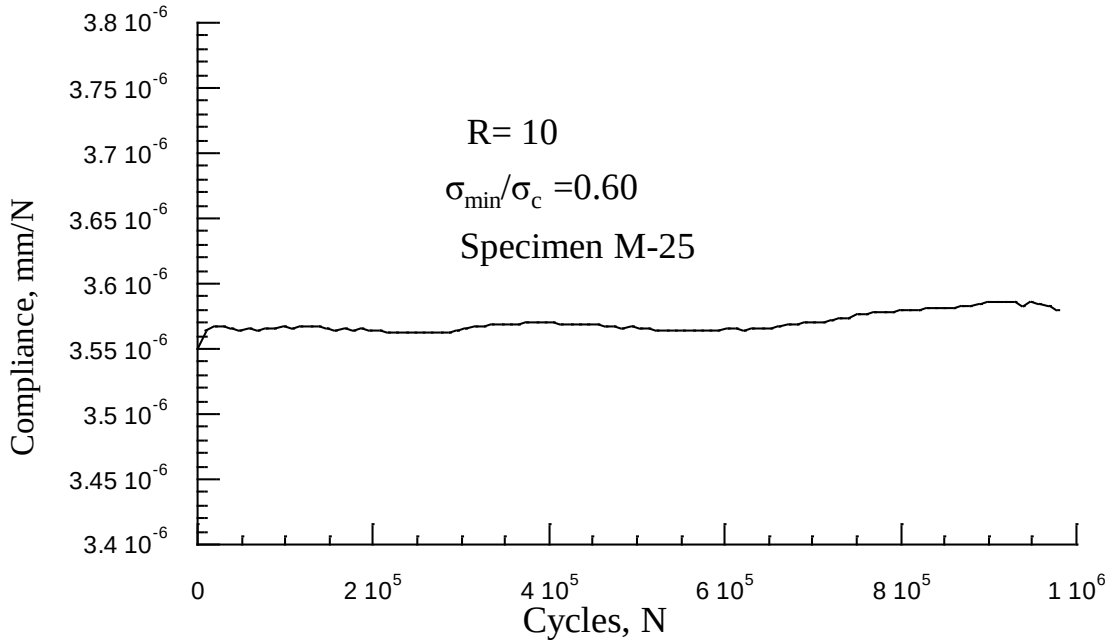

Figure B 8. Compliance versus number of cycles (M-25) for σ_{min}/σ_c = 0.60, R=10.

B.9 Compliance Versus Number of Cycles Curves of the Specimens for σ_{max}/σ_c = 0.95, R=5.

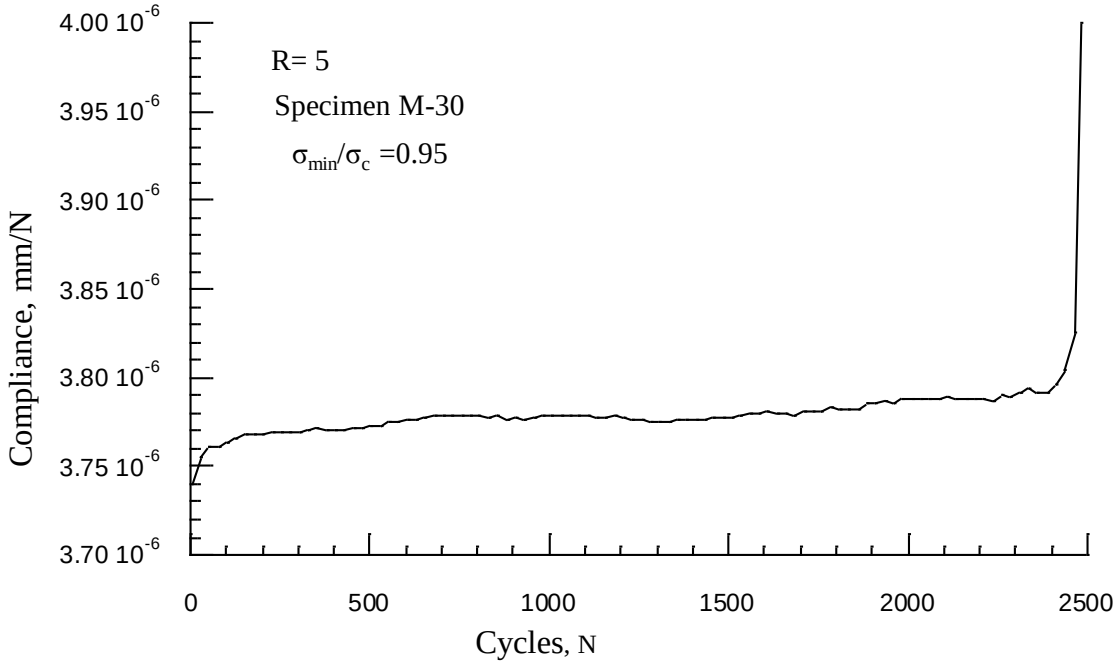

(a) Compliance Versus number of cycles curve for specimen M-30

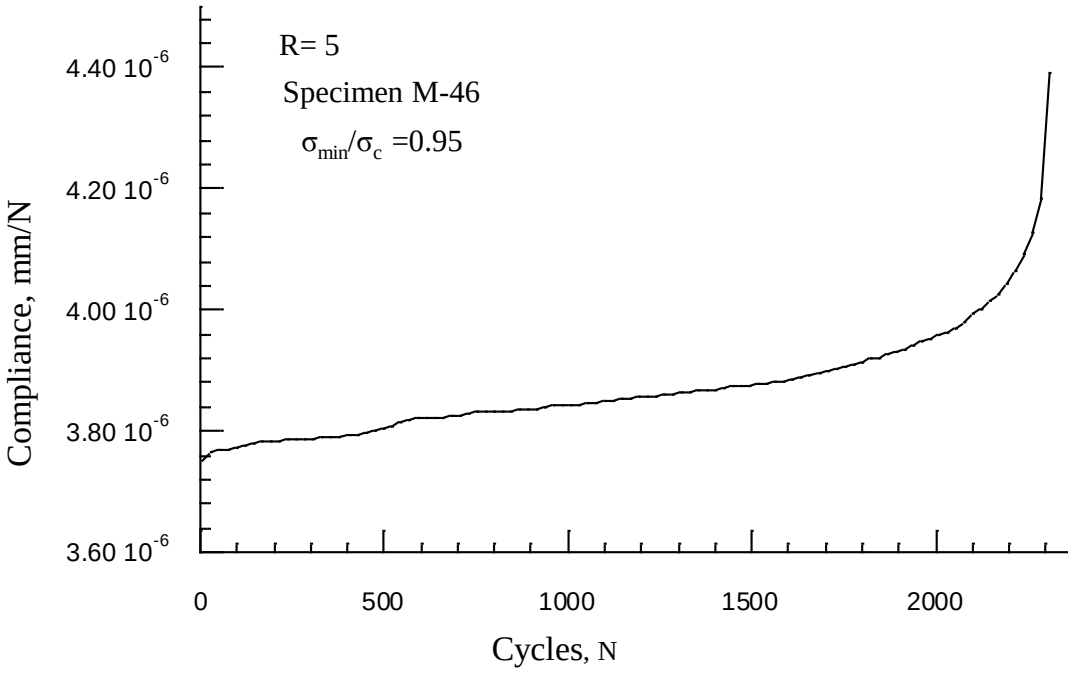

(b) Compliance Versus number of cycles curve for specimen M-46

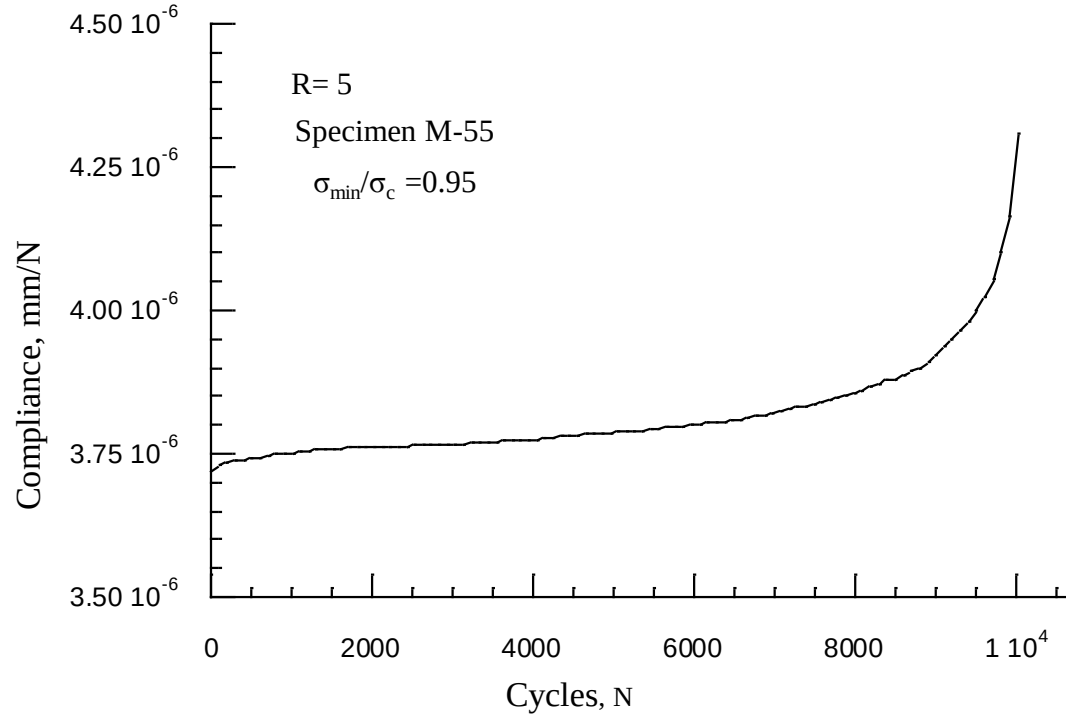

(c) Compliance Versus number of cycles curve for specimen M-55

Figure B 9. Compliance versus number of cycles (M-30, M-46, M-55) for σ_{min}/σ_c = 0.95, R=5.

B.10 Compliance Versus Number of Cycles Curves of the Specimens for σ_{max}/σ_c = 0.90, R=5.

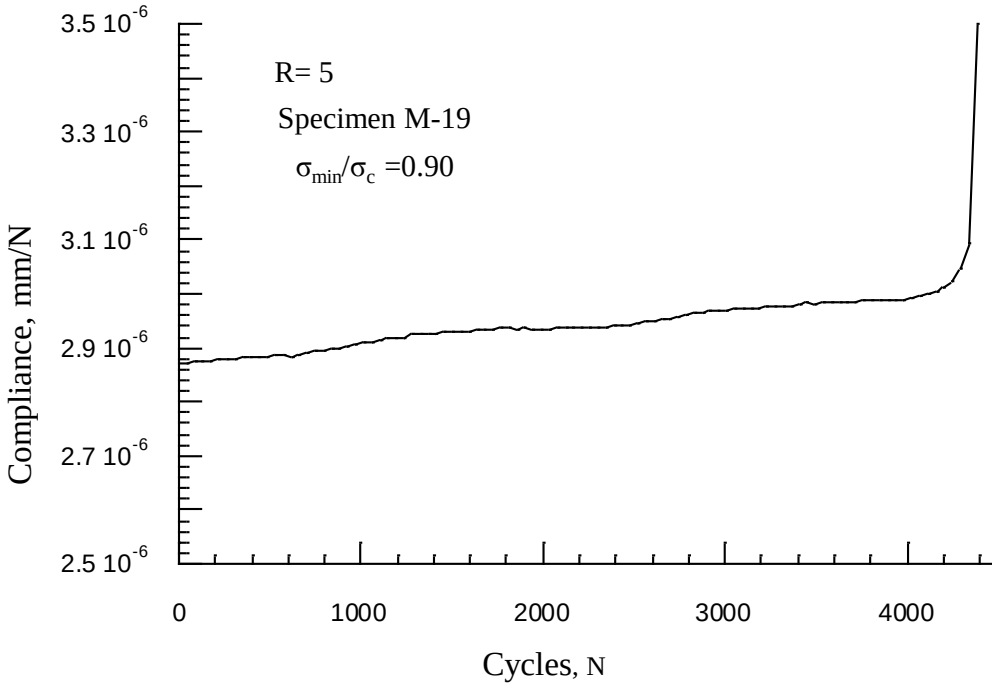

(a) Compliance Versus number of cycles curve for specimen M-19

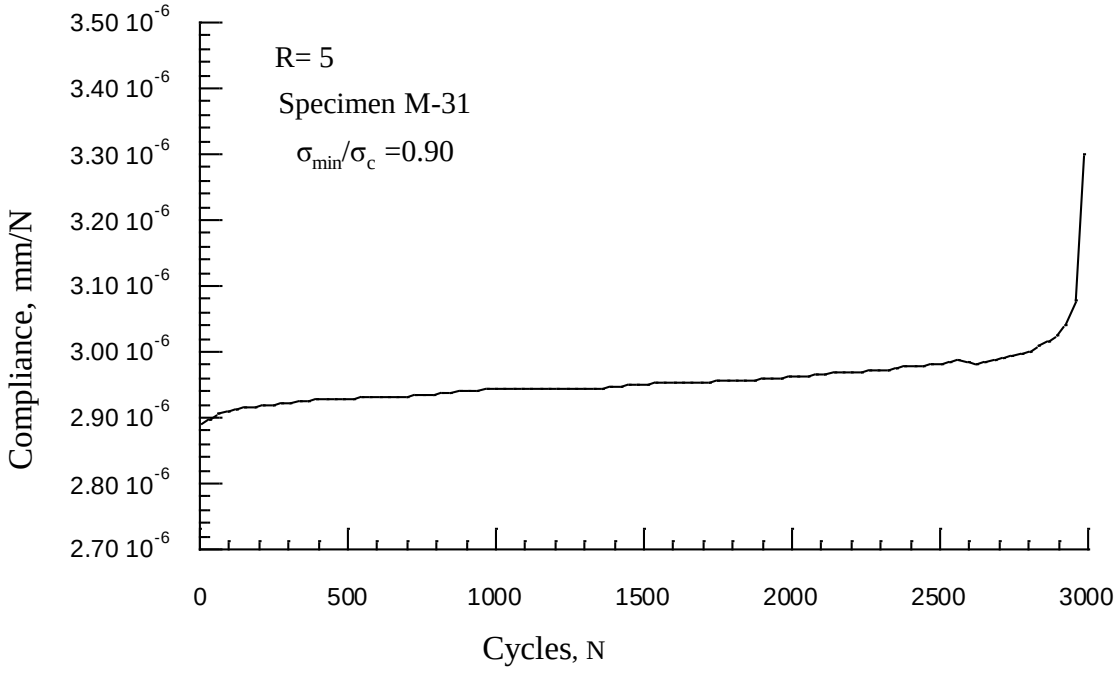

(b) Compliance Versus number of cycles curve for specimen M-31

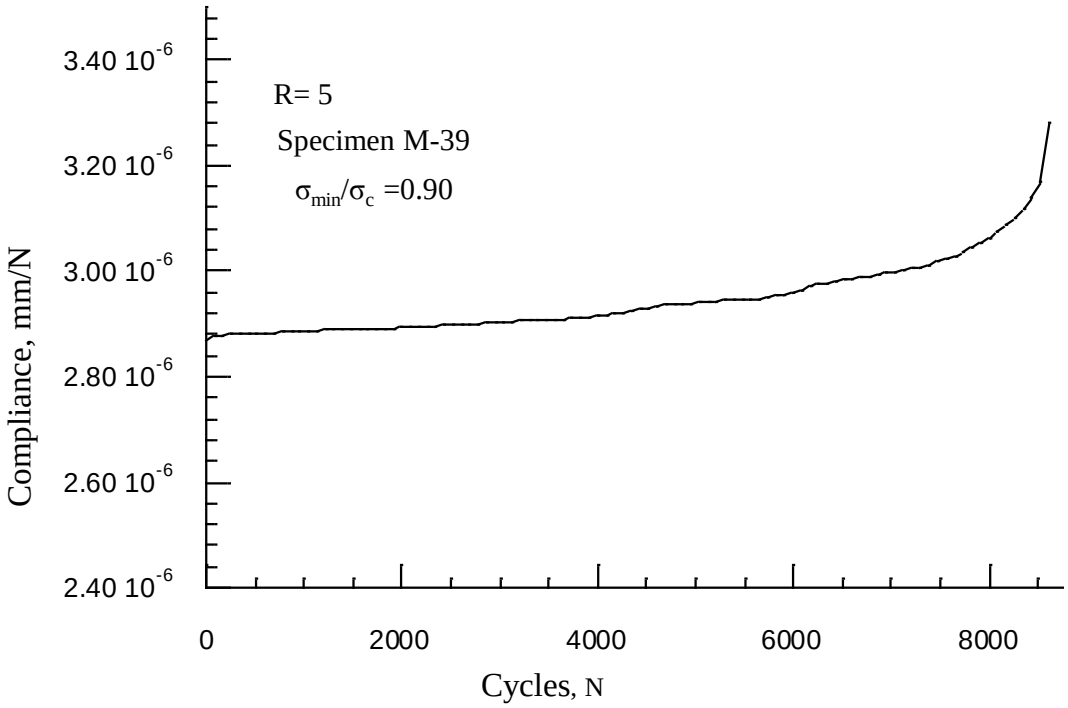

(c) Compliance Versus number of cycles curve for specimen M-39

Figure B 10. Compliance versus number of cycles (M-19, M-31, M-39) for $\sigma_{min}/\sigma_c = 0.90$, R=5.

B.11 Compliance Versus Number of Cycles Curves of the Specimens for $\sigma_{max}/\sigma_c = 0.85$, R=5.

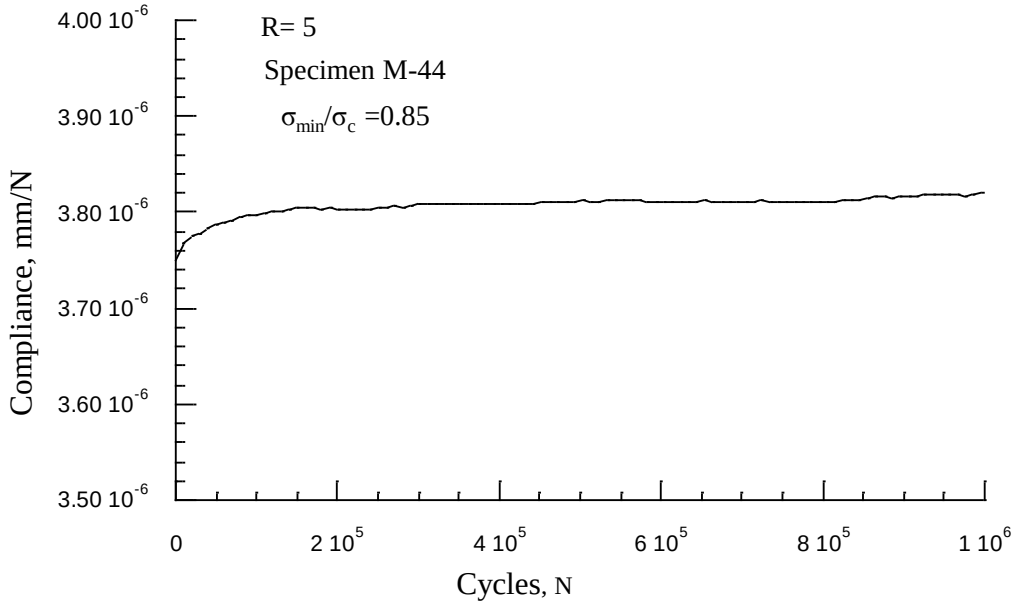

(a) Compliance Versus number of cycles curve for specimen M-44

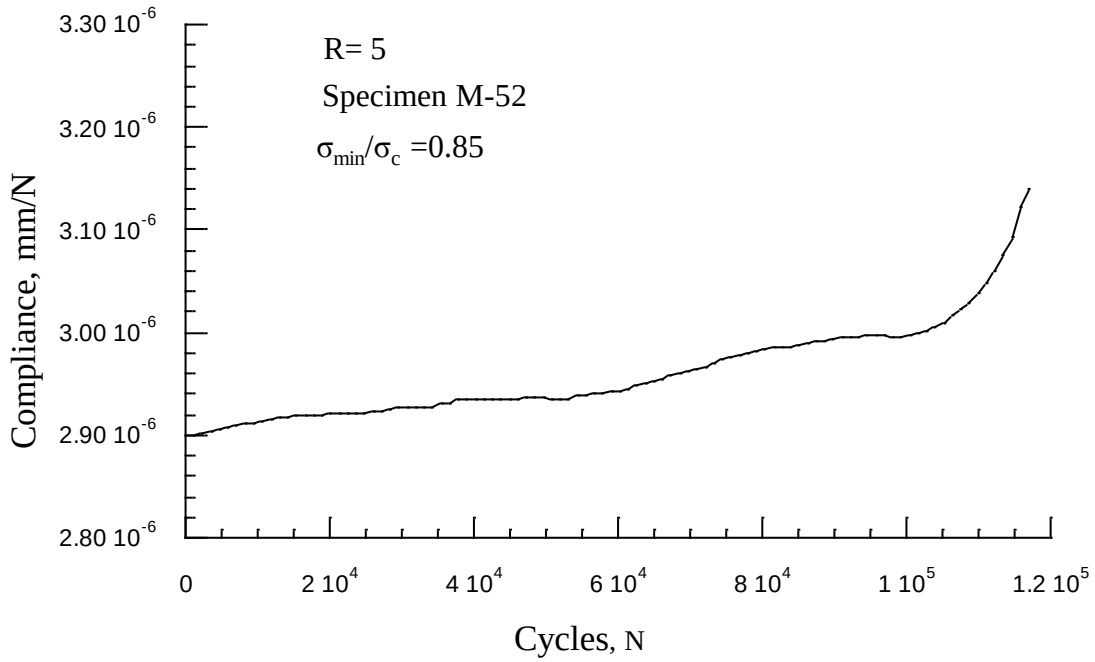

(b) Compliance Versus number of cycles curve for specimen M-52

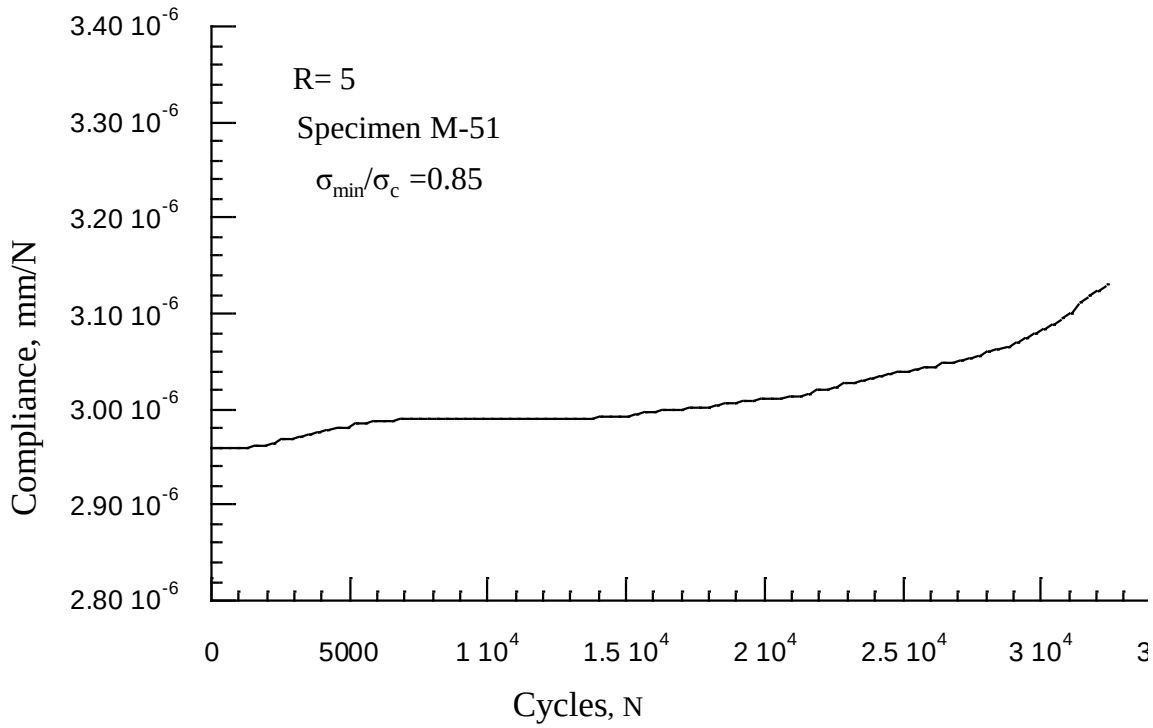

(c) Compliance Versus number of cycles curve for specimen M-51

Figure B 11. Compliance versus number of cycles (M-44, M-52, M-51) for σ_{min}/σ_c = 0.85, R=5.

B.12 Compliance Versus Number of Cycles Curves of the Specimens for σ_{max}/σ_c = 0.80, R=5.

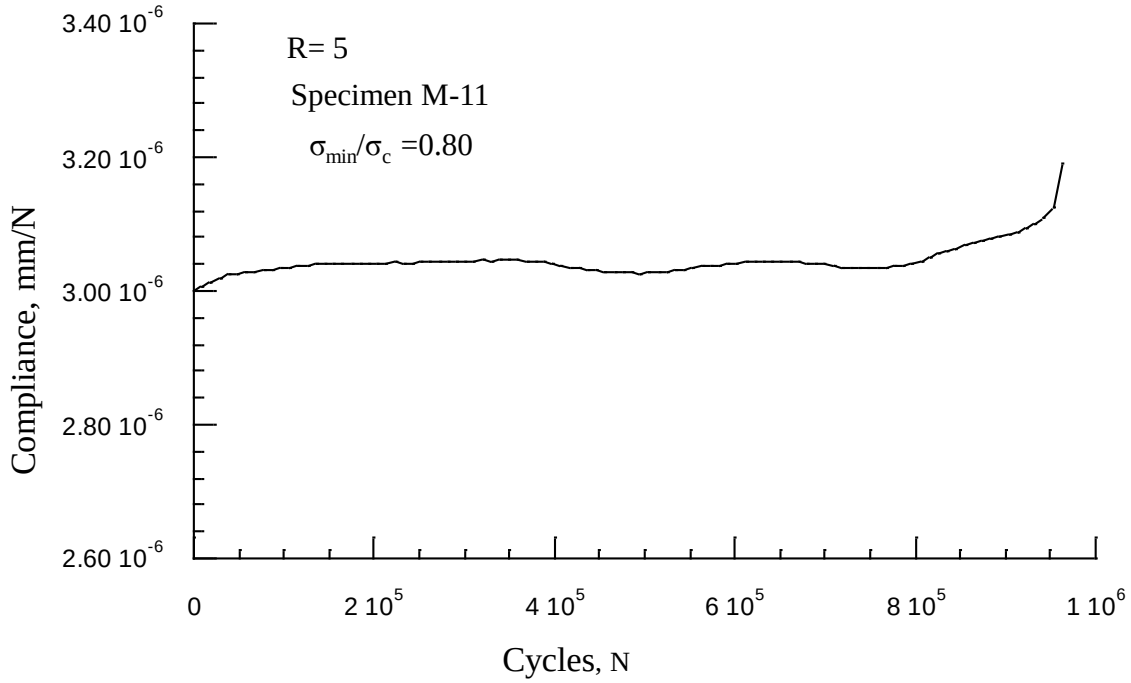

(a) Compliance Versus number of cycles curve for specimen M-11

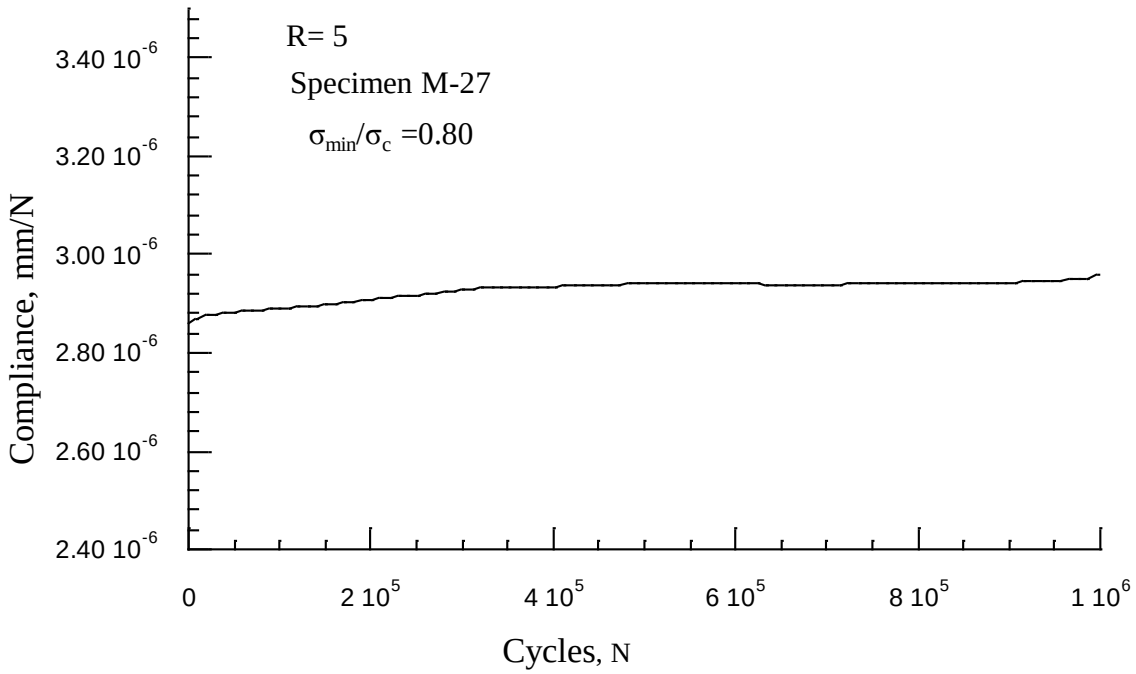

(b) Compliance Versus number of cycles curve for specimen M-27

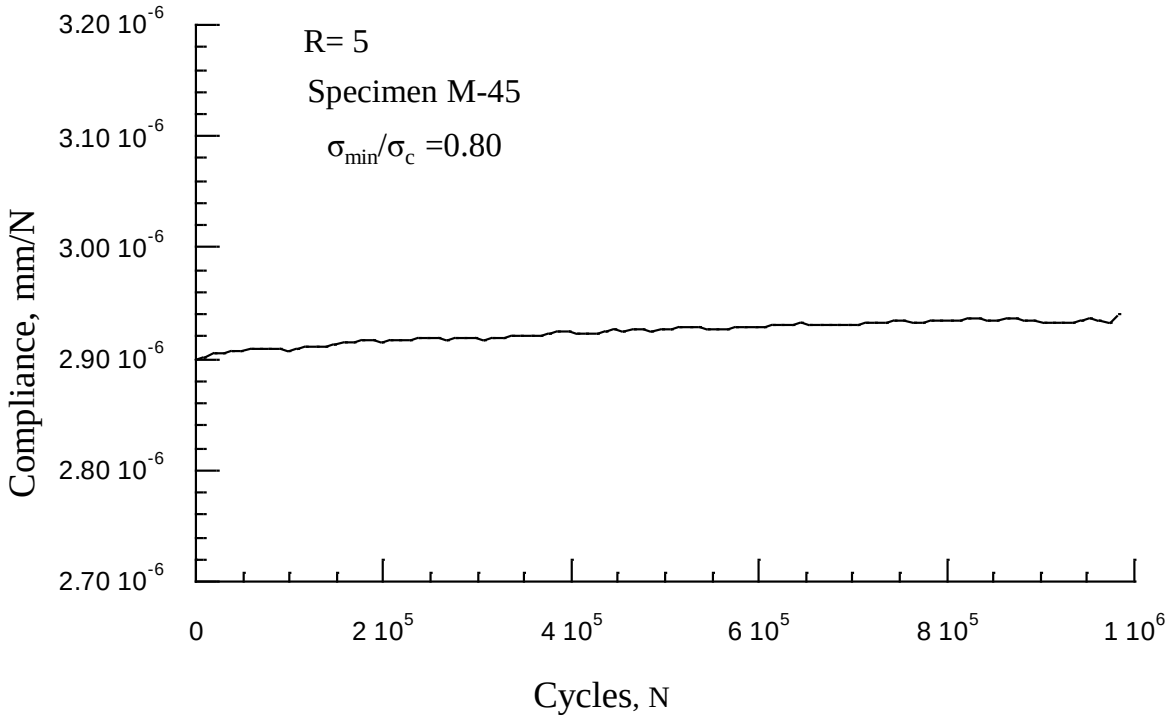

(c) Compliance Versus number of cycles curve for specimen M-45

Figure B 12. Compliance versus number of cycles (M-11, M-27, M-45) for σ_{min}/σ_c = 0.80, R=5.

B.13 Normalized stress versus N for 5% and 7% compliance change for R=10 and 5

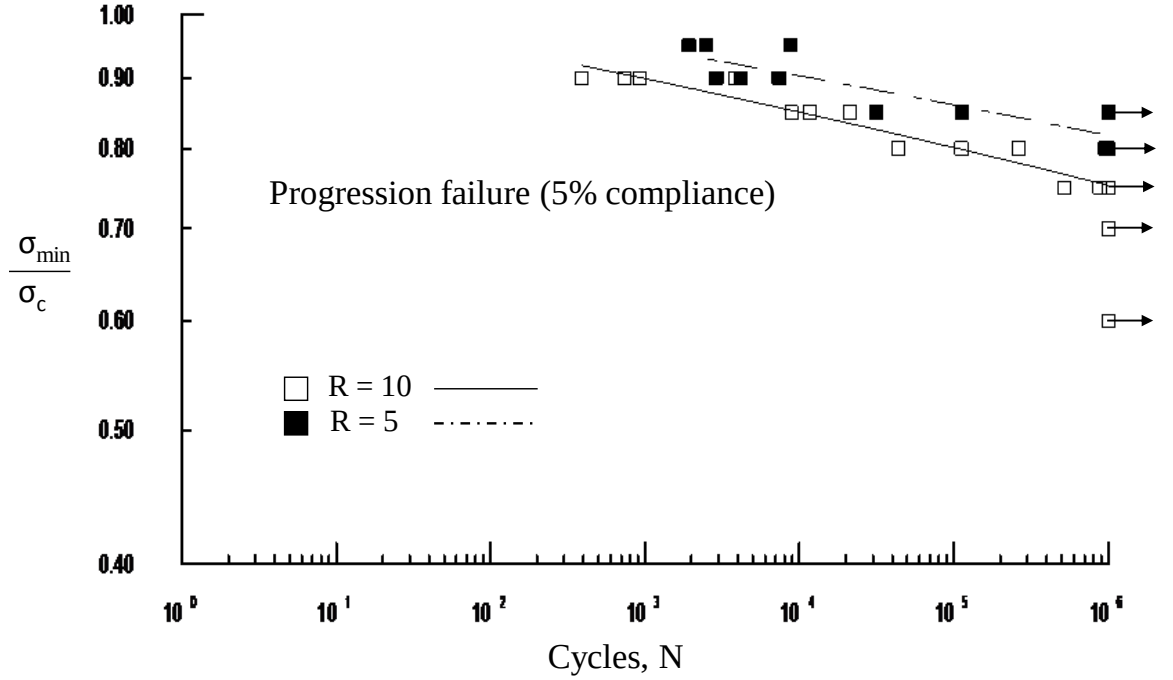

(a) For 5% compliance change failure

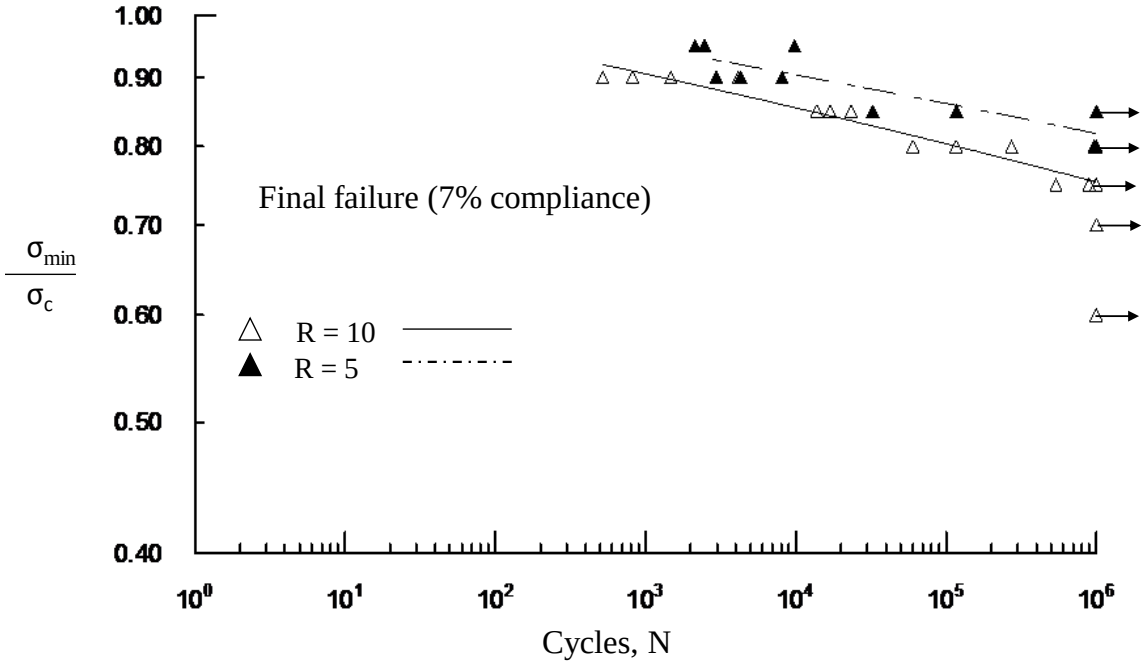

(b) For 7% compliance change failure.

Figure B 13. Normalized stress versus N for 5% and 7% compliance change for R=10 and 5.

B.14 Normalized Stress Range Versus N for 5% and 7% Compliance Change for R=10 and 5.

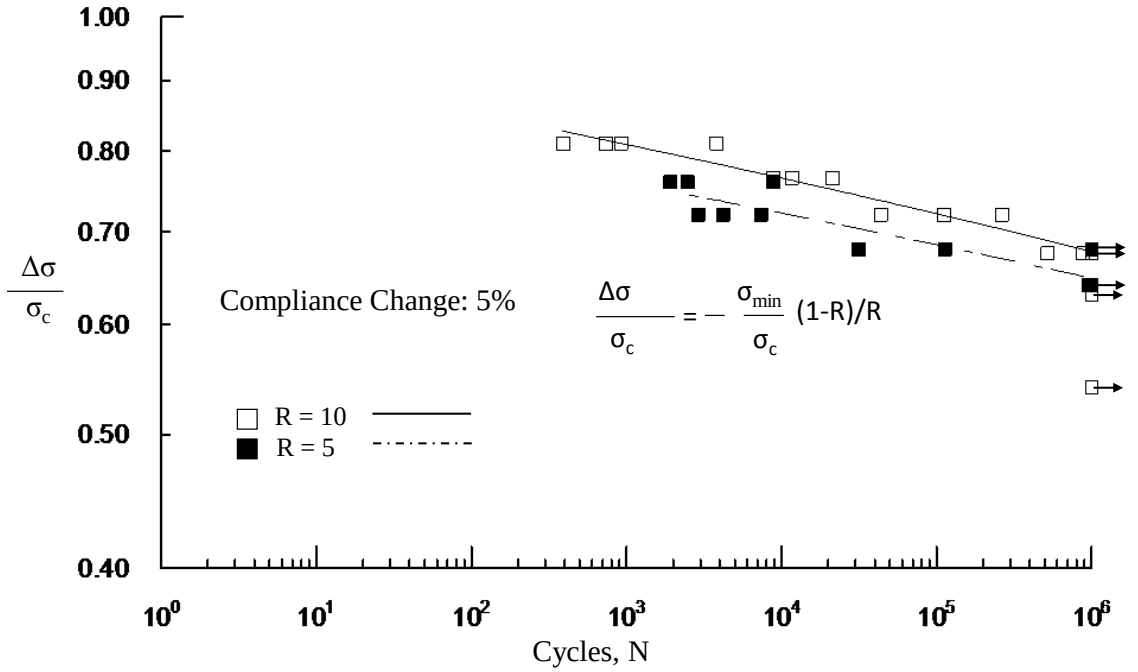

(a) For 5% compliance change failure

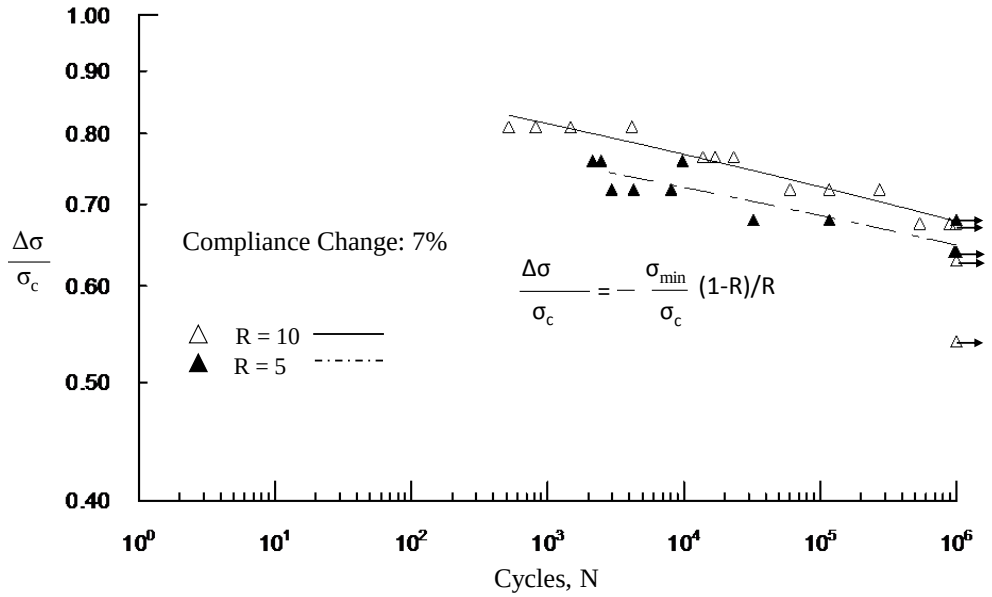

(b) For 7% compliance failure

Figure B 14. Normalized stress range versus N for 5% and 7% compliance change for R=10 and 5.

B.15 Normalized Mean Stress Versus N for 5% and 7% Compliance Change for R=10 and 5.

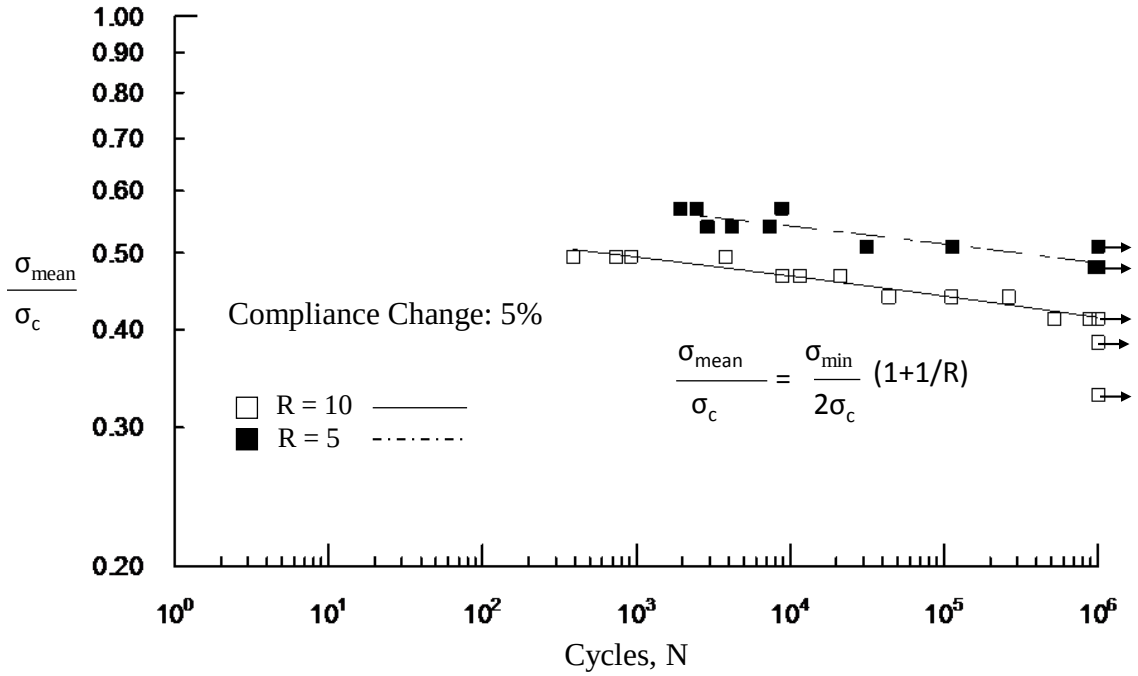

(a) For 5% compliance change failure.

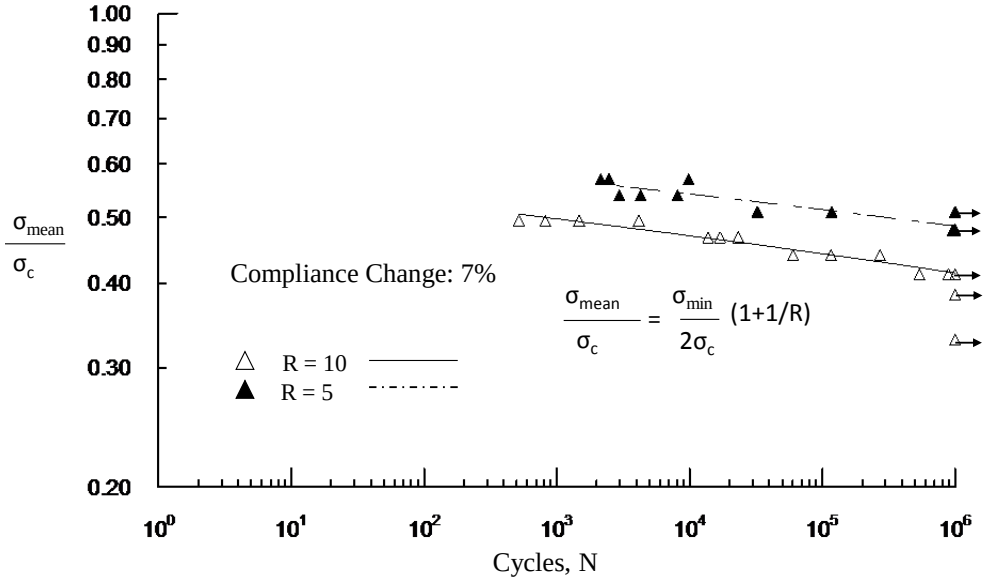

(b) For 7% compliance change failure.

Figure B 15. Normalized mean stress versus N for 5% and 7% compliance change for R=10 and 5.

Appendix C

Additional Figures of Chapter 3

Compliance versus number of cycles (N) curves of the fatigue tested specimens for τ_{max}/τ_c = 0.90, 0.80 and 0.75 are given below.

C.1 Compliance Versus N Curves of the Specimens for τ_{max}/τ_c = 0.90, R=0.1.

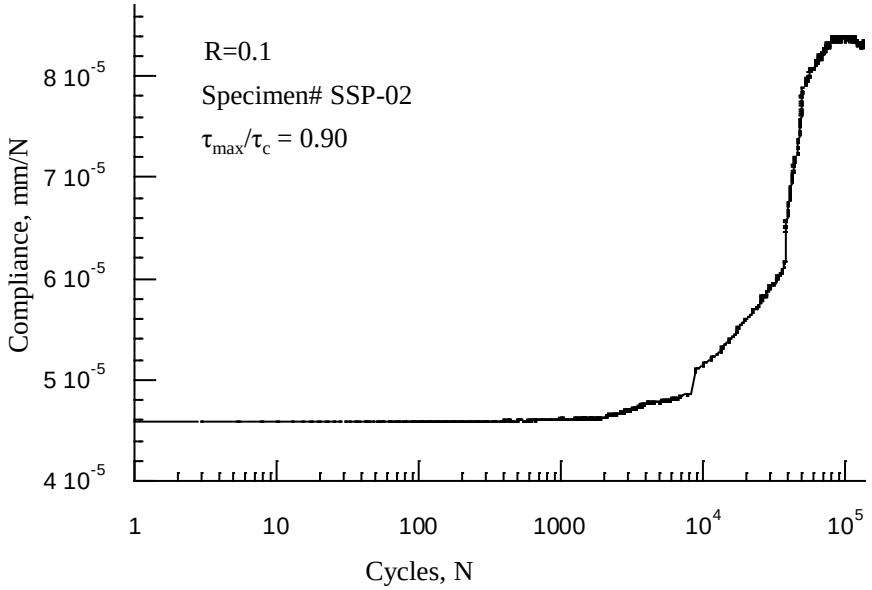

(a) Compliance versus number of cycles curve for specimen SSP-02

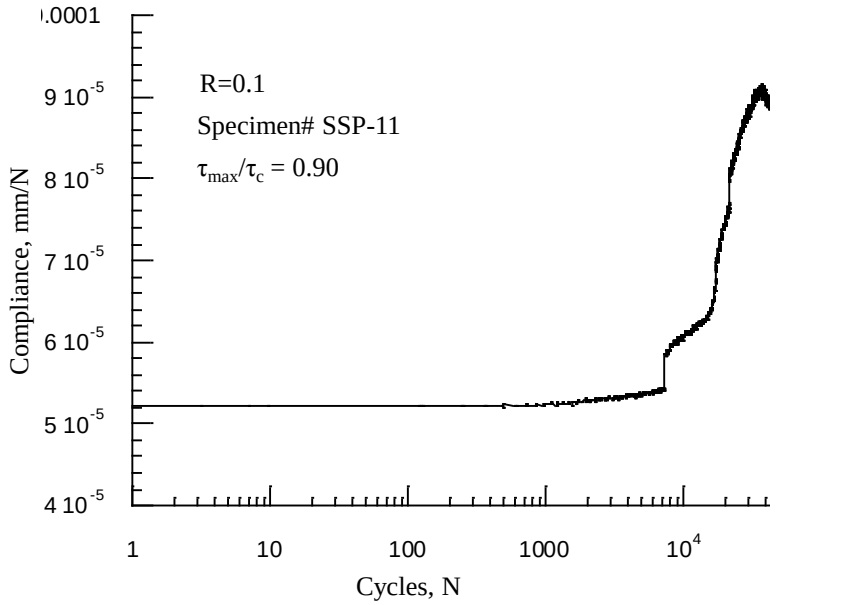

(b) Compliance versus number of cycles curve for specimen SSP-11

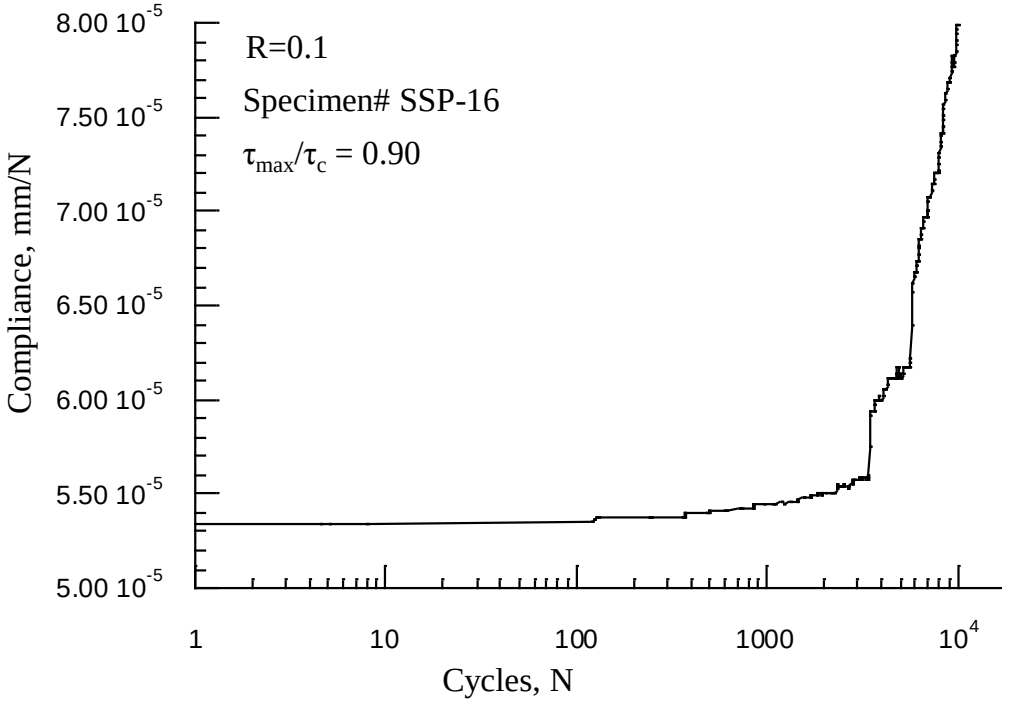

(c) Compliance versus number of cycles curve for specimen SSP-16

Figure C 1. Compliance versus N curves (SSP-02, SSP-11, SSP-16) for $\tau_{max}/\tau_c = 0.90$, R=0.1.

C.2 Compliance Versus N Curves of the Specimens for $\tau_{max}/\tau_c = 0.80$, R=0.1.

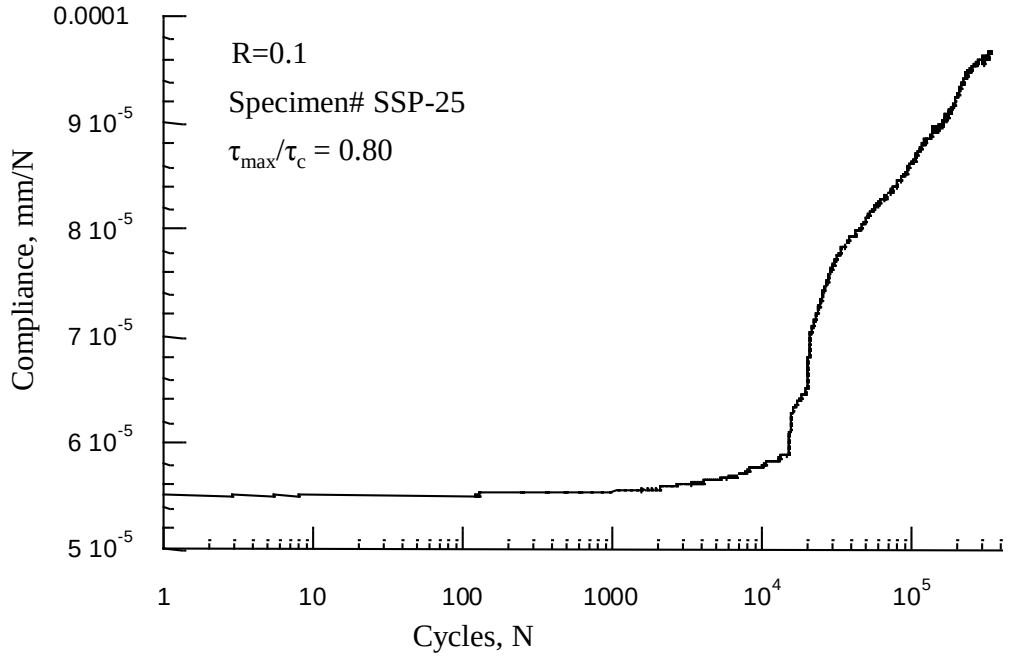

(a) Compliance versus number of cycles curve for specimen SSP-25

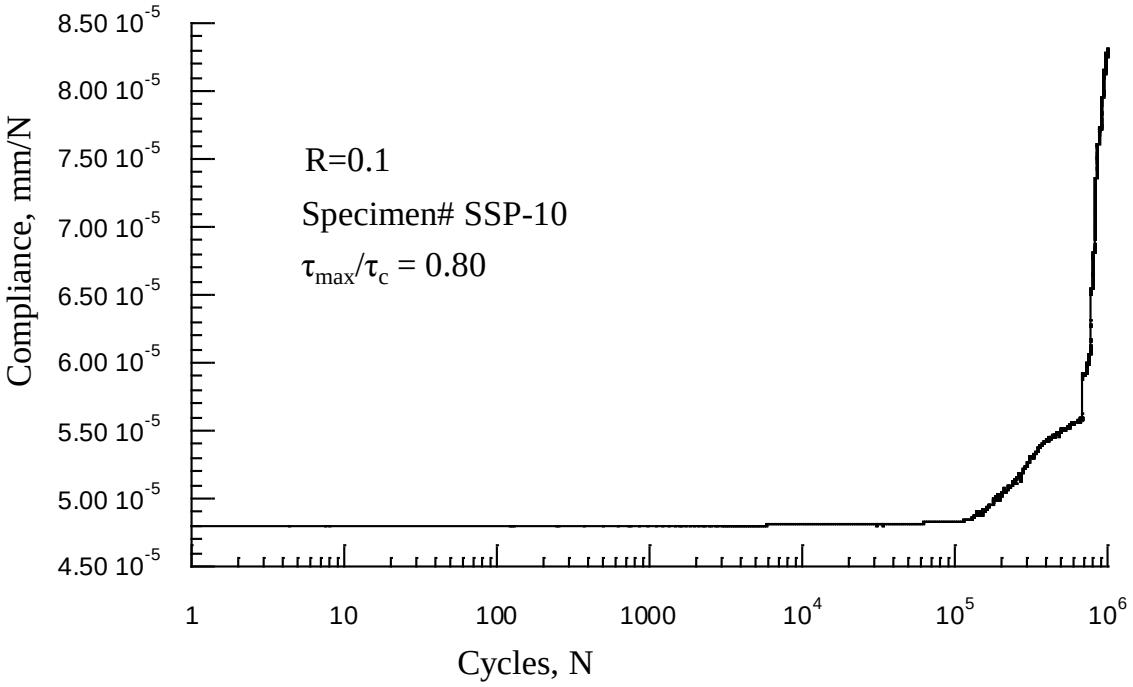

(b) Compliance versus number of cycles curve for specimen SSP-10

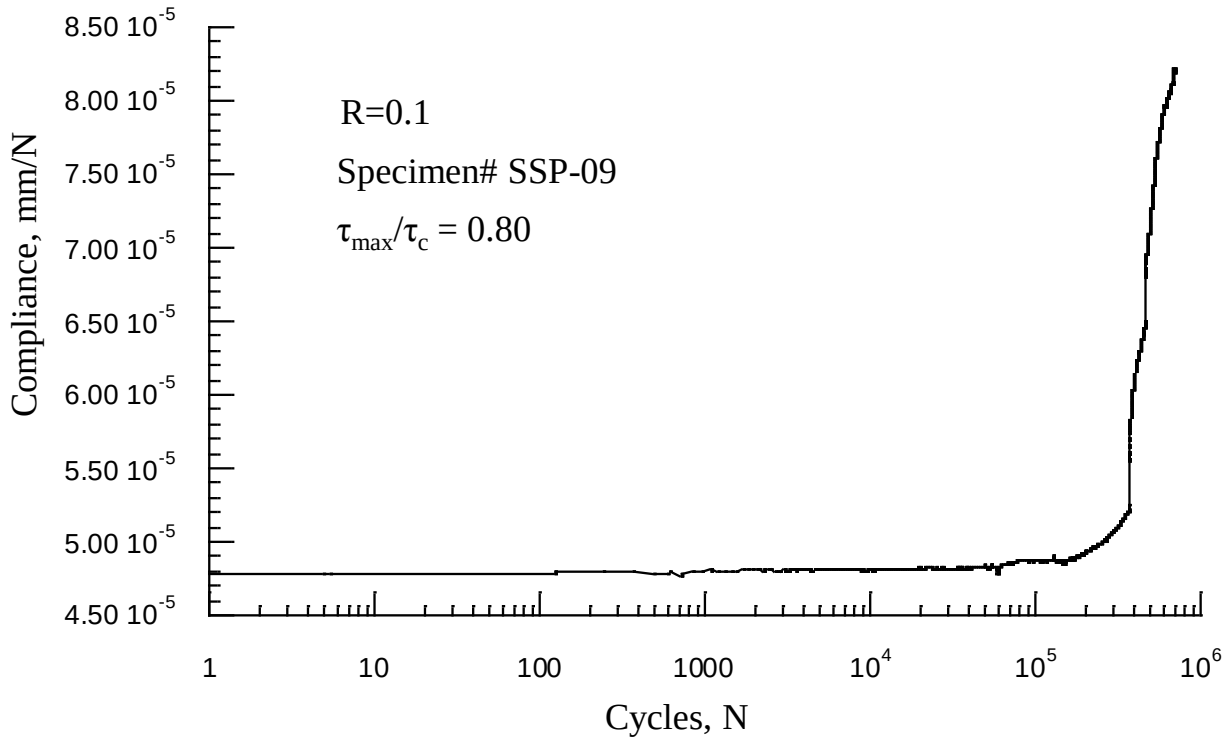

(c) Compliance versus number of cycles curve for specimen SSP-09

Figure C 2. Compliance versus N (SSP-25, SSP-10, SSP-09) for $\tau_{max}/\tau_c = 0.80$, R=0.1.

C.3 Compliance Versus N Curves of the Specimens for τ_{max}/τ_c = 0.75, R=0.1.

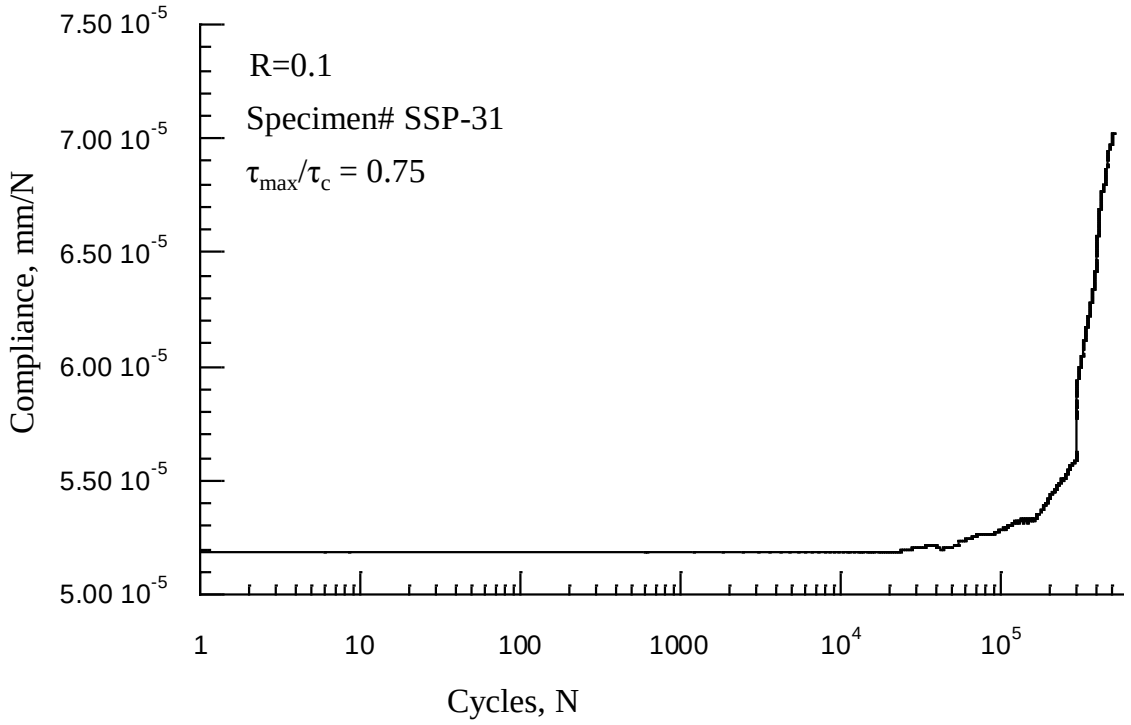

(a) Compliance versus number of cycles curve for specimen SSP-31

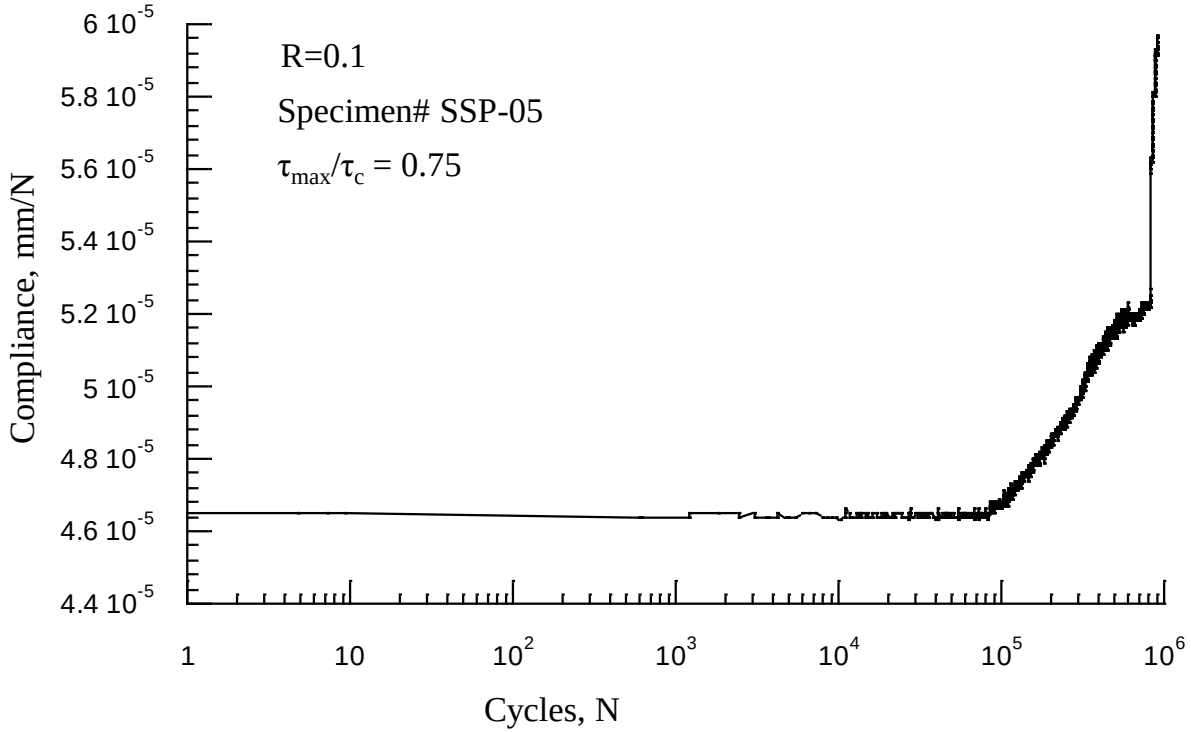

(b) Compliance versus number of cycles curve for specimen SSP-05

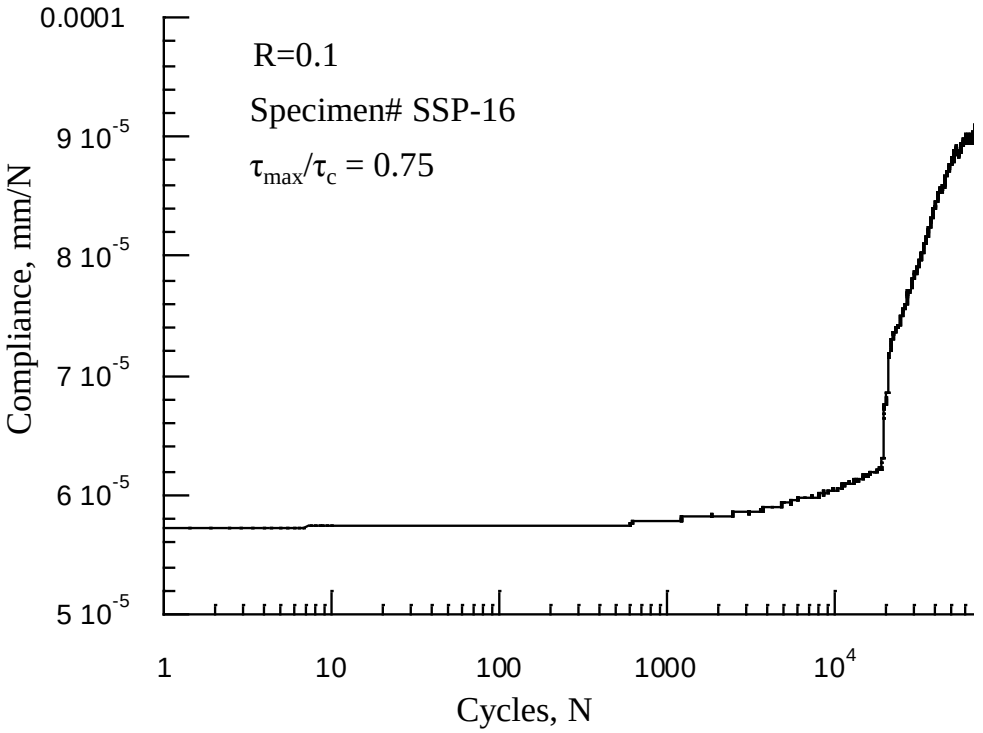

(c) Compliance versus number of cycles curve for specimen SSP-16

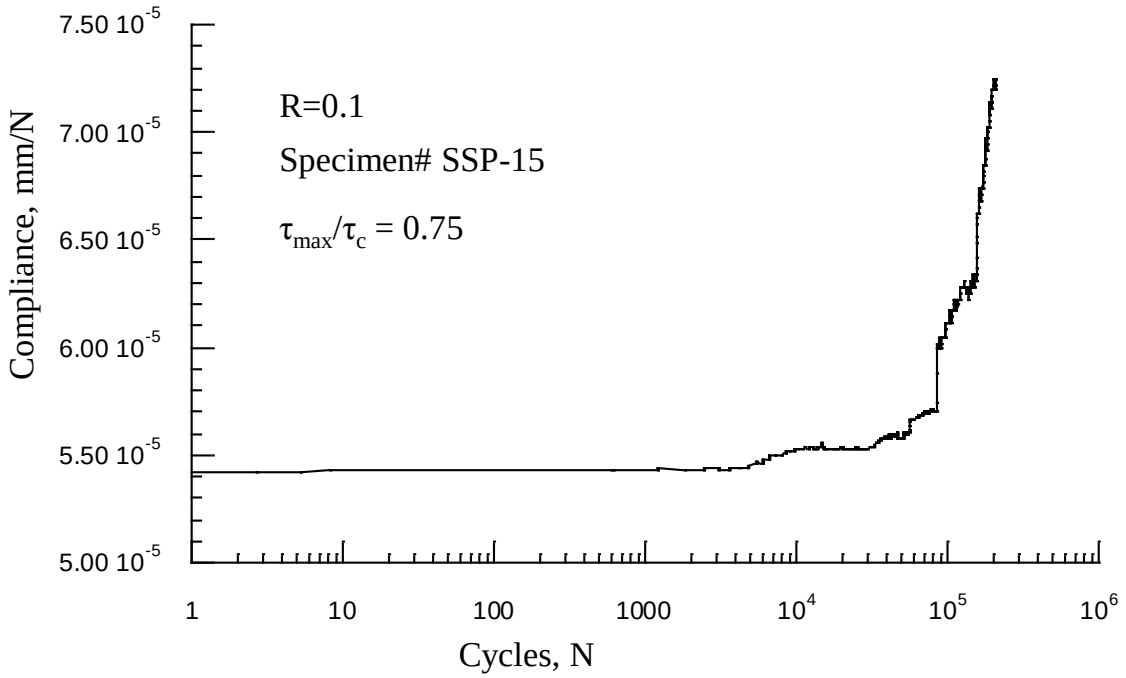

(d) Compliance versus number of cycles curve for specimen SSP-15

Figure C 3. Compliance versus number of cycles (SSP-31, SSP-05, SSP-16, SSP-15) for τ_{max}/τ_c = 0.75, R=0.1.

Appendix D

Additional Figures of Chapter 4

Compliance versus number of cycles (N) curves of the fatigue tested specimens for σ_{max}/σ_{ct} = 0.90, 0.80 and 0.75 are given below.

D.1 Compliance Versus N Curves of the Specimens for σ_{max}/σ_{ct} = 0.90, R=0.1.

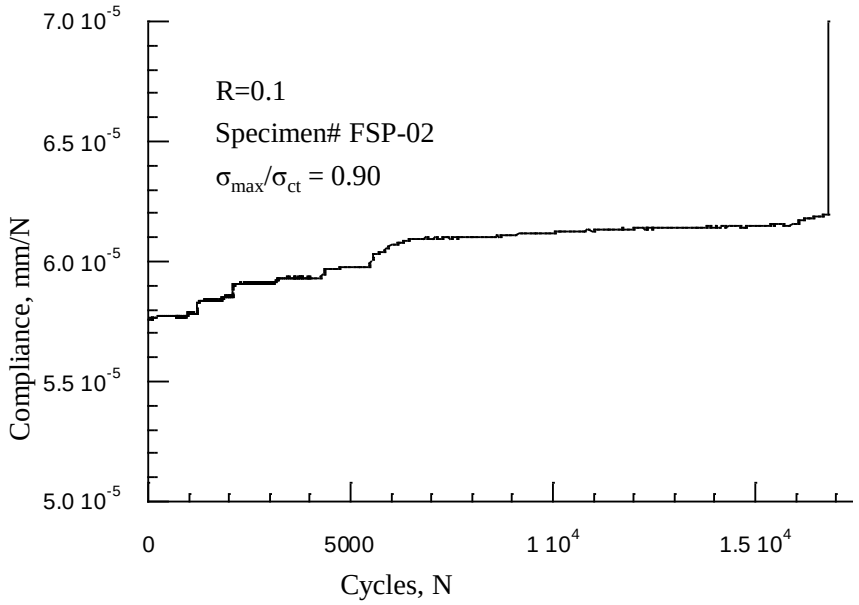

(a) Compliance versus number of cycles cureve for specimen FSP-02

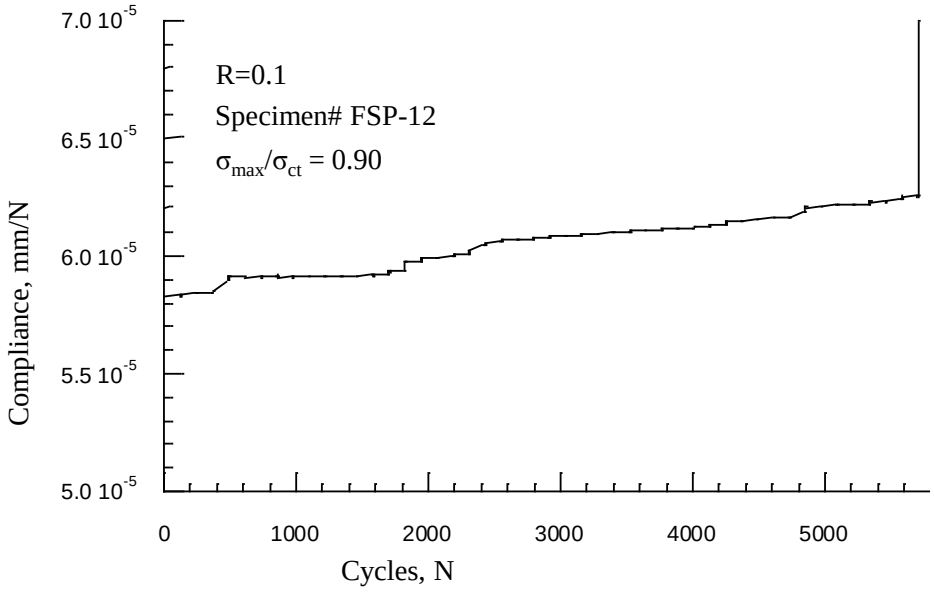

(b) Compliance versus number of cycles cureve for specimen FSP-12

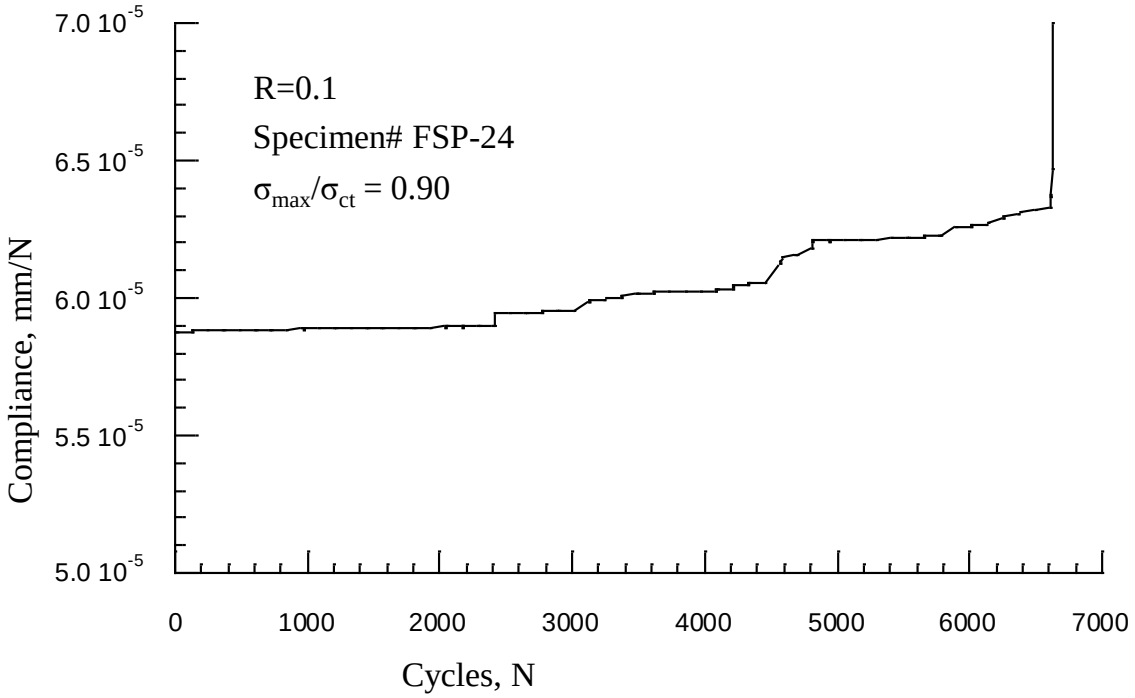

(c) Compliance versus number of cycles cureve for specimen FSP-24

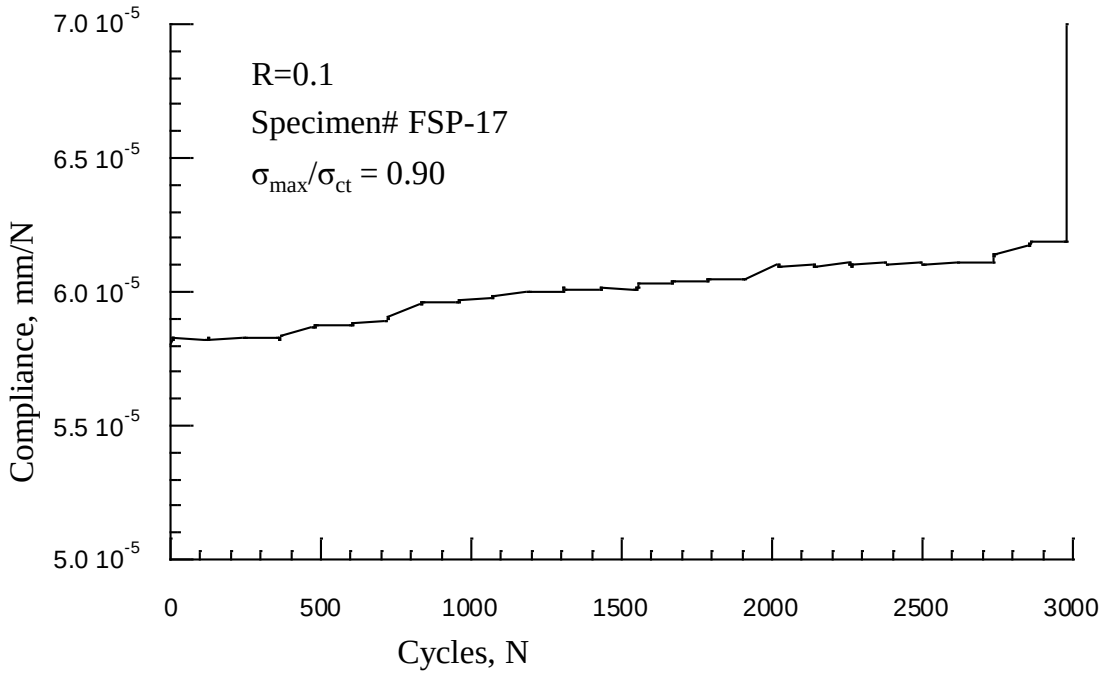

(d) Compliance versus number of cycles cureve for specimen FSP-17

Figure D 1. Compliance versus N curves (FSP-02, FSP-12, FSP-24, FSP-17) for $\sigma_{max}/\sigma_{ct} = 0.90$, R=0.1.

D.2 Compliance Versus N Curves of the Specimens for σ_{max}/σ_{ct} = 0.80, R=0.1.

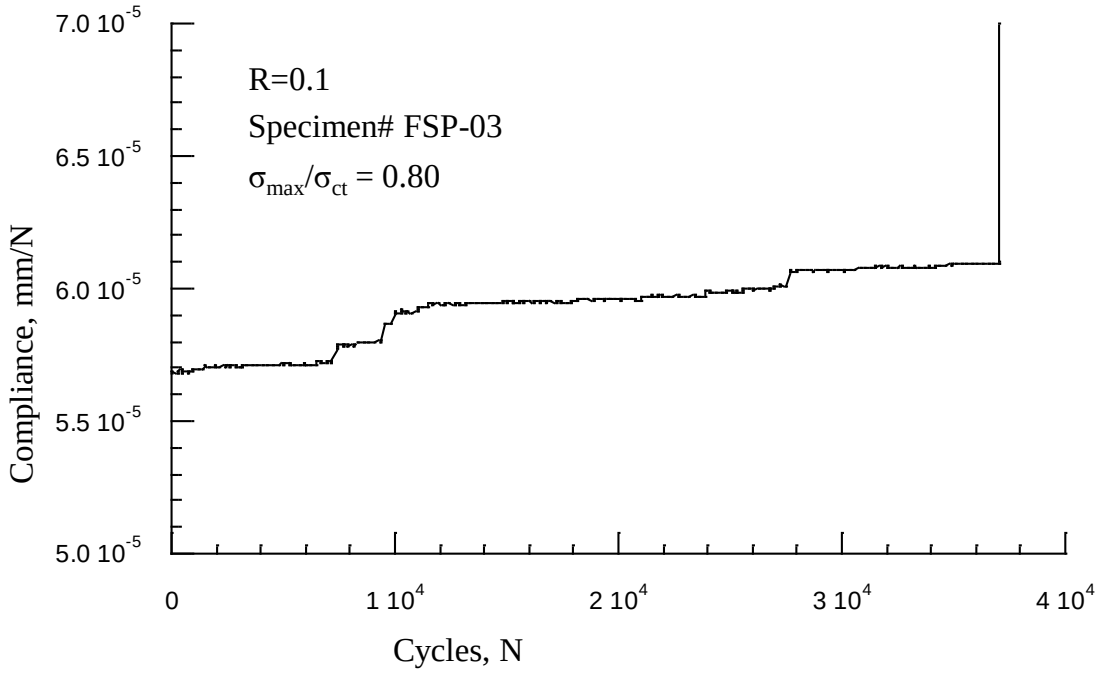

(a) Compliance versus number of cycles cureve for specimen FSP-03

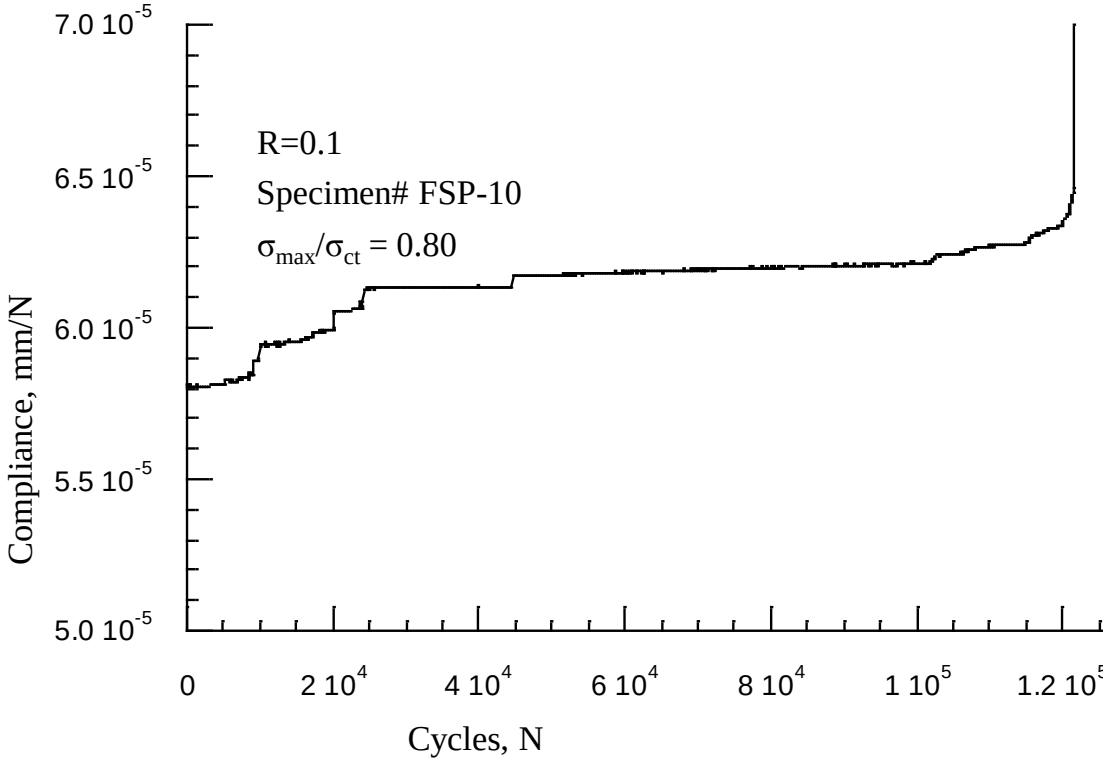

(b) Compliance versus number of cycles cureve for specimen FSP-10

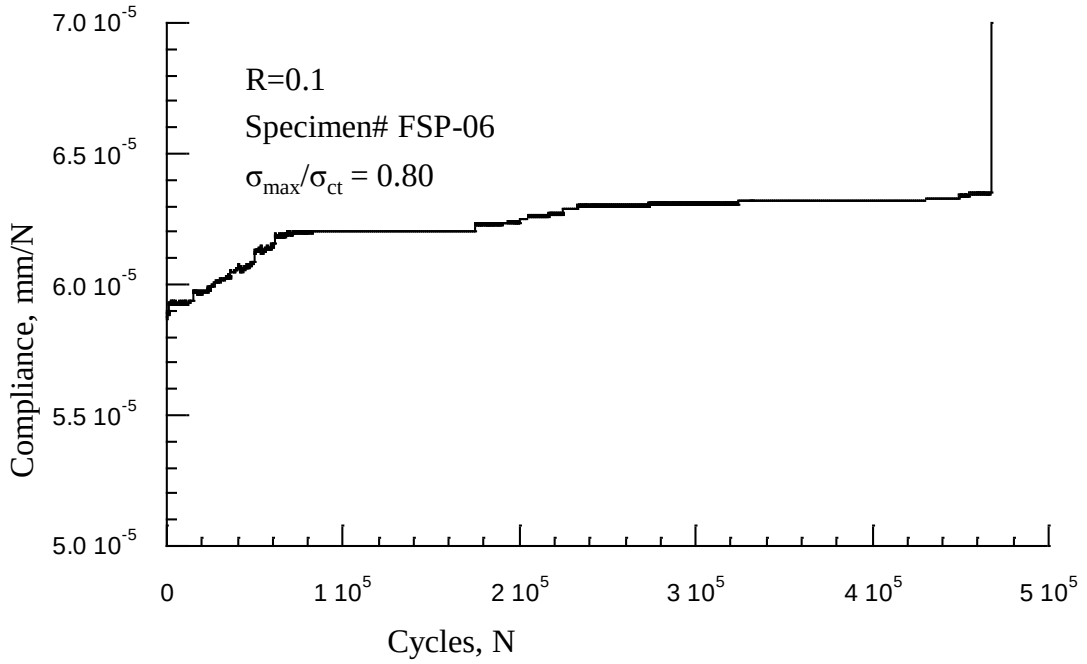

(c) Compliance versus number of cycles cureve for specimen FSP-06

Figure D 2. Compliance versus N curves (FSP-03, FSP-10, FSP-06) for σ_{max}/σ_{ct} = 0.80, R=0.1.

D.3 Compliance Versus N Curves of the Specimens for σ_{max}/σ_{ct} = 0.75, R=0.1.

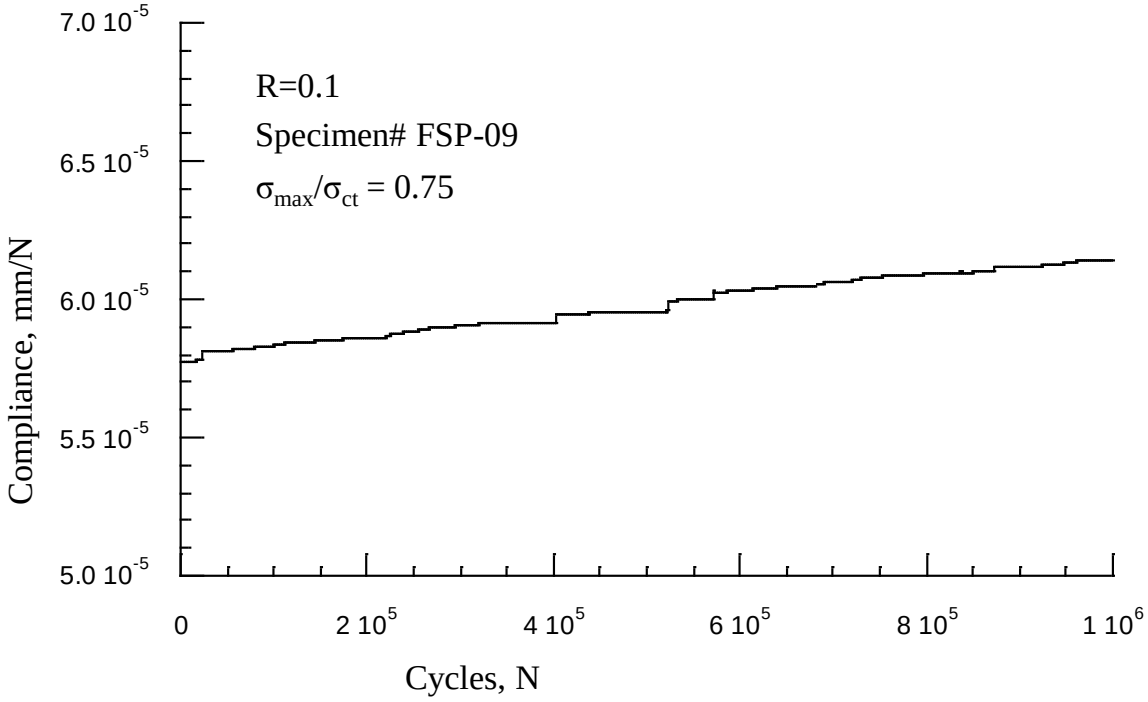

(a) Compliance versus number of cycles cureve for specimen FSP-09

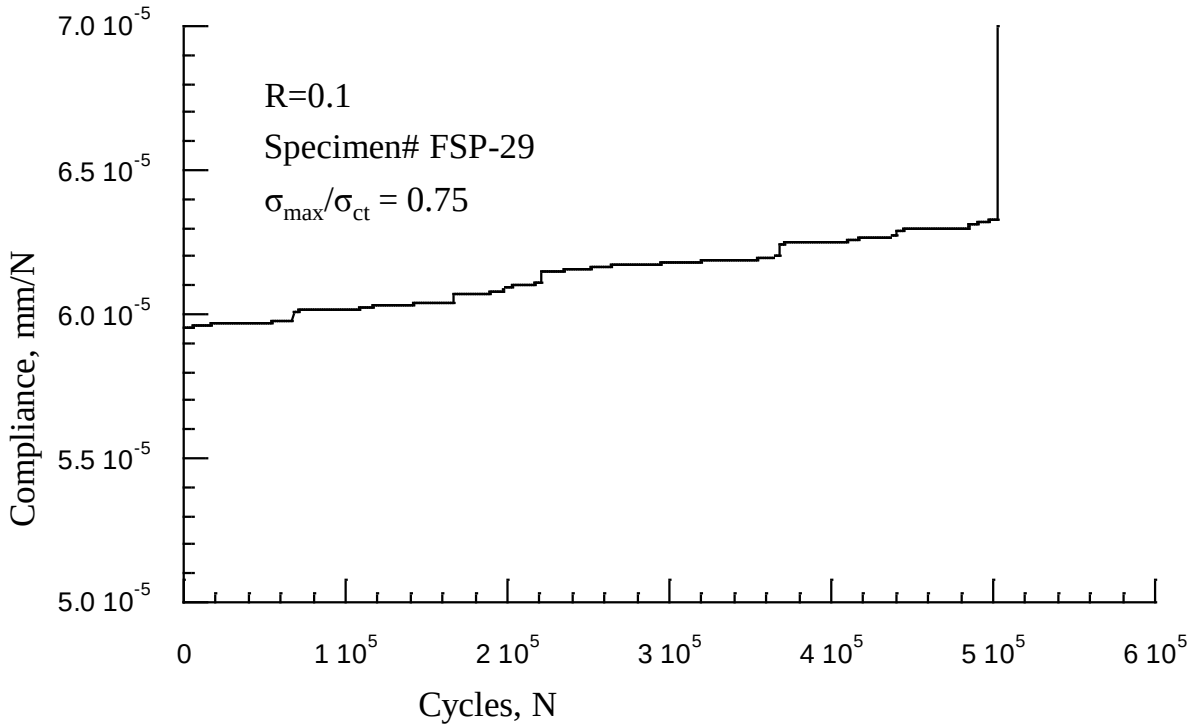

(b) Compliance versus number of cycles cureve for specimen FSP-29

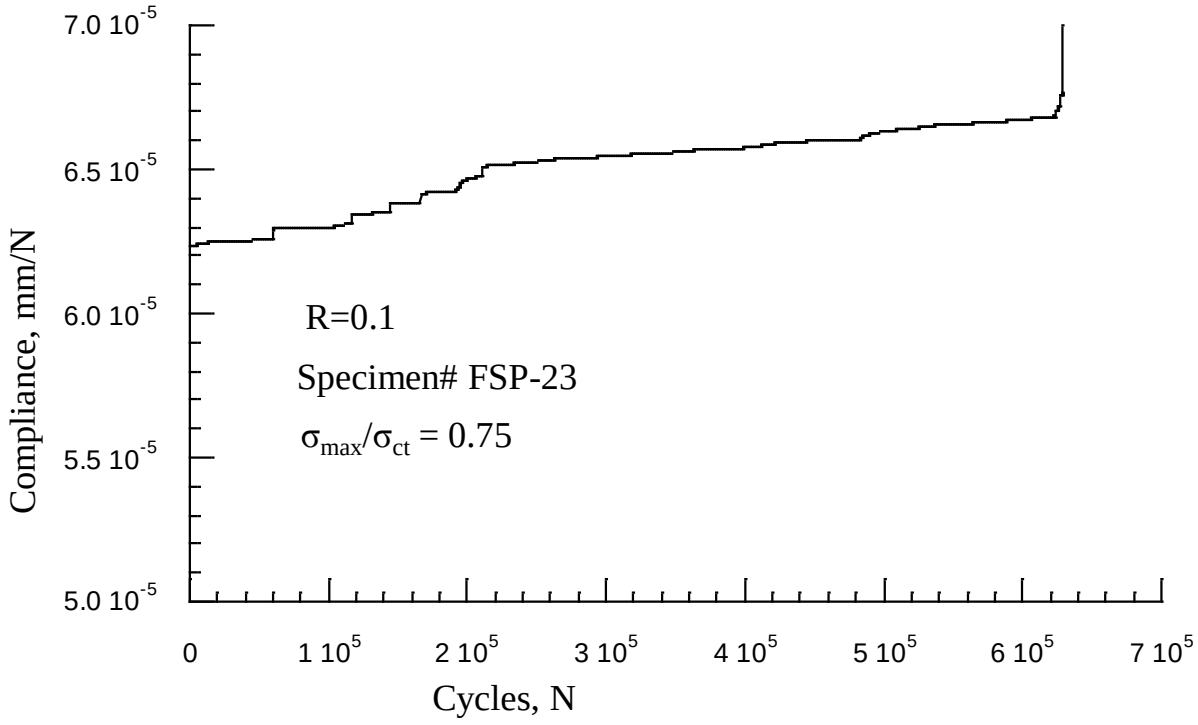

(c) Compliance versus number of cycles cureve for specimen FSP-23

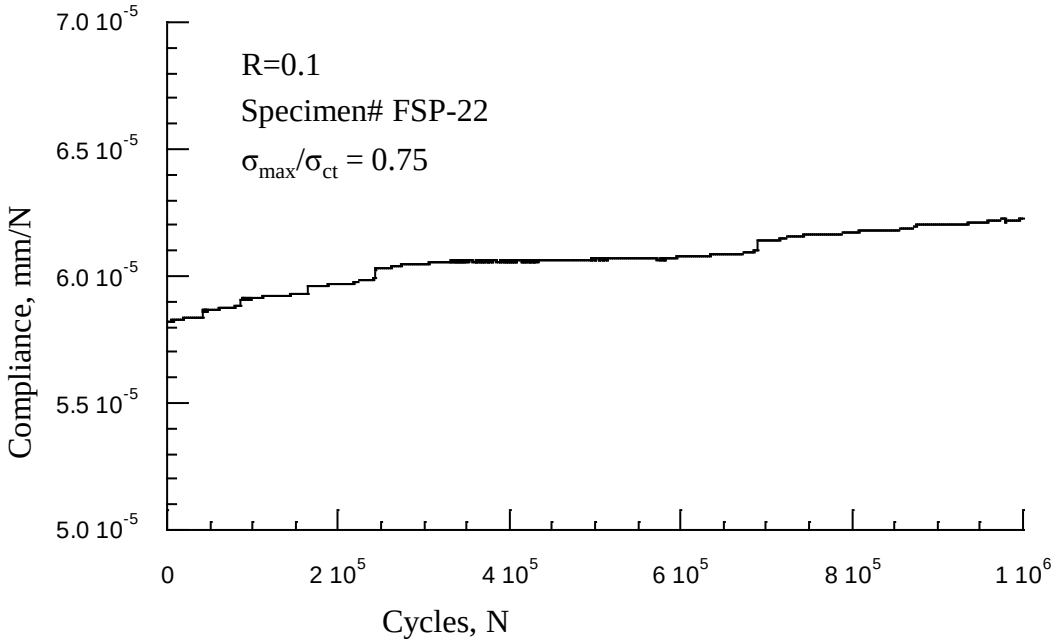

(d) Compliance versus number of cycles cureve for specimen FSP-22

Figure D 3. Compliance versus N curves (FSP-09, FSP-29, FSP-23, FSP-22) for $\sigma_{max}/\sigma_{ct} = 0.75$, R=0.1.